Class I p110alpha-PI3Ks crosstalk with nutrient sensing mTOR signalling regulates stress and injury responses in the intestinal epithelium

Ph.D. Thesis

Thesis Submitted in Partial Fulfilment of the requirements of the Degree of Doctor of Philosophy

Laura Medrano González

Queen Mary University of London

October 20, 2019

William Harvey Research Institute

Barts & the London School of Medicine and Dentistry

Amara lento tempera risu

"Temper the bitter things in life with a smile."

STATEMENT OF ORIGINALITY

I, Laura Medrano González, confirm that the research included within this thesis is my own work or that where it has been carried out in collaboration with, or supported by others, that this is duly acknowledged below, and my contribution indicated. Previously published material is also acknowledged below.

I attest that I have exercised reasonable care to ensure that the work is original and does not to the best of my knowledge break any UK law, infringe any third party's copyright or other Intellectual Property Right, or contain any confidential material.

I accept that the College has the right to use plagiarism detection software to check the electronic version of the thesis.

I confirm that this thesis has not been previously submitted for the award of a degree by this or any other university.

The copyright of this thesis rests with the author and no quotation from it or information derived from it may be published without the prior written consent of the author.

Signature:

Date:

Details of collaboration and publications:

ACKNOWLEDGEMENTS

I would like to express my especial thank of gratitude to my main supervisor Dr. Ezra Aksoy for her constant support, guidance and wisdom through my PhD. I have thoroughly enjoyed my time with you, and I know will enjoy your friendship for long to come. Thank you for sharing with me your extended knowledge and your passion towards science. My thanks also to Dr. Dianne Cooper for her co-supervision, advice and guidance as well. I would additionally like to thank everyone in Biochemical Pharmacology, current and past members, for all your help and support, especially to: Ula Stopka-Farooqui, Shani Austin Williams, Anton Zarafov, Patricia Regina-Souza, Louise Topping, Hefin Rhys, Jose Garrido, and others; I could not have been more grateful for your friendship and constant support during these years. I must extend my gratitude to Dr. Alba Bosquets-Agudo and Dr. María González-Núñez, co-workers and friends in Ezra's group, thank you for your unlimited help and advice through this journey inside and outside work. My deepest acknowledgements to Dr. Esther Castellano and her group for her advice and support in this project, as well as providing the p110α-RBD mouse strain and αRBD MEFs, which made a big impact in this project. Finally, additional thanks to the other members of the William Harvey Research Institute and all core facilities at the Charterhouse Square for making a friendly environment and the best of work quality in a day to day basis. Thank you to the Derek Willoughby Fund for Inflammatory Research at Queen Mary University for funding this project.

My home and heart will always belong to Barcelona, where many great friends and family had always believed in me and give me unconditional love and support. It is impossible for me to put in words all my gratitude and love towards everyone back home but most importantly: to my brother, Daniel Medrano-González, for his unlimited energy and admiration; to my father Jordi Medrano-García, for his constant positive energy and giving me always his greatest smile no matter what; and thank you with all my heart to my beloved mother Alícia González-Díaz, for giving me strength, empowerment, and being always a great example for any human being. Special acknowledgement to my basketball team Camden Panthers Woman, who had made my journey though PhD lighter and funnier. Working out and training with you after work to become our best all these years has not been easy but has helped me to organise myself and clear my mind day by day, giving me the consistency and balance needed for a PhD. Competition is a great effort which helped me learn how to be the very best version of myself. I was fortunate to found you Barbara Kaufmann-Kaufmann and Evelyn Oyebanjo, great friends who have always believed in me and gave me their very best energy and support to keep going. To all my basketball team, thank you for always being there and bringing great times of joy and amazing energy by winning the league and playing great finals.

**Acknowledgments in Spanish for my family:*

A toda mi familia, tíos, tías, primos y primas, que me demuestran su amor incondicional cada día, gracias. A mi tía Mari por ser mi conciencia, por todas las charlas y todas las locuras. A mi tío Julio, por no ser el "César" de aquellas Navidades, por llegar, por aceptarnos y querernos, por estar siempre ahí, por todas las series, pelis, programas, música, por no quedarse nunca y aguantarnos pase lo que pase. A mi tía Nuri por ser la más juerguista, la más lianta y compartir conmigo

sus grandes consejos, por todos los gritos y risas, por contagiarme esa manía tan graciosa de guiñar el ojo mientras reímos. A mi tío Tito por su alegría, sus ganas de descubrir, explorar, por todo su apoyo y su sonrisa dulce. A mi tía Cristina por ser tan despistada, tan sensible, tan caroñosa, y por darme los mejores consejos, gracias por ser mi hermana mayor. A mis abuelos: Nati & Vicente, y Conchita & Manolo, gracias por ser mis segundos padres, por haber hecho que mi infancia sea de ensueño, por todas las meriendas prohibidas, los macarrones, paellas y arroz con leche deliciosos. Por haberme transmitido tanto amor, por haber construido el Terreno y haber hecho de él mí segundo hogar. Por haberme cuidado y soportado tanto. Gracias por ser los mejores yayos que nunca nadie haya podido imaginar.

A mi hermano y mi mejor amigo Dani, gracias por ser mi media naranja, por conseguir que nunca me olvide de cantar, bailar a lo loco y despreocuparme de las tonterías que nos rodean. Gracias por tu apoyo e infinita admiración, que es y siempre será recíproca. Gracias por tu indiscutible sabiduría y ganas de girarlo y re-girarlo todo. Por ponerlo todo en duda y creer que siempre hay una mejor respuesta. Por ayudarme a seguir en los momentos más difíciles y estar siempre ahí. Gracias por tu habilidad de hacerme sonreír y valorar lo verdaderamente importante. Por enseñarme cuánto más tenemos que aprender y cuánto nos queda por batallar, y descubrir, eso sí, juntos. Gracias por tu serenidad y por tus inmensurables abrazos. Gracias por ser mi ángel de la guarda. Gracias por no ser niña y sobretodo, gracias por estar siempre ahí.

A mi papá Jordi, gracias por enseñarme el mundo, por hacerme soñar y ver que los sueños se pueden cumplir. Por ayudarme a entender que de todo se puede sacar el lado bueno y una broma sana. Gracias por tu insaciable alegría y positividad. Gracias por llegar a casa día tras día sonriendo y hacernos ver siempre

lo importante de la vida, por transmitirnos desde siempre tanto amor. Por despertarme cada día con optimismo y enseñarme que los resultados solo llegan con el trabajo duro. Por demostrarme que sí se puede trabajar de algo que disfrutas y te gusta, y cuando lo encuentras tienes que darlo todo, no por el premio, sino por el sencillo placer de hacer bien tú trabajo. Gracias por todos los partidos, torneos, entrenos y campeonatos a los que me has llevado sin rechistar ni una sola vez. Gracias por todos los partidos y entrenos en los que has estado ahí, apoyándome incondicionalmente y listo siempre para celebrar grandes victorias, y también para llorar derrotas y desilusiones. Gracias por defender nuestro hogar del dragón no con armas sino con rosas hermosas como las de de St Jordi. Gracias por cantar cada palabra y reír cada simple tontería. Gracias por tu apoyo incondicional y sobretodo, gracias por enseñarme que el amor de verdad existe. Gracias por ser mi héroe.

A mí querida madre Alícia, que decir que no sepas ya. Gracias por enseñarme a saber ser y estar, y por hacer que cada día que pasa quiera saber más y seguir aprendiendo. Gracias por hacerme valorar todo aquello que nos rodea y dar las gracias siempre con una gran sonrisa, pase lo que pase. Por enseñarme la importancia de intentar ser mejor persona sin escusas. Por hacer que levantarse para empezar un nuevo día sea siempre una gran aventura que tengamos ganas de comenzar. Gracias por todo el apoyo y cariño incondicional desde el día en que nací. Por abrirme las puertas del país de las maravillas que yo escogiera. Por permitirme soñar y volar tan alto como quisiera, sin limitaciones. Por ser una modelo y ejemplo a seguir, por todo lo que me has enseñado, por cada detalle, frase, gesto y abrazo que me han ayudado a ser la persona que soy el día de hoy. Por transmitirme esa fuerza imparable que con todo lo puede desde siempre. Gracias por ser una gran luchadora y mi superheroína hoy y siempre. Porque si este recorrido es posible es gracias a tus interminables consejos y grandes palabras de sabiduría. Porque sin ti no habría encontrado este camino. Gracias.

ABSTRACT

Phospoinositide-3-kinases (PI3Ks) are evolutionarily conserved lipid kinases that regulate essential organismal pathways for cell growth, division, proliferation, and are often deregulated in cancer and inflammation. PI3Ks regulate innate immune responses through detection of microbes via pathogen recognition receptors (PRRs)[1]. The oncogenic p110α-PI3K isoform is highly associated with several cancers and overgrowth diseases[2]. Nutrient sensing of amino acids (AAs), contributes to cell growth and proliferation involving PI3K-activation of the mammalian target of rapamycin (mTOR), known to regulate intestinal epithelial cells (IECs) regenerative activities[3,4]. NOD1/2 are cytosolic PPRs which detect D-amino-dipeptides from the bacterial-cell-wall component peptidoglycan and regulate stem cell renewal and wound healing in the intestine[5]. However, how p110α-PI3K regulates functions downstream PRR-signalling pathways in IECs is not well understood. Since, mutations in NOD2 have been associated with and increased risk of inflammatory bowel disease (IBD)[6–8], I hypothesized that NOD1/2-mediated activation of the p110α-mTOR axis, by intracellular detection of D-amino dipeptides, may be essential for initiating protective cellular responses to injury in IECs. Herein, by genetic and pharmacological targeting *in vivo* and *in vitro*, I established that NOD1/2 triggering by bacterial D-amino-dipeptides selectively couple to p110α, which activate AKT/mTOR pathways. Strikingly, temporal inactivation of p110α-RBD interaction in adult mice results in partial lethality following DSS-intestinal injury, due to defects in IEC repair and function, which can be comparably reproduced in mouse with IEC-intrinsic Rheb deletion or lacking NOD1/NOD2. Critically, I demonstrated *in vitro* that under AA low conditions, eukaryotic AA-sensing mTORC1 pathway requires p110α-RBD by extracellular protein uptake to sense

intracellular D-amino dipeptides, analogous to NOD pathway. These results establish for the first time that the p110α-RBD interaction mediates activation of mTOR by uptake of bacterial-peptides and couples to the intestinal repair and function, adding a new layer to the complexity of symbiotic host-microbiome interactions.

ACRONYMS

4EBP: eukaryotic initiation factor-4E (eIF4E)-binding protein - 43 -

4-OHT: 4-hydroxytamoxifen - 61 -

A66: p110α isoform selective inhibitor - 56 -

AA: amino acid - 47 -

AKT: AKR mouse that develops spontaneous thymic lymphomas, known as protein kinase B - 35 -

AMP: antimicrobial peptide - 80 -

APC: adenomatous polyposis coli - 90 -

APDS: activated PI3K-delta syndrome - 52 -

BAD: Bcl-associated death promoter - 42 -

BHD: BCR homology domains - 39 -

Bmi1: B cell-specific moloney murine leukemia virus integration site 1 - 82 -

BSA: bovine serum albumin - 108 -

BTK: bruton tyrosine kinase - 35 -

C2: putative membrane-binding domain - 37 -

CARD: caspase recruitment domains - 95/96 -

CBC: crypt base columnar cell - 82 -

CD: Crohn's disease - 90 -

CRC : colorectal cancer - 35 -

DAMPs: damage-associated molecular patterns - 95 -

DC: dendritic cell - 53 -

DLL: delta-like ligand - 76 -

DMEM: Dulbecco's modified eagle's medium - 103 -

DMSO: dimethyl sulfoxide - 103 -

DSS: dextran sodium sulphate - 113 -

EGF: epidermal GF - 82 -

RA: rheumatoid arthritis - 88 -

RBD: Ras-binding domain - 37 -

Rheb: Ras homolog enriched in brain - 43 -

RIP-2: receptor-interacting serine/threonine-protein kinase 2 - 97 -

RLR: RIG-I-like receptor - 92 -

RNA later: RNA stabilisation reagent - 114 -

RTKs: receptor tyrosine kinase -36 -

S6K: S6 kinase - 43 -

SERM: selective estrogen response modifier - 61 -

SH2: Src homology 2 - 37 -

SLE: systemic lupus erythematosus - 88 -

TA cells: transit-amplifying cells - 82 -

TAE: Tris-Acetate-EDTA - 109 -

TAK1: transforming GF beta-activated kinase 1 - 97 -

TBS-T: TBS Tween-20 - 108 -

TLRs: Toll-like receptors - 89 -

TMB: tetramethylbenzidine - 124 -

TNF: tumour necrosis factor - 94-

TSC: tuberous sclerosis protein - 43 -

UC: ulcerative colitis - 90 -

Wnt: wingless-related MMTV integration site 1 - 76 -

WT: wild type - 61 -

TABLE OF CONTENTS

LIST OF FIGURES

LIST OF TABLES

1. INTRODUCTION

"It is always best to start at the beginning"

The Wizard of Oz

1.1. Phosphoinositide 3-kinase family

Phosphoinositide 3-kinases (PI3Ks), are an important family of lipid kinases evolutionary conserved all the way from unicellular organisms such as *Amoeba*[9]. PI3Ks generate lipid second messengers for intracellular signalling after cell activation[10]. PI3Ks contribute to a number of essential biological processes including; proliferation, survival, migration, and vesicular trafficking. In particular, PI3Ks have important functions in the immune system[11]. Localised at the plasma membrane, PI3Ks phosphorylate the 3'-hydroxyl group of phosphatidylinositols (PIs) upon activation by G protein-coupled receptors (GPCRs) and receptors tyrosine kinase (RTKs)[12]. PI3Ks are heterodimeric lipid kinases composed of catalytic and regulatory subunit variants encoded by separate genes and alternative splicing. Mammals have eight PI3K isoforms, which are organised into three classes according to the primary structure of their catalytic subunits, substrate specificity, and regulation[13]. PI3Ks are also known to be important regulators of cellular growth, differentiation, adhesion, apoptosis, and motility and such, knockout (KO) and kinase inactivate (KI) mouse models of PI3K isoform exhibit a number of deficits including embryonic, lethality, overgrowth, T- and B-lymphocyte defects, liver necrosis, and colorectal cancer (CRC).

Class I PI3K is the best-characterised family and one of the most clearly implicated in human cancer and inflammation. Class I PI3Ks phosphorylate PI (4,5)-bisphosphate (PIP_2) to generate PI (3,4,5)-trisphosphate (PIP_3) which acts as a lipid messenger downstream and activates proteins with lipid-binding pleckstrin homology (PH) domains as found in phosphoinositol dependent kinase 1 (PDK1), AKT/protein kinase B (PKB), bruton tyrosine kinase (BTK) and phospholipase c gamma (PLCG)[14]. The tumour suppressor phosphatase and tensin homolog (PTEN)

dephosphorylates PIP_3 to PIP_2, therefore playing a role as an inhibitor of class I PI3Ks. Based on the structure of the catalytic domain (p110) and regulatory subunits, the four class I PI3K-isoforms are divided into two subgroups: class IA and IB. Class I PI3K catalytic subunits in mammals are p110α, p110β, p110δ, and p110γ, which are encoded by four different genes *PIK3CA*, *PIK3CB*, *PIK3CD* and *PIK3CG,* respectively. Catalytic subunits p110α and p110β transduce signals downstream of the insulin receptor (IR) and are expressed ubiquitously. In contrast, p110δ and p110γ are mainly expressed in hematopoietic cells (**Figure 1**).

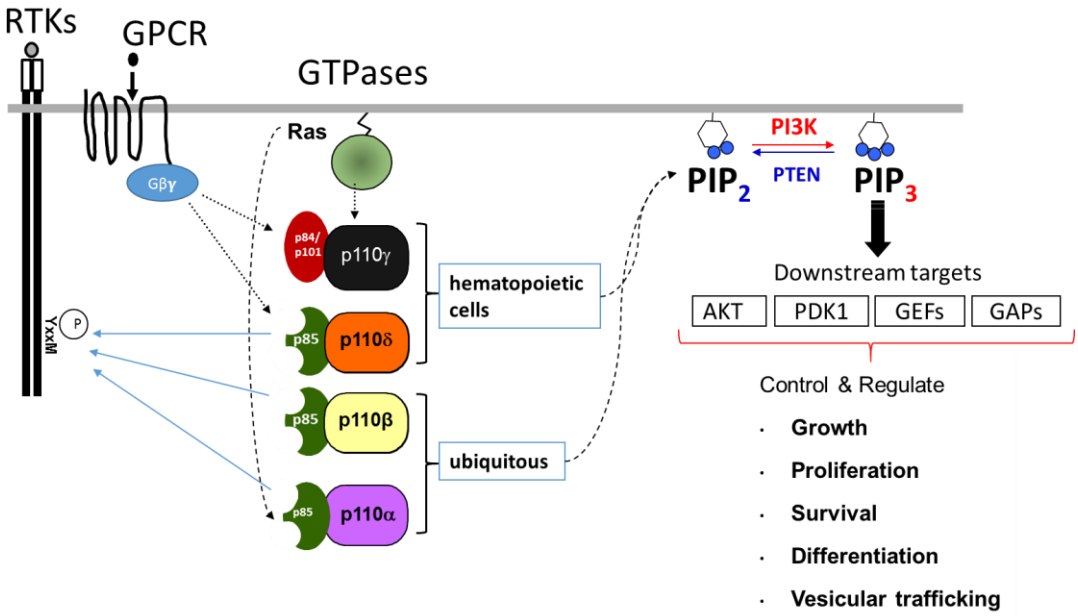

Figure 1: Class I PI3Ks classification and pathway. Phospoinositide 3-kinases (PI3Ks) class I subclasses. G protein-coupled receptors (GPCR), Gβγ heterodimers, receptor tyrosine kinase (RTK), enzymes that can bind and hydrolyze guanosine triphosphate GTP (GTPases), PI (2,4,5)-biphosphate (PIP_2), PI (3,4,5)-trisphosphate (PIP_3), and phosphatase and tensin homolog (PTEN). Downstream targets: AKT, phosphoinositol dependent kinase 1 (PDK1), GEFs, and GAPs. (Adapted from Aksoy E et al., unpublished).

Class II PI3K consists of three enzymes: C2α, C2β, and C2γ. The precise cellular roles of class II PI3Ks are less understood and remains to be established.

Recent studies suggest that class II PI3K regulate angiogenesis, cellular growth and survival functions. The sole member of class III PI3K, referred as vesicle-mediated vacuolar protein sorting (VPS)34 is ubiquitously expressed in mammals and has important functions in intracellular trafficking and autophagy[15]. Although, the PI3K pathway is conserved across organisms and cell subpopulations, the study of each isoform structure, function, and their signalling pathways; is required to identify isoform-specific roles of PI3Ks in cell and tissue specific processes. In this study, I investigated class IA PI3Ks signalling, specifically p110α and p110δ roles in innate immune cells and mucosal epithelial cells.

1.1.1. Class I PI3K – Structure & function

Class I PI3Ks catalytic subunits share a common domain organization composed of an N-terminal adaptor binding domain or p85-bindingdomain (p85-BD), a guanosine triphosphate GTP (GTPase) interacting, Ras-binding domain (RBD), a putative membrane-binding domain (C2), the helical domain, and the carboxy-terminal kinase catalytic domain. Class IA catalytic subunits: p110α, p110β and p110δ have a p85-BD, and their catalytic subunit is activated via the p85 regulatory subunit. There are five isoforms of the p85 regulatory subunit named: p85α, p55α, p50α, p85β, and p55γ[16]. All p85 isoforms contain two Src homology 2 (SH2) domains, which bind phosphorylated tyrosine (pTyr) in specific motifs on RTKs[17]. They share three core domains, including a p110-binding domain called the inter-Src homology 2 (iSH2) domain, along with two SH2 domains. The two longer isoforms, p85α and p85β, have an SH3 domain and a BCR homology domain (BHD) located in the extended N-terminal regions. Class IB PI3K isoform p110γ associates with p84 or p101 regulatory subunits and it is activated exclusively downstream of GPCRs through Gβγ heterodimers (**Figure 2**). Similar to p110γ,

p110β also preferentially couples to GPCRs. Upon specific stimulation, regulatory subunits release the catalytic p110 subunit leading for further PI3K activation. Both p110δ and p110γ have functions in immunity and inflammation, being implicated in inflammatory pathologies. Overall, the data published on class I PI3K subclasses suggests that these kinases mainly control cell biological processes within organ systems, associated with vesicular trafficking events involving endocytosis and phagocytosis. Class II PI3Ks sequence analysis show that they have the core domain organization of the class I enzymes with an extended N-terminal proline-rich region, RBD, and a C-terminal extension with Phox homology (PX) and CD2 domains. Class III PI3K, VPS34+VPS151 is the only PI3K identified in yeast and it has been evolutionarily conserved through mammals. Vps34 plays an essential role in autophagy, a process linked to human health and disease. Class III sequence analysis shows the presence of C2, helical and catalytic domains but absence of RBD[5].

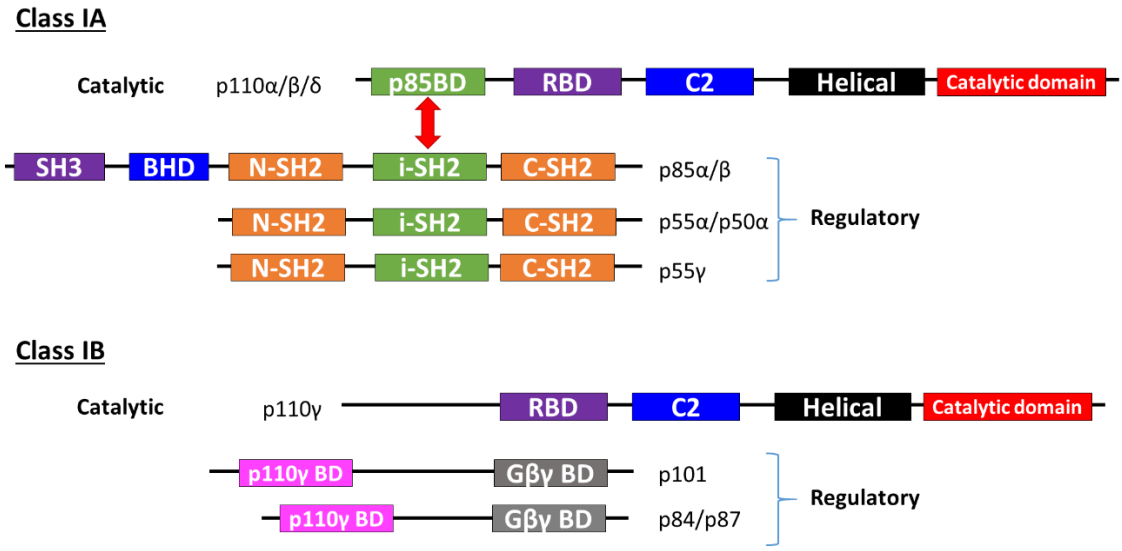

Figure 2: Class IA and class IB PI3Ks structure and classification. Class IA catalytic subunits: p110α, p110β and p110δ have a p85-binding domain (p85-BD), Ras-binding domain (RBD), putative membrane-binding domain (C2), the helical domain, and the carboxy-terminal kinase catalytic domain. The catalytic subunit is activated via p85 regulatory

subunit. There are five isoforms of the p85 regulatory subunit named: p85α, p55α, p50α, p85β, and p55γ. All p85 isoforms contain two Src homology 2 (SH2) domains, three core domains, including a p110-binding domain called the inter-Src homology 2 (iSH2) domain, along with two SH2 domains. The two longer isoforms, p85α and p85β, have an SH3 domain and a BCR homology domain (BHD) located in the extended N-terminal regions. Class IB PI3K isoform p110γ associates with p84 or p101 regulatory subunits[20]. (Adapted from: Thorpe et al., 2015).

1.1.2. Class I PI3K – Signalling pathways

Stimulation of class I PI3Ks occurs through three different type of activation. However, there are some differences between the four class I PI3Ks isoforms. RTKs can activate class IA PI3Ks through binding of the SH2 domains of the regulatory subunit to pTyr at the YXXM motif[21,22]. In the cytosol, catalytic p110 subunits are stabilised and maintained in an inhibited state by constitutive binding to their regulatory, p85 subunit. The inhibitory effect on the p110 subunit from the SH2 domain of the p85 regulatory subunit can be released by addition of RTK derived phosphopeptides or by point mutations in the regulatory subunits. PI3K activity can also be regulated by phosphorylation of the p85 regulatory subunit. Class I PI3K-isoforms p110β, and p110γ are mainly stimulated downstream of GPCRs through Gβγ heterodimers instead of RTKs although, it can also be activated through pY phosphopeptides. Whereas, p110γ can only be activated by Gβγ heterodimers, full activation of p110γ requires the p101 regulatory subunit. Activation by Gβγ heterodimers happens selectively in p110β and p110γ isotypes while p110α and p110δ coupling to Gβγ heterodimers is minimal.

Small G proteins of the Ras superfamily can also specifically activate p110α and p110γ. Ras family GTPases proteins are highly conserved across species and

have a key role in numerous basic cellular functions[23]. The five main families are Ras, Rho, Ran, Rab and Arf GTPases. The Ras family itself is further divided into 6 subfamilies: Ras, Ral, Rap, Rheb, Rad and Rit. Ras proteins are molecular switches that cycle between two conformational states: the active form (when they bound to GTP), and the inactive form (when bound to GDP). Activation of Ras stimulates a wide range of important downstream signalling pathways such MEK-ERK, key regulators of cell polarization, motility, and chemotaxis. Another Ras effector family is PI3Ks, which play important roles as cell survival and proliferation. Ras genes (the H-Ras, K-Ras, and N-Ras genes) are found mutated in 20 to 25% of human tumours and some of these mutations can lock Ras proteins into a constitutively activated state in which they signal to downstream effectors even in the absence of external stimuli[24]. PI3K can also activate Rho GTPase family member Rac, and this activation is involved in cytoskeleton reorganisation. A broader range of Ras family GTPases can activate p110α and p110γ. The RBD domain of p110α catalytic subunit is recruited to the plasma membrane through direct binding to the GTP-bound active form of membrane-bound Ras similar to p110δ[25]. Mutations in the RBD that prevent binding of p110 to Ras show that Ras is required for the signalling and transforming ability of p110α, p110β, and p110γ. However, activation of p110β by Ras family GTPases was not observed *in vitro*. The contribution of Ras to activation of PI3Ks is unclear in normal physiology and in diseases such as cancer where Ras can be constitutively activated. Mutation in the RBD (T208D/K227A) of p110α in mice, in which p110α can no longer interact with Ras, showed some perinatal lethality in homozygotes[25]. These mice showed resistance to tumorigenesis induced by endogenous oncogenic Ras, indicating that p110α is an effector of oncogenic Ras in cancer development. Further studies reported the importance of Ras binding to the single *Drosophila* type I PI3K for developmental growth through the insulin-pathway (**Figure 3**)[26].

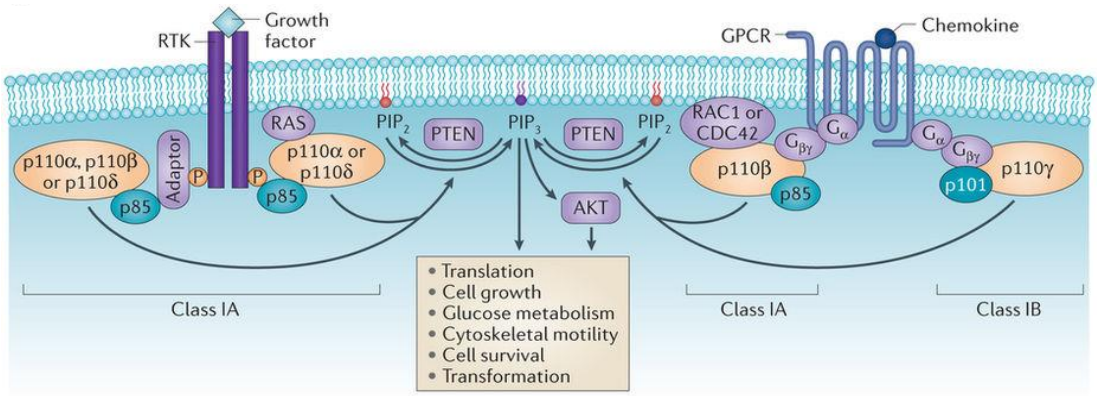

Figure 3: Scheme showing different mechanisms upon activation of class I PI3K signalling. PI3Ks are localised at the plasma membrane and phosphorylate the 3'-hydroxil group of phosphatidylnositides (PIs) on activation by G protein-coupled receptors (GPCR) and tyrosine kinase receptors (RTK)[27]. (Illustration from Burke et al., 2015).

1.1.2.1. The AKT pathway

The activity of class I PI3K is highly regulated and negligible under resting conditions of cells. The signalling cascade begins with specific stimuli, which activates receptors, leading to the recruitment of PI3K from the cytoplasm to the cell membrane. PI3K/AKT signalling controls multiple pathways such as cell cycle, proliferation, cell survival, and protein synthesis via downstream intracellular signalling. Class I PI3Ks catalytic subunits activated, phosphorylate the D-3 position of the inositol ring of PIP_2 to generate the second messenger PIP_3 at the plasma membrane. PIP_3 generated by PI3Ks, recruit proteins with PH domain-containing proteins such as PDK1, which selectively phosphorylates AKT at Threonine residue (Thr308) in order to phosphorylate Serine residue (Ser473) to finally activate AKT. Activation of AKT promotes cell cycle progression by inhibiting glycogen synthase kinase 3β (GSK3β) as well as growth, metabolism, and tumorigenesis in part by inhibiting the Forkhead box (FOXO) family of

transcription factors. At the nucleus, AKT can inhibit the activity of transcription factors, which prevent the expression of cell death genes and promote activation of anti-apoptotic genes. FOXO3 is a well-known substrate of AKT, which can induce apoptosis. AKT also promotes cell survival by inhibiting the ubiquitin E3 ligase MDM2 and the proapoptotic factor Bcl-associated death promoter (BAD). Other functions of AKT are the activation of the nuclear transcription factor kappa B (NF-κB) pathway, which induces activation of a classical inflammatory cascade (**Figure 4**).

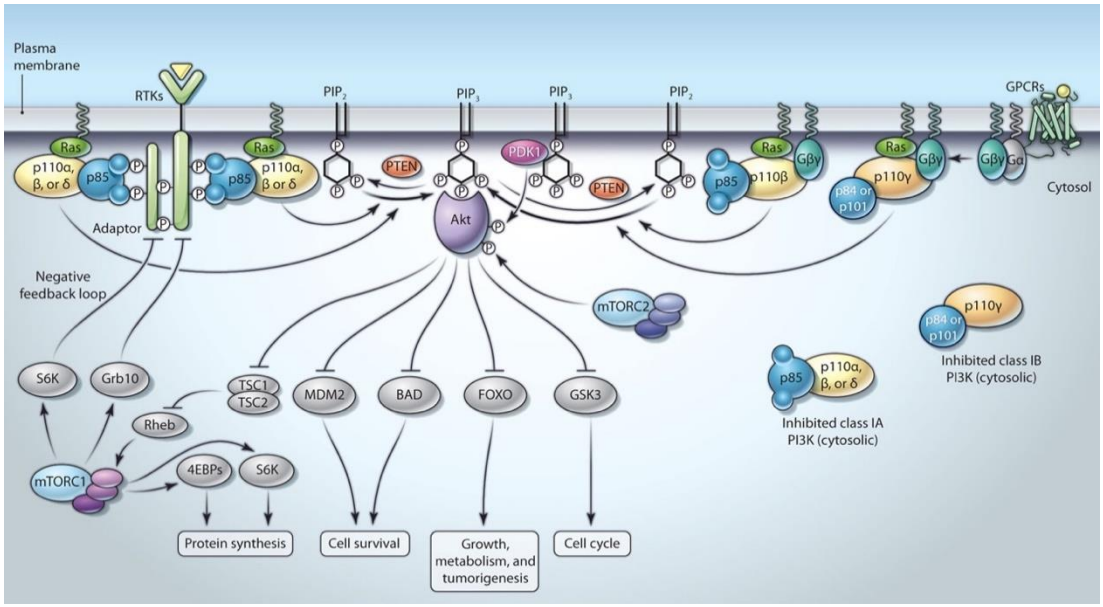

Figure 4: Schematic representation of class I PI3K signalling pathway downstream effects on cellular functions. PIP_3 generated by PI3Ks activates the kinases PDK1 and AKT. AKT is also activated by mTORC2. AKT promotes cell survival by inhibiting the ubiquitin E3 ligase MDM2 and the proapoptotic factor BAD. AKT promotes growth, metabolism, and tumorigenesis by inhibiting the Forkhead box (FOXO) family of transcription factors. AKT promotes cell cycle progression by inhibiting glycogen synthase kinase 3β (GSK3β). AKT promotes mTORC1 activity by phosphorylating and inhibiting the tuberous sclerosis proteins 1 and 2 (TSC1 and 2), thereby enabling the GTPase Rheb to activate mTORC1. Two proteins, S6 kinase (S6K) and the GF receptor-bound protein 10 (GRB10), are phosphorylated by mTORC1 and act in a feedback loop that inhibits signalling by the insulin receptor, insulin-like GF (IGF) receptor, and the adaptor protein IRS-1 (104). The mTORC1 promotes protein synthesis by phosphorylating translational regulators S6K and eIF4E binding proteins 4EBP1 and 4EBP2[28]. (Illustration from Vadas et al., 2011).

1.1.2.2. The mTOR pathway

The mammalian target of rapamycin (mTOR) is a highly conserved member of the PI3K-related protein kinase that controls cell growth and metabolism in response to nutrients. The mTOR is found in two functionally and structurally distinct multiprotein complexes: mTORC1 and mTORC2. Their main difference is that mTORC1 is composed by Raptor, whereas mTORC2 consists of Rictor, and other proteins. Another important difference between mTORC1 and mTORC2 is their activation directly or indirectly through AKT. The mTORC2 activates AKT directly whereas AKT regulates mTORC1 activity by phosphorylating and inhibiting the tuberous sclerosis proteins 1 and 2 (TSC1 and 2), thereby enabling the Ras homolog enriched in brain (Rheb) GTPase, to activate mTORC1. Two proteins, S6 kinase (S6K) and the growth factor (GF) receptor-bound protein 10 (GRB10), are phosphorylated by mTORC1 and act in a feedback loop that inhibits signalling by the insulin receptor, insulin-like GF (IGF) receptor, and the adaptor protein IRS-1. The mTORC1 promotes protein synthesis by phosphorylating translational regulators S6K and the eukaryotic initiation factor-4E (eIF4E)-binding proteins (4EBPs), which are key substrates that control cell proliferation and survival (**Figure 5**). The mTORC1 and mTORC2 complexes, are responsible for different physiological functions. Nutrient sensing mTORC1, is considered mostly involved in the regulation of the translation initiation machinery influencing cell growth, proliferation and cell survival. Whereas, mTORC2 participates in actin cytoskeleton rearrangements and cell survival. Signalling from GFs is mediated through PI3K-AKT-TSC1/2 pathway and upregulates mTORC1 to stimulate translation initiation, whereas energy or nutrient depravation and stress supresses mTORC1 via LMB1-AMPK cascade to trigger off the process of autophagy. On the contrary, mTORC2 is insensitive to nutrients or energy conditions, and so the

mTORC2 complex phosphorylates AKT regulating actin cytoskeleton and cell survival in response to GFs and hormones.

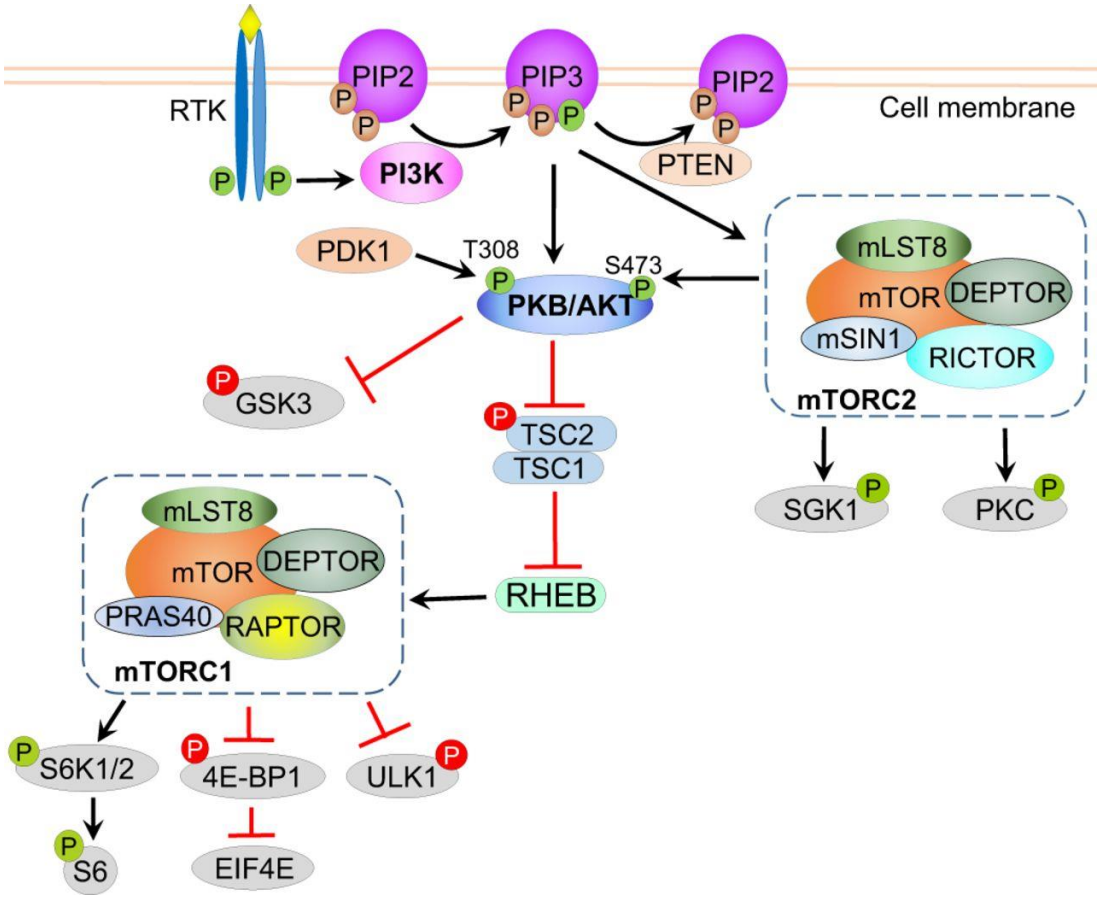

Figure 5: PI3K signalling pathway downstream effects on mTORC1/2 cellular functions. Receptor tyrosine kinase (RTKs) upon growth factor stimulation active phosphoinositide 3-kinases (PI3K) activate and phosphorylate PI (4,5)-bisphosphate (PIP_2) to PI (3,4,5)-trisphosphate (PIP_3), which then activates the kinases PDK1 and PKB/AKT. AKT is also activated by mTORC2/Rictor/Deptor complex. AKT promotes mTORC1 activity by phosphorylating and inhibiting the tuberous sclerosis proteins 1 and 2 (TSC1 and 2), thereby enabling the GTPase Rheb to activate mTORC1. S6 kinase 1 and 2 (S6K 1/2) are phosphorylated by mTORC1. The mTORC1 promotes protein synthesis by phosphorylating translational regulators S6K and eIF4E binding proteins 4E-BP1[29]. (Illustration from Yu et al., 2016).

The complexity of mTOR regulation is amplified by the crosstalk with other signalling pathways such as mitogen-activated protein kinase (MAPK) and the multiple site-specific phosphorylation of the main mTOR targets. Moreover, positive feedback loops propagate AKT-signalling pathways, one of which is mTOR, phosphorylating AKT Ser473. This additionally activates AKT on top of PDK1 activation via AKT Thr308 phosphorylation. In addition, activated G-protein Ras enhances activities of the PI3K pathway, acting as a positive regulator. On the other hand, as well as the downregulation provided by PTEN, S6K influences as a negative feedback mechanism in which it phosphorylates IRS1, an adaptor molecule of PI3K, which downregulates the pathway. A better understanding of mTOR signalling is essential since mTOR inhibitors are widely used as drugs in therapy of cancer and neurodegenerative diseases. The mTOR pathway is a vital regulator of mammalian metabolism and physiology, having important roles in the function of several tissues such as liver, muscle, adipose and the brain[30]. Dysregulation of this pathway in these tissues lead two several pathophysiological conditions such as diabetes and obesity[31]. Moreover, over-activation of the mTOR pathway is implicated in the initiation and development of tumours and dysregulation of the pathway in many cancers such as breast and prostate cancer[32]. PTEN mutations are a common cause of these cancers due to loss of negative feedback of PI3K activity. Therefore, a further investigation of PI3K-mTOR signalling, as described in this thesis, is an important study for future therapeutic applications.

1.1.2.3. Ras/ERK pathway and macropinocytosis

Macropinocytosis is a cellular mechanism by which the cell ingestion extracellular liquid and digests molecules. It is defined functionally as the uptake

of fluid droplets that are visible by light microscopy. This endocytic mechanism is a highly conserved process by which extracellular fluid and its content are internalised into cells through large, heterogeneous vesicles known as macropinosomes[33]. Macropinocytosis occurs in different forms in a variety of cell types[34] and it resembles phagocytosis closely except for the fact that the vesicle is not formed around a solid object. Endocytosis, phagocytosis and macropinocytosis are all large-scale actin-dependent uptake homologous processes, by their descent from feeding mechanisms. The distinguished feature of macropinocytosis involves the formation of a hollow ring of actin polymerisation under the plasma membrane. The circular ruffle can form an expanding ring according to the size of the molecule requiring uptake (**Figure 6**). It is known that cancer cells are able to use macropinocytosis to scavenge extracellular proteins, and certain viruses or bacteria use it to invade host cells. Therefore, the usage of macropinocytosis therapeutically to deliver drugs or cause cell death is an important study in progress.

There is evidence that the Ras-PI3K interaction regulates the early events associated with macropinosome formation[35]. Ras activates class I P3Ks through their RBD causes increased generation of local PIP_3 which activates macropinosome formation[36]. Importantly, Ras and PI3K-PIP_3 mediated events are not diffuse through the plasma membrane but is restricted to intense patches that form the core of circular ruffles. Ras activity can control the size and localisation of macropinosomes and might play a direct organisational role in macropinosome formation[37]. However, the roles of oncogenic Ras in tumour cells are strikingly parallel to the Ras in the feeding behaviour. Oncogenic Ras mutations drive proliferation and metabolic adaptations of cancer cells to sustain growth in a harsh tumour microenvironment[33,38]. Cellular uptake of proteins via macropinocytosis is regulated by Ras-p110α interactions and was shown essential for growth and

survival of transformed cells under nutrient limiting, stressful conditions [39]. Therefore, p110α-Ras-binding-domain (p110α-RBD) interaction with Ras may provide transformed cells which a survival and growth advantage under low nutrient settings. Other studies have established that macropinosome formation activates mTORC1 pathway, which regulates cell growth. Amino acid (AA)–dependent signalling from GFRs to mTORC1 requires activation of Rheb and Rag GTPases, which are themselves activated by two signalling pathways: (1) PI3K-dependent activation of AKT leads to phosphorylation and inhibition of TSC1/TSC2, which relieves inhibition of Rheb on endolysosomes; and (2) AAs in endolysosomes are sensed by Ragulator on endolysosomal membranes, which in turn activates Rag GTPases. Active mTORC1 regulates cellular metabolism, stimulating protein synthesis by phosphorylation of S6K and 4EBP1. How AAs reach endolysosomes so quickly in response to GF signalling is not well understood. However, endolysosomes and endocytic trafficking contribute to the activation of mTORC1 by AAs[40].

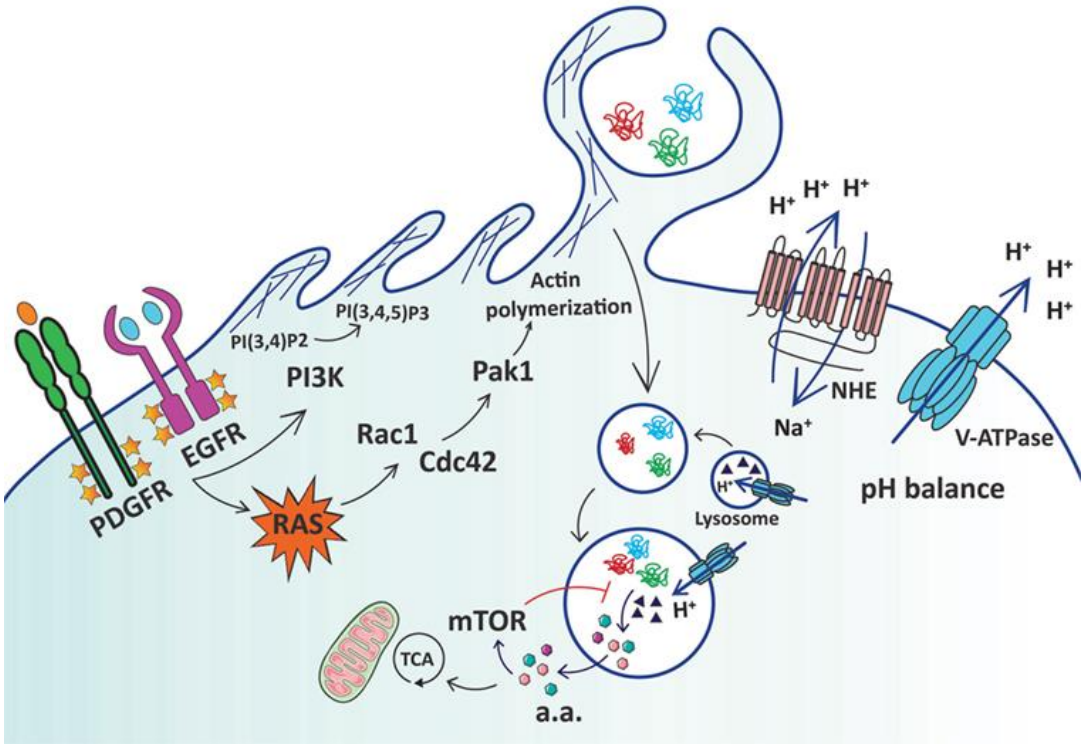

Figure 6: Cartoon deciphering extracellular protein uptake via macropinocytosis. Ras activation, either by GF stimulation or through oncogenic mutation, leads to increased membrane ruffling and macropinocytosis via activation of Rac1 and Cdc42, which in turn stimulate p21-activated kinase 1 (Pak1) to induce actin polymerization. Activation of Rac1 and Cdc42 is sensitive to changes in submembranous pH, and the activity of Na+/H+ exchangers (NHEs) and vacuolar H+-ATPase (V-ATPases) is crucial to maintaining pH homeostasis. Conversion of membrane phosphoinositides by PI3K is also necessary for macropinocytosis. Macropinosomes containing extracellular proteins such as albumin and collagen are internalized and subsequently fuse with lysosomes. Lysosomal proteases (▲) allow the catabolism of extracellular proteins into free amino acids (AA) that can fuel the TCA cycle to promote cell growth and survival. The mTORC1 regulates the utilization of extracellular protein derived AAs by inhibiting macropinocytosed protein catabolism when free AA are abundant. Yellow stars represent phosphorylation of GF receptors. (Illustration from Recouvreux et al., 2017)[35].

1.1.3. Class I PI3K – Mutations and related pathologies

Class I PI3Ks play an important role in controlling biological processes such as cell survival, proliferation, migration and vesicular trafficking and thus regulate immune and metabolic functions, as previously described. Dysregulations in class I PI3K signalling are mostly associated with severe diseases such as cancer, overgrowth and primary immunodeficiency diseases (PID)[27].

1.1.3.1. Cancer

Mutations causing constitutive activation of *PIK3CA* gene are one of the most frequently mutations associated with a wide variety of human cancers including ~30% of CRCs, 27% of glioblastomas, 25% of gastric cancer, 8% of breast cancer, and 4% of lung cancer; as well as other severe developmental disorders [41]. The 80% of cancer-causing mutations on the *PI3KCA* gene were found to be specific to one of the three residues, which become substituted in either the helical or the kinase domain. The two most common "hotspots" are E542K/E545K and H1047R. The helical domain mutant E545K removes the inhibitory interaction, provided by p85 regulatory subunit onto p110α, and requires signalling downstream of oncogenic Ras for activation. The kinase domain mutant H1047R can still bind to the p85 subunit but no longer requires Ras-binding for constitutive activity[42]. Both mutations lead to extensive changes in phosphorylation of the kinase, leading to constitutive activation of downstream pathways (**Figure 7**)[43]. Structural analysis have shown that the mutations alter the shape of the enzyme, mimicking its active conformation, causing constitutive activation of the PI3K pathway. Other less common *PI3KCA* mutations such as N345K or C420R disrupt the interface of the C2 domain with iSH2. Tumour-associated mutations in other class I PI3K genes are very rare but frequently occur in brain and endometrial cancers.

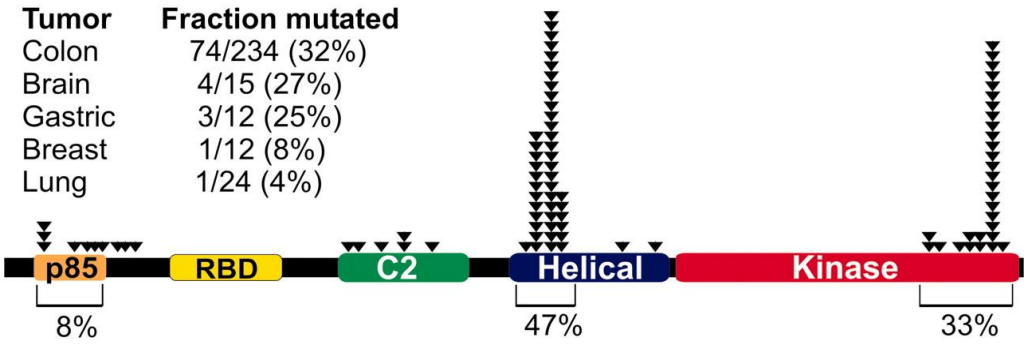

Figure 7: Scheme showing mutations in *PIK3CA* gene associated with cancer. Cancer mutations showing *PIK3CA* mutations encoding p110α PI3K isoform[18]. Arrowheads indicate the location of missense mutations, and boxes represent functional domains (the p85 binding domain (p85), Ras binding domain (RBD), C2 domain, helical domain, and kinase domain)[41]. (Illustration from Samuels et al., 2004).

Although, PTEN-deficient cancers show increased p110α signalling[44], the p110β isoform has also been implicated in the development of PTEN-null prostate cancer[45]. The role of p110β in cancer has been shown to be due to its continuous production of high basal levels of PIP_3, which is sensitive to the diminished PTEN[45]. The p110β mutations, characterised in the helical domain, upregulate the kinase activity of p110β, independent of RTK and Gβγ activation[2], indicating that the mutations induce a conformational change leading to constitutive signalling. Mutants of p110γ and the p101 regulatory subunit have been found to play a role in the development of tumours, studies on mice epithelial cancer cells demonstrated that the depletion of these two proteins inhibits metastasis and tumour development[46,47]. The inhibition of this isoform was also found to suppress growth and inflammation of implanted tumours in mice models. The overexpression of the p101 regulatory subunit in T cells results in hyperactivity of p110γ and protects cells from apoptosis[48].

1.1.3.2. Tissue overgrowth

Some cancer-associated *PI3KCA* mutations, were also reported to occur during development and result in mosaic tissue overgrowth syndromes, venous malformations, and brain malformations associated with epilepsy[49]. Activating mutations in *PIK3CA* have also been linked to noncancerous disease conditions such as spectrum of regional overgrowth syndromes including: congenital lipomatous overgrowth, vascular malformations, and epidermal nevi (CLOVE) syndrome; mosaic overgrowth with fibroadipose hyperplasia (**Figure 8**)[50]; and/or PIK3CA-related overgrowth syndromes (PROS). These *PIK3CA* mutations caused due to activating mutations mainly in the kinase or helical domain of p110α, are present at birth and occur in a mosaic pattern in contrast with the somatic *PI3KCA* mutation associated with cancer[51,52]. CLOVE syndrome is characterised by regional tissue overgrowths and malformations affecting the epidermis, internal organs, skeleton, and central nervous system. PROS is caused by mosaic gain-of-function mutations in the *PIK3CA* gene, which are associated with potentially life-threatening clinical features including excessive tissue growth, blood vessel malformations and scoliosis. Syndromes collectively termed PTEN hamartoma tumour syndrome (PHTS), consist of a heritable germline loss-of-function mutation in *PTEN* which results in a cluster of tissue overgrowth syndromes[53]. The most representative member of PHTS is Cowden's syndrome (CS), a multi-organ system disorder characterised by anomalous tissue overgrowths. CS confers a considerably more significant risk of cancer development.

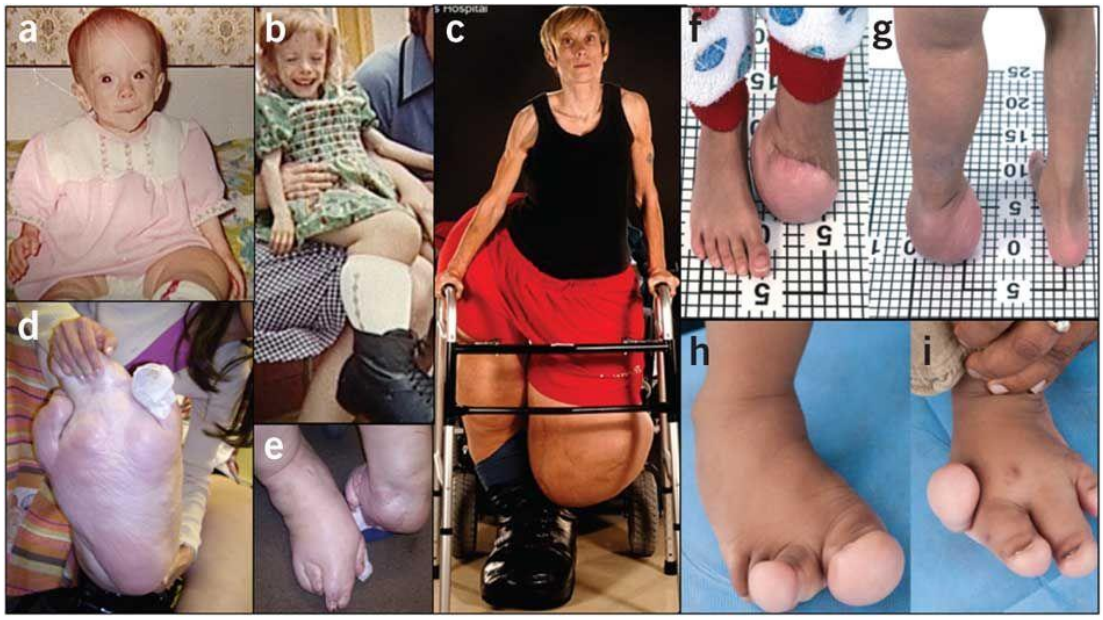

Figure 8: Mosaic overgrowth with fibroadipose hyperplasia. (A- I) Images of patients with other pathologies of activating mutations in *PIK3CA* gene such as mosaic overgrowth with fibroadipose hyperaplasia[50]. (Illustration from Lindhurst et al., 2012).

1.1.3.3. Immune deficiency

Other syndromes have been recently shown to be associated with mutations in the *PIK3CD* gene encoding the p110δ isoform, including activated PI3K-delta syndrome (APDS) or p110δ-activating mutation causing senescent T cell, lymphadenopathy, and immunodeficiency (PASLI)[54]. APDS is a PID, caused by gain-of-function mutations in the *PIK3CD* gene, caused by the E1021K variant in the C-lobe of the p110δ kinase domain is by far the most frequently reported APDS, mainly in a heterozygous state (**Figure 9**). Patients with this condition often have increased PIP_3 levels and display abnormally increased T and B cell proliferation[55,56]. The immunodeficiency is suggested to result due to recurrent bacterial and/or fungal infections particularly by *Streptococcus pneumonia* and/or Aspergillus in the respiratory track. Furthermore, the APDS patients show hyper-

susceptibility to Epstein-Bar virus and Herpes virus infections[57], potentially due to defects in patients antigen presenting cells such as dendritic cells (DCs) (Zarafov A. et *al*. personal communications). Interestingly, inactivating mutations in the *PIK3CD* gene that result in the deletion and absence of full-length protein expression were recently cause of PID, marked by enterocolitis in patients[58,59].

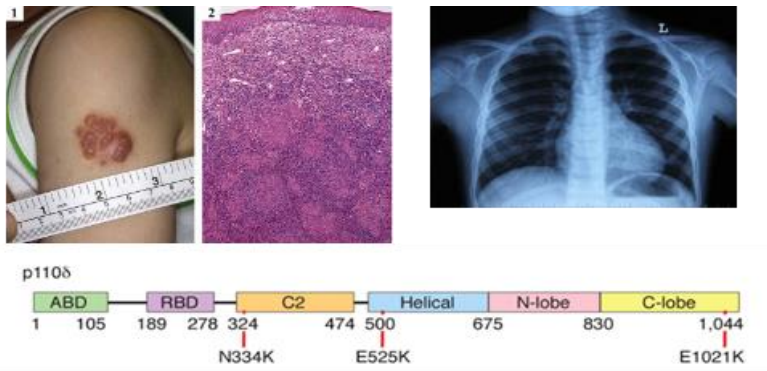

Figure 9: Activated PI3K delta syndrome (APDS). APDS is an autosomal dominant monogenic disorder caused by activating mutations in the gene encoding p110δ PI3K isoform. The symptoms of APDS are consistent with immunodeficiencies, lymphadenopathy, sinopulmonary infections, and bronchiectasis. (Adapted from Aksoy E et al., unpublished).

1.1.4. Class I PI3K – Pharmacological targets

Class I PI3Ks are important therapeutic drug targets in cancer, inflammation and monogenic diseases associated with increased activity of these kinases in related pathologies. For this reason, many pharmaceutical companies have largely invested developing inhibitors targeting isoform-selective PI3K. Several isoform-selective PI3K inhibitors are currently being used in clinical trials, some of which are approved for treatment by the Food and Drug Administration (FDA). PI3K selective enzymes are most generally small molecule inhibitors that

target and occupy the ATP-binding pocket of the selected PI3K isoform with up to 10-100-fold selectivity over the non-targeted isoforms. Initial clinical trials of these inhibitors showed partial effectiveness due to dose-limiting side-effects as well as the development of drug resistance in which alternative cell survival pathways were activated. Combinational-therapies with these inhibitors were then developed to solve these issues by acting on multiple pathways to prevent the development of resistance. PI3K selective inhibitors are effective treatments in treating pathologies related to naturally occurring activating p110α or p110δ PI3K mutations such as overgrowth syndromes and APDS, respectively.

Rapalogs were the he most established mTOR inhibitors (rapamycin and its analogs), and the first PI3K-pathway inhibitors which acted on the downstream target mTOR and demonstrated anti-tumour activity in few neoplasms such as renal cell carcinoma[60]. These were then used to develop agents targeting the PI3K, AKT and mTOR (PAM) inhibitors[61]. The development of PAM inhibitors has progressed in the past decade, indicated by the rise in the number of clinical trials evaluating many agents targeting PI3K, AKT and mTOR. Initially, Rapalogs showed limited clinical efficacy in treatment due to the emergence of resistance mechanisms, which decreased the activity of the drugs. However, they have shown effectiveness in combinational therapies in the treatment of breast cancer[62] that led to the development of second-generation PAM inhibitors[61]. Buparlisib (a pan-PI3K inhibitor capable of blocking all class I PI3Ks), and alpelisib (a p110α selective-isoform inhibitor), are currently being used in metastatic breast cancer patients. Although, a drug with a broader spectrum of targets is usually associated with higher clinical toxicity, a better understanding of buparlisib and alpelisib awaits the results from current clinical trials[63]. Idelalisib, an orally available p110δ-selective inhibitor, was the first selective PI3K inhibitor approved by FDA and showed antitumor activity in patients with leukemia. However, a high percentage

of patients developed severe adverse events and colitis-associated syndrome[64]. There are currently several types of PAM inhibitors under development (**Table 1**).

PAM Inhibitor	Description/example(s)
AKT inhibitors	Target downstream PI3K target AKT isoforms of which there are allosteric inhibitors and also catalytic inhibitors. Example: MK-2206 (allosteric) and GDC-0068 (catalytic)
Dual pan-class I-mTOR inhibitors	These target the catalytic domain of mTOR as well as the p110 subunit of PI3K as they are structurally similar. Example: GSK1059615
Irreversible pan-PI3K inhibitor	Targets all four class I isoforms, however, irreversibly binds to the ATP binding site of the enzymes. Example: PX-866 and wortmannin, which can irreversibly inhibit all PI3K classes.
Isoform-specific inhibitors	Target specific class I PI3K isoforms. Examples: CAL-101 (p110δ) and INK1117 (p110α)
mTOR inhibitors	Target the catalytic domain of mTOR. Example: INK128
Reversible ATP competitive /PI3K pan-inhibitors	Target all four class I PI3K isoforms. Example: GDC-0941 (Pictilisib)

Table 1: PAM inhibitors under development. (Adapted from LoRusso et al., 2016)[65]

Generally, the safety profile of PI3K inhibitors, with the exception of p110δ, have been tolerable, with no reported adverse and toxic effects. Side effects previously reported have been mild to moderate, and can be managed with medication[61]. However, several issues due to dose-limiting were reported with the usage of multiple PAM inhibitors, which included hyperglycaemia, gastrointestinal intolerance (nausea, vomiting, etc) and maculopapular rash[66]. Although these PAM inhibitors have displayed some degree of clinical efficacy from clinical trials, there have been a number of unresolved questions identified. These include pharmacological issues such as optimal extent and duration of inhibition for anti-tumour effects. Moreover, there has been patient selection

issues due to variations in different types of mutations in cancers, which affects the sensitivity to inhibitors[61]. In summary, there remains yet-to-be addressed questions regarding the biology of isoform selective roles of PI3Ks such as the role of the different isoforms in different types of tissue and in tumours. All of these questions are yet to be addressed and will need to be answered in ongoing and future studies. In this study, established p110α isoform-selective inhibitor (A66), p110β isoform-selective inhibitor (TGX-221), p110δ isoform-selective inhibitor (IC87114), and a pan-class I PI3K inhibitor (GDC-0941) were used *in vitro* in order to study isoform-selective role of class IA PI3Ks in innate immune receptor specific signalling pathways with links to nutrient sensing.

1.1.5. Mouse models to investigate isoform-selective roles of PI3K/mTOR pathway

To uncover the involvement of each PI3K isoform in the immune system and cancer development, genetically modified mouse models lacking and/or expressing mutant forms of class I PI3K isoforms, have been developed and studied in the last two decades. PI3Ks in transgenic mice have been approached and targeted on different sides such as: mutations at the regulatory subunits (i.e. p85), defects in PI3Ks upstream regulators (i.e. CD19 or CD28), and catalytic subunits (p110). Mice deficient in PI3Ks regulatory subunits were studied and concluded not to be the best model due to their non-selective interaction with class IA catalytic PI3K-isoforms and their mutlifunctionality and effect beyond those on p110 lipid kinase signalling[67–69]. Mice with loss or inhibition of p110γ or p110δ kinase functions are viable and healthy but they show significant defects in their innate and adaptive immune compartments[70]. Inhibition of p110γ results in major defects in cell motility in almost all immune cell types[71], as well as specific defects

in inflammatory and immune cell development and activation[27,46,72–75]. Catalytic inactivation of p110δ show impaired B and T cell antigen receptor signalling[14,76] and immunodeficiency in the presence of pathobionts in mice[77]. Genetic studies targeting PI3K isoforms have shown that incomplete deletion of p110α or p110β can cause deregulation of a number of signalling pathways[16]. Mice deficient in p110β isoform are partially viable but show small size and are infertile[45,78]. On the contrary, inhibition of p110α is lethal during embryogenesis between E9.5 and E10.5 due to delayed development and inability to proliferate, whereas heterozygotes were normal in appearance[79].

A constitutive p110δ$^{D910A/D910A}$ kinase inactive (also called p110δ KI) mouse model was used and studied in our laboratory in parallel to this project (González M. *et al.,* unpublished data). This constitutive KI mouse model was generated by introduction of a germline point mutation at the ATP-binding site of the p110δ KI catalytic subunit, on the C-terminus[80]. The KI mutations render p110 kinase dead albeit normal levels of the protein (**Figure 10**). The p110 KI model has been showed to be a more reliable and accurate model to use rather than the p110 KO model in which the gene encoding p110δ is deleted. This is because in the p110 KI mice model, p110 protein is still expressed while in the KO model it is not, therefore the space and role (even non-functional) that p110 occupies in the cell will not be substitute and/or compensated by other PI3Ks isoforms in the long term along with no deregulations in the regulatory p85 protein levels[16].

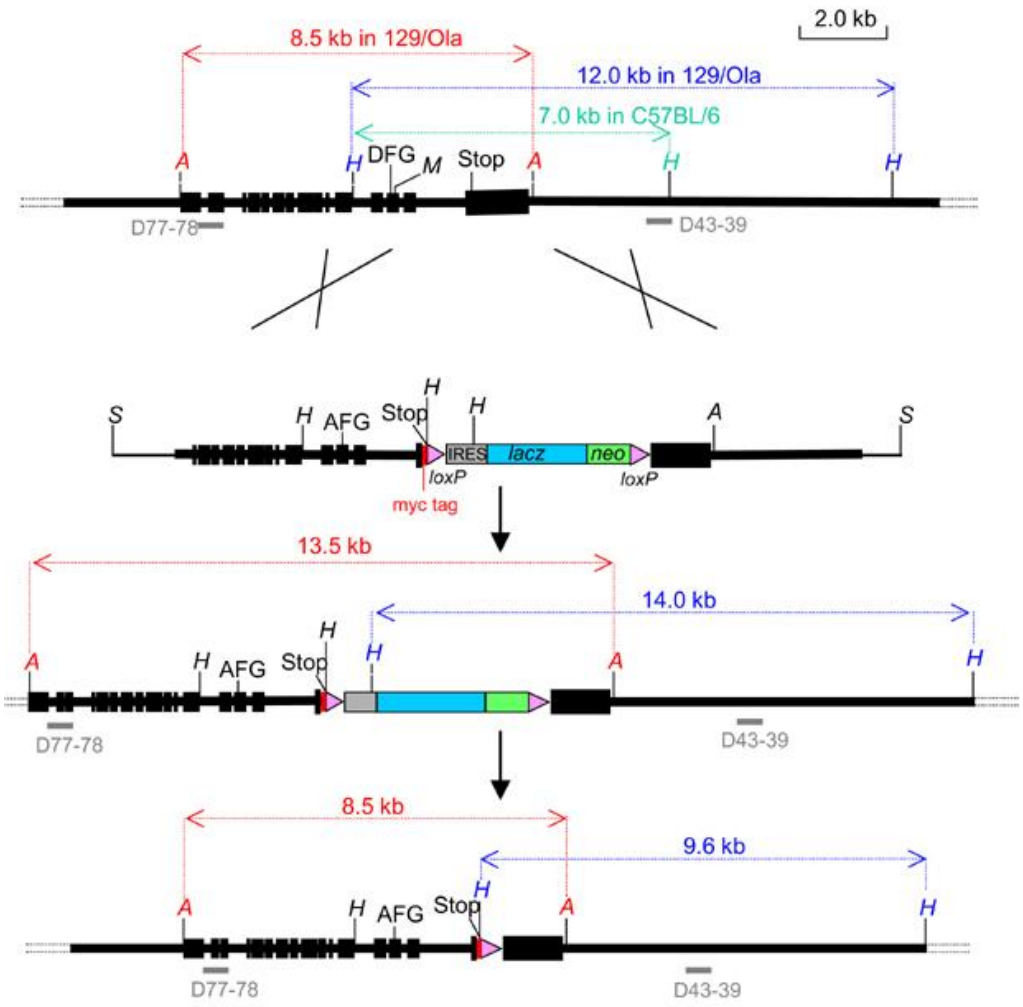

Figure 10: Gene targeting for p110δ$^{D910A/D910A}$ also named p110δ KI. Two genomic clones covering the coding region of the p110δ, *PIK3CD*, were isolated. The *PIK3CD* gene is encoded by 22 coding exons, a knock-in vector containing the last 4 exons of the *PIK3CD* locus was constructed and designed to introduce a point mutation, converting the conserved DFG motif in the C-terminal p110δ kinase domain to AFG. Two additional features were incorporated into the targeting vector: a sequence encoding a Myc-epitope tag introduced immediately 5' of the stop codon, and a reporter/selection cassette flanked by loxP sites inserted into the 3' UTR sequence. This cassette contained an IRES sequence followed by β-galactosidase (lacZ) coding sequence and a neomycin resistance gene expressed from its own promoter (MC1neopA). Note also that a vector-derived HindIII site was introduced just 5' of the cassette insertion site[81].

In order to understand and target a p110δ in gut immunity and inflammation, we investigated the role of p110δ in tissue specific cell subtypes.

Since p110δ is mainly expressed in leukocytes, conditional p110δ$^{flox/flox}$ mouse models were developed in order to deplete p110δ specifically in innate immune cells (**Figure 11**). Conditional deletion of p110δ in T cells, using CD19-Cre, CD4-Cre, or Ox40-Cre mouse strains results in reduction of T cell numbers in spleen and inhibition of T follicular helper (T_{FH}) formation[82]. In our laboratory, we have generated a myeloid/neutrophil specific LysM-Cre (Lyz2) mouse crossed onto p110δ$^{flox/flox}$ transgenic mice (p110δ$^{\Delta Lyz2}$) to study the role of p110δ in cells of myeloid origin (monocytes, macrophages and neutrophil). Moreover, we have generated a DC-specific CD11c-Cre mice by crossing them onto p110δ$^{flox/flox}$ transgenic mice (p110δ$^{\Delta CD11c}$) to study the role of p110δ selectively in DCs. CD11c-Cre mice are a Cre-lox tool for deletion of floxed sequences (p110δ in this study) in CD8^{-} and CD8^{+} DCs, tissue-derived DCs from lymph nodes, lung and epidermis, as well as plasmacytoid DCs. In order to study the role of p110δ in the intestinal epithelium, Villin-Cre mice from Jackson Laboratory were also used in this study and crossed with transgenic p110δ$^{flox/flox}$ mice to deplete p110δ in the intestinal epithelial cells (IECs) to obtain a transgenic mouse named here as p110δ$^{\Delta IEC}$ mouse.

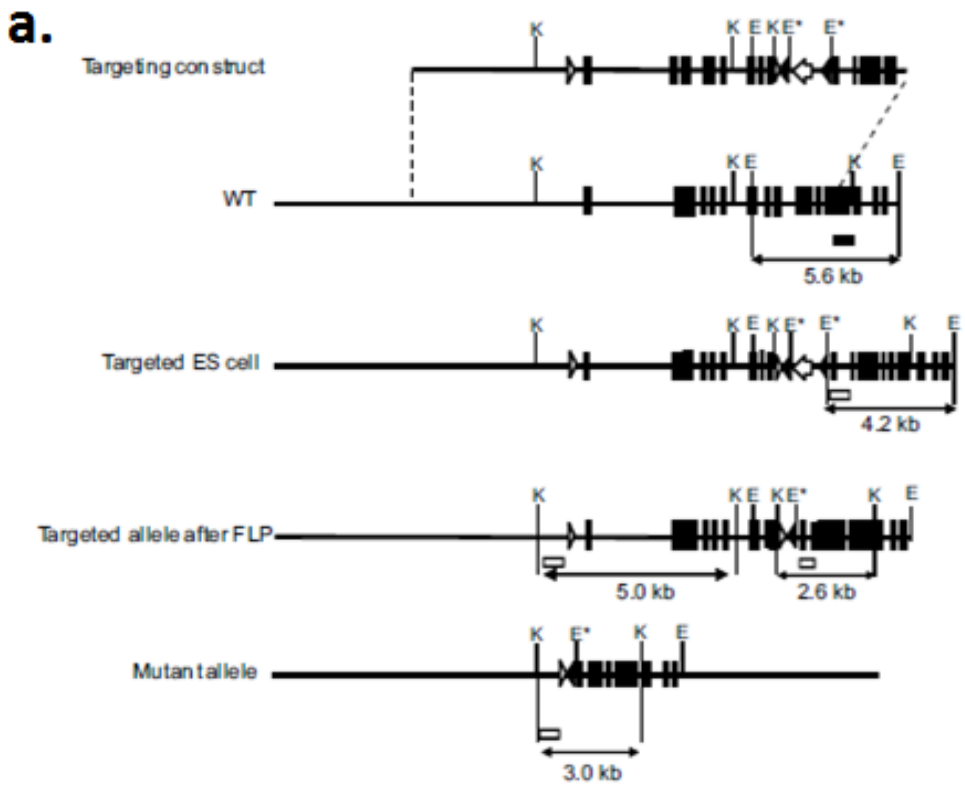
a.
Targeting construct
WT
5.6 kb
Targeted ES cell
4.2 kb
Targeted allele after FLP
5.0 kb
2.6 kb
Mutant allele
3.0 kb
b.
Exon 2
Exon 18
c.
B p110δ fl/fl
p110δ fl/fl
δ-/-
p110δ
β-actin
δ-/-
T p110δ fl/fl
p110δ fl/fl
p110δ
β-actin

Figure 11: Scheme showing gene-targeting strategy to generate conditionally targeted p110δ$^{flox/flox}$ mice. (A) A single LoxP site was introduced into the XhoI site upstream of the first coding exon. A neomycin cassette flanked by FRT sites and a single LoxP site (FRTneoFRT) was inserted into the EcoRV site between exons 9 and 10. **(B)** Strategy for assessing genomic deletion by quantification of exon 2 and exon 18 of PIK3CD. **(C)** Genomic DNA deletion efficiency of Cre determined by RT-PCR and western blotting in both B and T cell populations[82].

As previously mentioned, inhibition of p110α is lethal during embryogenesis[79]. In order to circumvent this issue, conditional mouse models for p110α inhibition are required to delineate its function, particularly in mice after birth. Therefore, a conditional mouse with an inactivating mutation in the Ras-binding domain (RBD, (i.e. GTPase interaction domain)) of the *PI3KCA* gene (p110α^{RBD}) was utilised to carry out this study[25]. This conditional mouse model was generated by introduction of two-point mutations (T208D and K227A) in the RBD of p110α, rendering p110α interaction with Ras GTPase and thus RBD-dependent lipid kinase activity null, without altering the overall kinase activity of the enzyme. Due to the lethality of homozygous p110α^{RBD} mice (similarly observed in p110α KI and p110α KO mice), heterozygous RBD were crossed onto p110α/loxP allele (p110α$^{RBD/flox}$). These mice expressed a constitutive mutation in the RBD of p110α, in a heterozygous manner, rendering p110α unable to interact with any GTPases, including Ras, and hence unable to generate PIP_3 via GTPase interactions. The second p110α was floxed, in a heterozygous manner, which allowed us to conditionally and temporarily delete it in adult mice, bypassing embryonic lethality. The p110α$^{RBD+/-}$/p110α-flox$^{+/-}$ (referred as p110α$^{RBD/flox}$) mice were then crossed with Rosa26-CreER (p110α$^{RBD/flox}$/Rosa26$^{CreER/+}$) and tamoxifen was used to enable the recombination of CreER allele in this conditional gene targeting mice such as p110α$^{RBD/flox}$/Rosa26$^{CreER/+}$. This Cre/lox system consists of an inducible Cre fused to a mutated hormone-binding domain of the estrogen receptor (ER), so-called CreER recombinases. The CreER recombinase is inactive

but can be activated by the synthetic estrogen receptor ligand 4-hydroxytamoxifen (4-OHT), allowing for external, temporal control of the Cre activity. Tamoxifen is a selective estrogen response modifier (SERM) and anti-angiogenic factor that is metabolized to active metabolites 4-OHT and is currently used as a therapy for breast cancer. These p110α$^{RBD/flox}$ mice after tamoxifen treatment, showed to have removed the p110α floxed allele ubiquitously leaving one copy of p110α^{RBD} expressed in these mice (p110α$^{RBD/-}$)[25] (**Figure 12**). These mice were compared with p110α$^{WT/flox}$/Rosa26$^{CreER/+}$ (p110α$^{WT/flox}$) mice, leaving one copy of p110α^{WT} expressed after tamoxifen (p110α$^{WT/-}$). An inbreed wild type (WT) colony of C57BL/6 (named here as p110α$^{WT/WT}$ after tamoxifen treatment), was used as a control in order to compare all groups.

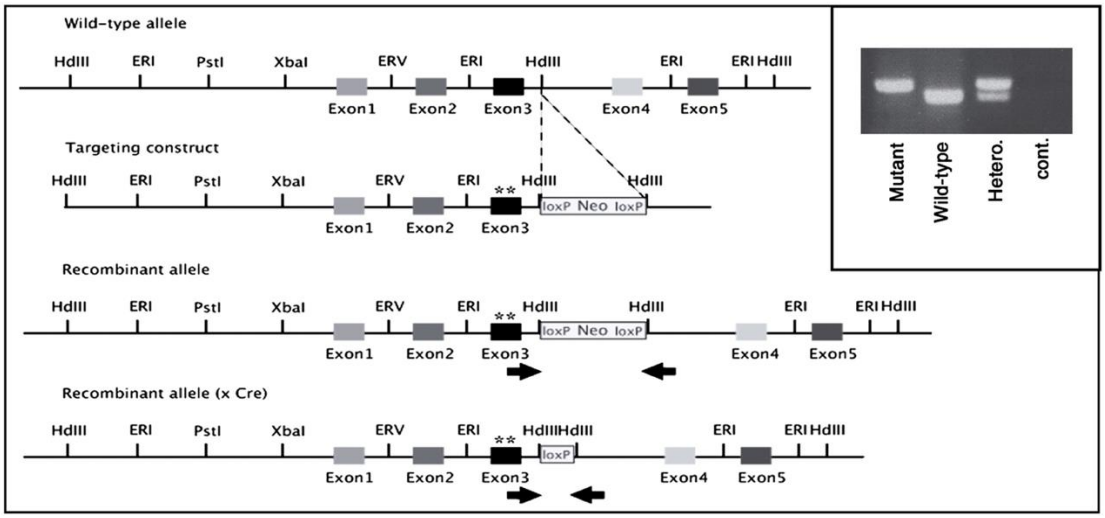

Figure 12: Gene targeting used to generate p110α$^{RBD/flox}$ mice generation. Scheme showing point mutations T208D and K227A into exon 3, RBD of *PI3KCA* gene. Arrows indicate the location of genotyping primers. Inset: genotyping PCR of samples after Cre-mediated excision of the neomycin selection cassette. The upper band represents the mutant allele (containing a residual 30 base pairs of the loxP site). The lower band represents the wild-type allele[25].

Finally, the role of mTORC1 target Rheb GTPase in nutrient sensing and innate immune receptor signalling pathways, was investigated using homozygous $Rheb^{flox/flox}$ transgenic mouse in this project. As previously discussed, Rheb couples GF signalling to activation of mTORC1. Recent studies showed that inactivation of the Rheb gene in mice leads to embryonic lethality during mid-gestation, with the viability of the homozygous mutants declining sharply around E12.5, likely due to circulatory failure[83–85]. Therefore, in order to determine the specific role of the Rheb/mTORC1 pathway in gut immunity and inflammation, conditionally targeted Rheb transgenic mouse in the IECs population were considered for this study. Transgenic Villin-Cre mice, directing expression of Cre recombinase to villus and crypt epithelial cells of the small and large intestine, were crossed with $Rheb^{flox/flox}$ transgenic mice (named here as $Rheb^{\Delta IEC}$ mouse), to deplete Rheb/mTORC1 activity in the intestinal epithelium (villin 1 promoter). A summary of all mouse models to investigate isoform-selective roles of PI3K already studied are described in **Table 2**. All mouse models and groups used in this study are discussed in detail in the **Materials and Methods** section.

Targeted subunit	Viability	Metabolic phenotype	Immunological phenotypes	Alterations in PI3K subunit	Ser473 AKT	Lipid kinase activity
p85α +p55α +p50α Homozygous[86–89]	Perinatal lethality	Hypoglycaemia Hypoinsulina	**B cells:** ↓number of peripheral mature cells; ↓proliferation induced by anti-IgM, anti-CD40 or LPS; ↓survival upon IL4-stimulation B1 cells: absent **T-cell** development and proliferation not affected **Mast cells:** ↓SCF- or IL3-induced proliferation, FcεRI-induced degranulation not affected	↑p85β, ↓p110α, ↓p110β and ↓p110δ	**Liver and skeletal muscle:** not affected upon intravenous insulin **MEFs:** ↓upon insulin and ↓upon IGF-1ES cells: ↓upon IGF-1 (Thr308 AKT also ↓)	**Liver and skeletal muscle:** ↓pY-associated activity upon intravenous insulin Adipocytes: ↓upon insulin **MEFs:** ↓ PIP_3 levels in vivo upon IGF-1 stimulation (compared with WT) in early phase and ↑ at later time points, ↓pY-associated activity upon IGF-1 stimulation

p85α +p55α +p50α Heterozygous[88,90]	Viable	↑Glucose tolerance ↑Insulin sensitivity		↑p85β; p110α and p110β not affected	**Liver and skeletal muscle:** ↑upon intravenous insulin **MEFs:** ↑upon IGF-1	**Liver and skeletal muscle**:↑pY-associated activity upon intravenous insulin **MEFs:** ↑ PIP_3 levels in vivo upon IGF-1 stimulation and pY-associated activity upon IGF-1 stimulation not affected
p85α-only[91,92]	Viable	↑Insulin sensitivity	**B cells:** ↓numbers of B1 and mature B cells; ↓proliferation in response to anti-IgM, anti-CD40 or LPS; ↓T-cell-independent antibody production **T cells:** altered Th1–Th2 balance in vivo: immune response becomes Th1-skewed, ↑in vitro Th1 cytokine production by popliteal lymph node cells upon Leishmania major infection; ↓in vitro Th2	↑ p55α and ↑p50α in muscle and fat cells; p110α and p110β not affected	Adipocytes: not reported	**Adipocytes:** ↑PIP_3 levels *in vivo* upon insulin stimulation **Skeletal muscle and adipocytes:** ↓pY-associated activity upon insulin stimulation **Skeletal muscle:** ↑IRS2-associated activity and ↓pY- and IRS1-associated activity upon insulin stimulation

		cytokine production by mesenteric lymph node cells upon helminth infection **Mast cells:** moderately reduced numbers of tissue mast cells; gastrointestinal mast cells absent; ↓c-kit-induced proliferation; IL3-induced proliferation not affected; ↓in vivo acute bacterial clearance; ↓sensitivity to infection by intestinal nematode Strongyloides venezuelensis **DC:** ↑IL12 production; ↓ sensitivity to Leishmania major infection **Platelets:** ↓aggregation by collagen and collagen-related peptide; aggregation by ADP, thrombin, thromboxane A2 analogue or phorbol myristate acetate unaltered			
p55 +p50[93]	Viable	↑Insulin sensitivity		In muscle, ↓p85α; not affected in adipocyte and	**Skeletal muscle**: ↑upon insulin stimulation (vena cava injection)	

				liver; p110α, p110β not tested	Isolated adipocytes: not affected upon insulin stimulation	
p85β[94]	Viable	↑Insulin sensitivity; hypoglycaemia; hypoinsulinaemia	**B cells:** not affected **T cells:** ↑proliferation and survival in response to anti-CD3 **Mast cells**: not affected	p85α, p55α, p50α, p110α and p110β not affected	Skeletal muscle: ↑upon insulin stimulation Liver: not affected upon insulin stimulation	**Skeletal muscle:** ↑IRS2-associated activity
p55γ and p101	Not reported					
p110α KO[95]	Embryonic lethal (E.10.5)			p85 embryo↑	Not assessed	Not assessed
p110β KO	Embryonic lethal (E3.5)			Not assessed	Not assessed	Not assessed
p110β KI	Viable					
p110δ KO[14,96]	Viable	Not reported	**B cells:** ↓numbers of mature B cells; B1 and M1 cells absent; ↓proliferation upon anti-IgM or anti-CD40; ↓T-cell-dependent and T-cell-independent antibody production **Neutrophils:** ↓chemotaxis	**B cells:** weak ↓p85α, weak ↓p55α and weak ↓p50α	**B cells:** ↓upon anti-IgM Neutrophils: not reported	**B cells:** ↓ PIP_3 levels in vivo (in response to antigen-receptor stimulation). Neutrophils: ↓ PIP_3 levels in vivo (in response to GPCR stimulation)

p110δ KI[76,77,97]	Viable	Not reported	**B cells:** ↓numbers of mature B cells; B1 and M1 cells absent; ↓proliferation upon anti-IgM or anti-CD40; ↓T-cell-dependent and T-cell-independent antibody production **T cells:** ↓proliferation to anti-CD3 or peptide presented by APC **Mast cells:** ↓numbers of mast cell in some tissues; ↓proliferation in response to SCF or IL3; ↓degranulation and cytokine production downstream of FcεRI; ↓in vivo allergic response	**B cells, T cells and mast cells:** no alteration in class IA PI3K subunit expression	**B cells:** ↓upon anti-IgM **T cells:** ↓upon anti-CD3Mast cells: ↓upon SCF, ↓upon IL3 and ↓upon IgE-antigen (FcεRI)	**B and T cells:** ↓YxxM phosphopeptide- or p110δ- or pan-p85-associated in vitro activity **Mast cells:** ↓YxxM phosphopeptide- or p110δ- associated activity (unstimulated); ↓ PIP_3 levels in total lysates (in response to SCF)
p110γ KO[71,98]	Viable	↓Glucose-stimulated insulin secretion; ↑pancreatic β-cell mass; ↑intraperitoneal insulin tolerance	**B cells:** not affected. **T cells:** ↑ CD4+:CD8+ thymocyte ratio; ↓thymocyte apoptosis; ↓proliferation of mature T cells in response to anti-CD3Mast cells: tissue distribution and differentiation not affected; ↓degranulation downstream of FcεRI; in vivo	**Neutrophils, macrophages, lymphocytes and monocytes:** no alteration in class IA PI3K subunit expression	**Macrophages, mast cells and neutrophils:** ↓upon various GPCR ligands	**Neutrophils, macrophages and mast cells:** ↓ PIP_3 levels in vivo (in response to GPCR stimulation)

			resistance to (IgE-Ag) allergic challenge **DCs:** ↓in vivo and ex vivo migration; ↓contact- and delayed-type hypersensitivity response **Neutrophils:** ↑ numbers; ↓oxidative burst; ↓in vitro chemokine-induced chemotaxis; ↓ in vivo recruitment (septic peritonitis) **Macrophages:** ↓ in vitro chemokine-induced chemotaxis; ↓ in vitro VEGF-induced migration; ↓ in vivo recruitment (septic peritonitis)			
p110γ KI	Viable	Not reported	**Neutrophils and macrophages:** ↓ in vivo chemotaxis	**Macrophages:** no alteration in p110γ or p110β expression	**Macrophages:** ↓ upon CCL5 and C5a	Not reported

Table 2: The metabolic and immunological phenotypes from mice with targeted PI3K subunits. (Adapted from Vanhaesebroeck et al., 2005)[16].

1.2. Stem cell biology

Stem cells are unspecialised cells, capable of indefinitely give rise to more cells of the same type (self-renew) and can differentiate into mature cells with specialised functions. In humans, stem cells have been identified in the inner cell mass of the early embryo. From totipotency (the ability of a zygote to give rise to all the lineages of the embryo and extra-embryonic tissues), and ability of embryonic stem cells (ESC) to generate all lineages of the embryo (pluripotency), differs from the ability of adult stem cells to reconstitute multiple (multipotency), a few selective (oligopotency) or a single lineage (unipotency) of a tissue (**Figure 13**). Stem cells govern tissue homeostasis as well as wound repair although in mature tissues, self-renewing of stem cells becomes more restricted. They reside in niches, which are local tissue microenvironments that maintain and regulate stem cells and their future fates. Their main functions are: maintenance of a steady-state tissue known as homeostasis, a rapid regenerative response, and restoration of tissue integrity when wounded[99,100]. Stem cells have the ability to divide asymmetrically to produce one stem cell and one non-stem daughter cell or differentiated cell. Stem cells are also capable of dividing symmetrically to produce more of the same type of stem cell. Due to this stemness, stem cells are capable to undergo long-term self-renewal and multilineage differentiation via regeneration of differentiated cells loss or re-population of the stem cell niche. Stem cells regenerative capacity varies across different tissues. Recent studies have shown that symmetric stem cell divisions play an important role in adult mammalian homeostasis[101–103]. Adult stem cells are undifferentiated cells that occur in a differentiated tissue, such as bone marrow, intestinal epithelium, skin, or the brain in the adult body. Cell plasticity in the intestine refers to differentiated intestinal cells ability to de-differentiate and adopt an alternate cell fate in response to perturbation such as adult stem cells[104].

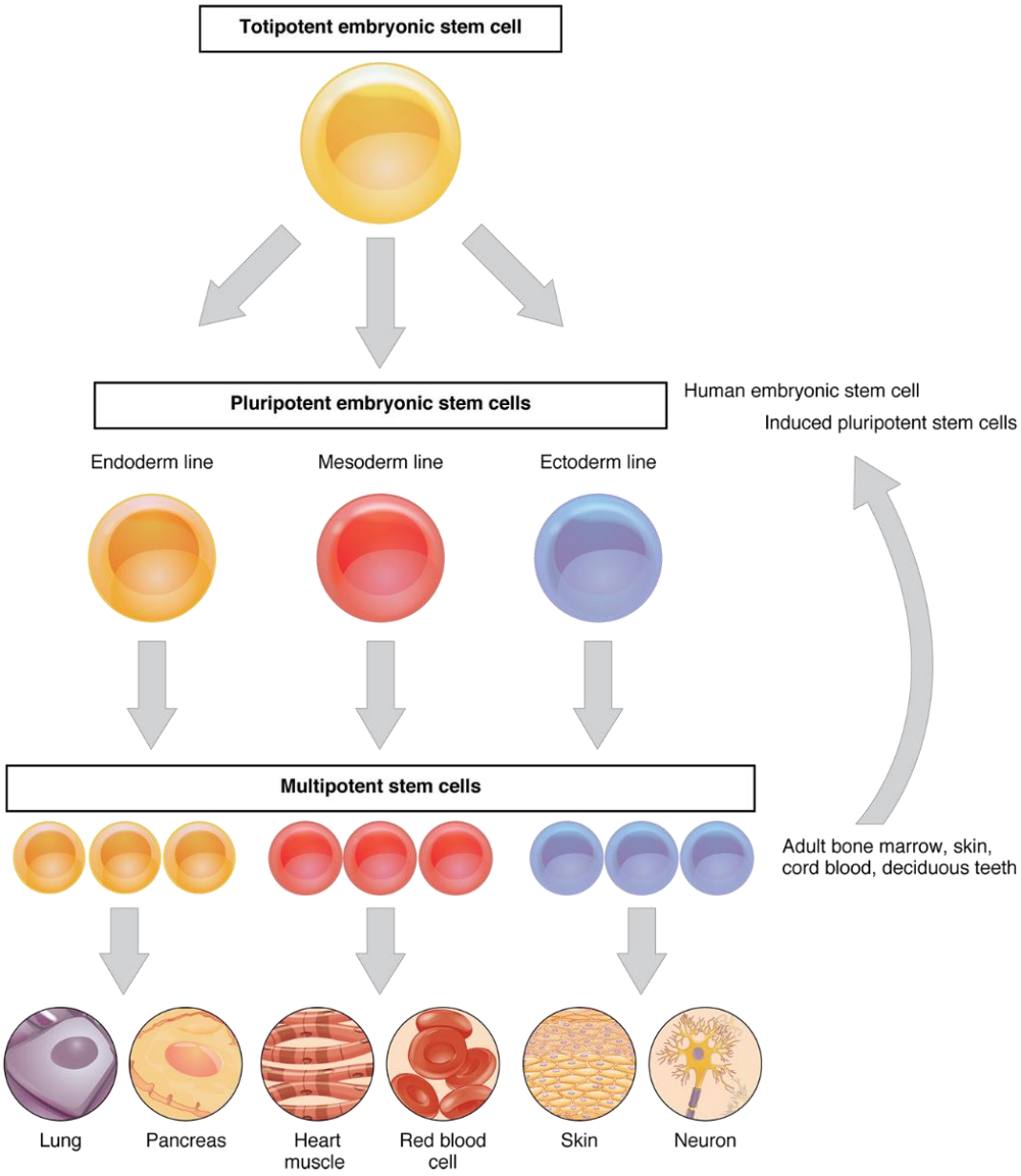

Figure 13: The schematic illustration depicts embryonic stem cell development in humans. From totipotent to pluripotent stem cells, the embryonic stem cells (endoderm, mesoderm, and ectoderm lines) differentiate into multipotent stem cells and then into specific tissues. (Illustration from Bindu et al., 2011).

1.2.1. PI3K signalling regulate stem cell fate

PI3K signalling has been shown to be important for controlling self-renewal of hematopoietic and embryonic stem cells[105]. Important pathways that control stem cell self-renewal and have important roles in embryonic development and differentiation include; Notch, Hedghog (HH), and wingless-related MMTV integration site 1 (Wnt). Notch signalling via transmembrane ligands and receptors is primarily involved in the communication between neighbouring cells. The Notch signalling pathway is complex and multifaceted, it comprises five canonical Notch ligands (Delta-like ligand 1 (DLL1), DLL3 and DLL4, and Jagged1 and Jagged2) and four Notch receptor paralogues (Notch1–4). Studies in *Drosophila* showed that Notch1 regulates the expression of PTEN and the activity of PI3K/AKT signalling pathway in normal and leukemic T cells [106]. Crosstalk with the Wnt and/or HH pathways might also determine the overall effect of Notch signalling (**Figure 14**). The HH signalling pathway is implicated in tissue patterning during embryonic development and the repair of normal tissues, and epithelial-to-mesenchymal transition. The signalling cascade initiated by smoothened (SMO) leads to activation and nuclear localization of GLI transcription factors, which drive expression of HH target genes; most of the target genes are involved in proliferation, survival, and angiogenesis. Recent studies showed that SMO expression was inversely associated with phosphorylated AKT expression in colorectal cancer, suggesting that SMO activation may tend to be mutually exclusive with AKT activation in colorectal cancer development[107]. The PI3K pathway regulates β-catenin, a crucial transcriptional factor in Wnt signalling, which is essential for the maintenance of somatic stem cells and committed progenitor cell compartments. Simultaneous hyperactivation of the Wnt–β-catenin pathway and inhibition of PI3K-AKT signalling at the plasma membrane promote nuclear accumulation of β-catenin, promoting cell metastasis by regulating a defined set of target genes[108,109]. The pathway is also involved in tissue regenerative processes following injury[110].

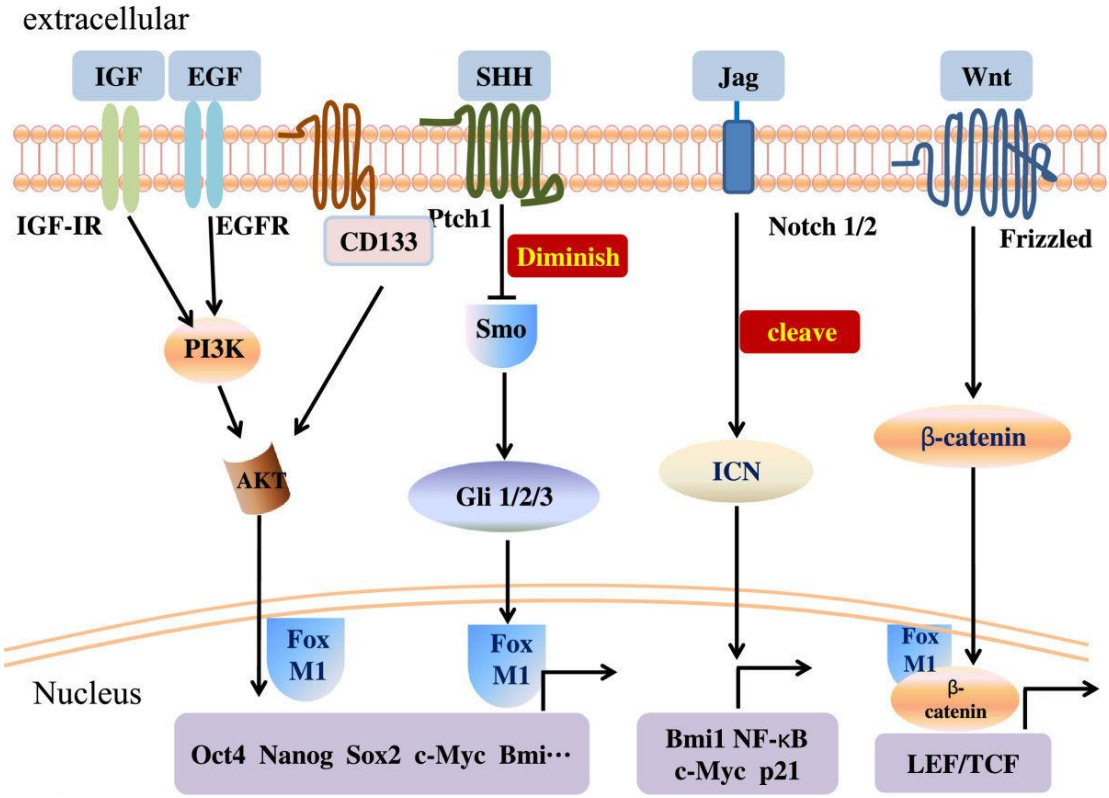

Figure 14: The PI3K/AKT signalling promote nuclear accumulation of β-catenin. Schematic representation of PI3Ks, Sonic Hedghog (SHH), Notch and Wnt pathways. Receptors insulin GF (IGF), epidermal GF (EGF), SGG, Jag and Wnt; activate downstream cascade through PI3K, Smo, Notch and β-catenin for further gene activation of Oct4, Nanog, Sox2, c-Myc, Bmi1, and NF-κB[111]. (Adapted from Oliveira et al., 2017).

The PI3K signalling was reported to play an essential role in asymmetric and symmetric stem cell division. Asymmetric PI3K activity has been initially reported in lymphocytes organised by PI3K nutrient uptake and cell polarity depending on PI3K signalling[112]. Since stem cells produce differentiated progeny while self-renewing themselves, recent studies have also shown that unequal transmission of PI3K signal transduction causes one cell to differentiate while its sister cell remains pluripotent[113]. Moreover, class I PI3Ks play an important role in proliferation, differentiation and cell division when regulating centrosome localisation and separation (**Figure 15**). Recent studies hypothesise that PI3K isoforms play important and specific roles in the growth, self-renewal, survival,

and epithelial-mesenchymal transition (EMT) phenotype of cancer stem cells in oncology[114]. Understanding of PI3K pathways in stem cell biology has major clinical implications for the diagnosis, prevention, and treatment of human diseases, as well as for regenerative medicine.

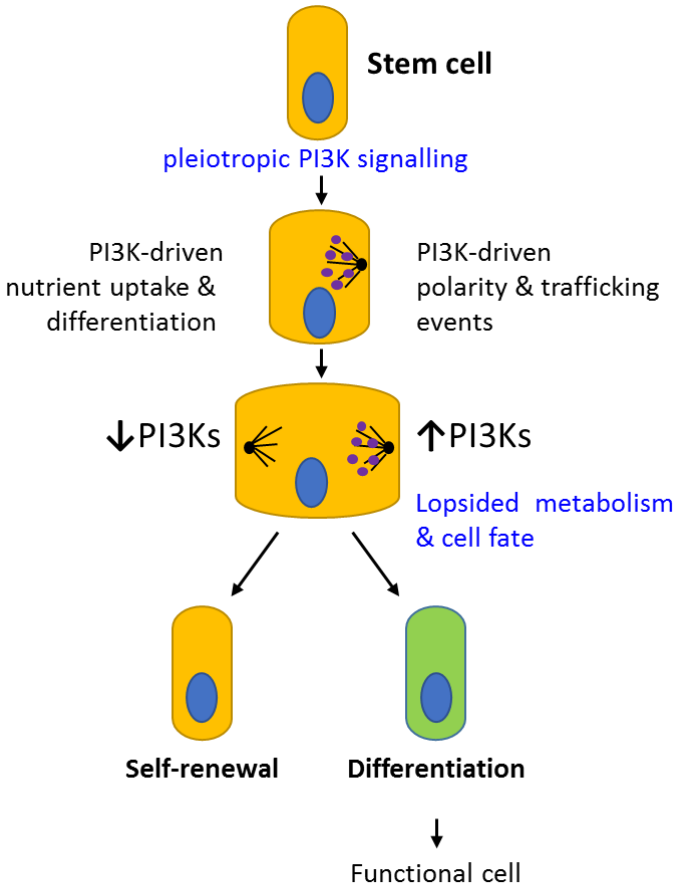

Figure 15: Scheme showing asymmetric PI3K activity in lymphocyte towards self-renewal vs. differentiation. Depending on PI3K-driven nutrient uptake, it has been shown that lymphocytes divide towards self-renewal or differentiation[112]. (Illustration from Laura Medrano-González).

1.3. Gastrointestinal physiology

The gastrointestinal tract (GI) is the largest specialised tissue in organisms whose primary function involves digestion and absorption of solutes and nutrients, as well as providing physical barrier protection against pathogens or external particles. The intestinal epithelium is the most central site of barrier defence against over 100 trillion of microbes that it hosts[115]. Direct interfacing between the host and microbial symbionts, is important for the maintenance of homeostasis and immunomodulation because it allows the host to tolerate intimate relationships with potentially beneficial microorganisms[116]. The GI wall is composed of four layers: mucosa, submucosa, muscular layer (or muscularis propria) and serosa[117]. The serosa is a thick fibrous cover that separates the intestine from the surrounding peritoneal cavity. The muscularis propria, composed by longitudinal and radial fibres, generates the peristaltic movements that push the content of the lumen onwards. The underlining connective layer, the submucosa, takes part in the control of this process being the place where the parasympathetic innervation makes its plexus. Finally, the gut mucosa is the most dynamic immunological environment of the body. The mucosa comprises itself a thin muscular layer (muscularis mucosa), the lamina propria and an overlying monolayer of epithelium[118]. The lamina propria is a loosely packed layer of connective tissue that constitutes the scaffolding for the different mucosal structures and maintains the shapes adopted by different regions of the gut to adapt to their distinct physiological functions. It also contains the blood, lymph drain-age and nervous supply, playing an important role in the regulation of mucosal function. Due to its size, the intestinal tract is the largest mucosal immune system, anatomically divided into upper and lower GI tract. The lower GI track is composed by the small and large intestines, separated by the ileocecal valve and the caecum.

Intestinal epithelial cells (IECs) play an essential role in gut immunity as the first physical and biochemical barrier of defence against food antigens, commensal microbiota, and pathogens. The IECs can detect and respond to microbial stimuli to reinforce their barrier function and coordinate appropriate immune responses such as tolerance or anti-microbial immunity. The intestinal epithelium is formed by a single layer of cells organised into villi and crypts. The villi are formed by enlarged IECs differentiated often into three cell types: goblet cells, enteroendocrine cells, and enterocytes[119]. The majority of the IECs are absorptive enterocytes, adapted to metabolise and digest nutrients. However, in the intestinal lumen there are also secretory IECs specialised in maintaining the protective barrier function of the intestine. The function of goblet cells is to secrete gel-forming mucins, the major components of intestinal mucus. Enteroendocrine cells secrete hormone regulators that link the central and enteric neuroendocrine systems and regulate the appetite, serotonin, and histamine release. Crypts of the small intestine are invaginations in the epithelial inner surface where intestinal stem cells (ISCs) and Paneth cells reside[120]. Paneth cells secrete protective antimicrobial peptides (AMPs) and the hydrolytic enzyme, lysozyme[121]. They are the unique IECs that migrate opposite direction (upside-down) compared to all the rest of IECs and have the longest life span of around three weeks. Paneth cells have important functions in immunity and antibacterial defence and are present throughout the small intestine. Secretory goblet cells and Paneth cells secrete mucus and antimicrobial proteins (AMPs) to promote the exclusion of bacteria from the epithelial surface. The transcytosis and luminal release of secretory IgA (sIgA) further contribute to this barrier function[119]. Microfold cells (M cells) and goblet cells mediate transport of luminal antigens and live bacteria across the epithelial barrier to dendritic cells (DCs), natural killer cells (NKs), and intestine-resident macrophages sample the lumen through transepithelial dendrites. In contrast to the small intestine, the colon epithelium is characterized by a high

density of goblet cells and the almost absence of Paneth cells (**Figure 16**). Many severe diseases have been associated with dysbiosis in the intestinal epithelium. Understanding the function of commensal microbiota in health and disease states, and the mechanism of regulation and signalling in gut immunity, is essential for targeting many diseases such as cancer auto-inflammatory and autoimmune diseases[122–124].

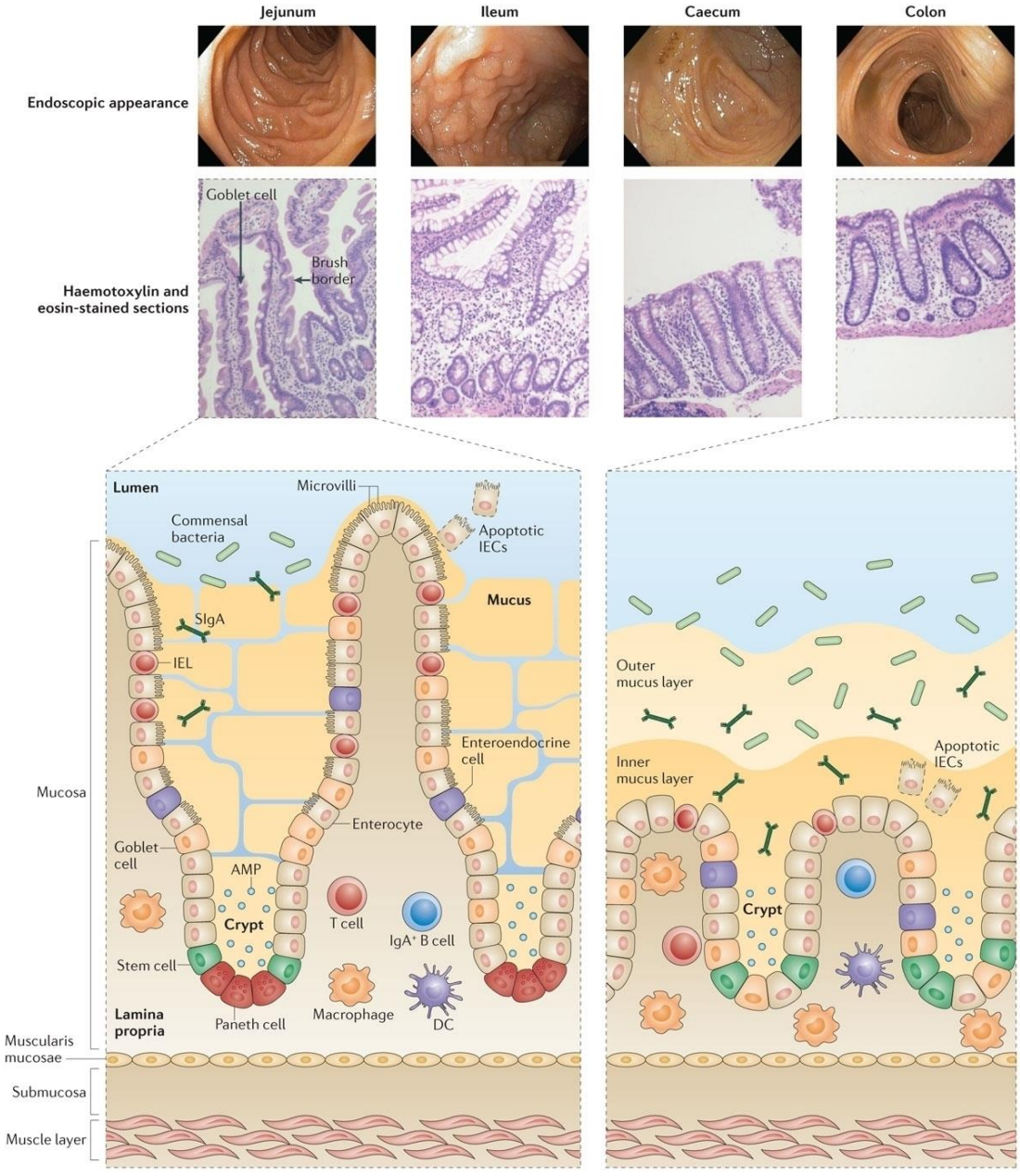

Figure 16: Scheme representing the anatomy, architecture, and organisation of the intestinal mucosa. Distinct appearances of the different segments of the intestine observed from the lumen using endoscopy (top panels). The upper small intestine, as exemplified by the jejunum (middle and lower panels), has long thin villi, which become progressively shorter and broader going down the length (the ileum is shown as an example), and goblet cells and Paneth cells become more numerous and IELs less frequent. The caecum has no villi and numerous goblet cells throughout the crypts. Villi are absent from all parts of the colon and crypts are smaller; Large number of goblet cells are found here, which produce an extensive and thick layer of protective mucus. Paneth cells are very rare in the colon and IELs are much rarer than in the small intestine[119]. (Adapted from Peterson et al., 2014).

1.3.1. Self-renewal of the intestinal epithelium

The intestinal epithelium is the fastest and most complex self-renewing tissue in mammals. The process of epithelial renewal takes approximately 3-6 days and is regulated by a small number of stem cells, located at the bottom of the crypts. More than 300 million new epithelial cells are generated daily in the small intestine to compensate for the high rate of cell death on the villi[125,126]. The complexity and extended architecture of the intestinal epithelium allows up to six invaginations or crypts of Lieberkühn per intestinal villus. These crypts comprise stem cell populations and progenitor cells such as ISCs and Paneth cells that can self-renew. ISCs divide asymmetrically or symmetrically into differentiated cells or progenitor stem cells (multipotent) whereas Paneth cells remain as they are for longer periods (3-6 weeks) in homeostasis. However, recent studies showed that Paneth cells can acquire multipotency after injury[127]. This renewal process involves a rapid and continuous proliferation followed by migration along the crypt-villus axis.

There are two populations or zone models of ISC identity: the crypt base columnar cells (CBCs)[128], and the +4 model. The populations occupy distinct but proximal locations in the crypts and regulate different or at times complementary roles[129]. CBCs intercalated with Paneth cells, are actively phagocytic cells and they give rise to the four major cell lineages in the intestinal epithelium, as discussed below[130]. CBCs are slow cycling adult stem cells that reside in a specialised niche at the very base of the crypt. CBCs generate daughter cells that exit the niche and commit to multi-lineage differentiation throughout the intestine. The primary marker for CBCs, Leu-rich repeat-containing G protein-coupled receptor 5 (Lgr5), was identified as a Wnt target gene selectively expressed at the base of adult intestinal crypts[131,132]. Other markers such as Ascl2 and ofactomedin 4 (Olfm4) are also used as indicators for CBCs. Wnt signalling in the adult intestine promotes proliferation of progenitor transit-amplifying cells (TA cells), as well as commitment toward differentiation of certain secretory lineages (Atoh1), whereas high Notch signalling promotes absorptive lineages differentiation (Hes1)[133,134]. Both Paneth cells and pericryptal stromal cells supply essential factors (including; Wnt, the Notch ligand DLL4, epidermal GF (EGF), and Noggin) to regulate the survival and function of the CBC stem cells *in vivo*. The +4 model or +4 stem cells, comprise a group of progenitor stem cells localised at the +4 position from the base of the crypt, just above of the Paneth cell compartment, as shown in **Figure 17**. Resident +4 stem cells can divide, differentiate, and then migrate until the top of the villi, where they die by apoptosis further in their lifecycle. These +4 stem cells are generally considered quiescent and are resistant to acute injury, displaying an inherent ability to retain DNA labels. The primary marker for +4 stem cells is B cell-specific Moloney murine leukemia virus integration site 1 (Bmi1), a proto-oncogene necessary for efficient self-renewal in different stem cell niches[135,136].

In the small intestine, Lgr5+ CBC stem cells are intercalated with Paneth cells, which express specific genes such as *Mmp7*, *Wnt3*, and *Wnt11*[137], and are localised at the base of the crypt. Paneth cells have been shown essential for supporting the Lgr5+ ISCs niche at the crypts and control tissue renewal[138]. Lgr5+ ISCs continuously divide and give rise to rapidly proliferating TA cells (*Wdr43*)[139], which occupy the remainder of the crypt[129,140]. TA cells differentiate into the various functional cells on the villi (i.e. enterocytes, tuft cells, goblet cells (*Muc2*) and enteroendocrine cells) to replace the epithelial cells that are lost by apoptosis at the villus-site. The quiescent Bmi1+ ISCs, have the ability to revert and restore the Lgr5+ CBC stem cell compartment in case of injury or damage to crypts. Under homeostasis, epithelial turnover occurs every 3-5 days and new Paneth cells are generated from the TA cells every 3-6 weeks. Although, many +4 stem cell markers such as: Leu-rich repeats and immunoglobulin-like domains 1 (Lrig1), and homeodomain-only (Hopx) were strongly expressed in Lgr5+ stem cells, recent studies showed that Bmi1 and Lgr5 markers mark functionally distinct ISCs[136]. The quiescent Bmi1+ ISCs induce proliferation upon intestinal damage and give rise to the progeny of Lgr5+ ISC that repopulate the crypt-villus axes disrupted. The Lgr5+ population, had been shown to be the constant promoter of IECs differentiation although its depletion can be replenished by quiescent Bmi1 populations as well as Paneth cell since both populations can revert to Lgr5+ cell type. Unlike the small intestine, the colon surface does not present enlarged cells forming villi. There are no Paneth cells in the colon, but the number of goblet cells are higher than in the small intestine. Similar to the small intestine, crypt base localised Lgr5+ CBC stem cells generate rapidly proliferating TA cells, which subsequently differentiate into the mature lineages of the epithelium, in the colon the epithelial turnover occurs every 5-7 days.

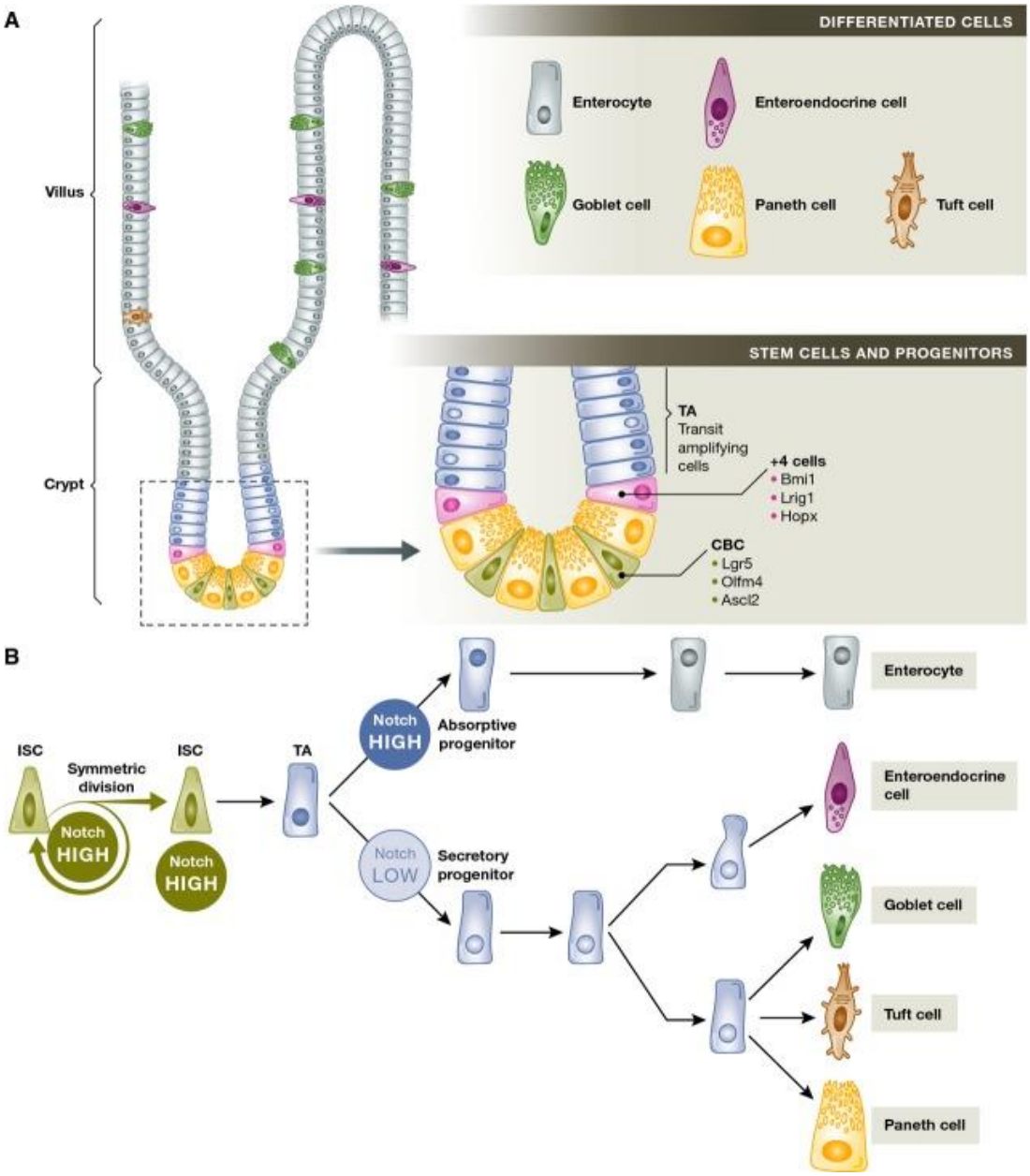

Figure 17: Scheme depicting villus-crypt organisation and localisation of IEC subpopulations. (A) The scheme depicts the organisation of intestinal epithelium according to their villus and crypt localisation. The figure indicates stem cells and progenitors, starting from the bottom of the crypt: CBC stem cells (Lgr5, OLfm4, and Ascl2 markers), +4 stem cells (Bmi1, Lrig1, and Hopx), and transit-amplifying (TA) cells); and differentiated cell: goblet cells, Paneth cell, tuft cell, enterocytes, and endteroendocrine cell. **(B)** Scheme representation of mammalian ISCs differentiation[141]. (Illustration from Sancho et al., 2015).

1.3.2. Intestinal regeneration: proliferation vs. differentiation

The homeostasis between differentiation and proliferation of ISCs are essential to maintain the integrity and protection of the mucosal barrier. ISC maintenance results in mainly symmetric division of progenitor stem cells (Lgr5+ CBCs) into daughter cells or same progenitor stem cells in order to maintain numbers of both cell populations[102]. Symmetrical division potentially predominates the Lgr5+ CBC population and it has been shown the mechanism of cell-fate decision from Lgr5+ CBCs to become a ISCs or TA cells[103]. Previous studies showed that asymmetric division in ISCs occur stochastically, although recent studies showed some controversial findings[101]. Recent studies have shown that epigenetic regulation via DNA methylation does not seem to play a major part in directing their fate[142]. After injury in the intestinal epithelium, the loss of Lgr5+ CBC population can activate +4 stem cells (also called 'reserve' stem cells), which regenerate Lgr5+ CBCs via asymmetric or symmetric division in order to maintain intestinal homeostasis (**Figure 18**). The ISCs role in repair and regeneration has been also documented by a number of studies in the skin[143,144]. ESCs are generated during development and are controlled by epithelial-mesenchymal interactions. Despite morphological and functional differences among epithelia, common signalling pathways appear to control epithelial stem cell maintenance, activation, lineage commitment, and differentiation. Furthermore, deregulation of these pathways can lead to severe disorders including cancer and inflammatory diseases[145–148].

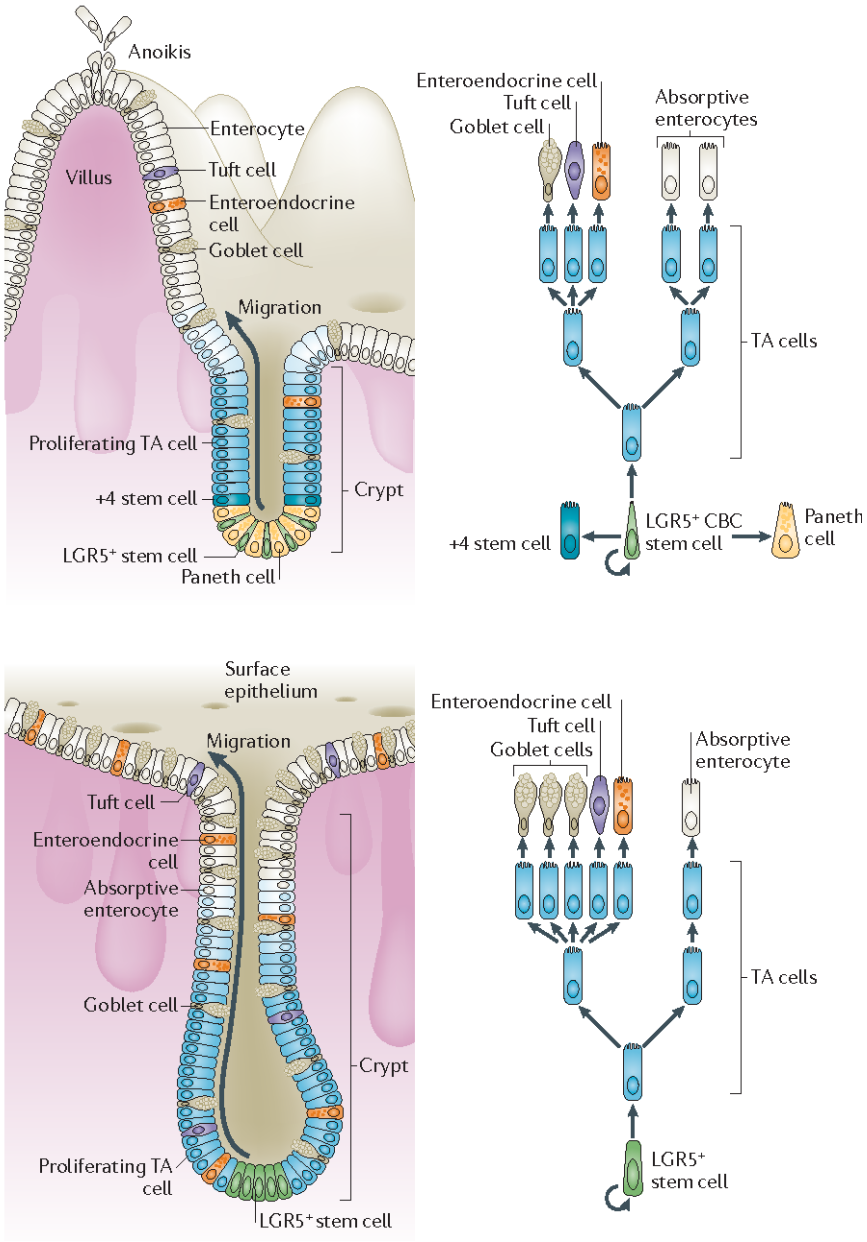

Figure 18: Cartoon comparing the stem cell niches and their differentiation process between the small intestine and the colon in homeostasis. (A) The small intestine architecture, organisation and cell type subpopulations in the small intestine such as: Lgr5+ crypt base columnar, CBC, stem cells, +4 'reserve' stem cells, Paneth cells, transit-amplifying cells (TA cells), and differentiate cells including enterocytes, tuft cells, goblet cells and enteroendocrine cells. The differentiation hierarchy is shown in the lineage tree on the right panel. **(B)** The colon architecture, organisation and cell type subpopulations represents Lgr5+ stem cells, TA cells, goblet cells, enterocytes, enteroendocrine cells and tuft cells, as shown in the lineage tree on the right panel. (Illustration from Barker 2013).

1.4. Immunity and tolerance

The immune system is a host defence system that comprises a number of biological structures and processes within an organism to protect host against disease and stress. The major role of the immune system is to maintain homeostatic tissue functions. The mammalian immune system is classified into two subsystems: the innate immunity, the first barrier and general defence, and the adaptive or humoral immunity, specialised defence involving memory. The immune system detects a wide variety of single or multicellular agents, referred as pathogens, from viruses to parasitic worms, and distinguish them as “foreign” from the organism's own healthy tissue. Innate immunity is the most ancient and evolutionary conserved biological system across species, from lower organisms including sea sponges[150]. The innate immune system has a number of signalling receptors that recognise foreign molecular structures as well as self-molecules that are altered, have become too abundant or emerge in areas normally devoid of these molecules. This conserved set of cell-surface bound, or soluble proteins are referred as pattern recognition receptors (PRRs)[151]. PRRs in immune cells may be membrane-bound receptors or soluble proteins that recognize molecular structures from foreign organisms known as pathogen-associated molecular patterns (PAMPs), such as lipopolysaccharide, flagellin, and bacterial DNA/RNA, and they activate the innate immune recognition and inflammatory alarm to protect against pathogens.

1.4.1. Immunity of the intestinal tract

The intestinal epithelium is protected by the coordinated action of immune cell effectors. These include: T and B lymphocytes, intra-epithelial lymphocytes, mononuclear phagocytes, and innate lymphoid cells which populate the epithelial

layer, the underlying lamina propria, and the IECs. These cells are often organized into specialized gut-associated lymphoid tissues (GALTs) such as in Peyer's patches. Due to the constant exposure to food antigens and microbes in the lumen, a sophisticated homeostatic system is needed to balance inflammation and tolerance in order to avoid inflammatory pathology, as well as microbial invasion (**Figure 19**). For example, microfold cell (M cell) in Peyer's patches efficiently capture luminal antigens through transcytosis for antigen presentation. In addition to immune effectors, specialized secretory cells in the intestinal lining such as goblet cells and Paneth cells secrete mucus and/or AMPs, respectively, which help fend off pathogenic microbes. Moreover, commensal bacteria that reside in the intestinal lumen also contribute to tissue homeostasis through production of metabolites such as short chain fatty acids, which facilitate the functional development of immune effectors. In turn, microbial metabolites are sensed by GPCRs such as GPR43 in colonic epithelial cells, which subsequently stimulate potassium efflux and NLRP3 inflammasome activation. Dysbiosis in the gut immunity causes severe autoinflammatory and autoimmune disorders including multiple sclerosis (MS), rheumatoid arthritis (RA), systemic lupus erythematosus (SLE), and inflammatory bowel disease (IBD). Understanding and studying the mechanisms of regulation and regeneration of IECs in gut immunity and inflammation is an important tool for future therapies in colon cancer and inflammatory diseases[119,125].

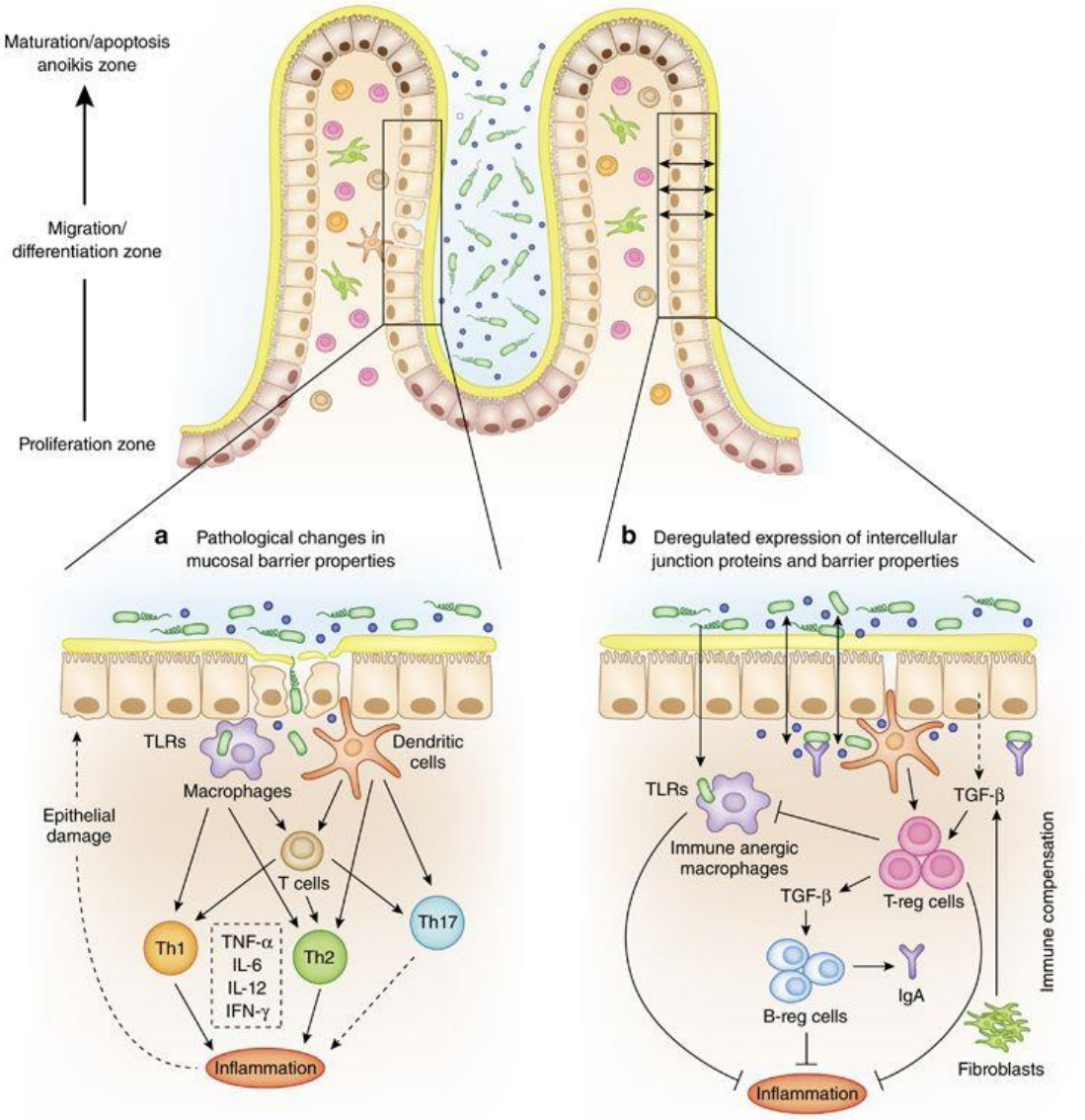

Figure 19: The intestinal epithelium selectively controls the passage of commensal bacteria and pathogens across the mucosal barrier. Schematic representation of the gastrointestinal epithelial barrier, a single layer of intestinal epithelial cells (IECs) proliferate across the villus and differentiate for further maturation and apoptosis. IECs form a physical barrier which selectively limits the permeation of commensal microbiota or pathogens though the intestinal epithelium. **(A)** Pathological changes in the mucosal barrier cause the break of commensal microbiota and pathogens across the IECs and induce hyper-activation of the mucosal immune system and inflammation. Bacterial ligands are recognised via pathogen recognition receptors (PRRs), such as toll-like receptors (TLRs), from macrophages and/or dendritic cells which prime T lymphocytes (T cells) and activate an excessive inflammatory response. **(B)** On the other side, deregulated expression of intracellular junctional proteins in IECs and barrier properties, which maintain the epithelial barrier tight, may not be adequate for the induction of mucosal inflammation

but for adaptive immune responses via regulatory T and/or B lymphocytes[152]**.** (Illustration from Ahmad et al., 2017).

IBD is a chronic inflammatory condition of the GI system with a high incidence in young adults, particularly effecting western societies. Over one million people in Europe and more than one and a half million in the United States are estimated to suffer from IBD[153]. There is no cure for IBD, and current therapies administered to IBD patients are not effective and may result in severe side effects leading, to a very poor life quality with high morbidity. IBD is classified into two subclasses according to the area of the GI track affected, named Crohn's disease (CD) and ulcerative colitis (UC). While CD affects the terminal ileum and colon, UC patients show inflammation of the colon. Treatment of IBD includes conservative measures as well as surgical approaches in those who are non-responders to medical treatment. There are some differences between CD and UC in the underlying immunological disturbances. In CD the antigen presenting cells and macrophages produce mainly interleukin-12 (IL-12) and IL-18 resulting in a T helper 1-type (Th1) polarization and production of pro-inflammatory cytokines including tumor necrosis factor-α (TNFα), and interferon-γ (IFNγ)[154]. Subsequently these cytokines stimulate the antigen presenting cells to secrete other cytokines including: IL-1, IL-6, IL-8, IL-12, and IL-18, thus leading to a self-sustained cycle. Patients with UC exhibit an added contribution of Th2 responses characterized by increased secretion of IL-4, IL-5, and IL-13 and reduced amounts of IFN-γ[155]. Th17 cells were identified as a new subset of T helper cells unrelated to Th1 or Th2 cells. Th17 cells differentiate under the influence of IL-1β, IL-6, IL-21 and IL-23. Recently, it has been shown that transforming growth factor-β (TGF-β) regulates also the differentiation of Th17 cells, with the presence of cytokines favoring Th17 cell differentiation. A large number of biological agents against TNFα have been developed during the last decade, as well as many biochemical

substances and molecules specifically for the medical treatment of patients with IBD. Current pharmaceutical treatment of IBD includes anti-inflammatory drugs (mesalazine, corticosteroids); immunosuppressive drugs (azathioprine, 6-mercaptopurine, methotrexate, or cyclosporine); biologic agents (infliximab, adalimumab, certolizumab pegol); antibiotics (metronidazole, ornidazole, clarithromycin, rifaximin ciprofloxacin, anti-tuberculosis); probiotics; and drugs for symptomatic relief[156]. Numerous studies showed IBD caused by multiple factors such as intestinal microbiota alterations, environmental factors, disturbances in the innate and adaptive immune responses, and genetic variations. An increasing number of susceptibility genes in IBD have been identified after genome wide association studies (GWAS), the most relevant are *NOD2, ATG16L*, and *IRGM*[157] (**Figure 20**). Patients with IBD are at significantly increased risk of developing CRC, which constitute a colitis-associated cancer (CAC) subgroup. CRC is the third most common malignancy cancer in incidence and mortality worldwide. Most colon cancers are associated with mutations in the adenomatous polyposis coli (APC) gene, which results in activation of the Wnt pathway and dysregulated nuclear translocation of β-catenin. However, IBD and CAC, have been associated with microbial dysbiosis in the gut, facilitating adhesion of pathogens to the bowel wall. Investigating genes involved in epithelial barrier immunity and how IECs of the gut mucosa handle the commensal bacteria and interact with the local immune cells, is necessary for development of future therapies not only in IBD but also in other chronic inflammatory diseases and cancer with potential gut origin.

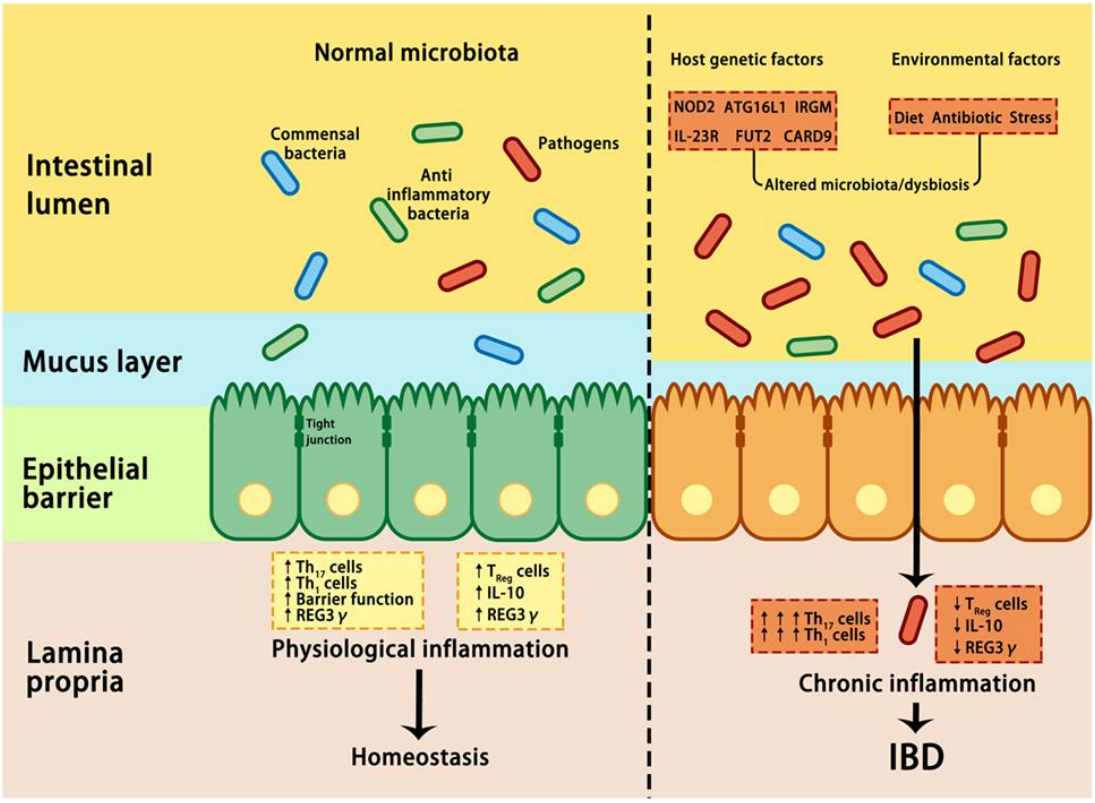

Figure 20: Intestinal microbiota, host genetic mutations and environmental factors cause a pathological chronic inflammation in the intestinal epithelium. In homeostatic conditions (left side), pathogens are supressed by beneficial commensal bacteria through the secretion of anti-inflammatory proteins such as interleukin -10 (IL-10). In pathological conditions such as inflammatory bowel disease (IBD), a combination of host genetic mutations (*NOD2, ATGL16, IRGM*) and environmental factors (such as diet), leads to dysbiosis which affects barrier integrity resulting in uncontrolled innate and adaptive immune responses: hyper-activation of T helper 1 and 17 (Th_1/ Th_{17}), reduction in regulatory T cells (Treg) and IL-10. (Illustration from Zhang et al., 2017).

1.4.2. Pathogen recognition receptors

Host immune molecules control the balance between immunity and tolerance. These molecules couple to a large family of innate PRRs including Toll-like receptors (TLRs), RIG-I-like receptor (RLR), and NOD-like receptors (NLRs). IECs express PRRs, which play an essential role in protection against intestinal

inflammation and controlling repair and regeneration of epithelial damage. These receptors can directly or indirectly recognise microorganisms, fungi, bacterial ligands, and parasites through their molecular structural signatures, while maintaining tolerance to food antigens. If required, PRRs can activate the NF-κB complex, which is important for pro-inflammatory, inflammasome formation, and anti-apoptotic responses. Defects in gut immunity, caused by dysregulation of PRR activity/PAMP recognition, are associated with autoimmune and inflammatory disease in animal models and humans, as well as cancer (**Figure 21**)[124,158,159].

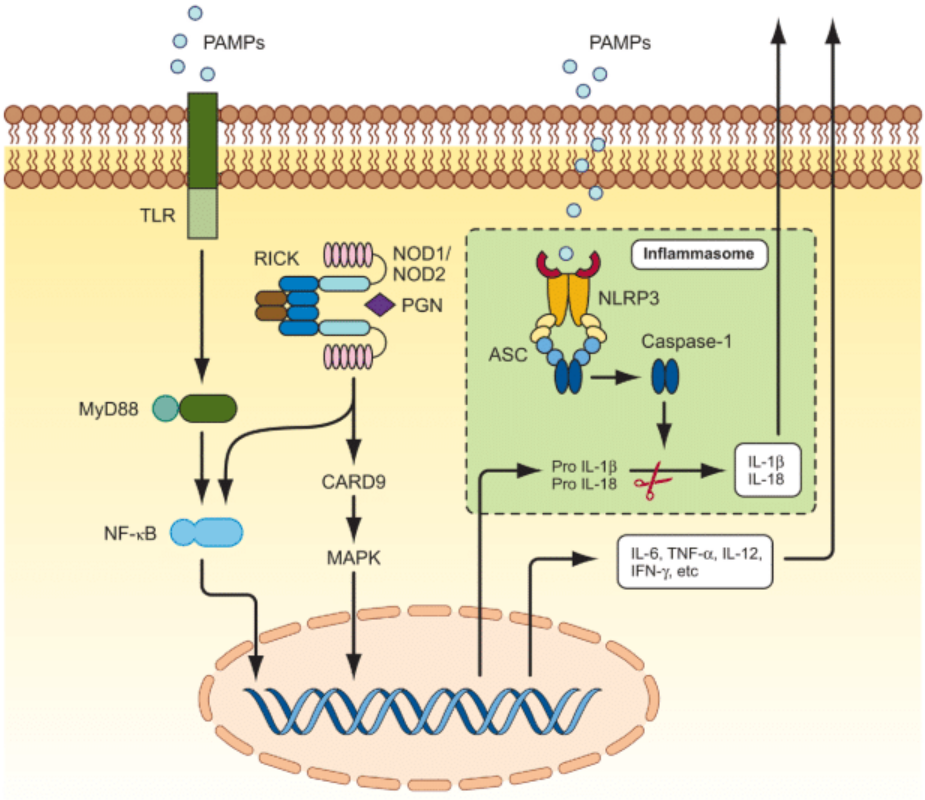

Figure 21: Intestinal epithelial cells (IECs) express pathogen recognition receptors (PRRs) which control and regulate inflammatory responses in the intestinal epithelium. Toll-like receptors (TLRs) recognise pathogen-associated molecular patterns (PAMPs) and activate classical inflammatory response via MyD88/NF-κB. Moreover, NOD-like receptors (NLRs) such as NOD1 and NOD2 sense intracellular presence of bacterial cell wall component peptidoglycan (PGN) which further activates CARD9/MAP Kinases (MAPK) and NF-κB. The NF-κB and MAPK pathways are the major signalling pathways that induce the

expression of pro-inflammatory cytokines. Another cascade of signalling is mediated by NLRP3, which senses bacterial ligands in the cytosol and forms the inflammasome; a multiprotein complex with associated speck like protein containing a caspase recruitment domain (ASC) and caspase-1. The inflammasome plays a central role in inflammatory process by activating caspase-1, and mediating production of pro-inflammatory cytokines IL-1β and IL-18[160]. (Illustration from Zaki et al., 2011).

1.4.3. TLRs signalling pathways

IECs express intracellular and extracellular receptors of the TLR family. TLRs trigger intestinal inflammation when pathogenic microbes or physical injury breaches the intestinal barrier. TLR signalling has been shown to be involved in epithelial cell proliferation, IgA production, maintenance of tight junctions and antimicrobial peptide expression. TLRs can also trigger pro-inflammatory responses by underlying lamina propria immune cells[161–163]. TLR1, TLR2, TLR3, TLR4, TLR5 and TLR9 have also been detected in IECs of the human small intestine. TLR2 and TLR4 are expressed at low levels by IECs in normal human colon tissues. TLR3 seems to be abundantly expressed in normal human small intestine and colon, whereas TLR5 is expressed predominantly in the colon. Recent studies show that TLR signalling in the IECs confers protection in acute inflammation. However, it has not been clearly addressed which cells mediate protection[164]. The TLR→MyD88→AREG/ERE-G→EGFR signalling pathway is represented in non-hematopoietic cells of the intestinal tract, responds to microbial stimuli once barriers are breached, and mediates protection against dextran sodium sulphate (DSS)-induced colitis (**Figure 22**). DSS induces damage to the small intestine and colon and it is the best known model utilised to investigate in a model of acute damage and microbial mediated inflammation[165,166]. IECs from patients with IBD have higher expression of TLRs, especially TLR4. Early studies

showed that IFNγ and tumour necrosis factor TNFα induce the transcription of TLR4[167].

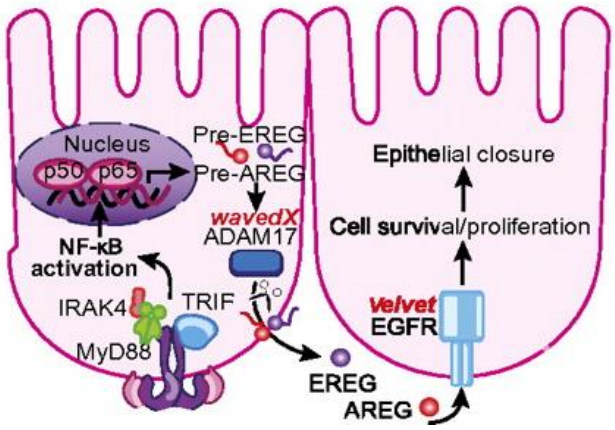

Figure 22: Cartoon depicting TLR intracellular signalling downstream of MyD88. TLR-MyD88 pathway in intestinal epithelial cells (IECs) activates NF-κB complex induce inflammatory response as well as amphiregulin (AREG)/ epiregulin (EREG) → epithelial GF receptor (EGFR) induce cell survival and proliferation after injury[164]. (Illustration from Brandl et al., 2010).

1.4.4. NLRs signalling pathways

Nucleotide-binding oligomerisation domain (NODs) are cytosolic innate receptor members of NLR family. Twenty-three mammalian NLRs have been identified, their classification in different subgroups are based on structural motifs and/or their function. NODs are characterised by their N-terminal effector domain, a centrally located nucleotide-binding domain (NBD) and multiple leucine-rich repeats (LRRs) in the C-terminal end of the molecule. NODs use the LRR scaffold domains to detect PAMPs and tissue injury induced damage-associated molecular patterns (DAMPs). NLRs are classified according to the protein domains on their N-terminal effector domain, which activate the NF-κB complex and initiate immune inflammatory responses.

NOD1 and NOD2 are the most studied isoforms, contain one or two caspase recruitment domains (CARD) respectively, which interact with the CARD-containing molecules involved in inflammation and apoptosis[168]. NOD proteins are intracellular sensors of bacterial cell wall component of peptidoglycan (PGN), NOD1 recognises γ-D-glutamyl-meso-diaminopimelic acid (iE-DAP), a dipeptide component of PGN from gram-negative bacteria whereas NOD2 can detect muramyl dipeptide (MDP) present in almost all gram-negative and gram-positive bacteria. MDP is the minimal bioactive motif, common to all bacteria required for immune stimulatory activity in vaccine adjuvants of bacterial cell wall components (**Figure 23**). NOD1/2 signalling leads to the activation of NF-κB and MAPK signalling pathways evolutionarily conserved throughout the innate immune system. Ligand sensing and activation of the receptors induces self-oligomerisation of NOD1/2, allowing the recruitment of the CARD containing receptor-interacting serine/threonine-protein kinase 2 (RIP-2)[169]. RIP2 subsequently activates transforming GF beta-activated kinase 1 (TAK1) through Lys63-linked ubiquitination, which finally activates NF-κB and MAPK. The activation of MAPK via NOD2 requires also the CARD-containing CARD9. Both CARD9 and RIP2 mutations are associated with IBD susceptibility. Mutations in the LRR domain cause a non-functional NOD, whereas mutations in the NBD domain were reported to promote an auto-inflammatory disorder called Blau syndrome or early-onset sarcoidosis[170,171].

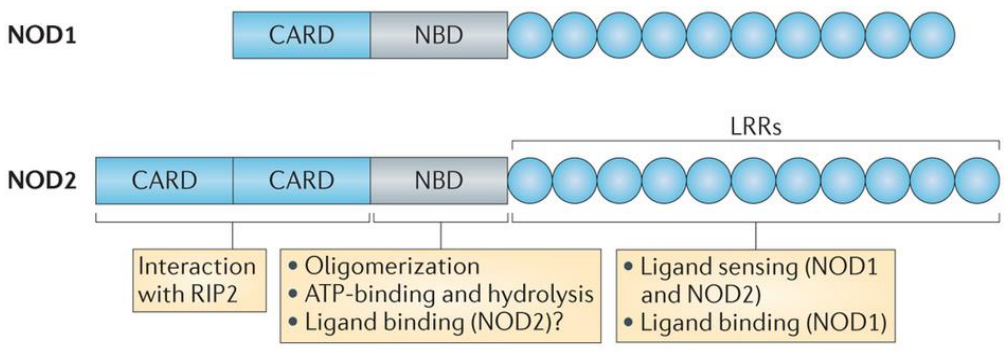

Figure 23: The molecular structure of NOD1 and NOD2s. Caspase recruitment domains (CARD), nucleotide-binding domain (NBD), leucine-rich repeats (LRRs), and Receptor-interacting serine/threonine-protein kinase 2 (RIP2)[172]. (Illustration from Philpott et al., 2014).

NOD1 is constitutively expressed in IECs and has been shown to activate NF-κB by pathogens in particular those which have developed methods to bypass sensing by TLRs. *NOD1* gene polymorphisms have been associated with increased susceptibility to human IBD[173]. While NOD1 is expressed ubiquitously, NOD2 is mainly expressed in myeloid cells and epithelial cells[168,174,175]. *NOD2* was the first susceptibility gene identified from CD patients and plays an essential role maintaining microbial tolerance at the mucosal barriers[176,177]. NOD2 has also been shown to supress CACs via downregulation of the TLR pathways[178]. Recent studies showed NOD2 expression in IECs protects toward the development of inflammation and CACs[179]. The roles of NOD1/2 receptors have been shown to be highly specific to the gut epithelium. NOD1/2 pathway in IECs have been reported to control intestinal homeostasis and wound healing[174,180–182]. Moreover, NOD1/2 are receptors expressed in the Paneth cell population[183] activated by the N-acetylmuramic acid-linked dipeptides from the gram-negative and/or gram-positive bacterial cell wall component peptidoglycan, expressed by almost all bacteria, with the exception of mycoplasma[184,185]. This leads to downstream activation of the NF-κB and MAPK pathways, promoting pro-inflammatory, immune-regulatory and wound healing responses[159,183].

2.AIMS

"The aim of science is not to open the door to infinite wisdom,

but to set some limit on infinite error"

Bertolt Brecht

Mammalian PI3Ks are lipid modifying enzymes involved in important cell biological events, often deregulated in cancer and inflammatory diseases[186–188]. Our laboratory has been studying how signalling events downstream of PRRs, mainly of NOD1/NOD2 can be regulated through phospholipid modifications in cell membranes by class I PI3K isoforms in immune and non-immune cells. Although current knowledge of the signalling pathways involved in NOD1/2 mediated gut immunity is rudimentary[8,176,189,190], our data suggests that PI3Ks couple and regulate NOD1/2 intracellular signalling and impact immune responses both *in vivo* and *in vitro*. Since NOD2 mutations cause colitis susceptibility and selective inhibition of class I PI3K isoforms, particularly p110δ, results in gut inflammation in humans and mice; I hypothesised that epithelial cell-intrinsic class I PI3K isoforms regulate important aspects of NOD1/2 signalling pathway, influencing gut immunity, repair and regenerative processes. Therefore, I proposed to investigate the role of class I PI3Ks in signalling downstream of PRRs in IECs, which may connect PI3K biology not only to inflammatory/immune responses but also repair and regeneration processes in the mammalian intestine.

Class I PI3Ks couple with RTKs, GPCRs and Ras and Rho GTPase mediated signalling pathways in the epithelium. Oncogenic Ras mutations, which augment Ras signalling, are established driver mutations associated with cell proliferation and provide metabolic adaptations to cancer cells to sustain their growth in harsh tumour microenvironment. It is also established that cellular uptake of proteins via macropinocytosis is regulated by Ras-p110α interactions and was shown essential for growth and survival of transformed cells from certain cancers under nutrient limiting, stressful conditions[25,191]. Therefore, previous studies have uncovered p110α-RBD interaction with Ras can provide cancer cells survival and growth advantages under low nutrient settings. Yet while, a number of works established important role of p110α in cancer settings, by which p110α increases the

oncogenic potential of epithelial cells, how p110α couples and regulates normal IEC functions and IEC responses under intestinal injury are not well established.

I hypothesised that evolutionarily conserved p110α-RBD interaction regulates physiological responses of IECs by coordinating the nutrient uptake processes, by macropinocytosis, necessary for cell growth and repair in cells, particularly under cell or tissue stress during injury. Herein, by genetic and pharmacological targeting *in vivo* and *in vitro*, I have investigated the role of p110α PI3K, particularly of p110-αRBD in the activation of mTORC1 pathway by extracellular eukaryotic AAs, and bulk proteins. Furthermore, by means of an analogous hypothesis, I have investigated whether prokaryotic D-amino-dipeptides from bacteria can utilise a similar pathway and activate mTORC1 through the cytosolic sensors for D-amino-dipeptides, NOD1/2 associated signalling pathways. The key aim of this thesis is to investigate and determine the IEC-intrinsic role of class I PI3K isoforms in gut health and inflammation mediated injury and/or NOD1/2 signalling. I propose to test my hypothesis by addressing the aims as listed below;

1. To investigate the effect of class I PI3K-isoforms inhibition on NOD1/2 signalling in human and mouse IECs.
2. To uncover the IEC-intrinsic roles of p110α and p110α-RBD mediated gut repair and regenerative responses *in vivo* in a model of intestinal injury.
3. To understand the role of p110α-RBD interaction regulating physiological responses upon injury by coordinating nutrient uptake events, necessary for cell growth and repair in cells under stress.
4. To investigate the activation of mTORC1 pathway by extracellular AAs, with similar to proteins, and if they require p110α-RBD interaction.

3.MATERIALS & METHODS

"I am not here to speak the Truth,

I am here just to give you a method to perceive it"

Jaggi Vasudev

3.1. Cell culture management

IEC lines from human (NCM-365), and mouse (CMT-93), were used in this study. The mouse embryonic fibroblasts (MEFs) WT and p110α-RBD homozygous mutant (αRBD) were generated from 9.5-10 day embryos from pregnant females as previously described (**Table 3**)[25,192]. All cell lines were immortalised by serial passaging and routinely cultured in 75 cm^2 flasks with complete Dulbecco's modified eagle's medium (DMEM) containing: 10% fetal bovine serum (FBS) dialyzed; 1% of penicillin-streptomycin, 1% non-essential amino acids (NEAAs), and 1% of sodium pyruvate. Cells were cultured in this complete medium in a humidified cell culture incubator at 37°C with 5% CO_2. Subculture of cell lines was followed daily and allowed to proliferate up to 85-90% confluent status. Once confluent, each cell line was passaged using Trypsin-EDTA (0.05%), phenol red for less than 4 min at 37°C. Adherent cells were then detached and suspended in twice the volume of complete medium in order to inactivate Trypsin-EDTA, and centrifuged at room temperature 1500 rpm for 5 min. Pellets were suspended in complete medium and passaged to a new flask in 1:4 to 1:10 dilution, according to each cell line growth. In order to cryopreserve stocks of each cell line, $1 \cdot 10^6$ cells which were passaged less than 3 times, were re-suspended in 10% dimethyl sulfoxide (DMSO) FBS and kept at -80°C in a freezing container (Nalgene Mr. Frosty) overnight. Cryovials with frozen cells were then transferred into the liquid nitrogen storage facility. When required, frozen cells were thawed at 37°C and diluted rapidly in pre-warmed complete medium, cells were then centrifuged at room temperature 1500 rpm for 5 min and pellet was re-suspended in complete medium for further subculture.

NCM-365 and CMT-93 cell lines, were plated and treated for *in vitro* experiments. When sub-confluent status was reached, cells were detached, collected and counted 1:4 with Trypan blue solution (**Figure 24**). IECs lines were suspended in complete medium and 30,000 cells/cm^2 were plated in 6-well cell culture for 4 – 6 h prior stimulation or FBS starvation. When IECs were adherent, some plates had their complete medium replaced in order to treat the cells with IL-1β (20 ng/mL), TNFα (20 ng/mL), LPS (1 µg/mL), or PGN (200 µg/mL) overnight. Other plates with IECs engaged for a different experiment, were replaced with 0.5% FBS starvation medium DMEM overnight. On the following day, stimulated cells were collected whereas 0.5% FBS starved IECs were treated with PI3K isoform-selective inhibitors: p110α A66 (1 µM), p110β TGX-221 (0.25 µM), p110δ IC87114 (1 µM), pan-class I PI3K-inhibitor GDC-0941 (0.5 µM), or DMSO (vehicle) for 4 h prior to stimulations (**Table 4** & **Table 5**). Time kinetic stimulations were optimised for 0 – 30 – 60 min of iE-DAP (30 µg/mL), MDP (30 µg/mL), or LPS (1 µg/mL). Stimulations were given to IECs with or without PI3K isoform-selective inhibitors.

$$\boldsymbol{Number\ of\ cells \times 10^4 \times Dilution\ factor\ (1:4)}$$

Figure 24: Formula used to obtain the cell count. Cell lines cultured in DMEM were counted with a haemocytometer and Trypan blue staining technique. Cells that lied within the 1mm2 square of the haemocytometer were counted at x10 magnification on a light microscope.

Immortalised WT and homozygous mutant αRBD MEFs, were engaged for *in vitro* experiments following the same procedures as described above. Briefly, 30,000 cells/cm^2 WT and mutant αRBD MEFs were plated in 6-well cell culture plates overnight in a humidified cell culture incubator at 37°C with 5% CO_2. On

the following day, complete medium was replaced with 5% FBS starvation medium in DMEM 4 h prior to stimulations with EGF (20 ng/mL) for 5 – 10 – 15 min; iE-DAP (30 µg/mL) for 0 – 20 – 40 min; or MDP (30 µg/mL) for 0 – 20 – 40 min. For the essential amino acid (AA) starvation assays, MEFs were replaced with AA starvation medium with 5% of special FBS dialyzed without nutrients and 1% glutamine in Earle's balanced salt solution (EBSS). Cells were AA starved for 4 h prior to treatment and stimulation as follows; EIPA (50 µM) inhibitor was added 45 min before stimulations, other cells were treated with Bafilomycin A1 (100 nM) 20 min before stimulations. Samples were compared to basal levels and stimulated with iE-DAP (30 µg/mL) for 0 – 45 – 90 min, L-Leucine (1 mM) for 0 – 45 – 90 min or 3% albumin for 0 – 90 – 180 min.

3.1.1. Cell lines

Cell Type	Organism	Tissue	Morphology	Growth properties	Levels p110α/δ	Source
CMT-93	*Mus musculus*	Rectum, colon epithelium	Epithelial C57BL/icrf	Adherent	p110α↑p110δ↓	ATCC CCL223
MEFs p110α WT	*Mus musculus*	Embryonic fibroblasts	Fibroblast	Adherent	p110α↑p110δ↓	Generated by Prof Julian Downward, F.Crick Institute
MEFs p110α RBD	*Mus musculus*	Embryonic fibroblasts	Fibroblast	Adherent	p110α+/-p110δ↓	Generated by Prof Julian Downward, F. Crick Institute
NCM-365	*Homo sapiens*	Colon immortalised epithelium	Intestinal epithelial	Adherent	p110α↑p110δ↓	INCELL Corporation LLC

Table 3: Cell lines cultured and treated in our laboratory.

3.1.2. Inhibitors

Name	Original name	Source	Description	Concentration used
Bafilomycin	Bafilomycin A1	Sigma-Aldrich	Streptomyces griseus	100 nM
EIPA	EIPA	TOCRIS	1154-25-2	50 µM
p110α	A66 SY-A66	Symansis	IC_{50} p110α 32 nM	1 µM
p110β	TGX-221	Calbiochem	IC_{50} p110α 5 µM IC_{50} p110β 0.005 µM	0.25 µM
p110γ	AS-252424	SelleckBio		0.5 µM
p110δ	D030 IC87114	SelleckBio	IC_{50} p110δ 130 nM	1 µM
Pan-class I PI3K-inhibitor	GDC-0941 957054-33-0	Axon-Medchem	Ref. Axon 1377	0.5 µM

Table 4: Class I PI3K specific-isoforms inhibitors used in this thesis.

3.1.3. Stimulations

Name	Description	Concentration used	Source
EGF	Protein produced by skin fibroblasts which stimulates epidermal GF receptors (EGFRs), type of RTK which in turn activates PI3K	20 ng/mL	Peprotech
iE-DAP	Found in Gram-negative bacteria and activates the NOD1 receptor	30 µg/mL	Invivogen
IL-1β	Interleukin 1 beta	20 ng/mL	Peprotech
LPS	TLR-4 ligand L2880-10MG	1 µg/mL	Sigma-Aldrich
MDP	Fragment of Gram-positive or Gram-negative bacterial PGN component that activates NOD2 receptor.	30 µg/mL	Invivogen tlrl-mdp
PGN	Peptidoglycan, PGN-from Staphylococcus auresu ultrapure	200 ng/mL	Invivogen tlrl-sipgn
TNFα	Tumor necrosis factor alpha	20 ng/mL	Peprotech

Table 5: Ligands, proteins and GFs used for in vitro assay stimulations.

3.2. Western blotting

Western blotting (or protein immunoblotting) is a biochemical analysis technique used in molecular biology to detect and quantify protein expression from cell or tissue samples. Cell lysates are the most common form of samples used for western blotting and were used and described in this study. Cellular lysates were extracted from all cell types after indicated treatments and stimulations. Cells were processed with lysis buffer containing: 20 mM Tris HCl pH 7.5; 150 mM NaCl; 1 mM EDTA; 1% IGEPAL; 10% glycerol; 10 mM β-glycerophosphate; 10 mM NaF; 10 mM Na_2VO_3; 1X Protease inhibitor cocktail tablet; 1X Phosphatase Inhibitor Cocktail Set II. Following stimulations and respective kinetics, cells treated rested on ice whilst medium was removed from each sample and washed 2-3 times with PBS. Once samples were washed, 150 µL of lysis buffer was added per sample and rested for 20 min on ice. Since the samples processed were adherent cells, each sample was scraped before collection. Cell lysates were centrifuged at 13500 rpm for 10 min at 4°C. Supernatants were collected and pellet discarded. Protein quantification assays were carried out to enable equal protein loading. Protein concentrations were measured using the Pierce BCA protein assay kit and spectrophotometer at 570 nm was used to measure the optical density. Cell lysates were diluted into a 4X Laemmli sample buffer [193]. Polyacrylamide gel electrophoresis (PAGE) was used to separate proteins according to their electrophoretic mobility such as length, conformation and charge of the molecule. Sodium dodecyl sulphate-PAGE (SDS-PAGE) is a method of separating molecules based on the difference of their molecular weight and is the one used in this report. SDS-PAGE requires two types of polyacrylamide gels were in SDS: stacking and separating gel. Stacking gel is the first gel where samples were loaded, is acidic (pH 6.8) and forms all samples into thin and defined bands. The second gel is basic (pH 8.8) and has a higher polyacrylamide content, which allows proteins to separate by

size; smaller proteins travel more easily and rapidly than larger proteins. In this report, the gels used were 10% of acrylamide due to the size of our proteins of interest. Electrophoresis was carried out at 80V for two h at room temperature in 1X running buffer.

Once SDS-PAGE was completed, gels were transferred onto a nitrocellulose membrane in order to make the proteins accessible to antibody detection. A transfer sandwich was prepared (sponge-paper-gel-membrane-paper-sponge), and electroblotting was carried out at 80V for one hour at 4°C in 1X transfer buffer. Proteins were transferred from the SDS-PAGE onto the membrane while maintaining the organization they had within the gel. Membranes were marked and cut for further antibody detection. Protein marker ladder was loaded at the edge of each gel before running to analyse molecular weight and to cut the membranes at the right size. Membranes were incubated in 5% non-fat dry milk in tris-buffered saline with 0.05% of TBS Tween-20 (TBS-T) for one hour at RT in order to avoid non-specific binding. After blocking, primary antibody, was incubated with the respective membrane size overnight at 4°C on a shaker. Antibodies used were diluted in 5% bovine serum albumin (BSA) in TBS-T (**Table 20**). After washing membranes with TBS-T four times for ten min, secondary antibody was incubated for one hour at RT on a shaker. Membranes were washed as previously described before being developed using darkroom development techniques for chemiluminescence.

3.3. Polymerase chain reaction

Each mouse colony was generated and reared at the QMUL animal facility under HO regulations. I personally checked the colonies previously described every other day, genotyped and arranged the required breeders in order to obtain the desired mouse strain. Mice were numbered/ID via ear clipping and so, used that sample for further genotyping. Ear clips were digested individually with 42 µl TNES buffer, 4 µl proteinase K, and 4 µl proteinase E and kept at 55ºC overnight in the water bath. Once digested, all samples were diluted in 200 µl of TE buffer in order to obtain ~200 µg/mL of DNA and kept at 4ºC. The DNA fragments of interest were amplified by carrying out polymerase chain reaction (PCR) using the protocol from our laboratory. All DNA samples were processed with the same reagents and reaction as follows: 32.75 µl of ddH_2O, 2 mM dNTP mix, 10X Titanium Taq PCR Buffer, 50X Titanium Taq DNA Polymerase, and 2 µl of DNA for a final volume of 50 µl (**Table 6**). Each strain or genotyped required a different set of primers and PCR thermocycling conditions at **Table 7.** Sets of primers and reactions are described at **Table 8**. In order, to separate the DNA of interest, DNA was mixed with loading dye (40% (w/v) sucrose in Tris-EDTA and loaded into 1.5% agarose gel containing 1:100 µl of GelRed Nucleic Acid Gel Stain in 1X Tris-Acetate-EDTA (TAE) buffer (Geneflow Limited, 20 mM Tris-acetate, 1 mM Na_2).

Component	50 µl Reaction	Final Concentration
10X Titanium Taq PCR Buffer	5 µl	1X
2 mM dNTP mix	5 µl	0.20 mM
10 µM Forward Primer	5 µl	0.5 µM
10 µM Reverse Primer	5 µl	0.5 µM
50X Titanium Taq DNA Polymerase	0.25 µl	1X
Template DNA	2 µl	<1,000 ng
Nuclease-Free Water	to 50 µl	

Table 6: PCR reaction set up.

Step	Temperature ºC	Time
Heat lid	110	
Initial Denaturation	94	2 min
Start cycle (30-40 cycles according to each pair of primers)		
Denaturation	94	30 sec
Annealing	51-57-68	30-60 sec
Extension	72	1min
End cycle		
Final Extension	72	10 min
Hold	4-10	Store

Table 7: PCR Thermocycling Conditions.

PCR product	Forward Primer (5'-3')	Reverse Primerb (5'-3)	Base Pairs (bp)	Cycles	Tm
p110δ KI	GCGTAACAGAGAGCAAAGTCCC	AGGGAACCGCCGTATGAC	WT = 232; HET = 232+404; KO = 404	39	65
p110δ flox/flox	CATGCCTACAGTTGATTAAGT	AAGTTCAAAACCAGCTTGATG	WT = 361; Floxed = 400	20	65
p110δ flox/flox R2	-	TCAGGCCCCAAAGCAGGAAG	Recombined = 477	20	55
p110α-RBD	GGGCAAGTATATTCTGAAAGTGTG TGGCTGTG	CACTCATCCCAAAGGGGGTGAATAT GAGCC	WT = 250; HET = 250 + 300	40	57
p110α loxP	CTGTGTAGCCTAGTTTAGAGCAACC ATCTA	ACAGCCAAGGCTACACAGAGAAACC CTGTCTTG	WT = 400; HET = 400 + 500	40	57
NOD1 WT	GCTTGGCTCCTTTGTCATTG	ACTGCTGCTTGGCTTTATTCTC	WT = 373	10	65-68
NOD1 Mutant	TTGGTGGTCGAATGGGCAGGTA	CGCGCTGTTCTCCTCTTCCTCA	KO = 400	28	60
NOD2 WT	GTCATTTCCTGACCTCTGACC	-	WT = 606	34	60
NOD2 Mutant	GCCTGCTCTTTACTGAAGGCTC	AACCGCATTATTCCATGGGGC	KO = 459	34	60
Rheb flox/flox	GCCCAGAACATCTGTTCCAT	GGTACCCACAACCTGACACC	WT = 653; Floxed = 850	30	51
Villin-Cre	TTCTCC TCT AGG CTC GTC CA	CATGTC CAT CAG GTT CTT GC	Transgene = 195	28	50
Internal Positive control	CTAGGCCACAGAATTGAA AGATCT	GTAGGTGGAAAT TCT AGCATCATCC	Internal positive control = 324	10	65

Table 8: PCR primers used for amplifying mouse genes.

3.4. Mouse strains

To investigate the role of PI3Ks-NODs-mTOR in the intestine, we have used specific transgenic mice strains described in this section. All mice were kept under conventional facilities, fed *ad libitum* and were all backcrossed over n>10 generations on the C57BL/6 background. All animal experimentation protocols carried out in the study, were approved by the local ethics committee and the Home Office (agreement number 70-8462). As a model of injury, we used a model of experimental acute inflammation induced by oral administration of dextran sodium sulphate (DSS) soluble in water for each mouse colony. DSS induces damage to the small intestine and colon, and this is the best-known model utilised in immune studies to investigate acute damaged and microbial induced inflammation, and as a very similar model of human colitis in mice. Other models such as 2,4,6-trinitrobenzene sulfonic acid (TNBS) is only colon specific inflammation, and radiation does cause crypt damage but not relevant microbial mediated inflammation[194]. The mechanism by which DSS induces intestinal inflammation is unclear but is likely the result of damage to the epithelial monolayer lining the small and large intestine allowing the dissemination of bacteria and their inflammatory contents into the underlying tissue such as lamina propria. In our laboratory the mice were given 2.5% DSS for 5 consecutive days in order to establish the same protocol viable for all our mouse models and follow up on preliminary data.

At day 0, 2.5% DSS was freshly dissolved in water and given to the desired group of mice, always having matching numbers, ages, and genotypes for controls (baseline or vehicle). At day 5, DSS was removed from the bottles and replaced with fresh water until day 7. Weights for all mice were checked and recorded daily at the same time. Mice with more than 20% weight loss since day 0 were

euthanised in a CO_2 chamber as per established in my project licence and common ethical procedures in animal research. Mice have undergone 2.5% DSS injury for 5 days and their control counterparts, were euthanised at day 7 in a CO_2 chamber. After euthanasia, mice were kept on ice and dissection was carried for each specimen as follows. First, tail from each specimen was collected for reconfirmation of the genotypes by genomic PCR. Abdominal area was cleaned with 70% ethanol and a small incision was made in order to remove skin carefully and to perform necropscopy aseptically to collect organs including the liver, spleen, and gastrointestinal tract. The duodenal end was grabbed with forceps and the intestine carefully pulled. This action separates most of the mesentery from the intestine while preserving its integrity. Spleens and livers were measured and kept with RNA stabilisation reagent (RNA later) and kept at -80^{o}C for further RNA isolation. The gastrointestinal tract was kept intact and removed gently all the way until the anus in cold PBS in order to measure colon length. Both the small intestine and colon were cleaned and kept in 10 mL of cold PBS until intestines from all specimens were collected.

Once colons were measured and compared within groups for an image capture, a small portion of cecum was collected for further stool analysis as well as 1-2 cm the very end of the rectum in RNA later. At this stage, some intestines were collected for histology (tissue fixation) or for further intestinal epithelial cell isolation. Total of samples collected and number of mice used from each colony engaged for experiments can be found in **Table 9**, **Table 10**, **Table 11**, and **Table 12**. Small intestines and colons engaged for fixation and histology were then washed with cold PBS and fixed with IHC zinc fixative in a Swiss roll, starting with the cecum in the middle and leaving the rectum at the end, for future tissue embedding. Tissues were kept overnight with zinc fixative (BD Bioscience) and replaced with 70% ethanol. Same procedure of fixation was carried out with ~10

cm of small intestines washed once with PBS, starting in the middle with the duodenum, followed by jejunum and finishing with the ileum at the end. About 1-2 cm of ileum were also kept in RNAlater at -80ºC for further RNA isolation and analysis.

3.4.1. Conditional p110δ mutant mouse model

Transgenic p110δ$^{flox/flox}$ mice were generated by Dr. Martin Turner (Babraham Inst. Cambridge) and crossed in our animal facility with Villin-Cre mice (p110δ$^{\Delta IEC}$) from Jackson Laboratory (obtained from Brigitta Stokinger Crick Institute) to study the role of p110δ in the intestinal epithelium. All mice were genotyped (**Figure 25**) and reared in order to obtain a required number of groups and controls for further assay. When indicated, animals were given 2.5% DSS for 5 days and euthanised at day 7. All numbers (n) used, age, treatment given, and experiments engaged are detailed in **Table 9**.

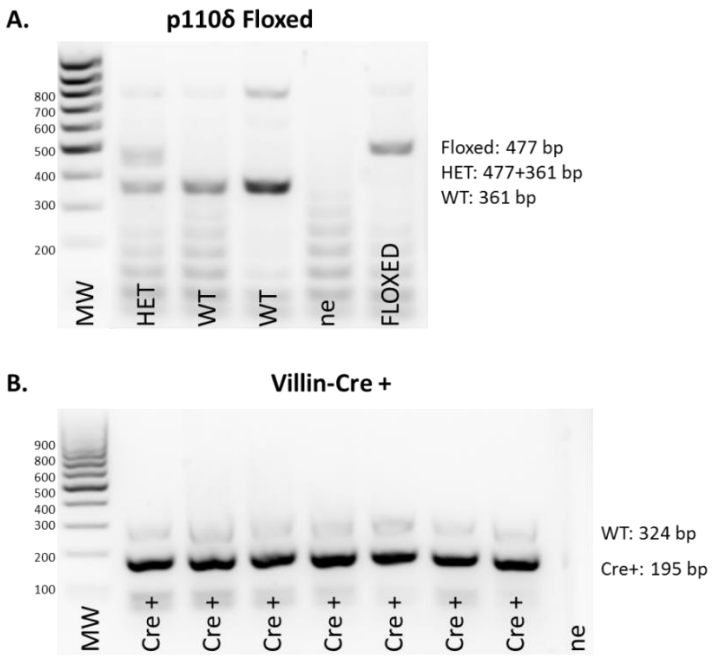

Figure 25: Genoytping results for p110δ$^{flox/flox}$ mice. The 1.5% agarose gels show genotyping results for a group of mice in order to identify if they were **(A)** p110δ$^{WT/WT}$ (WT: 361 bp), p110δ$^{WT/flox}$ heterozygous (HET: 477+361 bp), or p110δ$^{flox/flox}$ (Floxed: 477 bp). **(B)** A separate PCR reaction had to be done for the same group of mice in order to detect if they were Villin-Cre+ (Cre+) or not (WT). MW indicates MassRuler Low Range DNA Ladder (Thermo Scientific #SM0383). Ne inidicates negative control using same PCR reaction with ddH2O instead of DNA in order to confirm no contamination nor unspecific banding detection.

Diet	Genotype	n =	Age (w)	±Colon (cm)
Baseline	p110δ$^{\Delta IEC}$	6	14	10.68
	p110δ$^{flox/flox}$	5	14	9.96
	Villin-Cre	4	14	9.2
DSS	p110δ$^{\Delta IEC}$	10	14	7.8
	p110δ$^{flox/flox}$	4	14	8.13
	Villin-Cre	3	14	8.75
	Total	32		

Table 9: Conditional p110δ mutant mice and controls used in this thesis. The genotype of each mouse strain p110δ$^{\Delta IEC}$, p110δ$^{flox/flox}$, and Villin-Cre used as baseline or after DSS treatment (2.5%), is indicated in this table are indicated in this table together with the

number of mouse used per strain (n), average of age from each mouse strain in weeks old (w), and colon length (cm).

3.4.2. Conditional p110α-RBD mutant mouse model

Conditional transgenic adult male mice Rosa26$^{CreERT2/+}$/p110α$^{RBD/flox}$ (so called p110α$^{RBD/flox}$) and Rosa26$^{CreER/+}$/p110α$^{WT/flox}$ (so called p110α$^{WT/flox}$) were administered with tamoxifen (40 mg/mL) thrice by oral gavage every other day. Tamoxifen was prepared in 5 mL corn oil, previously heated at 42ºC for 30 min. Tamoxifen was added into the warmed corn oil, and then the solution was placed on a rocker at 37ºC for several hours. The solution was kept at 4ºC for up to a month prior to administration. We administered tamoxifen to live mice using oral gavage technique for three times every other day. Following tamoxifen treatment, so called p110α$^{WT/-}$ mice from p110α$^{WT/flox}$ mice, and p110α$^{RBD/-}$ from p110α$^{RBD/flox}$ mice were generated by depleting one copy of p110α by Cre recombinase expressed under the estrogen receptor (ER) induced by tamoxifen (**Figure 26**). Mice were genotyped (**Figure 27**), and weights from each mouse were checked and recorded daily for 15 days due to the established weight loss after tamoxifen treatment. Once mice recovered original weight, they were given 2.5% DSS for 5 days as previously described. All mice used in this study were adult males (14-17 weeks old). All numbers (n) used, age, treatment given, and experiments engaged are detailed in **Table 10.**

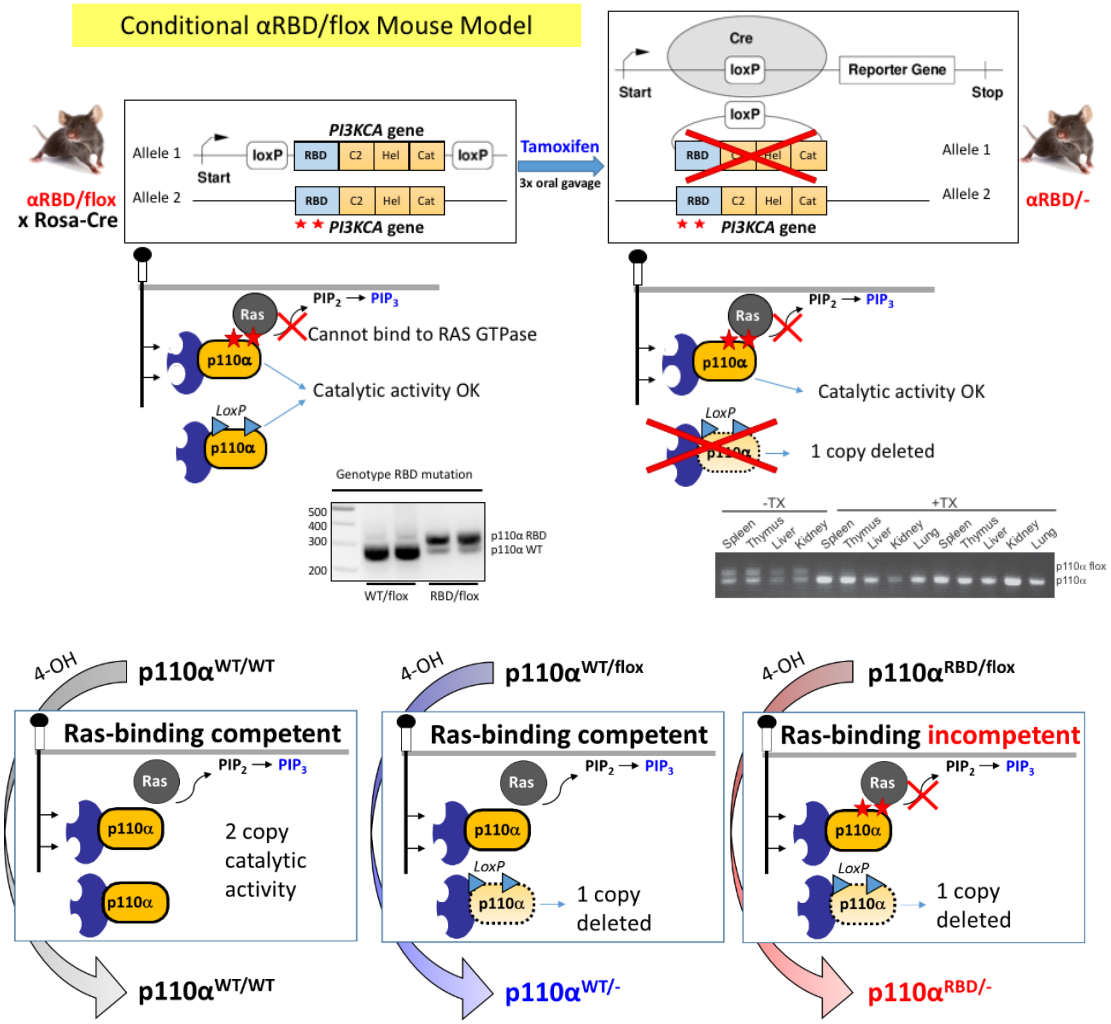

Figure 26: **Gene targeting used for p110α$^{RBD/-}$ and p110α$^{WT/-}$ mice generation. (A)** Scheme showing two-point mutations RBD of *PI3KCA* gene. Arrows indicate the location of loxP site. Inset: genotyping PCR of samples after Cre-mediated excision of the neomycin selection cassette. The upper band represents the mutant allele (containing a residual 30 base pairs of the loxP site). The lower band represents the wild-type *PIK3CA* allele[25]. **(B)** p110α$^{WT/flox}$ and p110α$^{RBD/flox}$ were reared carrying a single floxed *PIK3CA* allele were crossed onto mouse strain, carrying a conditional Cre recombinase (*Cre-ERT2*) allele targeted to the Rosa26 locus. Tamoxifen administration efficiently removed floxed *PIK3CA* allele in tail skin (Medrano et al.) and tissues. Illustrated by Laura Medrano-González.

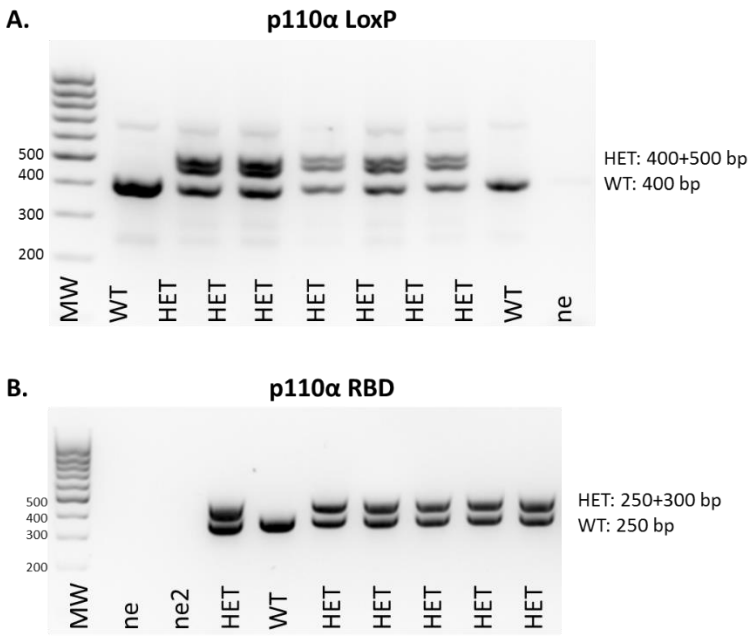

Figure 27: Genotyping results for p110α-LoxP and p110α-RBD mice. The 2% agarose gels show genotyping results for a group of mice in order to identify if they were **(A)** p110α without LoxP (WT: 400 bp), or p110α-LoxP heterozygous (HET: 400+500 bp). **(B)** A separate PCR reaction had to be done for the same group of mice in order to detect if they were p110α-RBD heterozygous mice (HET: 250+300 bp) or p110α-WT mice (WT: 250 bp). MW indicates Mass Ruler Low Range DNA Ladder. Ne indicates negative control using same PCR reaction with ddH2O instead of DNA in order to confirm no contamination nor unspecific banding detection.

Diet	Genotype	n =	Age (w)	±Colon (cm)
Baseline	$p110\alpha^{WT/WT}$	6	±13	11.96
	$p110\alpha^{WT/flox}$	13	±14	11.13
	$p110\alpha^{RBD/flox}$	6	±12	11.33
	$p110\alpha^{WT/WT}$ +TAM	8	±13	11.96
	$p110\alpha^{WT/-}$	12	±15	11.49
	$p110\alpha^{RBD/-}$	12	±15	11.44
DSS	$p110\alpha^{WT/WT}$	7	±14	10.64
	$p110\alpha^{WT/flox}$	9	±15	8.93
	$p110\alpha^{RBD/flox}$	8	±17	9.42
	$p110\alpha^{WT/WT}$ +TAM	8	±14	8.94

$p110\alpha^{WT/-}$	7	±14	8.21
$p110\alpha^{RBD/-}$	9	±14	7.94
Total	105		

Table 10: Conditional p110α-RBD mutant mice and controls used in this thesis. The genotype of each mouse strain with or without tamoxifen given: $p110\alpha^{WT/WT}$, $p110\alpha^{WT/flox}$, $p110\alpha^{RBD/flox}$, $p110\alpha^{WT/WT}$ + tamoxifen (TAM), $p110\alpha^{WT/-}$, and $p110\alpha^{RBD/-}$ used as baseline or after DSS treatment (2.5%); are indicated in this table together with the number of mouse used per strain (n), average of age from each mouse strain in weeks old (w), and colon length (cm).

3.4.3. Conditional Rheb mutant mouse model

$Rheb^{flox/flox}$ mice were generated by Dr. Paul Worley (John's Hopkins, USA) and crossed in our animal facility with Villin-Cre mice from Jackson Laboratory to study the role of Rheb in the intestinal epithelium. Healthy age and sex-matched mice $Rheb^{\Delta IEC}$, $Rheb^{flox/flox}$, and Villin-Cre; were reared in conventional housing facility and genotyped and were then subjected to 2.5% DSS in drinking water or vehicle for 5 days to induce acute chemically-induced colitis. All mice were genotyped (**Figure 28**) and reared in order to obtain a required number of groups and controls for further assay. All mice health status was checked daily and euthanised at day 7. All numbers (n) used, age, treatment given, and experiments engaged for are detailed in **Table 11**.

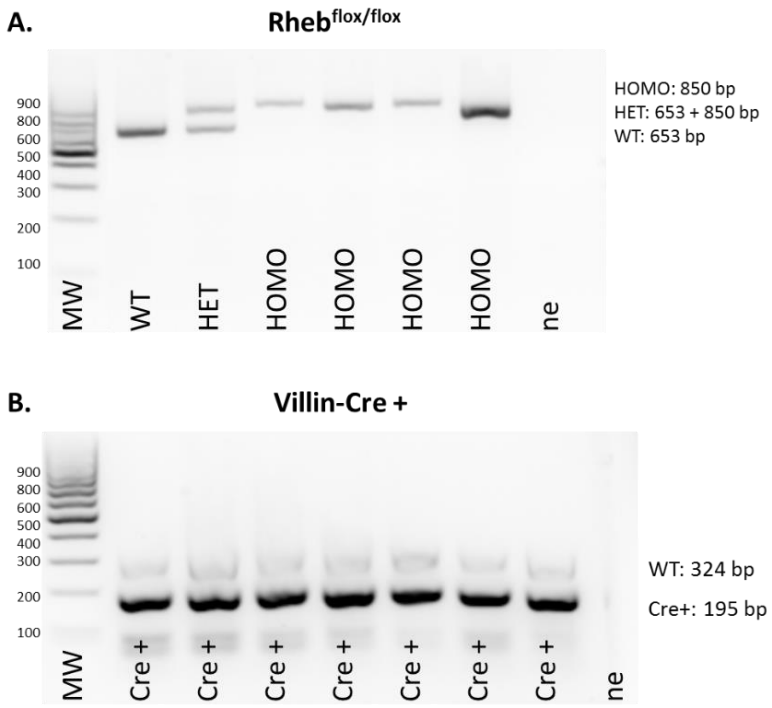

Figure 28: Genoytping results for Rheb$^{flox/flox}$ mice. The 1.5% agarose gels show genotyping results for a group of mice in order to identify if they were **(A)** Rheb$^{WT/WT}$ (WT: 653 bp), Rheb$^{WT/flox}$ heterozygous (HET: 653 + 850 bp), or Rheb$^{flox/flox}$ (Floxed: 477 bp). **(B)** A separate PCR reaction had to be done for the same group of mice in order to detect if they were Villin-Cre+ (Cre+) or not (WT). MW indicates MassRuler Low Range DNA Ladder. Ne inidicates negative control using same PCR reaction with ddH2O instead of DNA in order to confirm no contamination nor unspecific banding detection.

Diet	Genotype	n =	Age (w)	±Colon (cm)
Baseline	Rheb$^{\Delta IEC}$	11	±15	10.87
	Rheb$^{flox/flox}$	7	±18	9.75
	Villin-Cre	4	±16	9.71
DSS	Rheb$^{\Delta IEC}$	16	±15	6.25
	Rheb$^{flox/flox}$	11	±16	7.33
	Villin-Cre	7	±16	8
	Total	56		

Table 11: Conditional Rheb mutant mice and controls used in this thesis. The genotype of each mouse strain: Rheb$^{\Delta IEC}$, Rheb$^{flox/flox}$, Villin-Cre used as baseline or after DSS treatment

(2.5%); are indicated together with the number of mouse used per strain (n), average of age from each mouse strain in weeks old (w), and colon length (cm).

3.4.4. NOD1^{KO} and NOD2^{KO} mouse model

Card4/Nod1-deficient (NOD1^{KO}) mice were generated by Millennium Pharmaceuticals Boston. Card15/Nod2-deficient C57BL/6J (NOD2^{KO})[195] mice were provided by J.-P. Hugot (Hôpital Robert Debré, Paris, France). Healthy age and sex-matched NOD1^{KO}, NOD1^{KO} and WT mice; reared in conventional housing facility and genotyped (**Figure 29**), were orally treated with 2.5% DSS in drinking water or vehicle for 5 days to induce acute chemically-induced colitis. The health status of all mice was checked daily and euthanised at day 7. All numbers (n) used, age, treatment given, and experiments engaged for are detailed in **Table 12**.

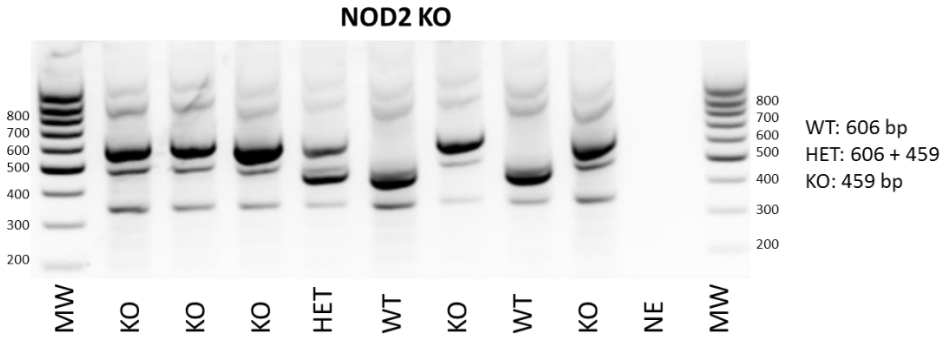

Figure 29: Genoytping results for NOD2^{KO} mice. The 1.5% agarose gel shows genotyping results for a group of mice in order to identify if they were **(A)** WT (606 bp), HET heterozygous (606 + 459 bp), or NOD2^{KO} (459 bp). MW indicates MassRuler Low Range DNA Ladder. Ne inidicates negative control using same PCR reaction with ddH2O instead of DNA in order to confirm no contamination nor unspecific banding detection.

Diet	Genotype	n =	Age (w)	±Colon (cm)
Baseline	NOD1^{KO}	6	17	10.1
	NOD2^{KO}	10	15	9.84
	WT	14	13	10.98
DSS	NOD1^{KO}	6	17	7.8
	NOD2^{KO}	13	15	7.85
	WT	14	13	9.08
Total of mouse used		63		

Table 12: NOD1^{KO}, and NOD2^{KO} mice used in this thesis. The genotype of each mouse strain: NOD1^{KO}, NOD2^{KO}, WT used as baseline or after DSS treatment (2.5%); are indicated in this table together with the number of mouse used per strain (n), average of age from each mouse strain in weeks old (w), and colon length (cm).

3.1. Enzyme-linked immunosorbent assay

Enzyme-linked immunosorbent assays (ELISAs), were used to quantify and compare secretory cytokines from mouse intestinal explants. Colon and small intestines were dissected, washed in PBS, sectioned, and weight. Similar weights (70-100 mg of tissue) of colon and small intestine explants from each mouse were cultured 18 h prior to bacterial ligand stimulation: LPS (1 µg/mL), MDP (30 µg/mL); or basal levels at 37°C in DMEM media. The ELSA kits used are described at **Table 19**. High affinity 96-well plates were coated with coating antibody diluted in PBS pH 7.2. Coated plates were covered and incubated overnight at 4°C. Plates were washed 4 times with TBS-T and blocked with 300µl of PBS 1% BSA for at least 2 h at room temperature. Samples were prepared in duplicate with 2-fold dilutions made in DMEM media. Standards were made in eight 2-fold dilutions in DMEM media. Once blocked, plates were washed again 4 times with TBS-T. Samples and standards were added (100 µl/well) and incubated for 2 h at room temperature. Detection was achieved by adding detection antibody diluted in PBS 1% BSA and incubated for 2 h at room temperature. The reaction was visualized by the addition of 50µl chromogenic liquid substrate Tetramethylbenzidine (TMB) for 10 min under the colour change was observed. The reaction was stopped with 50 µl of 2N H_2SO_4 solution. An ELISA plate reader measured an absorbance at 450nm. Due to the different colon sample weight per condition, each sample was normalised according to their initial weights measured. A positive signal was defined as an OD450 $\geq 2 \times$ plate background.

3.1. Immunohistochemistry

Mouse under 2.5% DSS injury for 5 days together with their baselines control, were euthanised at day 7 with a CO_2 chamber. Straight after euthanasia, mice were kept on ice and dissection was carried for each specimen as described in **Section 3.3**. Colons already measured and engaged for histology, were washed with cold PBS and fixed with IHC zinc fixative in a Swiss roll, starting with the cecum in the middle and leaving the rectum at the end, for future wax embedding. Tissues were kept for 6 – 8 h with zinc fixative and replaced with 70% ethanol. Same procedure of fixation was carried out with ~10 cm of small intestines once washed with PBS. Small intestines were placed in histocassettes starting in the middle with the duodenum, followed by jejunum and finishing with the ileum at the end. Once fixed, samples were sent for tissue processing & embedding of paraffin block at the BCI Pathology Services. Cuts of 4 µm size were stained for hematoxylin and eosin (H&E), extra slides unstained were requested for further specific antibody staining (data now shown). Sections were scanned using NanoZoomer S210 digital microscope and pictures were analysed with NDP.view2 software. Semi-quantitative analyses were carried with the scoring described in **Table 13**. Each section from 4 different mouse of each strain and treatment, was triple blinded scored by the pathologist expert Dr. David Dombrowicz as well as the author of this thesis independently.

Score	Inflammation	Crypt Depth	Disrupted Villi / Crypt Loss	Hyperplasia
0-1	None	Normal	None	None
2	Mild	Abnormal	Mild	Mild
3	Moderate	Crypt loss; surface epithelium present	Moderate	Moderate
4-5	Severe	Crypt loss and surface epithelium loss	Severe	Severe

Table 13: Semi-quantitative scoring for H&E staining from colon and small intestine used in all mouse strains.

3.2. IECs isolation from murine intestine

Isolation of IECs from murine intestine, was carried as suggested by several protocols and relevant laboratories in the field. The main protocol followed for further cell sorting with specific cell biomarkers was optimised and adapted as described in this section. Mice were euthanised by CO_2 asphyxiation, small intestine and colon were collected as previously described in (**Section 3.3.**). After dissection, intestines were kept in cold PBS. The lumen of the intestines was flushed out with ice-cold PBS using a 10 mL syringe and 21G needle. Once cleaned, the intestines were opened longitudinally, cut into 5 mm pieces, and placed in a 15 mL conical tube containing 10 mL of dissociation reagent #1 (PBS, 30mM EDTA, 1.5 mM DTT). Intestines from each mouse were incubated for 20 min on ice. The fragments were vigorously homogenised by pipetting up and down into a 10 mL pipette 15 times. Fragments were left to settle down by gravity for 30 sec, dissociation reagent #1 was discarded without taking any fragments and 6 mL of dissociation reagent #2 (PBS, 30 mM EDTA) was added. Intestinal fragments were incubated at 37ºC for 10 min and homogenised vigorously every 30 sec. IECs were now dissociated and intestinal tissue fragments left were removed. IECs were centrifuged at 1000 x g for 5 min at 4°C. Pellets containing IECs were washed in 10 mL of PBS 10% FBS and centrifuged again at 1000 x g for 5 min at 4°C. Pellets were washed in 10 mL HBSS with 0.8 mg/mL of Dispase and incubated for 10 min at 37°C in a water bath. Conical tubes were homogenised vigorously every 2 min for a total of 4X, 10% FBS and 10 mg/mL DNase were added to each cell solution. Cell solutions were passed through a 70 μm filter into 50 mL conical tubes and centrifuged at 1000 x g for 5 min at 4°C. Supernatants were removed and cells were washed in 10 mL of HBSS 10% FBS to rinse Dispase. At this stage, IECs isolation from each mouse were counted and 300,000 cells/well were plated in a 96-well U-bottom plate for further fluorescence-activated cell sorting (FACS) staining.

3.3. Flow cytometry

In order to stain specific cell subpopulations from murine IEC isolation for further FACS analysis, I developed the following assay for FACS staining. IECs were already isolated and plated as previously described (**Section 3.7**). The 96-well U-bottom plates containing 300,000 IECs cells/well were centrifuged at 2000 rpm for 5 min at 4°C. Supernatants were discarded gently in the sink and IECs were resuspended in PBS 1% BSA or PBS FcR blocking reagent and incubated for 20 min on ice. After blocking, cells were centrifuged at 2000 rpm for 5 min at 4°C and supernatants were discarded gently in the sink. A cocktail of primary antibodies (**Table 20**) was added 100 µl/well and incubated on ice for 30 min in dark. Cells were centrifuged at 2000 rpm for 5 min at 4°C, supernatants were discarded gently in the sink and IECs cells were fixed in Fixation/Permeabilisation buffer for 20 min on ice. Antibodies for intracellular staining were used together with the FOXP3 Permeabilisation Buffer following the manufacturer's instructions and incubated for 45 min on ice. If secondary antibodies were required, they were added at this stage and incubated for 30 min on ice. Samples were kept no longer than one week at 4°C in Permabilisation buffer until acquired using LSR Fortessa (Flow Cytometry Core Facility, Charterhouse Square).

Flow cytometry panels and gating strategy were defined according to previous set up experiments and fluorescence minus one (FMO) controls. Data was analysed using FlowJo software (Tree Star, USA). Total count of each population was obtained, and results were expressed as total number of live cells, percentage of $EpCAM^{+}CD45^{-}$ live cells or percentage of the parent populations. For total number (used on small intestine and colonic epithelial cells), percentage of live cells from the analysis were multiplied by the cell count obtained after tissue

digestion and divided by the weight of the tissue fraction used for digestion/total organ. In order to quantify proliferative levels, CBCs secretory/Paneth cells; and Lgr5+ stem cell population, the gating strategy and analysis used for each mouse strain and experiment is described in the results section.

3.4. Real-time quantitative PCR analysis

In order to quantify relative expression of specific transcription factors in the ileum from each mouse colony engaged for acute chemically induced DSS injury, and study their differences, real-time quantitative PCR (RT-PCR) analyses were carried out. RNA isolation from ileum previously collected and kept with RNAlater at -80ºC, was carried out following PureLink RNA mini kit protocol. Tissues were first weight (mg) and homogenised as indicated with lysis buffer in Precellys steel beats (2.8 mm 2 mL). After RNA isolation, RNA quality (260/280) and concentration (ng/mL) per sample were obtained using UV-Vis spectrophotometer Nanodrop. Dilutions per sample were calculated in order to use 1-2 μg/mL of RNA for further transcription to cDNA using SuperScript™ II Reverse Transcriptase kit. RNA is very unstable and susceptible, for this reason, samples were always processed on ice rapidly. Once RNA was reverse transcribed to cDNA, the RT-PCR reaction was prepared for each sample using SYBR green protocol for a final volume of 25 μl (**Table 14**). All cDNA samples were processed with each pair of primers and thermocycling conditions are described in **Table 15** and **Table 16**.

The Cq or Ct value obtained after RT-PCR reaction, refers to the cycle quantification value, which is the PCR cycle number at which the sample's reaction curve intersects the threshold line. This value tells how many cycles it took to detect a real signal from your samples. Once the Ct values were obtained from the PCR reaction, the following data analysis was performed using the formula $\Delta Ct = C_{(TR)} - C_{(REF)}$; in which $C_{(TR)}$ refers to the Ct value reported our targeted gene, and $C_{(REF)}$ refers to the Ct value reported our reference gene or housekeeping (GAPDH in this case). Once the ΔCt value was obtained, $\Delta\Delta Ct = \Delta Ct_{TR} - \Delta Ct_{REF}$ was

calculated for further $2^{-\Delta\Delta Ct}$ relative expression normalised from control mouse strain and vehicle treatment. An example of Ct values obtained, and control are shown in **Figure 30**.

Component	25 µl Reaction	Final Concentration
SYBR Green	12.5 µl	1X
Forward primer	1 µl	10 uM
Reverse primer	1 µl	10 uM
cDNA sample (1-2 µg/mL)	5 µl	100 ng
RNase-free water	5.5 µl	Bring up to final volume

Table 14: RT-PCR reaction set up.

Step	Temperature ºC	Time
Initial Denaturation	95	15 min
Start cycle (40 cycles)		
Denaturation	94	15 sec
Annealing	65	30 sec
Extension	72	30 sec
End cycle		
Final Extension	95	15 sec
	60	15 sec
	95	15 sec

Table 15: RT-PCR thermocycling conditions.

RT-PCR product	Description	Base pair (bp)
Wdr43 Forward	AGTCACACGAGAGGCCTGGCTT	22
Wdr43 Reverse	GCCTCTTGTTTTCTGGCACAGGG	23
Bmi1 Forward	TCCCCACTTAATGTGTGTCCT	21
Bmi1 Reverse	CTTGCTGGTCTCCAAGTAACG	21
Ascl2 Forward	AAGCACACCTTGACTGGTACG	21
Ascl2 Reverse	AAGTGGACGTTTGCACCTTCA	21
Lgr5 F	CCTACTCGAAGACTTACCCAGT	22
Lgr5 R	GCATTGGGGTGAATGATAGCA	21
Hprt F	TCAGTCAACGGGGGACATAAA	21
Hprt R	GGGGCTGTACTGCTTAACCAG	21
Muc2 F	ATGCCCACCTCCTCAAAGAC	20
Muc2 R	GTAGTTTCCGTTGGAACAGTGAA	23
Mmp7 F	CTGCCACTGTCCCAGGAAG	19
Mmp7 R	GGGAGAGTTTTCCAGTCATGG	21
Notch2 F	GACTGCCAATACTCCACCTCT	21
Notch2 R	CCATTTTCGCAGGGATGAGAT	21
Olfm4 Forward	CAGCTGCCTGGTTGCCTCCG	20
Olfm4 Reverse	GGCAGGTCCCATGGCTGTCC	20
Ki67 Forward	CCTTTGCTGTCCCCGAAGA	19
Ki67 Reverse	GGCTTCTCATCTGTTGCTTCCT	22
Epcam Forward	TTGCTCCAAACTGGCGTCTA	20
Epcam Reverse	ACGTGATCTCCGTGTCCTTGT	21
RTc-Myc1	CTGGATTTCCTTTGGGCGTT	20
RTc-Myc2:	TGGTGAAGTTCACGTTGAGGG	21
RTc-Myc probe	AAACCCCGCAGACAGCCACGAC	22

Table 16: Primers used for RT-PCR.

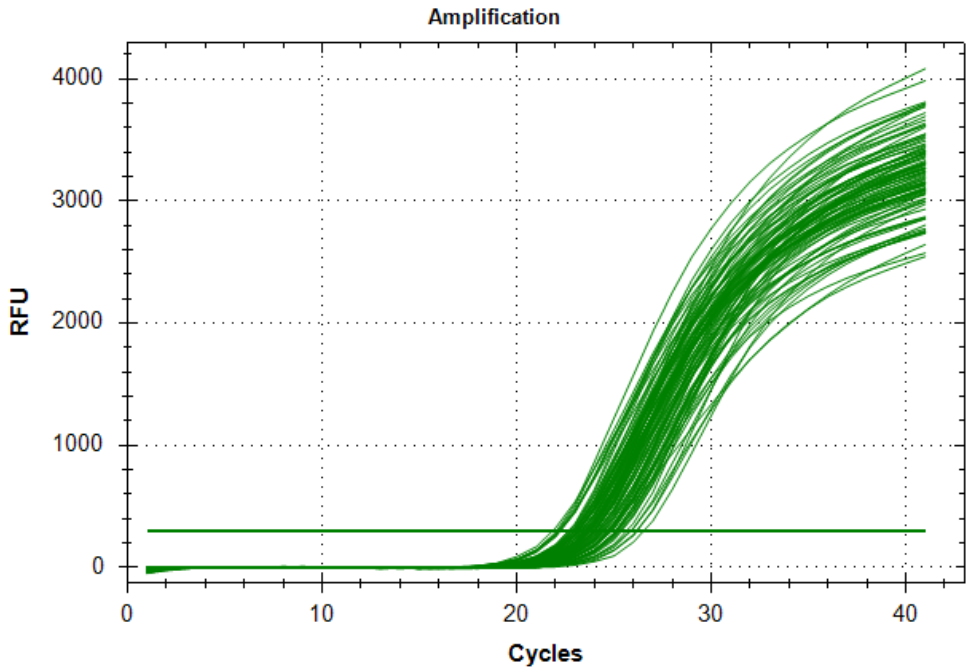

Figure 30: Example of melt curve and control line after gene amplification using housekeeping and target

3.5. Statistics

Statistical analysis was performed using Graphpad Prism 7 and 8 software. Data are expressed as mean ± standard error of mean (SEM). For cytokine comparisons, non-parametric data (DAI values), and colon length graphs; linear regression with a 95% confidence interval, and unpaired, two-tailed Student's *t*-test were used, unless indicated otherwise. One-way analysis of variance (ANOVA) was used in circumstances where three or more groups were being tested with one variable (histological score, Western blot quantification, flow cytometry analysis, and RT-PCR assays). Two-way ANOVA was used in circumstances where two or more groups existed with two variables (e.g. time and treatment) with Bonferroni post-hoc test.

3.6. Materials

3.6.1. Reagents

Name	Source	Catalogue
1 M Tris-HCL pH 6.8	Severn Biotech	20-7901-10
1 M Tris-HCL pH 7.5	Severn Biotech	20-7901-10
1 M Tris-HCL pH 8	Severn Biotech	20-7901-10
1.5 M Tris-HCL pH 8.8	Severn Biotech	20-7900-10
10X Titanium Taq PCR Buffer	Clontech	S1793
200µl Round Gel-Loading Tip	Starlab	I1022-0600
30% Acrylamide/Bis Solution	Serva	10688.01
50X Titanium Taq DNA polymerase	Clontech	S1792
Agarose	Bioline	41025
Albumin	Sigma-Aldrich	A7284-50ML
All Blue Prestained Protein Standard	Bio-Rad	1610393
Ammonium persulphate solution (APS)	Sigma-Aldrich	A3678
Bovine serum albumin (BSA)	Sigma-Aldrich	A79006
CD326 (EpCAM) MicroBeads, mouse	Miltenyi biotec	130-105-958
Complete EDTA tablets	Roche	04693116001
cOmplete EDTA-free protease inhibitor	Sigma Aldrich	11873580001
Corn oil	Sigma-Aldrich	C-8267
Dextran sulfate sodium salt colitis grade (DSS)	Mp biomedicals	0216011080
Dimethyl sulfoxide (DMSO)	Sigma-Aldrich	D2650-100ML
Dispase		
Dithiotreitol (DTT)	Thermofisher	R0862-25gr
DNase I recombinant, RNase-free	Sigma-Aldrich	4716728001
dNTP Mix (2 mM each)	Thermofisher	R0242
Dulbecco's modified eagle's medium (DMEM)	Sigma-Aldrich	D5796
Earle's balanced salt solution (EBSS)	Thermofisher	240-10-043

EDTA complete tablets	Roche	04693116001
FBS dialyzed without nutrients	Thermofisher	A3382001
Fetal bovine serum dialyzed (FBS)	Thermofisher	
Fixation/Permeabilization buffer	eBioscience	421402
FOXP3 bermeabilization buffer	eBioscience	421402
FUJIFILM Super RX-N 18x24	Fisher scientific	100NIF
Gel Red Nucleic Acid gel stain	Biotium	89139-140
Hank's balanced salt solution (HBSS)	Thermofisher	14025092
HEPES (1 M)	Thermofisher	15630080
Hydrogen peroxide		
IGEPAL CA630	Sigma-Aldrich	I8896-50ML
IHC Zinc Fixative	BD Pharmingen	550523
L-glutamine	Sigma-Aldrich	G7513
L-leucine	Sigma-Aldrich	61819-25G
Luminol	Sigma-Aldrich	A8511-25G
Non-essential amino acids 100X (NEAAs)	Thermofisher	1140-035
NT Nitrocellulose Transfer Membrane	Pall Corporation	66485
p-Coumaric acid	Sigma-Aldrich	C9008-25G
Paraformaldehyde solution 4% in PBS	Santa Cruz	sc-281692
Penicillin-streptomycin 100X	Sigma-Aldrich	P4333-100ML
Phosphatase Inhibitor Cocktail Set II	EMD Millipore	524625-1SET
Phosphatase buffered saline (PBS)	Sigma-Aldrich	D8537
Power SYBR® Green PCR Master Mix (5ml)	Thermofisher	4367659
Protease from Streptomyces griseus	Sigma-Aldrich	P6911-100MG
Proteinase K from Tritirachium album	Sigma-Aldrich	P6556-100MG
RNA Stabilization Reagent RNAlater	Qiagen	76106
Sodium azide	Sigma-Aldrich	S2002-100G
Sodium dodecyl sulfate (SDS)	Sigma-Aldrich	L3771
Sodium fluoride (NaF)	Sigma-Aldrich	S7920
Sodium orthovanadate (Na_2VO_3)	Sigma-Aldrich	S6508-50G
Sodium pyruvate 100 mM 100X	Thermofisher	11360070

Tamoxifen	Sigma-Aldrich	T-5648
TEMED	Sigma-Aldrich	BCBR7160V
TMB Chromogen Solution (for ELISA)	Thermofisher	2023
Trichloroacetic acid (TCA)	Sigma-Aldrich	T6399
Trypan blue solution, 1:2 in PBS	Sigma-Aldrich	T8154
Trypsin-EDTA (0.05%), phenol red	Thermofisher	25300062
Tween20	Sigma-Aldrich	P1379
UltraPure™ 0.5M EDTA, pH 8.0	Invitrogen	15575-038
Vectashield Hardset Antifade Mounting Medium with Phalloidin	Vector Laboratories	LS-J1032
β-Glycerophosphate disodium salt hydrate	Sigma-Aldrich	G-9891

Table 17: Reagents purchased in our laboratory and used in this study.

3.6.2. Buffers and solutions

Name	Description	
0.05% TBS-Tween	30 mL 5 M NaCl; 10 mL 1 MTris pH 8; 0.5 mL Tween20 in ddH_2O	
10% APS	10% in ddH_2O	
10% SDS	10% in ddH_2O	
10% SDS-PAGE	For 50 mL: 20 mL ddH_2O; 16.6 mL 30% Acrylamide; 12.5 mL 1.5 M Tris pH 8.8; 0.5 mL 10% SDS; 0.5 mL 10% APS; 0.02 mL TEMED	
10X Running buffer	For 1000 mL ddH_2O: 142 g Glycine; 30.2 g Tris; 10 g SDS	
10X Transfer buffer	For 1000 mL ddH_2O: 144 g Glycine; 30 g Tris	
1M DTT	154.2 mg DTT in 1 mL ddH_2O	
1X Transfer buffer	100 mL 10X Transfer buffer; 200 mL 100% ethanol; 700 mL ddH_2O	
1X Tris-acetate-EDTA (TAE)	20 mM Tris-acetate; 1 mM Na_2	
4X sample loading	1X: 200 mM Tris pH 6.8; 400 mM DTT; 8% SDS; BPBlue; 40% glycerol; Store at -20 C	For 60 mL: 12 mL Tris pH 6.8; 3.69 g DTT; 4.8 g SDS; 0.02 – 0.06 g BPBlue; 24 mL glycerol; 24 mL ddH_2O
500 mM luminol	0.886 g in 10 mL DMSO	
5M NaCl	292 g NaCl in 1000 mL ddH_2O	
Enhanced chemi luminescence solutions (ECL)	Solution A: 20 mL of 1M Tris-HCl pH 8.5; 180 mL ddH_2O; 120 µl 30% ddH_2O_2	Solution B: 20 mL 1M Tris-HCl pH 8.5; 178 mL ddH_2O; 1 mL luminol; 880 µl coumaric acid
	Make solutions separately and store at 4ºC in light protected bottles. For ECL mix solutions in equal parts	

Lysis buffer	20 mM Tris HCl pH 7.5; 150 mM NaCl; 1 mM EDTA 1% IGEPAL; 10% glycerol. supplemented with: 10 mM β-glycerolphospate; 10 mM NaF; 10 mM Na_2VO_3 in ddH_2O supplemented with:1X Protease inhibitor cocktail tablet; 1X Phosphatase Inhibitor Cocktail Set II
Na_2VO_3	Sodium orthovanadate, 10mM final from a stock of 0.5M stock dissolved in ddH_2O
NaF	10mM final from 0.5M stock dissolved in ddH_2O
p-Coumaric acid	0.09 M in DMSO
Stacking gel	For 10 mL: 6.8 mL ddH_2O; 1.7 mL 1 M Tris pH 6.8; 0.1 mL 10% SDS; 0.1 mL 10% APS; 0.01 mL TEMED
Stripping buffer	5% TCA in ddH_2O
TE Buffer	500 µl 1M Tris pH 8; 100 µl 0.5 M EDTA; mL ddH_2O

Table 18: Buffer and solutions prepared in our laboratory.

3.6.3. Kits and other materials

Name	Source	Catalogue
Mouse EGF DuoSet ELISA	R & D Systems	DY2028
Mouse Epiregulin DuoSet ELISA	R & D Systems	DY1068
Mouse IL-1 beta/IL-1F2 DuoSet ELISA	R & D Systems	DY401
Mouse IL-10 DuoSet ELISA	R & D Systems	DY417
Mouse IL-33 DuoSet ELISA	R & D Systems	DY3626-05
Mouse IL-6 DuoSet ELISA	R & D Systems	DY406
Pierce™ BCA Protein Assay Kit	Thermofisher	23227
Precellys steel kit 2.8mm 2mL beats		
PureLink™ RNA Mini Kit	Thermofisher	2183018A
SuperScript™ VILO™ cDNA Synthesis Kit	Thermofisher	11754050

Table 19: Assays and kits used in the materials and methods section.

3.6.4. Antibodies

Name	Supplier	Catalogue	Dilution	Application
AKT Total	Cell signalling Biotech. (CSB)	4658	1/1000	WB
Anti-CARD15 (NOD2)	Abcam	ab124348	1/500	WB
Anti-Mouse IgG HRP	GE Healthcare	NXA931V	1/5000	WB
Anti-PI3Kinase p110α	CSB	4249	1/1000	WB
Anti-PI3Kinase p110β	Santa cruz Biotech	sc-602	1/750	WB
Anti-PI3Kinase p110γ	CSB	4252s	1/1000	WB
Anti-PI3Kinase p110δ	Abcam	ab1678	1/1000	WB
Anti-Rabbit IgG HRP	GE Healthcare	NA934	1/5000	WB
Anti-Rat IgG HRP	GE Healthcare	NA935V	1/5000	WB
APC anti-mouse EpCAM	Biolegend	118214	1/200	FC
BV605 anti-mouse CD45	Biolegend	109841	1/200	FC
CARD9 (NOD1)	Abcam	ab122835	1/500	WB
GAPDH	Abcam		1/1000	WB

IKKα/β Total	CSB		1/1000	WB
Ki-67 mAb (7B11), FITC	eBioscience		1/200	FC
Lysozyme	Dako	A0099	1/200	FC, IHC, IF
Mouse Lgr5/GPR49	R & D Systems	MAB8240		FC, IHC, IF
p38 Total	CSB	8690	1/1000	WB
p4EBP1	CSB	9456		WB
p4EBP1 Ser 65	CSB	9451		WB
p4EBP1 Thr37/46	CSB	2855		WB
p70 S6K Total	CSB	2708	1/2000	WB
p85	CSB	4257S	1/1000	WB
p-AKT Ser473	CSB	4060	1/1000	WB
p-AKT Thr307	CSB		1/500	WB
PE anti-mouse CD24	Biolegend	138503	1/200	FC
p-IKKα/β Ser176/Ser177	CSB	2078	1/750	WB
p-mTOR Ser2448	CSB	5536		WB
p-p38 Thr180/Tyr182	CSB	9211	1/1000	WB
p-p70 S6K Ser 371	CSB	9208		WB
p-p70 S6K Thr 389	CSB	9205	1/750-	WB
p-p70 S6K Thr421/Ser424	CSB	9204		WB
p-S6Ribosomal 240/244	CSB	2215		WB
p-S6Ribosomal S235/236	CSB	4858	1/2000-	WB
p-TSC2 T1462	CSB	3617		WB
S6 Ribosomal Total	CSB	2217	1/2000	WB
TSC2 Total	CSB			WB
Anti-Rabbit AF 594	eBiosciences			FC
eF780 R780	eBiosciences		1/500	FC

Table 20: Antibodies used for cell signalling, immunofluorescence and cell sorting.

4.RESULTS

"Once you see results, it becomes an addiction"

4.1. The role of p110δ PI3K in gut immunology

4.1.1. Inactivation of p110δ PI3K isoform in transgenic mice results in increased susceptibility after acute chemical induced intestinal inflammation

In order to understand the role of p110δ in gut immunity, mice expressing an inactive version of the gene encoding p110δ (also called p110δ KI), were reared and observed daily in conventional animal facility. To investigate the role of p110δ in the intestine after acute inflammation, we have used a model of experimental colitis induced by oral administration of DSS soluble in water. DSS is commonly used in immune studies to cause acute chemically induced damage to the epithelial barrier, leading to bacterial translocation and inflammation, which is considered a similar model of human colitis in mice. The mechanism by which DSS induce intestinal inflammation is imprecise but is likely that the activation of inflammasome pathway[196], following damage to the epithelial monolayer lining of the small and large intestine might be an important driver. The DSS mediated damage and subsequent activation of the inflammasome in epithelial cells, results in cell death and dissemination of bacteria and their microbial contents into the underlying lamina propria, activating immune cells[196,197]. The p110δ KI mice showed significantly worst pathological signs of intestinal damage following 5 days of 2.5% DSS-injury compared to WT mice, marked by increased weight loss and colon shortening (**Figure 31**), overall resulting in significantly higher DAI (disease activity index). These results obtained in collaboration with Dr. María González Núñez (unpublished data for manuscript from our laboratory in preparation), indicated that p110δ kinase activity is required for restrain intestinal injury

responses that ensued after acute chemically induced gut injury by promoting resolution processes.

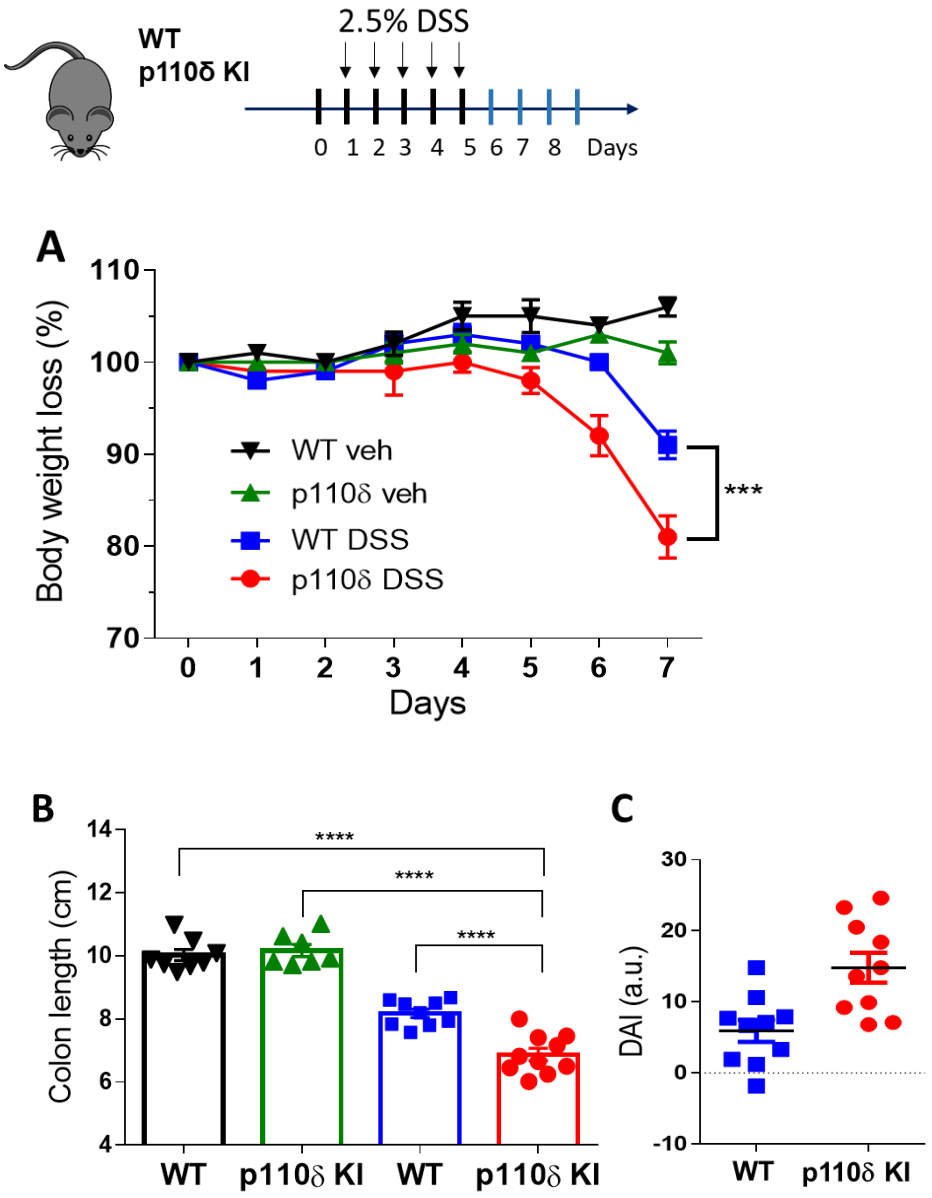

Figure 31: The p110δ inactivation in mice results in a significantly heightened colonic inflammation and after acute chemically DSS-induced colitis. Healthy age and sex-matched WT and p110δ KI mice, reared in conventional housing facility were orally treated with 2.5% DSS in drinking water for 5 days or vehicle (veh) to induce acute chemically-induced colitis. The mice engaged for acute analysis were euthanised at day 7. **(A)** The graph represents the percentage of weight loss for 7 days ensuing DSS injury (n=23 mice per

mouse strain). **(B)** The bar chart represents mean ± SEM colon length from indicated mouse strain. **(C)** The bar chart represents DAI (disease activity index), calculated in colon tissue from indicated mouse strains under DSS-injury (n=9-10 mice per mouse strain). **(A-B)** Statistical analysis of data expressed as mean ± SEM was **(A)** ***p<0.001 by Two-way ANOVA, and **(B)** ****p<0.0001 by Student t-test, and **(C)** **p<0.01 by Student t-test.

4.1.2. Genetic inactivation of p110δ PI3K kinase activity in mice results in hyper-activation of inflammatory responses mediated by bacterial ligand LPS *ex vivo*

Colon explants from p110δ KI mice were isolated and stimulated with LPS (TLR4 ligand) or vehicle (PBS) in medium, 18 h later supernatants from explants were collected. Inflammatory responses under basal (medium alone) and LPS-activated conditions were quantified using ELISA (see **Section 3.6**). We observed that colon explants from p110δ KI mice were marked by significantly increased inflammatory cytokines (IL-1β, and IL-6) but decreased anti-inflammatory cytokines (IL-10) compared to colon explants from WT mice (**Figure 32**). These results indicated that p110δ PI3K isoform regulates inflammatory responses to bacteria-derived ligands in the intestinal epithelium.

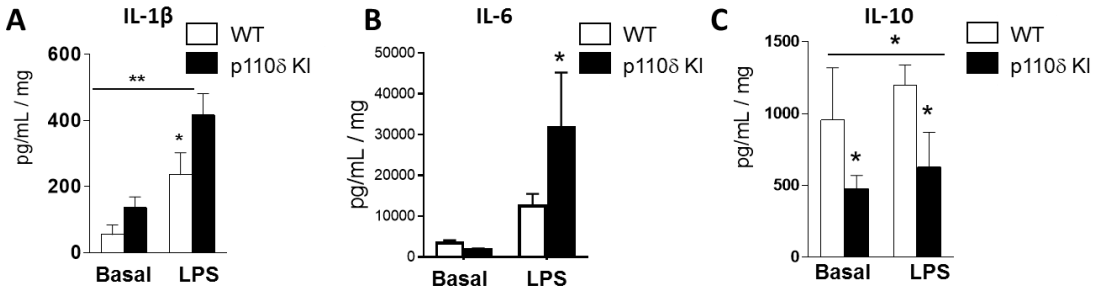

Figure 32: The p110δ kinase inactivation results in increased inflammatory, while decreased anti-inflammatory cytokines production from colon explants *ex vivo*. **(A–C)** The colon

explants from age and sex-matched WT and p110δ KI mice were isolated and similar weight of colon tissue from each mouse was stimulated by LPS (1 μg/mL) or (PBS) for 18 h. The levels of **(A)** IL-1β, **(B)** IL-6, and **(C)** IL-10 levels in culture supernatants were measured by ELISAs. The graphs are mean ± SEM cytokine level from the indicated mouse strains, (n=5-6 mice per mouse strain), *p≤0.05 or **p≤0.01 by Student t-test.

4.1.3. The p110δ is a key component of NOD2 signalling pathway and downregulates intestinal inflammation

Mutations in the genes encoding NOD2, ATG16L and IRGM have been associated with IBD susceptibility in humans[198–200]. Furthermore, genetic studies in mice have shown that NOD2-ATG16L axis are determining factors in gut immunity and inflammation[201]. Previous studies demonstrated that p110δ PI3Ks in DCs regulate the TLR-mediated innate immune responses and downstream signalling *in vitro* and *in vivo*[202]. In order to determine whether p110δ is also involved in the NOD2-mediated innate immune responses in a similar manner, we generated bone marrow-derived DCs (BMDCs) from p110δ KI, NOD2 knockout (KO), and WT mice, which were stimulated in a time dependent manner with the bacterial cell-wall component muramyl dipeptide (MDP) (NOD2 ligand) stimulation. For these experiments, the total cell lysates from BMDCs, which have been activated by MDP from indicated mouse strain, were analysed for the kinetic phosphorylation-dependent activation of AKT on Ser473 as well as p-IKKα/β, and p-p38 MAPKs. As shown in **Figure 33A**, MDP activation of BMDCs resulted in a strong phosphorylation of AKT and IKKα/β in WT cells, which was abolished in BMDCs from p110δ KI mice. In a similar setting, $NOD2^{KO}$ BMDCs showed completely abrogated AKT and IKKα/β phosphorylation, compared to their WT counterparts (**Figure 33B**). MDP activation of BMDCs binds to NOD2 and resulted in phosphorylation of p38, which was observed to be stronger in BMDCs from

p110δ KI mice compared to WT. However, NOD2^{KO} mice do not express NOD2 and therefore p38 could not be activated. There results indicated that p38 MAPK activation is NOD2-dependent (**Figure 33A, B**).

In order to investigate the role and coupling of p110δ to NOD2 pathway *in vivo*, we carried out peritonitis experiments by injecting MDP in the peritoneal cavity of WT or p110δ KI counterparts. The data, obtained by flow cytometry analysis of the peritoneal lavage fluid (PLF), indicated that p110δ KI mice, compared to the WT counterparts, displayed significantly heightened MDP-mediated inflammatory response, marked by increased neutrophil recruitment (**Figure 33C**). In line with increased neutrophil recruitment, p110δ KI mice also produced significantly higher IL-1β in PLF following MDP injection (**Figure 33D**). These results were obtained in collaboration with Dr. María González Núñez, unpublished data for manuscript from our laboratory in preparation (**Figure 33**). Overall our data demonstrated that p110δ PI3K isoform in DCs may couple to NOD2 signalling and downregulates inflammatory cell signalling upon detection of bacterial dipeptides.

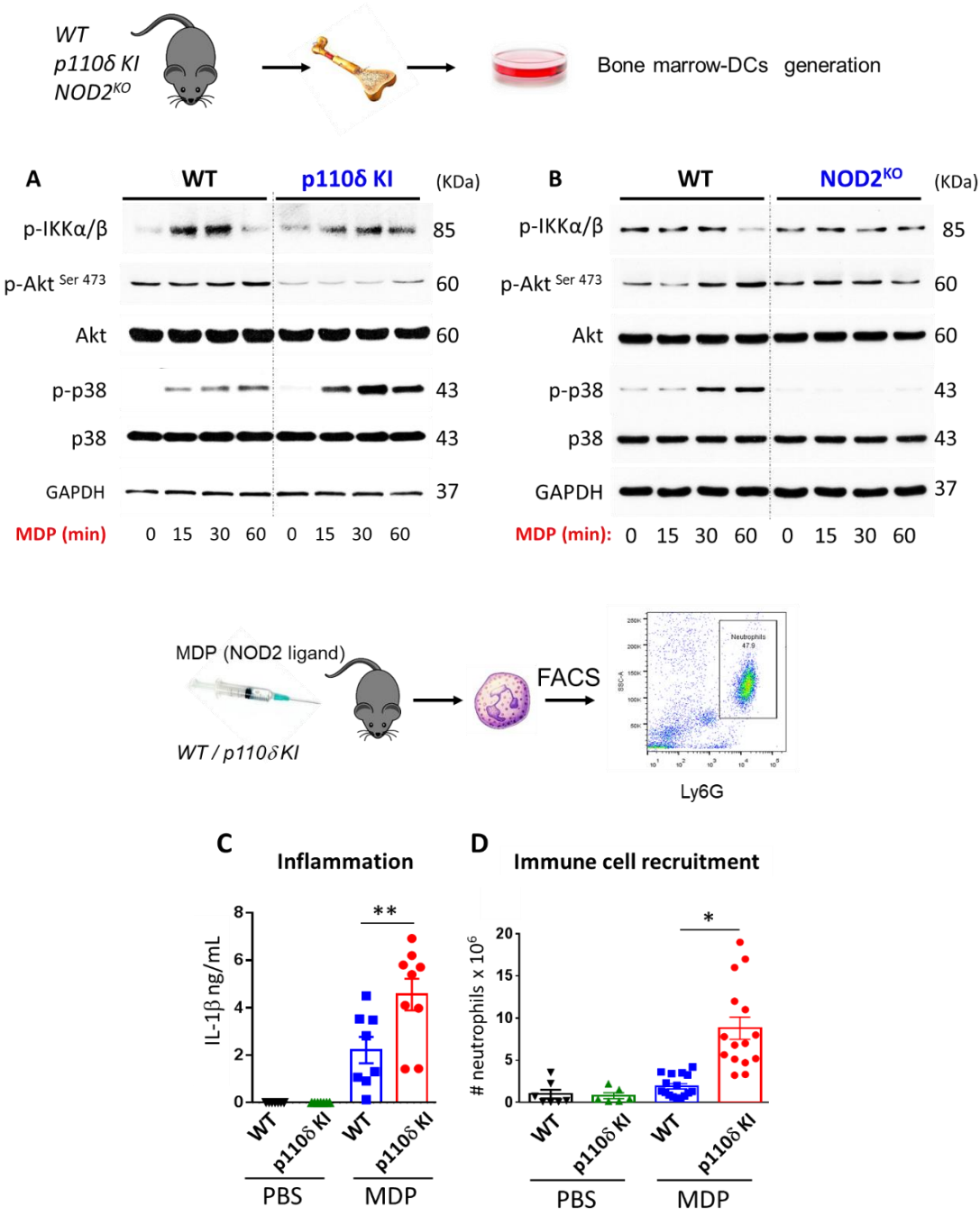

Figure 33: Genetic inactivation of p110δ abolishes AKT phosphorylation mediated by NOD2 stimulation *in vitro* and hyper-activates MDP-induced peritoneal inflammation *in vivo*. **(A-B)** BMDCs total cell lysates from WT and **(A)** NOD2^{KO} and **(B)** p110δ KI mice were stimulated by MDP (30 µg/ml) at indicated time intervals. Immunoblots were probed using; p- IKKα/β, p-AKT^{Ser473}, AKT, p-p38, p38, and GAPDH levels. AKT, p38, and GAPDH were used as loading controls. Data represent one out of 3 independent experiments from WT and p110δ KI mice (n=3). **(C-D)** The p110δ KI and WT mice were intra-peritoneally injected with 300 µg of MDP per mice. After 4 h, the mice were sacrificed and peritoneal lavage fluid (PLF), containing leukocytes was collected, counted,

and stained for flow cytometry analysis and cell-free supernatants were analysed by ELISA. The graphs show **(C)** IL-1β secretion in PLF from WT and p110δ KI mice and **(D)** neutrophil recruitment in peritoneal cavity, determined by flow cytometry analyses of $CD11b^{+}$ $Ly6G^{+}$ SSC^{high} leukocyte population. **(C-D)** Statistical analysis of data expressed as mean ± SEM (n=8-15) mice per group used by unpaired Student t-test **(C)** $^{**}p<0.01$, and **(D)** $^{*}p<0.05$.

4.1.4. The p110δ inactivation in DCs results in increased susceptibility to acute DSS intestinal injury

The $p110\delta^{\Delta Lyz2}$ (myeloid/macrophage specific) and $p110\delta^{\Delta CD11c}$ (DC specific) mouse were reared, genotyped and allowed to age up to 25 weeks of age in conventional animal facility. Interestingly, $p110\delta^{flox/flox}$ Cre-positive and Cre-negative strains did not show any signs of macroscopic intestinal pathology, indicative of intestinal inflammation (data not shown). The colon lengths of $p110\delta^{\Delta Lyz2}$ and $p110\delta^{\Delta CD11c}$ mice did not show any differences in comparison to the control $p110\delta^{flox/flox}$ Cre-negative strains. For this reason, our laboratory carried out acute DSS-induced colitis using the two different conditional mouse models in parallel. We observed that although $p110\delta^{flox/flox}$ mouse strains' weight loss was comparable to $p110\delta^{\Delta Lyz2}$ (**Figure 34**), the $p110\delta^{\Delta CD11c}$ mice lost significantly more weight in comparison to $p110\delta^{flox/flox}$ control counterparts (**Figure 35**). The $p110\delta^{\Delta CD11c}$ mice also showed significantly shorter colon length following DSS-induced colitis with no changes under basal conditions (results obtained in collaboration with Dr. María González Núñez & Dr. Ezra Aksoy, unpublished data for manuscript from our laboratory in preparation). We concluded that under basal conditions, conditional deletion of p110δ neither in myeloid cells nor in DCs resulted in a microbiota-mediated colitis in a conventional facility. However, conditional deletion of p110δ in CD11c+ DC population was observed to be

important in restricting inflammation and inducing tolerance to microbial insult and injury following breach of the intestinal barrier after DSS-induced injury (**Figure 35** and data not shown). These results indicated that other immune cell compartments, expressing p110δ PI3K alone or together with the intestinal phagocytes (DCs and macrophages) maybe important to achieve immune tolerance to the gut pathobionts under basal conditions in conventional housing. Since intestinal barrier functions are first mediated by the IECs, we decided to investigate the class I PI3Ks isoform-selective roles in IECs, which may impact their innate responses/inflammation, proliferation, survival and/or regeneration in the gut.

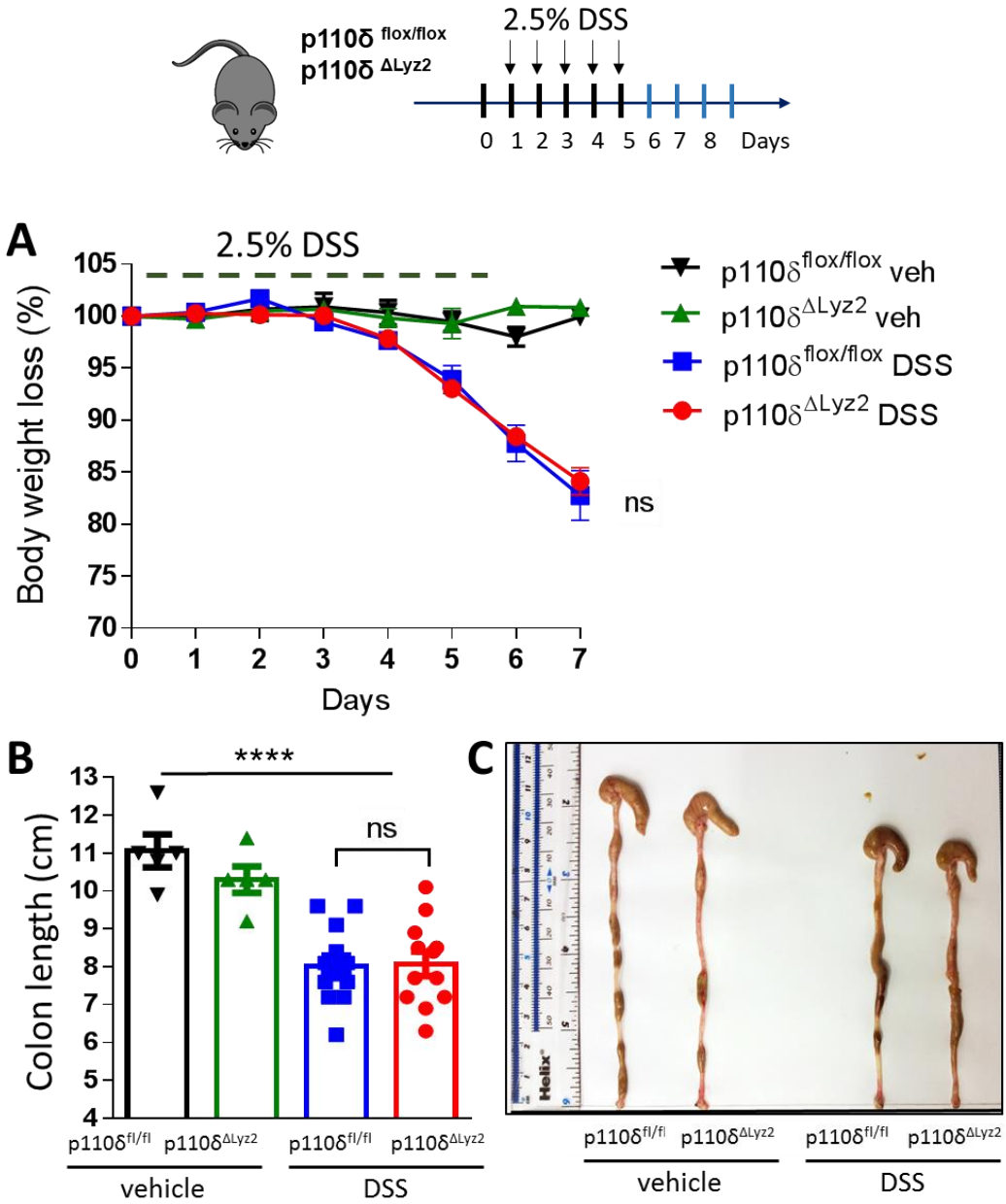

Figure 34: Specific p110δ kinase inactivity in myeloid cells (p110δ^{ΔLyz2}) in mice was comparable to p110δ$^{flox/flox}$ after acute DSS-induced colitis. Healthy age and sex-matched p110δ$^{flox/flox}$ and p110δ^{ΔLyz2} mice, reared in conventional housing facility were orally treated with 2.5% DSS in drinking water or 5 days or vehicle (veh) to induce acute chemically-induced colitis. The mice engaged for acute analysis were euthanised at day 7. **(A)** The graph represents the percentage of weight loss for 7 days ensuing DSS injury or vehicle-treatment (n=7-14 mice per mouse strain). **(B)** The bar chart shows mean ± SEM colon length. **(C)** The image shows colon lengths at day 7 after DSS injury in p110δ^{ΔLyz2} mice compared to Cre-negative p110δ$^{flox/flox}$ mice at day 7 after DSS or vehicle (n=5-12 mice per group). **(A-B)** Statistical analysis of data expressed as mean ± SEM was ****p<0.0001 One-way ANOVA after vehicle compared to DSS treatment; **(A)** no significant (ns) after DSS

treatment by Two-way ANOVA; and **(B)** Student t-test no significant (ns) after DSS treatment compared to p110δ$^{\Delta Lyz2}$ and p110δ$^{flox/flox}$ mouse strains.

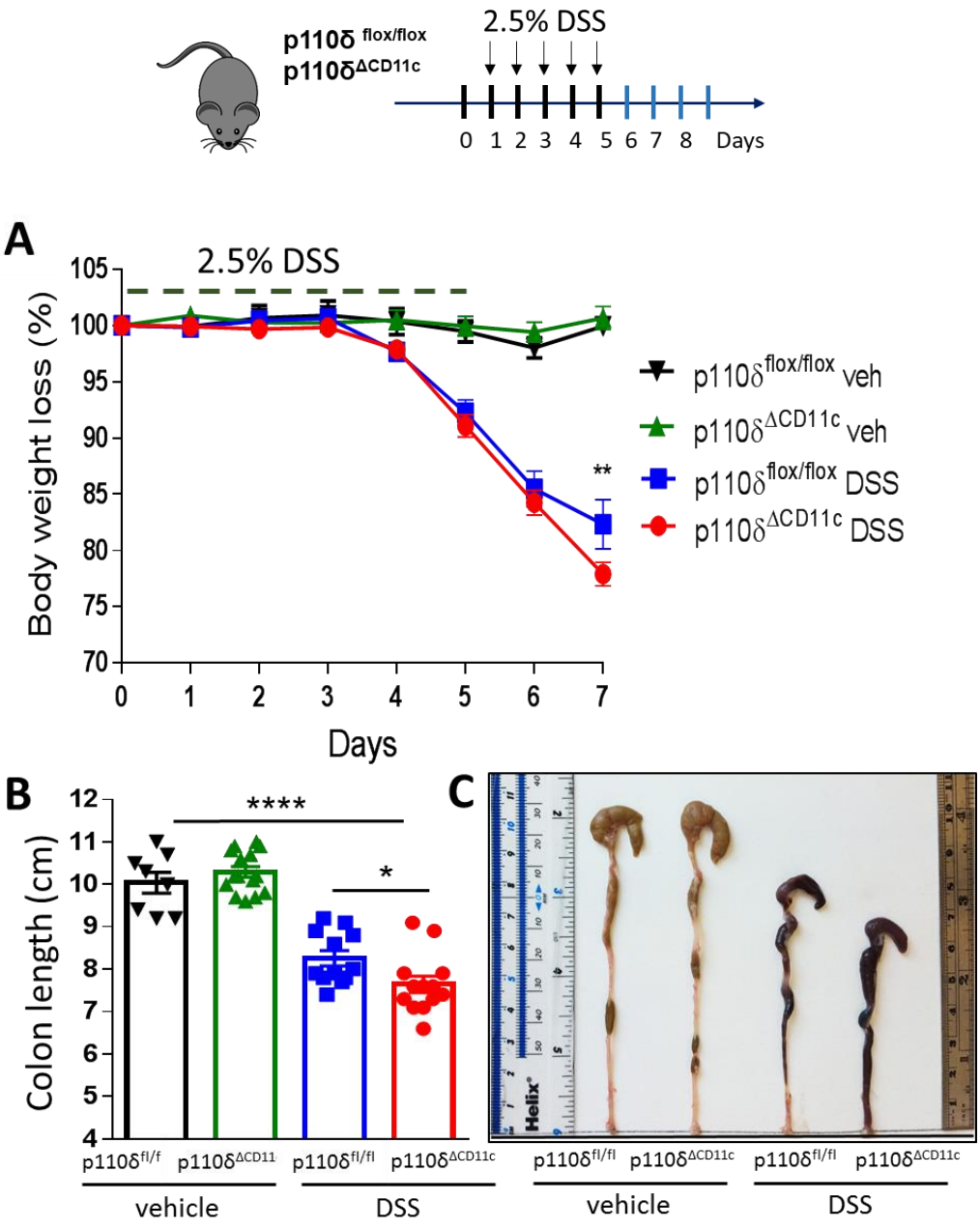

Figure 35: Specific p110δ kinase inactivity in DCs (p110δ$^{\Delta CD11c}$) in mice results in significant susceptibility after acute chemically DSS-induced colitis. Healthy age and sex-matched p110δ$^{flox/flox}$ and p110δ$^{\Delta CD11c}$ mice, reared in conventional housing facility were orally treated with 2.5% DSS in drinking water for 5 days or vehicle (veh) to induce acute chemically-induced colitis. The mice engaged for acute analysis were euthanised at day 7.

(A) The graph represents the percentage of weight loss for 7 days ensuing DSS injury or vehicle-treatment (n=11-21 mice per mouse strain). **(B)** The bar chart shows mean ± SEM colon length (n=7-12 mice per mouse strain). **(C)** The image shows colon lengths at day 7 after DSS injury in $p110\delta^{\Delta CD11c}$ mice compared to Cre-negative $p110\delta^{flox/flox}$ mice at day 7 after DSS or vehicle. **(A-B)** Statistical analysis of data expressed as mean ± SEM was $^{****}p<0.0001$ by One-way ANOVA after DSS treatment compared to vehicle; **(A)** $^{**}p<0.01$ by Two-way ANOVA; and **(B)** $^{*}p<0.05$ by Student t-test after DSS treatment compared to $p110\delta^{\Delta CD11c}$ and $p110\delta^{flox/flox}$ mouse strains.

4.1.5. The p110δ expression is induced by PAMP or inflammatory cytokines exposure in human and mouse IECs *in vitro*

Western blotting analysis of the IECs cultures (see **Section 3.1**) showed that p110α and p110β proteins expression levels were comparable between human (NCM3-65, and HTB-38) and mouse (CMT-93) cell lines (**Figure 36**). However, there was little or no p110δ protein expression in these cell lines ay basal levels. AKT residue serine 473 ($p\text{-}AKT^{Ser473}$) in the C-terminal hydrophobic was also variable between the IECs tested. To investigate the effects of PAMPs and inflammatory cytokines, CMT-93 and NCM-365 cell lines were treated with PAMPs including LPS (TLR4 ligand), PGN (TLR2 ligand), and inflammatory cytokines (TNFα and/or IL-1β) overnight. Western blotting analysis of the extracts demonstrated that mouse IECs, were only exclusively responsive to LPS, which upregulated p110δ protein expression. On the other side, human IECs were responsive to all PAMPs and inflammatory stimuli and upregulated p110δ expression. These data showed that human and mouse IECs express p110δ after PAMP and inflammatory cytokines exposure *in vitro.* However, these results also indicated that the main PI3K isoform expressed in IECs is p110α, being p110β the second most expressed.

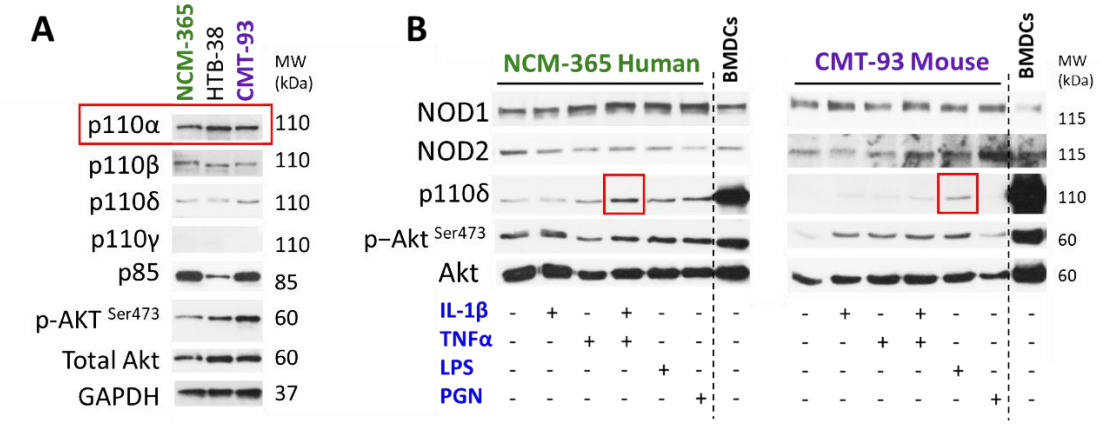

Figure 36: Protein expression levels of PI3K isoforms and AKT levels in human and mouse IECs. (A) Human (NCM-365, HTB-38) and mouse (CMT-93) IECs, were cultured under normal medium conditions containing 10% FBS in DMEM. Whole cell protein extracts were obtained from 30,000 cells/cm^2 after total cell lysis and were fractioned and separated by gradient concentrations of SDS-PAGE and then immunoblotted. Immunoblots were sequentially probed by using p110α, p110β, p110δ, p110γ, p85, p-AKT$^{Ser\ 473}$, total AKT, and GAPDH antibodies. Total AKT and GAPDH were used as loading controls. **(B)** NCM-365 and CMT-93 IECs, were cultured under normal medium conditions containing 10% FBS in DMEM and stimulated overnight with IL-1β (20 ng/ml), TNFα (20 ng/ml), IL-1β + TNFα, LPS (1 μg/ml), PGN (200 ng/mL). Immunoblots were sequentially probed by using NOD1, NOD2, p110δ, p-AKT^{Ser473}, and total AKT antibodies. Total AKT was used as loading controls. Basal and BMDCs lysates were used as positive and negative controls respectively. One representative out of three independently performed experiments is shown.

4.1.6. Conditional inactivation of p110δ PI3K in IECs does not alter susceptibility to colitis mediated by acute DSS-induced injury

As previously described, p110δ regulates gut immunity and inflammation in immune cell populations. We have attempted to unpick the relative contribution of p110δ kinase in the innate immune cell populations by conditional targeting of DCs (p110δ$^{\Delta CD11c}$) and macrophages (p110δ$^{\Delta LyzM}$) *in vivo*. Our

unpublished data showed that microbiota-mediated colitis was not observed in the selectively targeted DC or macrophage innate immune populations (data not shown). Furthermore, p110δ$^{\Delta CD11c}$ mice showed marked severity of colitis following acute injury by DSS colitis, phenocopying colitis data obtained in healthy p110δ KI animals under DSS injury (**Figure 35**). We have shown that p110δ expression in IECs can be induced after exposure to the PAMPs such as LPS and PGN and inflammatory cytokines (**Figure 36**). Therefore, we hypothesised whether p110δ in IECs contributed to intestinal homeostasis and tolerance to the microbiota. In order to study our hypothesis, we have targeted p110δ gene using transgenic p110δ$^{flox/flox}$ mice, which was crossed to Villin-Cre mice (referred hereafter p110δ$^{\Delta IEC}$) to delete p110δ in intestinal epithelium. In order to study the role of p110δ in the IECs after injury, p110δ$^{\Delta IEC}$ mice were given DSS for 5 days in order to chemically induce acute inflammation in the intestine. Mice were observed daily, and weights were recorded until day 7. Remarkably, we observed that p110δ$^{\Delta IEC}$ mice did not show susceptibility to colitis mediated by acute DSS injury compared their control p110δ$^{flox/flox}$ counterparts. Both the weight loss and the colon lengths within each mouse strain were comparable after DSS treatment at day 7 (**Figure 37**). These results showed that although p110δ isoform expression can be induced by PAMPs and inflammatory cytokines, it is not required in protection from acute gut injury and inflammation.

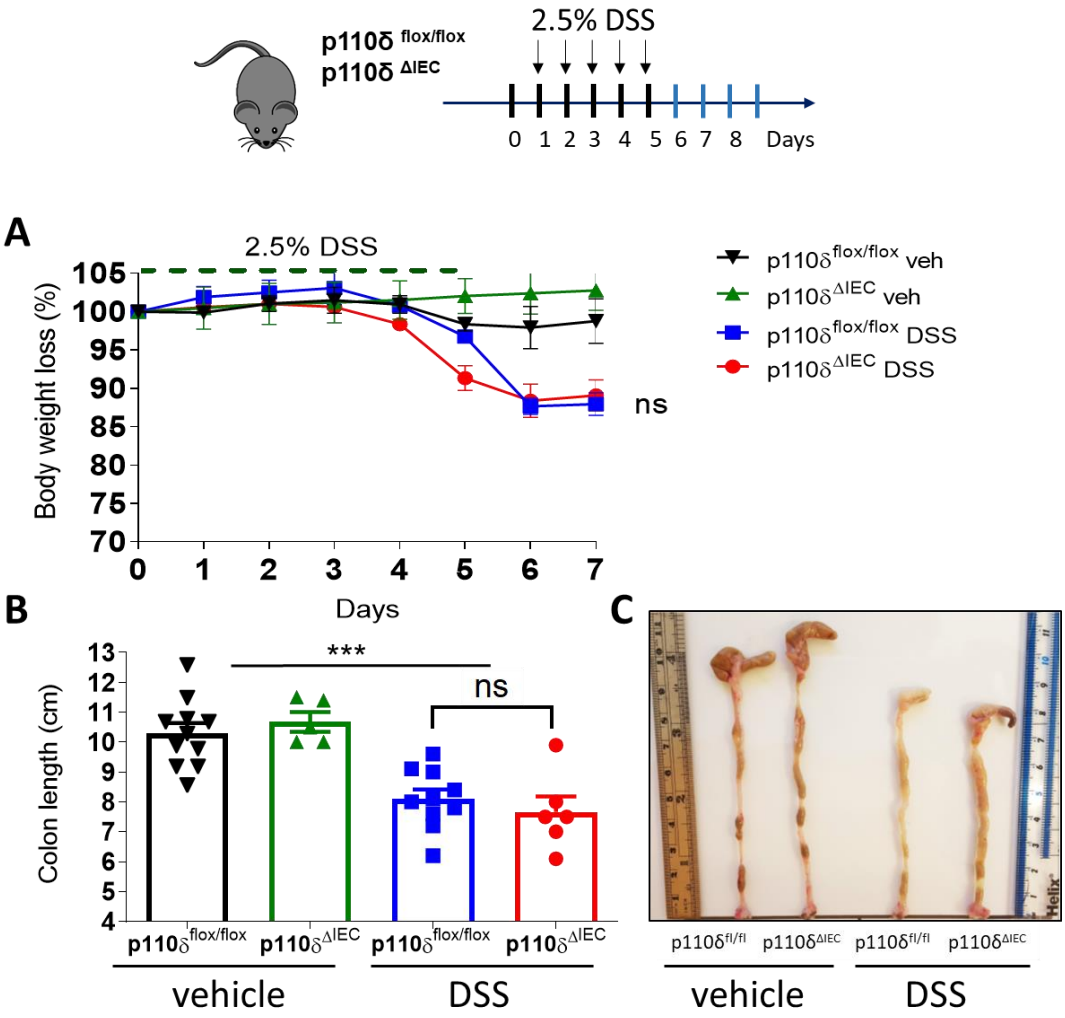

Figure 37: Conditional p110δ kinase inactivity in IECs (p110δ$^{\Delta IEC}$) in mice was comparable to p110δ$^{flox/flox}$ after acute DSS-induced colitis. Healthy age and sex-matched p110δ$^{flox/flox}$ and p110δ$^{\Delta IEC}$ mice in conventional housing were orally treated with 2.5% DSS in drinking water for 5 days or vehicle (veh) to induce acute chemically-induced colitis. The mice engaged for acute analysis were euthanised at day 7. **(A)** The graph represents the percentage of weight loss for 7 days ensuing DSS injury or vehicle-treatment (n=5-10 mice per mouse strain). **(B)** The bar chart shows mean ± SEM colon length (n=5-10 mice per mouse strain). **(C)** The image shows colon lengths at day 7 after DSS injury or vehicle in p110δ$^{\Delta IEC}$ mice compared to Cre-negative p110δ$^{flox/flox}$ mice. **(A-B)** Statistical analysis of data expressed as mean ± SEM was was ****p<0.0001 One-way ANOVA after vehicle compared to DSS treatment; **(A)** no significant (ns) by Two-way ANOVA after DSS treatment, and **(B)** Student t-test was no significant (ns) after DSS treatment compared to to p110δ$^{\Delta IEC}$ and p110δ$^{flox/flox}$ mouse strains.

4.2. The role of p110α PI3K in the intestine

Our previous data established that p110δ regulates innate immunity and inflammation in the gut. However, all animal models investigated using conditional deletion of p110δ in innate immune cell subsets (DCs and myeloid cells ($p110\delta^{\Delta LyzM}$, and $p110\delta^{\Delta CD11c}$, respectively), or IECs ($p110\delta^{\Delta IEC}$) did not develop microbiota-dependent colitis, indicating ubiquitous inactivation of p110δ kinase activity in mice cannot be phenocopied by conditional deletion of the p110δ in these cell populations. Furthermore, with the exception of DC-intrinsic p110δ deletion, neither myeloid-intrinsic nor IEC-intrinsic deletion of p110δ modified susceptibility to DSS-induced acute injury and ensuing inflammation in (**Section 3.1**). These results overall suggested that other class I PI3K isoforms may be important in the regulation of host-microbiota interaction and responses to gut injury.

NODs are cytosolic PRRs that detect bacterial dipeptides expressed by IECs[172]. NOD1/2 signalling pathways control innate immune cell and IEC inflammatory responses[203], while equally mediate tolerance to commensal bacteria in the gut[123]. However, much lesser investigated is the role of NOD1/2 pathway in IECs, reported to control intestinal repair and wound healing, particularly in the Paneth cell population[182]. As previously discussed, we have demonstrated that class I p110δ PI3K is a component of NOD1/2 signalling in innate immune phagocytes such as DCs and induces tolerance to host commensal bacteria (results obtained in collaboration with Dr. María González Núñez & Dr. Ezra Aksoy, unpublished data for manuscript from our laboratory in preparation). Therefore, we hypothesised that another class I PI3K isoform may couple to NOD signalling and regulate IEC responses in the gut tissue. Previous studies have shown that activation of colon

epithelial cells by NOD1/2 ligands induce a canonical innate immune response and stress signalling involving NF-κB (IKKα/β phosphorylation) and p38 stress-activated MAPK pathways[6]. Nevertheless, the NOD receptor coupling to PI3K-AKT pathway in IECs and its function remains yet to be established. In the next set of experiments, we set out to investigate the isoform-selective role and mechanism of action of class I PI3Ks in human and mouse IECs.

4.2.1. The p110α PI3Ks regulate AKT/mTORC1 activities downstream of NOD1/2 signalling pathways in human and mouse IECs *in vitro*

The western-blotting assays, carried out to visualise protein expression profiles of PI3K isoforms in human (NCM-365) and mouse (CMT-93) cell lines; showed that IECs mainly express p110α and p110β with negligible levels of p110δ and p110γ (**Figure 36**). Using PI3K isoform-selective inhibitors, we have addressed class I PI3Ks isoform-selective roles in mTORC1 and AKT signalling mediated by NOD1 pathways. The cells were incubated overnight 0.5% FBS starvation medium DMEM overnight and the next day were treated with PI3K-selective inhibitors for 4 h. In the following assays, the cells were acutely stimulated with iE-DAP (NOD1 ligand) at indicated time intervals, followed by western-blotting of cell extracts to visualise phosphorylation-dependent activation kinetics of PI3K downstream targets, specifically AKT and mTORC1 targets p70S6K and ribosomal S6. The data demonstrated that iE-DAP-mediated NOD1 stimulation resulted in the phosphorylation-dependent activation of AKT (Ser-473), p70-S6K (Thr-389) and ribosomal S6 (Ser-235/236) in NCM-365 and CMT-93. In the same conditions, pre-treatment of human or murine IECs with A66 (p110α isoform-selective) and GDC-

0941 (pan class I PI3K inhibitor) abolished the phosphorylation of AKT and p70 S6K. However, IC87114 (p110δ selective) did not alter iE-DAP mediated AKT phosphorylation at all-time points tested. Interestingly, TGX-221 (p110β selective) also resulted in a marked reduction in the AKT phosphorylation mediated by iE-DAP in both human and mouse IECs (**Figure 38**).

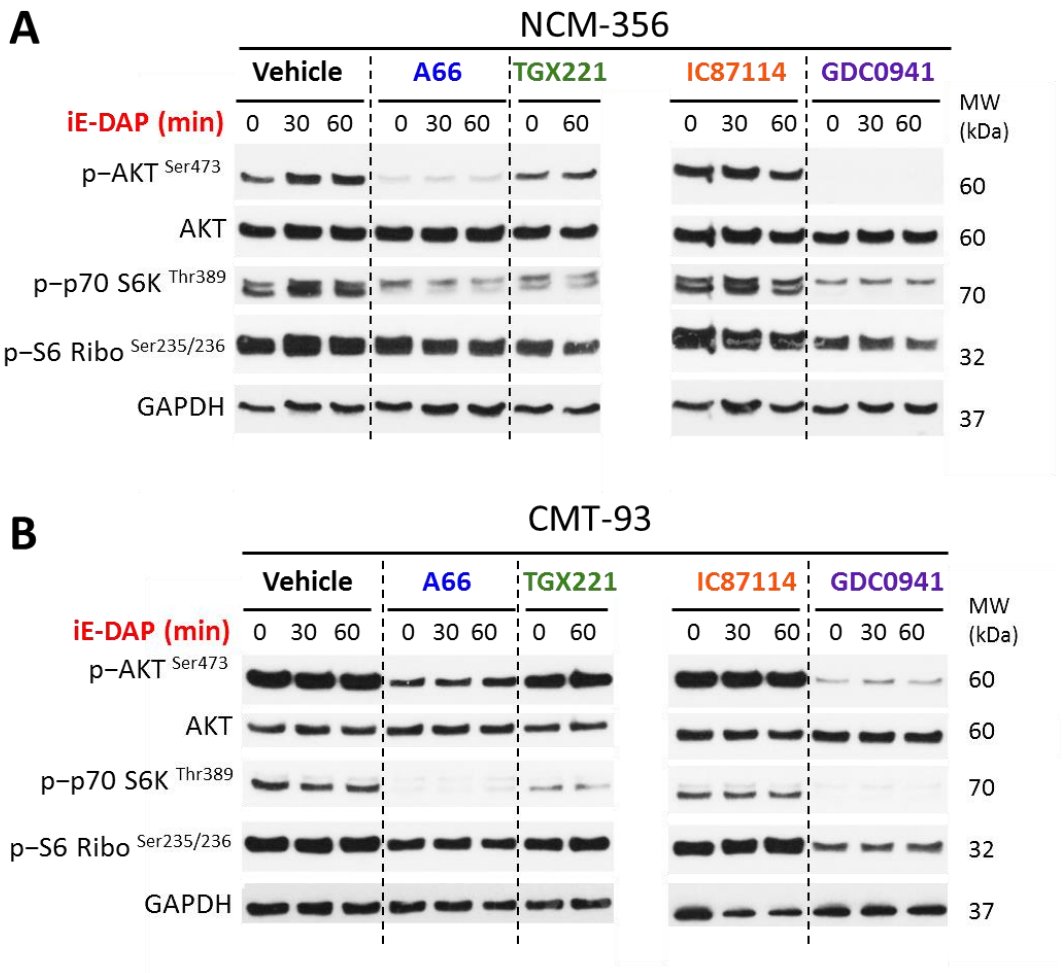

Figure 38: Class I p110α isoform induces AKT/mTORC1 pathway in IECs after acute NOD1 stimulation. The effects of PI3K isoform-selective inhibitors on NOD1 mediated PI3K-AKT and mTORC1 targets were analysed by immunoblotting assays using **(A)** human NCM-365 and **(B)** mouse CMT-93 cell lines. Cells were counted plated with 0.5% FBS starvation medium DMEM. On the following day, cells were treated with PI3K isoform-selective inhibitors: A66 (1 μM, p110α), TGX-221 (0.25 μM, p110β), IC87114 (1mM, p110δ), and GDC0941 (1 μM, pan-

class I PI3K-inhibitor); or DMSO (vehicle) for 4 h prior to stimulation by iE-DAP (30 μg/ml) at indicated time intervals. Immunoblots were probed using; p-AKT^{Ser473}, p-p70 S6K^{Thr389}, p-S6 ribosomal$^{Ser235/236}$ and GAPDH antibodies. AKT and GAPDH were used as loading controls. One representative out of three independently performed experiments is shown.

The next western-blotting assays were designed to analyse innate immune/inflammatory and stress signalling pathways by measuring canonical NF-κB and MAPK pathway targets IKKα/β, ERK/p38 MAPK, respectively. In these assays, none of the PI3K isoform-selective nor pan PI3K inhibitor had marked effect on the activation pattern and levels of IKKα/β and ERK phosphorylations mediated by iE-DAP (**Figure 39**). Strikingly, in the same settings, A66 mediated inhibition of p110α resulted in hyper-activation of p38 MAPK in both human and mouse cells. Overall, these data indicated that human and murine colon epithelial cells responded to iE-DAP (NOD1 ligand) and resulted in NOD1-mediated activation of p110α PI3K and its downstream targets AKT/mTORC1. Furthermore, NOD-mediated p110α PI3K activation dampened p38 MAPK activity, indicating that p110α activity negatively regulated stress mediated p38 MAPK pathway upon challenge by bacterial dipeptide. The biological relevance of our results is that NODs coupling to PI3Ks act as a homeostatic regulator of stress levels in epithelial cells and in innate immune cells. MAPKs are involved in many critical biological processes such as proliferation, differentiation, and cell death. Therefore, we observed a specific role of NOD-PI3K crosstalk in IECs downregulating uncontrolled activation of stress pathways that may be detrimental to the epithelial cell survival, proliferation, and differentiation.

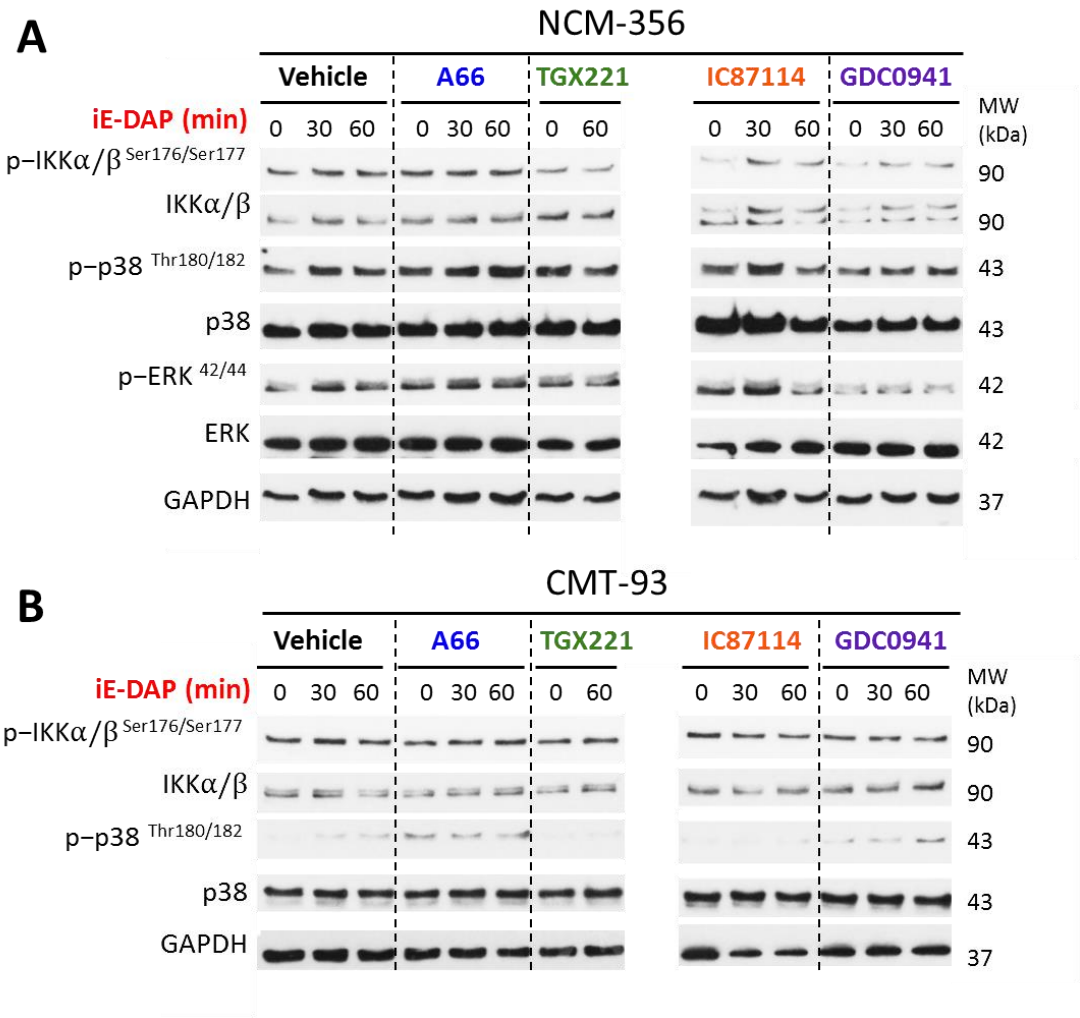

Figure 39: Acute NOD1 ligand does not mediate innate signalling canonical pathway in IECs treated with PI3K isoform-selective inhibitors. The effects of PI3K isoform-selective inhibitors on NOD1 mediated NF-κB and MAPK pathway activities is shown in **(A)** human NCM-365 and **(B)** mouse CMT-93 cell lines. Cells were treated with PI3K isoform-selective inhibitors, A66 (1 μM, p110α), TGX-221 (0.25 μM, p110β), IC87114 (1mM, p110δ), and GDC0941 (1 μM, pan-class I PI3K-inhibitor); or DMSO (vehicle) for 4 h prior to stimulation by iE-DAP (30 μg/ml) at indicated time intervals. Immunoblots were probed using; p-IKKα/β$^{Ser176/177}$, IKKα/β, p-p38$^{Thr180/182}$, total p38, p-ERK$^{42/44}$, and ERK antibodies. GAPDH was used as loading control. One representative out of three independently performed experiments is shown.

A similar pattern of NOD2 mediated AKT activation was observed in human and murine IECs since pre-treatment, which was abrogated by A66 and

GDC-0941, indicating that p110α is the major class I PI3K regulating NOD1/2 signalling pathways. Interestingly, under NOD2 stimulations, p110δ isoform-selective inhibitor IC87114 inhibited AKT and S6K phosphorylation in human IECs (**Figure 40A**). In a similar setting, stimulation by TLR4 ligand LPS resulted in a discernible activation of AKT and p70-S6K in murine IECs, which was likewise abrogated by A66 and GDC-0941 (**Figure 40B**). These results showed that bacterial ligands mediate AKT and mTORC1 pathway in human and mouse IECs through class I p110α isoform.

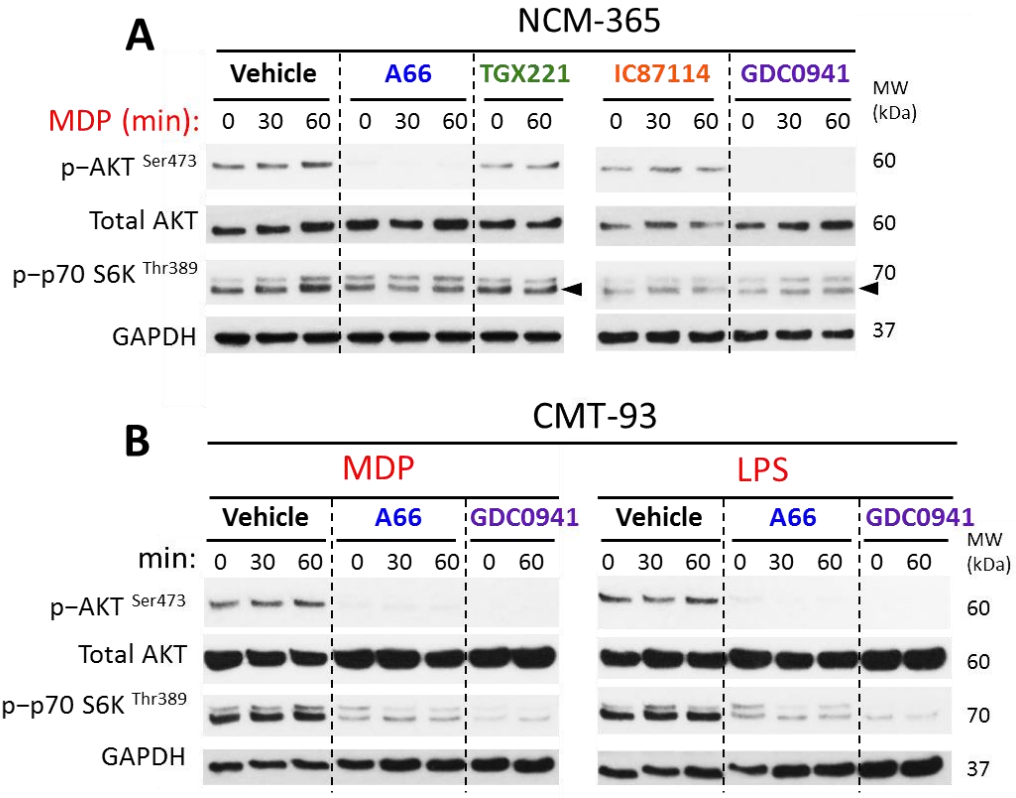

Figure 40: Class I p110α isoform induces AKT/mTORC1 pathway in IECs after acute NOD2 stimulation. The effects of PI3K isoform-selective inhibitors on NOD2 mediated PI3K-AKT and mTORC1 targets were analysed by immunoblotting assays using **(A)** human NCM-365 and **(B)** mouse CMT-93 cell lines. Cells were treated with PI3K isoform-selective inhibitors, A66 (1 μM, p110α), TGX-221 (0.25 μM, p110β), IC87114 (1mM, p110δ), and GDC0941 (1 μM, pan-class I PI3K-inhibitor); or DMSO (vehicle) for 4 h prior to stimulation by MDP (30 μg/ml) or LPS (1 μg/mL), at indicated time intervals.

Immunoblots were probed using; p-AKTSer473, p-p70 S6KThr389, and GAPDH antibodies. AKT and GAPDH were used as loading controls. One representative out of three independently performed experiments is shown.

4.2.2. Conditional inactivation of p110α-RBD interaction by tamoxifen results in colon shortening and overall delay in weight-gain *in vivo*

The p110α PI3K isoform is ubiquitously expressed by all somatic cells. Mutations enhancing p110α activity have been associated with a number of cancers, gastric cancers being one of the most prominent type showing p110α hyper-activating mutations[204,205]. As previously discussed in the introduction (**Section 1.1.5**), inhibition of p110α is lethal during embryogenesis between E9.5 and E10.5 due to defects in angiogenesis, whereas heterozygous mice appear normal[95,206]. Therefore, we have utilised a conditional mouse model for inactivating p110α to delineate p110α isoform selective function in intestinal injury. In this study, we have used a conditional mouse, carrying a genetic mutation in the RBD of the *PI3KCA* gene, which expressed two-point mutations at amino acid residues T208D and K227A, completely abolishing interaction with the GTPases such as Ras, but fully preserving the p110α enzymatic activity (referred hereafter as $p110\alpha^{RBD}$). The homozygous $p110\alpha^{RBD}$ mice, markedly phenocopied the *PIK3CA* knockout or p110α kinase inactivated strains, since all mice displayed perinatal lethality[25]. For these reasons, we have crossed the heterozygous $p110\alpha^{RBD}$ mice with the mouse strain, carrying a single p110α/loxP allele, which carried a gene encoding Cre recombinase under Rosa 26 promoter, in a heterozygous manner: **$Rosa26^{CreERT2/+}/p110\alpha^{RBD/flox}$** (referred hereafter as **$p110\alpha^{RBD/flox}$**). We have also crossed the non-RBD mutant ($p110\alpha^{WT}$) mice with the mouse strain p110α/loxP allele:

Rosa26$^{CreER/+}$/p110α$^{WT/flox}$ (referred hereafter as **p110α$^{WT/flox}$**). Tamoxifen was used to induce Cre recombinase expression in p110α$^{WT/flox}$ and p110α$^{RBD/flox}$ mice, resulting in the heterozygous deficiency of p110α either carrying a single WT copy of RBD-p110α or a single mutant inactive RBDp110α copy, (referred hereafter as **p110α$^{WT/-}$** and **p110α$^{RBD/-}$**, respectively). Since tamoxifen-induced toxicity is damaging to the stem cell populations[63,207], an internal control of inbred C57 black 6 mice (referred hereafter as **p110α$^{WT/WT}$**) was used to compare all groups, under similar conditions. Moreover, it is well known that tamoxifen inducible lines may not recombine all the cells, therefore expression of p110α was confirmed in several tissues from each mouse strain (**Figure 26**).

Tamoxifen was administrated using oral gavage technique for three times every other day. Following tamoxifen treatment, mice were genotyped and weights from each mouse were checked and recorded daily for 15 days in order to recover initial weight percentage (100%). Statistically significant differences in the percentage of weight loss after tamoxifen treatment were observed between age and sex-matched p110α$^{WT/WT}$ control mice and p110α$^{RBD/-}$ or p110α$^{WT/-}$ mice. While p110α$^{WT/WT}$ and p110α$^{WT/-}$ recovered their body weight back by 100% immediately after tamoxifen treatment, p110α$^{RBD/-}$ strain's weight recovery was tardy, and they only recovered 99.98% from their original weight after two weeks (day 14) following tamoxifen treatment. In these experiments, the colon length of p110α$^{RBD/-}$ mice was significantly decreased in comparison to the control p110α$^{WT/WT}$ counterparts, while p110α$^{WT/-}$ mice showed noticeable but statistically insignificant decrease in colon length (**Figure 41**).

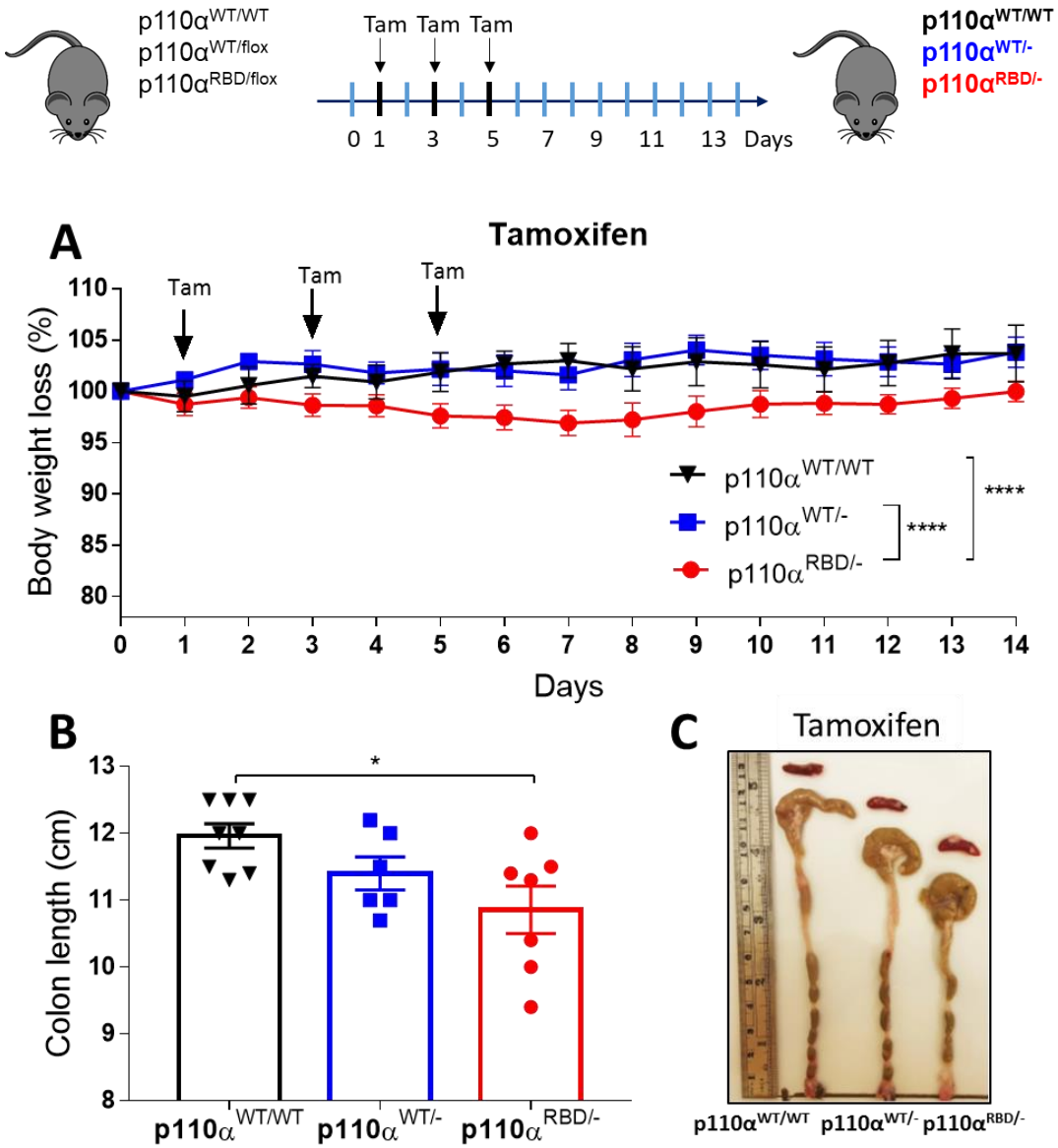

Figure 41: The p110α-RBD interaction weight gain and colon length following tamoxifen treatment to the intestine. Healthy age and sex-matched p110α$^{WT/WT}$, p110α$^{WT/flox}$, and p110α$^{RBD/flox}$ mice were given thrice tamoxifen (40 mg/mL) by oral gavage every other day. After 14 days, tissue sample were taken from each mice strain to confirm p110α heterozygous or homozygous expression. One representative out of three independently performed experiments is shown. **(A)** The graph represents means ± SEM percentage of weight loss following tamoxifen treatment (n=8-14 mice per mouse strain). **(B)** The bar graph represents means ± SEM of colon length of indicated mice strains (n=6–14 mice per mouse strain). **(C)** The photo shows colons length of indicated mouse strains. **(A-B)** Statistical analysis show mean ± SEM **(A)** ****p<0.0001 by Two-way ANOVA, and **(B)** *p<0.05 by One-way ANOVA.

4.2.3. Temporal and gene dosage-dependent deletion of p110α causes partial lethality and greater susceptibility to DSS-mediated intestinal injury

Following our observation that mice expressing a single copy of mutant p110α-RBD showed significant reduction in colon length and marked decrease in weight recovery, we interrogated the role of p110α and its RBD interaction in chemically induced acute intestinal injury and inflammation mediated by DSS. The next set of experiments were designed to investigate the in vivo effects of gene dosage-dependant deletion of p110α (in heterozygosity) along with p110α-RBD interaction (in heterozygosity) in acute intestinal damage. After two weeks following tamoxifen treatment, 2.5% DSS was given to 12-17 week adult $p110\alpha^{WT/WT}$, $p110\alpha^{WT/-}$, and $p110\alpha^{RBD/-}$ mice, respectively, for five 5 consecutive days and mice were kept for 7 days following DSS treatment. The mice were checked daily and weights were recorded in order to observe the pathological effects and weight loss of each mouse strain. Strikingly, $p110\alpha^{RBD/-}$ mice showed approximately 55.56% lethality, at and after day 6 and statistically significant susceptibility to DSS-mediated acute intestinal injury in comparison to $p110\alpha^{WT/WT}$ (**Figure 42A-B**). In the similar settings, $p110\alpha^{WT/-}$ displayed approximately over 30% lethality and marked susceptibility to DSS. Equally, the surviving $p110\alpha^{WT/-}$ and $p110\alpha^{RBD/-}$ mice showed significantly decreased colon lengths compared to $p110\alpha^{WT/WT}$ mice at day 7 upon DSS treatment (**Figure 42C-D**). Specifically, $p110\alpha^{RBD/-}$ mice showed the greatest decrease in colon length compared to all other groups after DSS injury. Interestingly, the $p110\alpha^{RBD/-}$ mice were observed to have little or no faecal matter in their colon, indicating disruption of absorptive functions in the gut. These results corroborated that p110α kinase activity and its RBD interaction with GTPases safeguards and contributes to intestinal health,

potentially by contributing to the intestinal repair and/or wound healing processes in response to acute intestinal injury.

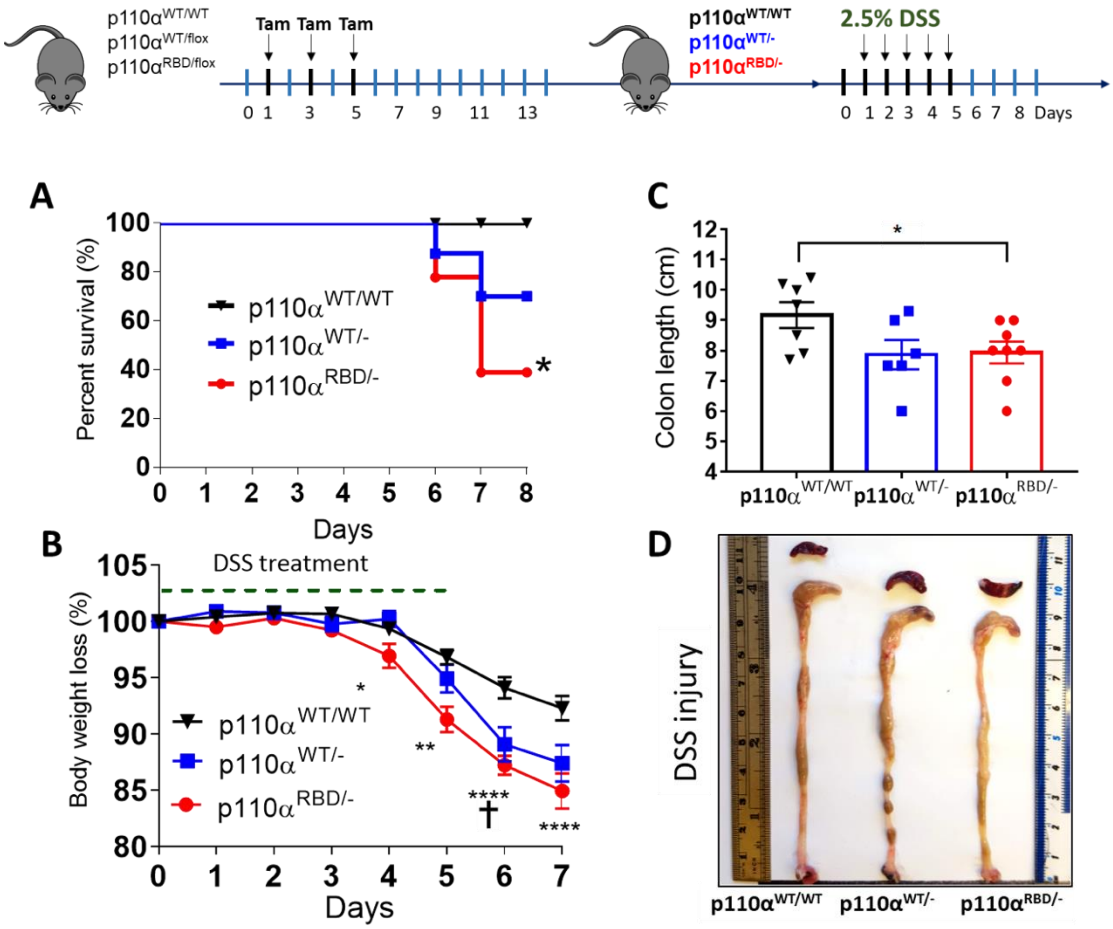

Figure 42: Inactivation of p110α-RBD interactions causes partial lethality following acute chemically induced DSS injury. Healthy age and sex-matched p110α$^{WT/WT}$, p110α$^{WT/flox}$ and p110α$^{RBD/flox}$ mice, reared in conventional housing facility were given thrice tamoxifen (40 mg/mL) by oral gavage every other day. After 2 weeks, p110α$^{WT/WT}$, p110α$^{WT/-}$ and p110α$^{RBD/-}$ mice were orally treated with 2.5% DSS in drinking water for 5 days or vehicle (day 0) to induce acute chemically-induced intestinal injury. The mice engaged for acute analysis were euthanised at day 7. One representative out of four independently performed experiments is shown. **(A)** The graph represents the percent survival after DSS injury (n=11 mice per mouse strain per experiment). **(B)** The bar graph shows mean ± SEM percent weight loss after DSS treatment (n=7-13 mice per mouse strain per experiment) **(C)** The graph shows colon length after DSS treatment of p110α$^{WT/WT}$, p110α$^{WT/-}$ and p110α$^{RBD/-}$ adult mice, (n=6–8 mice per group per experiment). **(D)** The image is representative of one of 6 colons from indicated mouse strain. **(A-C)** Statistical analysis

show mean ± SEM **(A)** *p<0.05 by Log-rank (survival curve) test, **(B)** ****p<0.0001 by Two-way ANOVA, and **(C)** *p<0.05 by One-way ANOVA.

In order to validate the selective role of p110α-RBD interaction in intestinal injury, we decided to use the heterozygous p110α-RBD mice which are viable and express a single copy of the mutant p110α-RBD together with single floxed copy of the gene encoding p110α (referred hereafter $p110\alpha^{RBD/flox}$) in order to bypass the potential additional toxic effects of tamoxifen to the crypt cells. The mice were subjected to 2.5% DSS treatment for 5 days. Remarkably, the $p110\alpha^{RBD/flox}$ mice showed increased susceptibility to DSS-mediated intestinal injury in comparison to the control counterparts (which express two functional copies of the p110α protein, albeit one copy being floxed). The $p110\alpha^{RBD/flox}$ mice showed shortened colon lengths, and a tendency toward greater weight loss (87.3%) in comparison to the control counterparts (91-94%) at day 8 and significant increased susceptibility to DSS-mediated intestinal injury day 17 (**Figure 43**). These data corroborated that p110α-RBD interaction is critical for protection against intestinal injury and the p110α kinase activity appears to depend on RBD-mediated interactions in the gut.

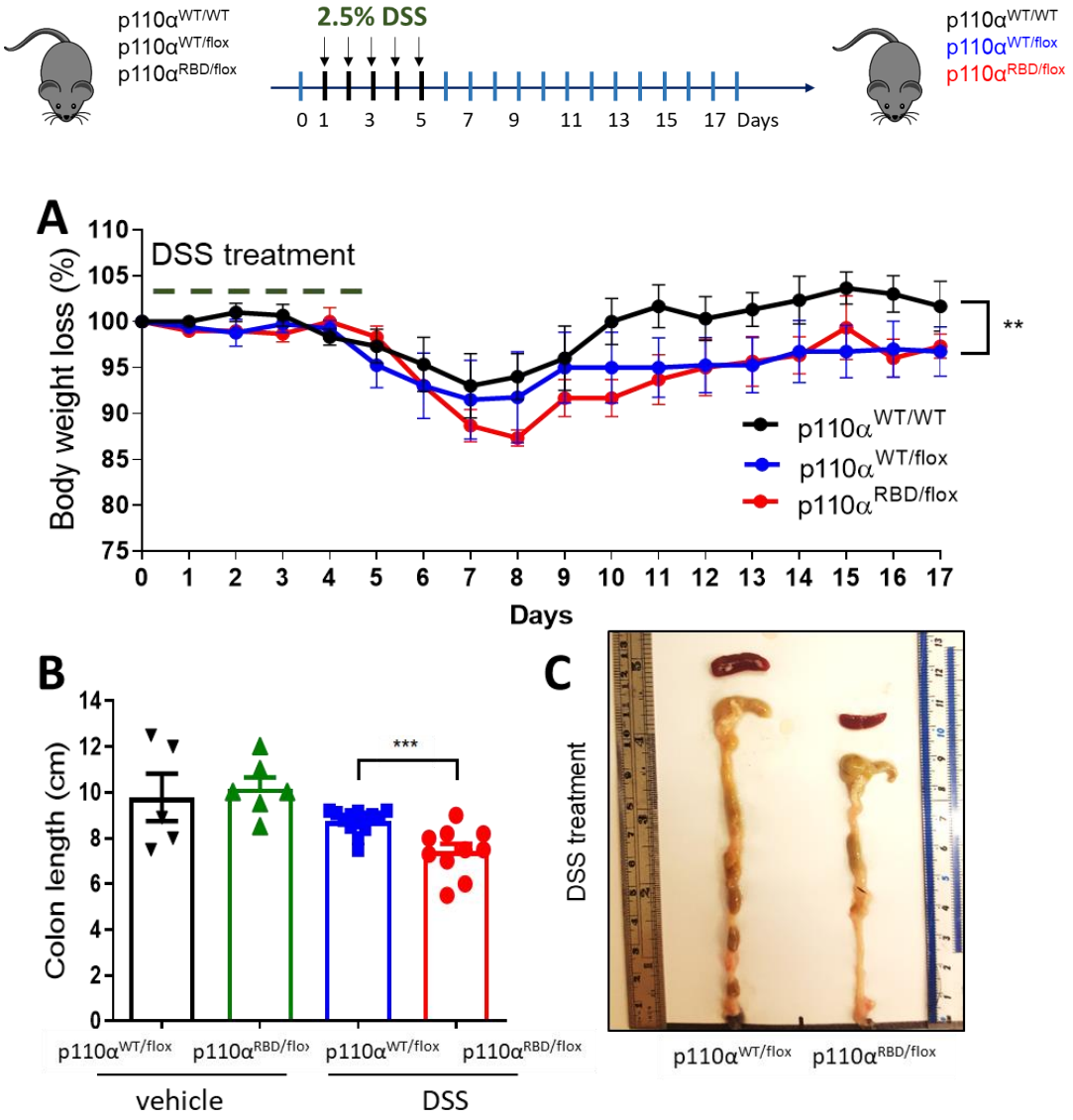

Figure 43: The p110α-RBD interaction causes long term susceptibility following acute chemically-induced DSS injury. . Healthy age and sex-matched p110α$^{WT/WT}$, p110α$^{WT/flox}$, and p110α$^{RBD/flox}$ mice were given 2.5% DSS treatment for five days. **(A)** The graph represents means ± SEM percentage of weight loss for 17 (n=10 mice per mouse strain). **(B)** The bar graph represents means ± SEM of colon length of indicated mice strains (n=5-10 mice per mouse strain). **(C)** The photo shows colons length of indicated mouse strains after DSS treatment. Statistical analysis of data expressed as mean ± SEM **(A)** **p<0.01 after DSS treatment at day 17 by Two-way ANOVA and **(B)** ***p<0.001 by Student t-test.

4.2.4. Disruption of p110α-RBD interaction in mice results in impaired intestinal architecture

In order to investigate the cause of partial lethality and disruption of the intestinal epithelium after DSS acute treatment in $p110\alpha^{WT/-}$ and $p110\alpha^{RBD/-}$ mice, we analysed H&E stained small intestinal and colonic tissue from each mouse strain after vehicle or DSS treatment. The H&E stained tissues from the small intestine under basal conditions following tamoxifen treatment, showed visually discernible alterations and graduate loss of villi architecture in the $p110\alpha^{WT/-}$ and $p110\alpha^{RBD/-}$ compared to $p110\alpha^{WT/WT}$ (**Figure 44A**). Following DSS injury, increased damage, abnormal architecture at the small intestine, and reduced crypt length, were observed in both mutant mice groups compared to our control group $p110\alpha^{WT/WT}$, being $p110\alpha^{RBD/-}$ the most prominent (**Figure 44B**). Colonic H&E stained tissues from the small intestine under basal conditions following tamoxifen treatment, did no show visible alterations (**Figure 44C**). However, following DSS injury, increased crypt loss and abnormal and damged colonic architecture were observed in both mutant mice groups compared to our control group $p110\alpha^{WT/WT}$, being $p110\alpha^{RBD/-}$ the most prominent (**Figure 44D**).

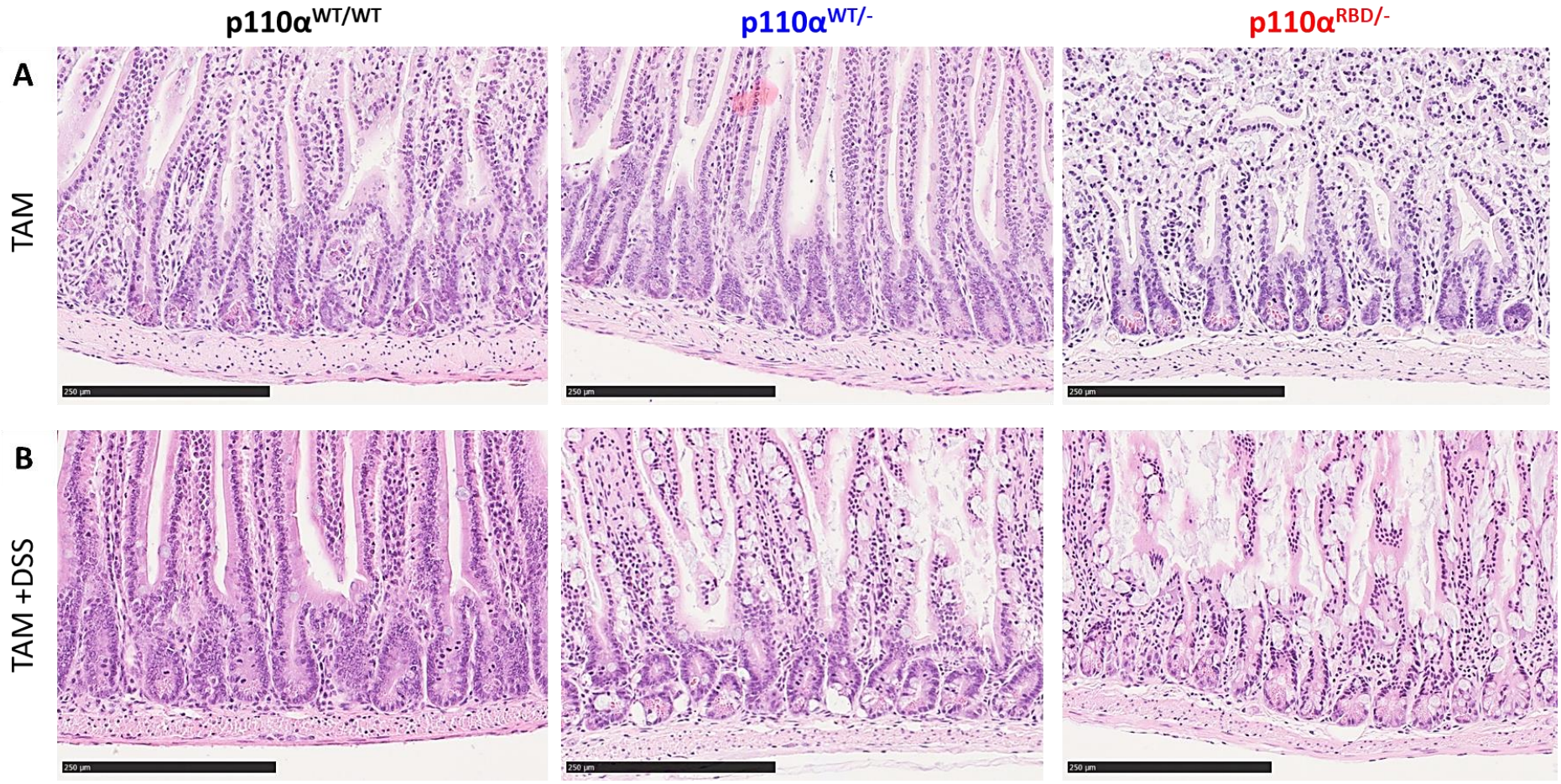
p110α^WT/WT
p110α^WT/-
p110α^RBD/-
A
TAM
B
TAM +DSS
250 µm

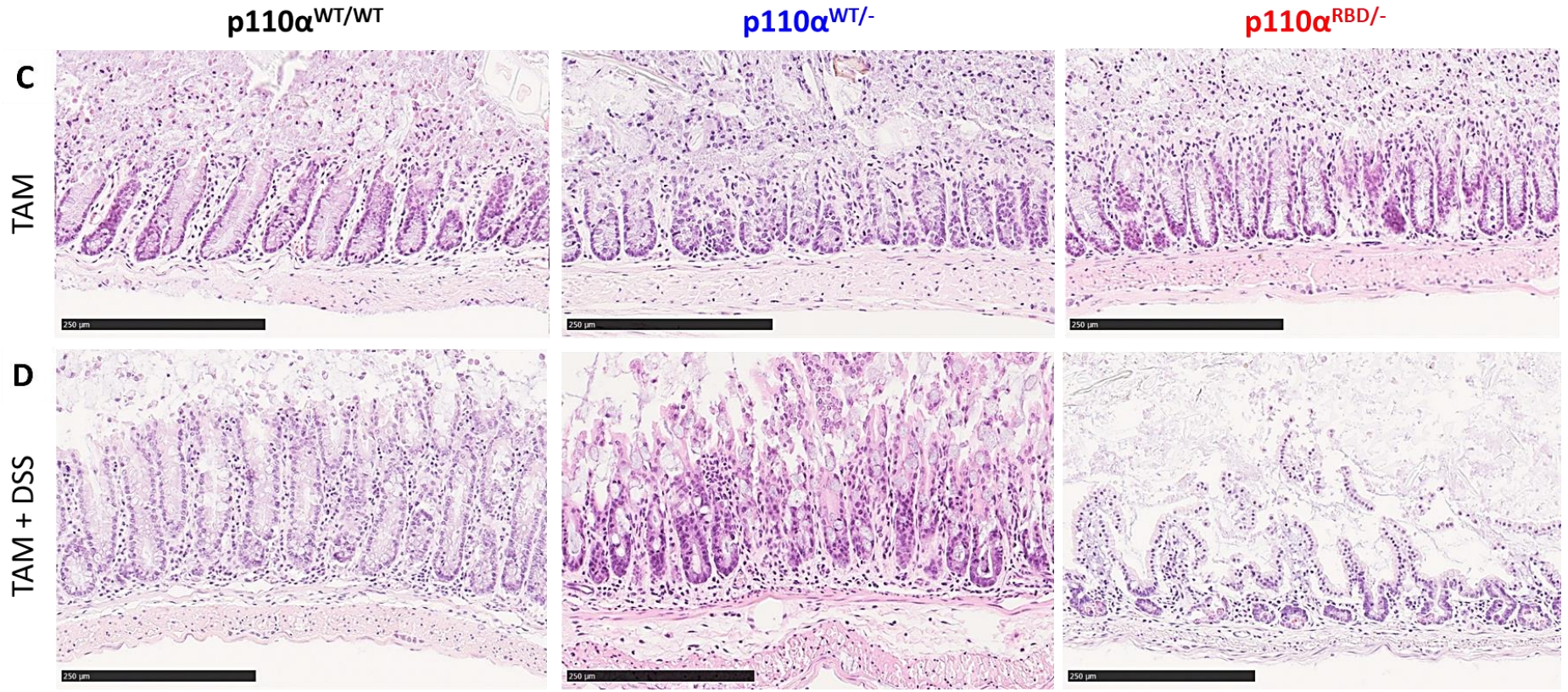
p110α^WT/WT
p110α^WT/-
p110α^RBD/-
C
TAM
D
TAM + DSS
250 µm

Figure 44: Acute DSS injury in p110α$^{RBD/-}$ and p110α$^{WT/-}$ mice result in disrupted intestinal architecture and organisation. Health age-matching p110α$^{WT/WT}$, p110α$^{WT/flox}$, and p110α$^{RBD/flox}$ males received tamoxifen 2 weeks prior to vehicle or 2.5% DSS treatment. The micrographs represent H&E staining of zinc fixative fixed and paraffin-embedded from **(A-B)** small intestine and **(C-D)** colon sections at day 7 after **(A-C)** vehicle or **(B-D)** 2.5% DSS treatment from indicated mice strains p110α$^{WT/WT}$, p110α$^{WT/-}$, and p110α$^{RBD/-}$. H&E staining tissues were scanned using NanoZoomer S210 digital microscope and pictures were analysed with NDP.view2 software. The photos represent one out of n=6-14 independent mouse from each strain and treatment tissue fixed and stained. Scale bars indicate 250 μm.

Based on the analyses of H&E stained small intestinal or colonic tissue from each mouse strain, a semi-quantitative histology scoring was carried. We observed no marked differences between the three groups regarding inflammation after DSS (**Figure 45**). These results suggested that p110α$^{RBD/-}$ and to a lesser extend p110α$^{WT/-}$ exhibited partial lethality after DSS injury which may potentially originate from a damaged villi and disruptive intestinal architecture. The disruption may be due to an induced apoptosis of multiple adult IECs, the reconstitution and regeneration of the intestinal tissue cannot be accomplished in time in p110α$^{RBD/-}$ and to a lesser extend p110α$^{WT/-}$ mice strains. However, what needs to be addressed is whether increased proliferation is met with increased cellular differentiation into secretory and absorptive cell types and whether p110α-RBD regulates intestinal cell proliferation or differentiation.

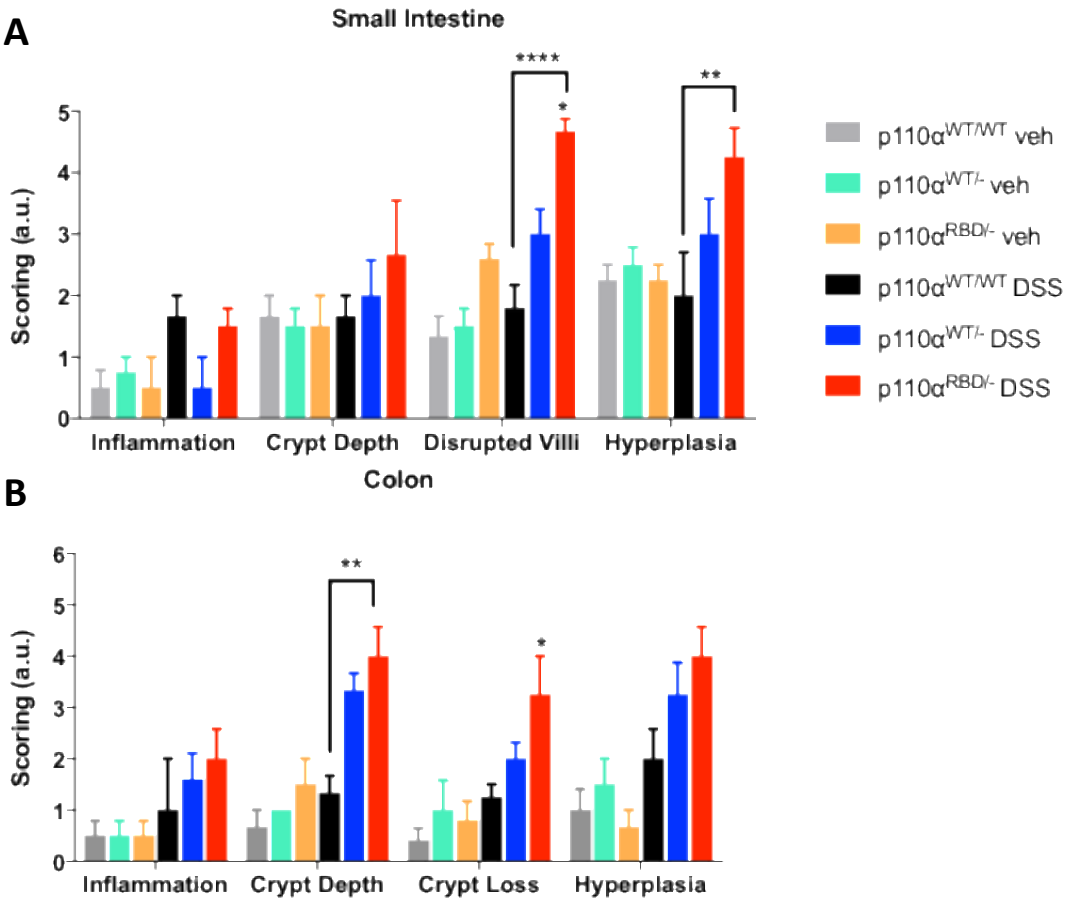

Figure 45: The p110α$^{RBD/-}$ and p110α$^{WT/-}$ mice result in increased damage and disruption of the intestinal architecture after DSS injury. The graphs show semi-quantitative analysis based on the histopathological scoring of H&E stained from **(A)** small intestine and **(B)** colon tissues from p110α$^{WT/WT}$, p110α$^{WT/-}$, and p110α$^{RBD/-}$ adult mice administered tamoxifen via oral gavage prior to by vehicle (veh) or DSS treatment. The graphs represent means ± SEM disease activity index (DAI) scoring of indicated mouse strains (n=3-4 mouse per mouse strain). **(A-B)** Statistical analysis from mean ± SEM (n=4 per mouse strain) by Two-way ANOVA are; **(A)** ****p<0.0001 disrupted villi, and **p<0.01 hyperplasia in p110α$^{RBD/-}$ mice after vehicle or DSS compared to p110α$^{WT/WT}$; **(B)** **p<0.01 crypt depth, and *p<0.05 of crypt loss in p110α$^{RBD/-}$ compared to p110α$^{WT/WT}$ after DSS.

4.2.5. Disruption of the p110α-RBD interaction does not alter inflammatory response to LPS but selectively upregulates GFs and IL-33 secretion from intestinal explants *ex vivo*

In the next set of experiments, we have analysed whether increased susceptibility to DSS injury may result from damage associated bacterial translocation and ensuing response to bacterial components. In these experiments, intestinal explants of similar size and regions were obtained from small intestine and colon tissue of $p110\alpha^{WT/-}$ or $p110\alpha^{RBD/-}$ mice, which were previously treated by tamoxifen. The tissues were stimulated with bacterial ligand LPS or MDP for 18 h and culture supernatants were analysed by ELISAs for inflammatory and anti-inflammatory cytokines, as well GFs and IL-33. Cytokine secretion of IL-1β, IL-6 (**Figure 46**), and anti-inflammatory IL-10 (**Figure 47**) were comparable following LPS or MDP simulations with the exception of IL-6, which tended to be significant lower under basal conditions from small intestinal explants of $p110\alpha^{RBD/-}$ mice. The secreted EGF tended to be significantly lower in all conditions from the small intestinal explants but not colons *ex vivo* (**Figure 48A-B**). Interestingly, epiregulin levels secreted from $p110\alpha^{RBD/-}$ small intestinal explants were significantly increased, while was unaltered in the colon explants (**Figure 48C-D**). IL-33 is a member of the IL-1 superfamily of cytokines that acts as an alarmin, released from the intestinal microenvironment such as the stroma-associated fibroblasts and intraepithelial lymphocytes during mucosal injury and inflammatory conditions by promoting epithelial cell proliferation and wound healing processes to initiate tissue restitution[208–211]. In line with the increased susceptibility of $p110\alpha^{RBD/-}$ mice to DSS damage *in vivo*, we observed an increase in the fold induction of LPS-induced IL-33 from the small intestinal explants of $p110\alpha^{RBD/-}$ mice in comparison to the fold increase in $p110\alpha^{WT/-}$ mice, indicating increased response to bacterial PAMPs

(**Figure 49**). Under basal conditions IL-33 levels were also higher in the p110α$^{RBD/-}$ mouse colons indicating increased damage response. Overall, our data suggested that p110α-RBD interaction reduces inflammatory alarm response to the barrier damage to the intestinal tissue either by a protective effect in IECs, supporting tissue repair or indirectly dampening IL-33 production from the intestinal microenvironment.

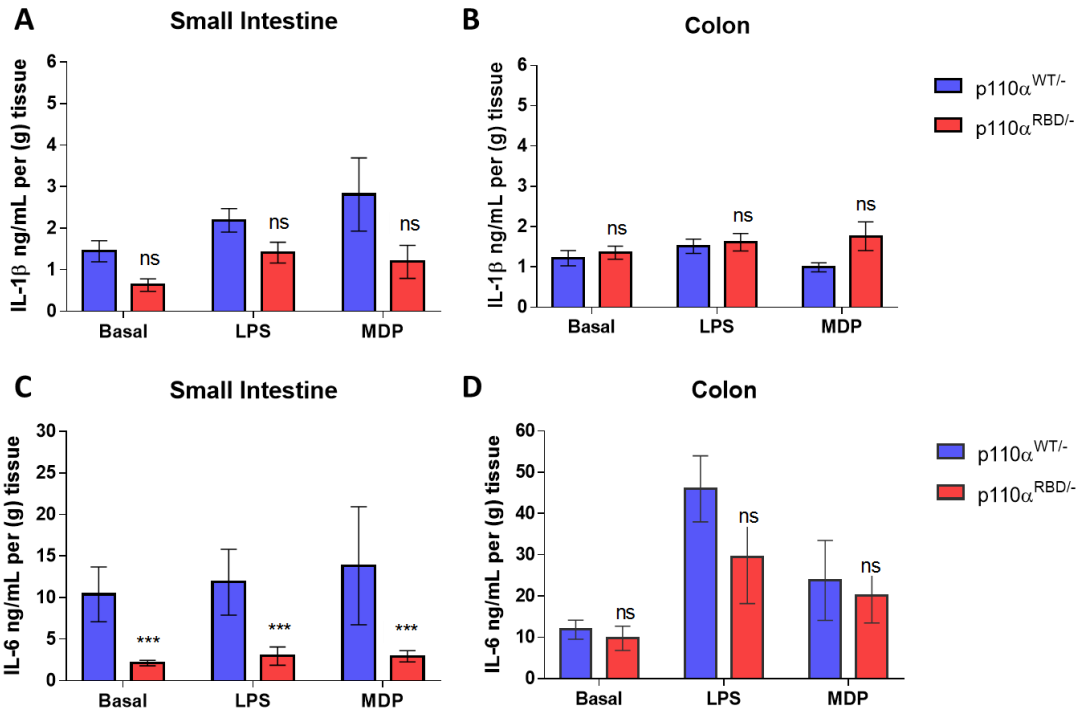

Figure 46: The p110α-RBD interaction does not alter Il-1β cytokine secretion but regulates IL-6 production from the small intestinal explants. The graphs represent ELISA analysis for **(A-B)** IL-1β, and **(C-D)** IL-6 secretion measured from culture supernatants obtained from p110α$^{WT/-}$ or p110α$^{RBD/-}$ mice **(A, C)** small intestine or **(D, E)** colon explants, which were activated by LPS (1 µg/mL), MDP (30 ng/mL), or basal (left in medium alone). **(A-D)** Statistical analysis from mean ± SEM (n=4-12 per mouse strain) by One-way ANOVA are; **(A, B, D)** no significant (ns), and **(C)** ***p<0.001.

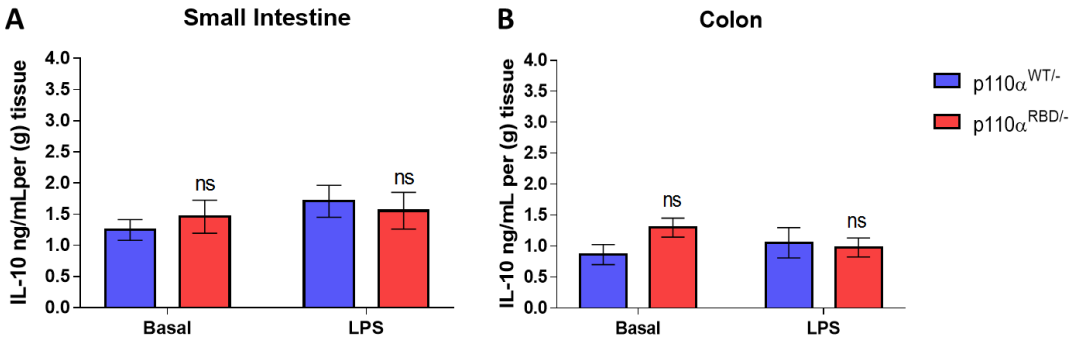

Figure 47: The p110α-RBD interaction is not critical for the anti-inflammatory cytokine secretion in mice intestinal explants *ex vivo*. The graphs represent ELISA analysis for IL-10 cytokine secretion measured in culture supernatants obtained from p110α$^{WT/-}$ or p110α$^{RBD/-}$ mice **(A)** small intestine and **(B)** colon explants, which were activated by LPS (1 µg/mL), or basal (left in medium alone). **(A-B)** Statistical analysis from mean ± SEM (n=7-12 per mouse strain) by One-way ANOVA are no significant (ns).

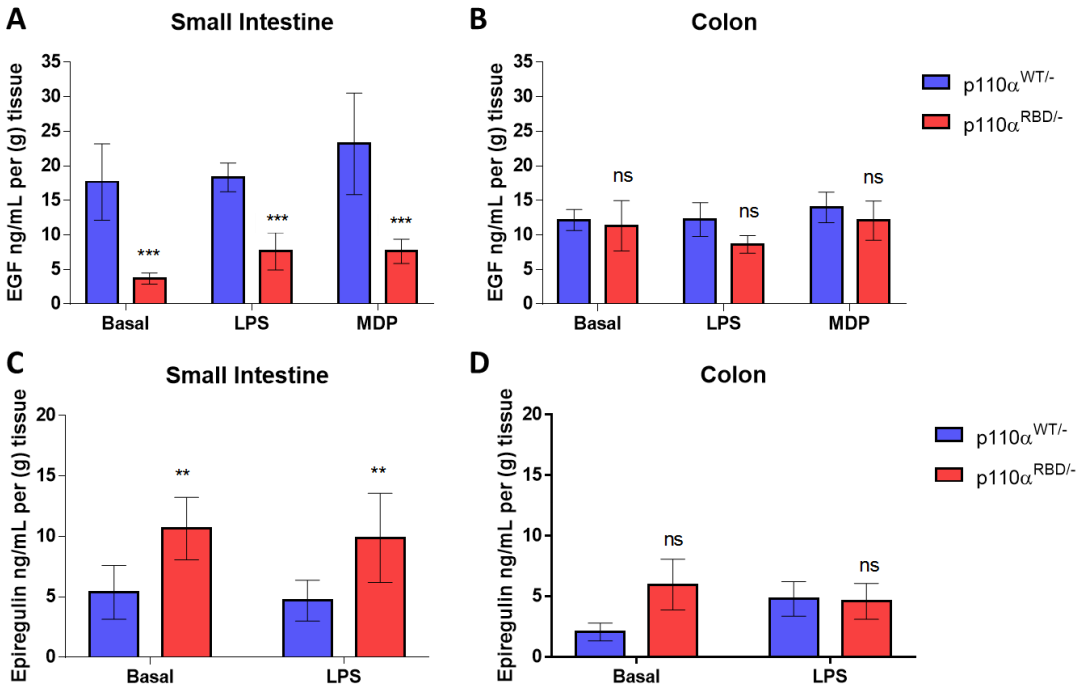

Figure 48: The p110α-RBD interaction regulates GFs secretion in mice small intestine but not colon explants *ex vivo*. The graphs represent means ± SEM cytokine levels from supernatants of indicated tissues, obtained from p110α$^{WT/-}$ or p110α$^{RBD/-}$ mice. ELISA analysis for **(A-B)** EGF in small intestine and colon explants activated by LPS (1 µg/mL), MDP (30 ng/mL), or basal (left in medium alone); and **(C-D)** Epiregulin in small intestine

and colon explants activated by LPS (1 µg/mL) or NS. **(A-B)** Statistical analysis from mean ± SEM (n=4-6 per mouse strain) by One-way ANOVA are **(A)** ***p<0.001; **(B)** no significant (ns), **(C)** **p<0.01, and **(D)** ns.

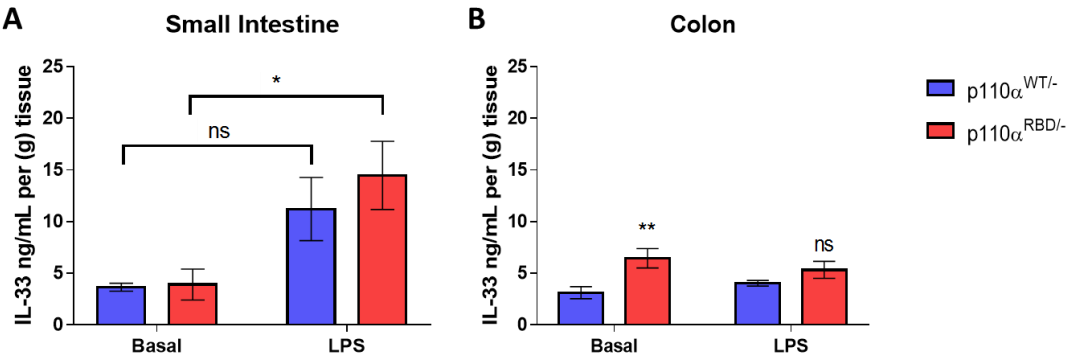

Figure 49: The p110α-RBD interaction mediates Il-33 cytokine secretion in mice after bacterial exposure in intestinal explants *ex vivo*. The graphs represent means ± SEM cytokine levels from supernatants of indicated tissues, obtained from p110α$^{WT/-}$ or p110α$^{RBD/-}$ mice. ELISA analysis for IL-33 cytokine secretion measured from culture supernatants obtained from **(A)** small intestine and **(B)** colon explants activated by LPS (1 µg/mL), or basal (left in medium alone). **(A-B)** Statistical analysis from mean ± SEM (n=4-6 per mouse strain) by One-way ANOVA are; **(A)** no significant (ns) in p110α$^{WT/-}$mice after LPS activation, **p<0.01 in p110α$^{RBD/-}$mice after LPS activation in small intestine; and **(B)** **p<0.01 in p110α$^{RBD/-}$ mice at basal conditions compared to p110α$^{WT/-}$ in colon explants.

4.2.6. The p110α-RBD inactivation results in increased proliferation and altered CBCs niche after acute DSS intestinal injury

IECs from p110α$^{WT/WT}$, p110α$^{WT/-}$, and p110α$^{RBD/-}$ after vehicle or DSS treatment, were isolated and stained as previously described (**Section 3.7 & 3.8**) in order to quantify through FACS proliferative levels, using Ki67 antibody, as well

as Lgr5+ stem cell population, and secretory/Paneth cells using CD24 antibody[138,212]. From whole sample of IECs isolated and stained (FSC-A, SSC-A), dead cells (Aqua, SSC-A) and doublets were excluded. IECs were positively selected with EpCAM-CD36 antibody and leukocytes discriminated with CD45 antibody ($EpCAM^{+}CD45^{-}$). Proliferative cells were selected from $EpCAM^{+}CD45^{-}$ subpopulation ($Ki67^{hi}$). Positive secretory/Paneth cells population ($CD24^{hi}$) as well as Lgr5+ stem cells ($Lgr5^{hi}$) were also selected from the $EpCAM^{+}CD45^{-}$ subpopulation. Gating strategy used and unstained/FMO controls are described in **Figure 50** & **Figure 51**.

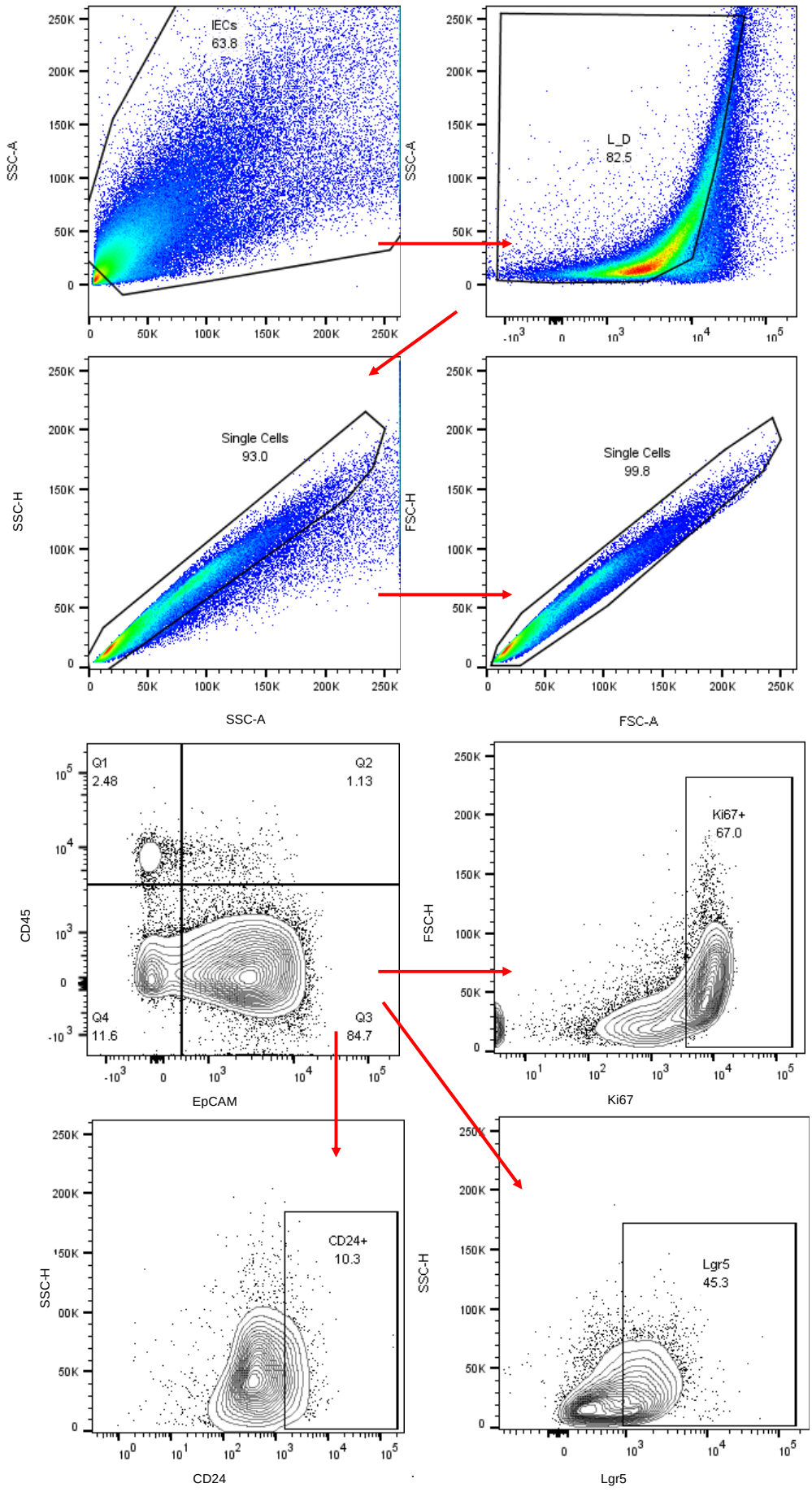
IECs
63.8
SSC-A
L_D
82.5
Single Cells
93.0
SSC-H
Single Cells
99.8
FSC-H
SSC-A
FSC-A
Q1
2.48
Q2
1.13
Q4
11.6
Q3
84.7
CD45
EpCAM
Ki67+
67.0
FSC-H
Ki67
CD24+
10.3
SSC-H
CD24
Lgr5
45.3
SSC-H
Lgr5

Figure 50: Gating strategy used for IECs staining. IECs isolated and stained from small intestine and colon (FSC-A, SSC-A), were excluded of dead cells (Aqua, SSC-A), and doublets (FSC-A, FSC-H). IECs were positively selected with EpCAM-CD36 antibody and leukocytes discriminated with CD45 antibody ($EpCAM^{+}CD45^{-}$). Proliferative cells were selected from $EpCAM^{+}CD45^{-}$ subpopulation ($Ki67^{hi}$, FSC-H). Higher expression secretory/Paneth cells population ($CD24^{hi}$, SSC-H) were also selected from the $EpCAM^{+}CD45^{-}$ subpopulation. One out of >100 is shown.

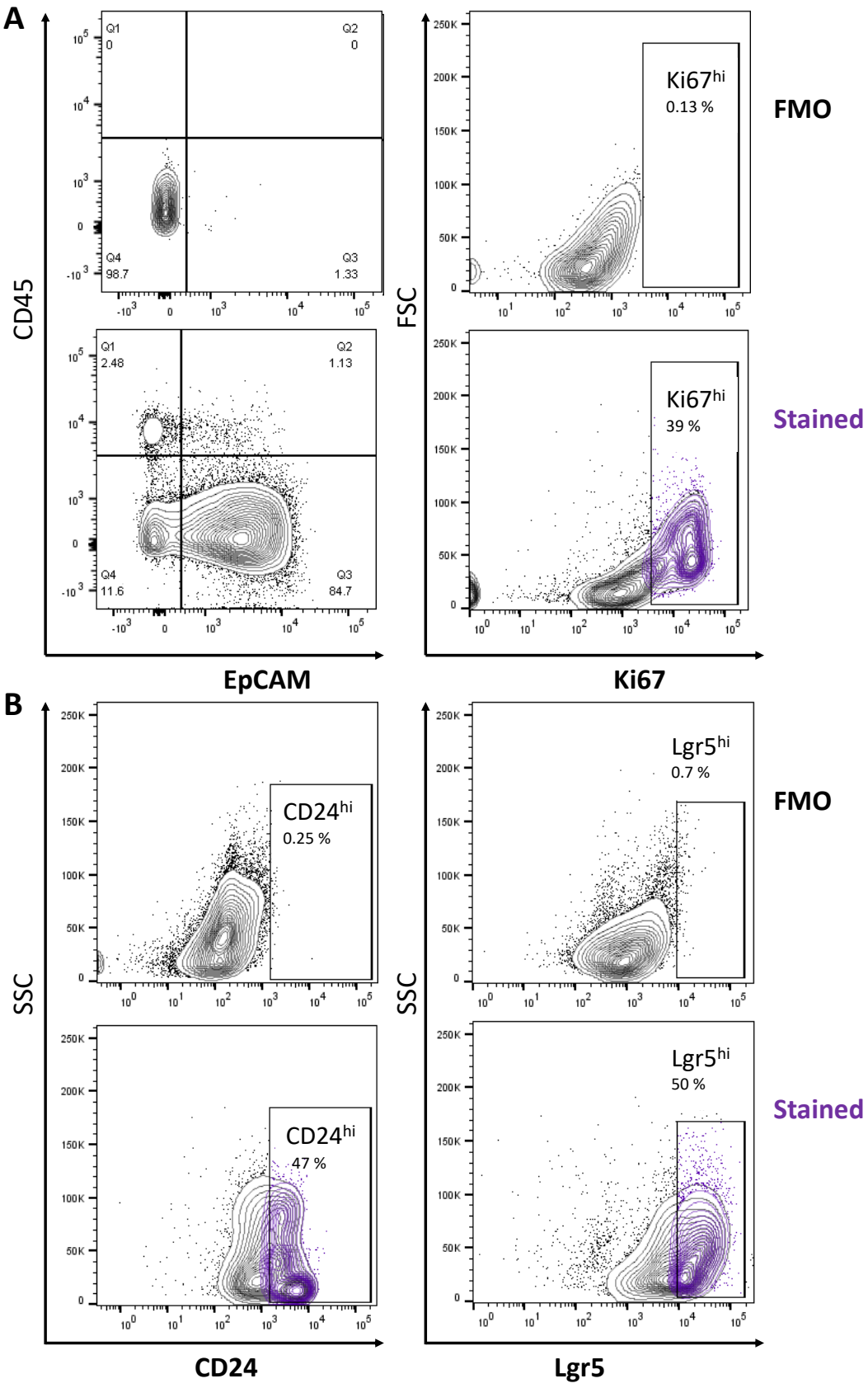
A
CD45
EpCAM
Q1
0
Q2
0
Q4
98.7
Q3
1.33
Q1
2.48
Q2
1.13
Q4
11.6
Q3
84.7
FSC
Ki67
Ki67hi
0.13 %
Ki67hi
39 %
FMO
Stained
B
SSC
CD24
CD24hi
0.25 %
CD24hi
47 %
SSC
Lgr5
Lgr5hi
0.7 %
Lgr5hi
50 %
FMO
Stained

Figure 51: Controls and unstained samples utilised for FACS gating strategy. The gates indicate a sample for each antibody utilised in the full staining compared to a sample engaged for a fluorescence minus one (FMO) staining, which includes all antibodies excluding the one desired in order to add the correct gate strategy for the assay. Unstained sample were also added to all the controls panel. The figure shows an example of FMO sample compared to the stained and gating strategy utilised for all the flow cytometry assays for **(A)** $EpCAM^{+}CD45^{-}$, $Ki67^{hi}$, **(B)** $CD24^{hi}$, and $Lgr5^{hi}$.

Isolation and staining of IECs from $p110\alpha^{WT/WT}$, $p110\alpha^{WT/-}$, and $p110\alpha^{RBD/-}$ were analysed and compared to each mouse strain with and/or without DSS treatment as described above. The $EpCAM^{+}CD45^{-}$ subpopulation from each mouse strain and group was consistent indicating purification of IECs isolation. Under basal conditions, there was no tendency or minimal toward increased expression of $Ki67^{hi}$ and $CD24^{hi}$ expression from $EpCAM^{+}CD45^{-}$ subpopulation from each mouse strain. However, the percentage of $Ki67^{hi}$ and $CD24^{hi}$ expression from $EpCAM^{+}CD45^{-}$ subpopulation, were significantly increased after DSS treatment in $p110\alpha^{RBD/-}$ mice compared to $p110\alpha^{WT/WT}$ and $p110\alpha^{WT/-}$ control counterparts (**Figure 52**). Furthermore, the percentage of $Lgr5^{hi}$ expression from $EpCAM^{+}CD45^{-}$ subpopulation, was significantly increased in in $p110\alpha^{RBD/-}$ and $p110\alpha^{WT/-}$ after DSS intestinal injury compared to $p110\alpha^{WT/WT}$ (**Figure 53**). The mean fluorescence intensity (MFI) of $EpCAM^{+}CD45^{-}$ and $CD24^{hi}$ subpopulations were comparable under DSS treatment. Our results showed significantly increased $Ki67^{hi}$ and $Lgr5^{hi}$ MFI expression in the $EpCAM^{+}CD45^{-}$ population under DSS treatment in the IECs of the $p110\alpha^{WT/-}$ and $p110\alpha^{RBD/-}$ in comparison to the control counterparts (**Figure 54**).

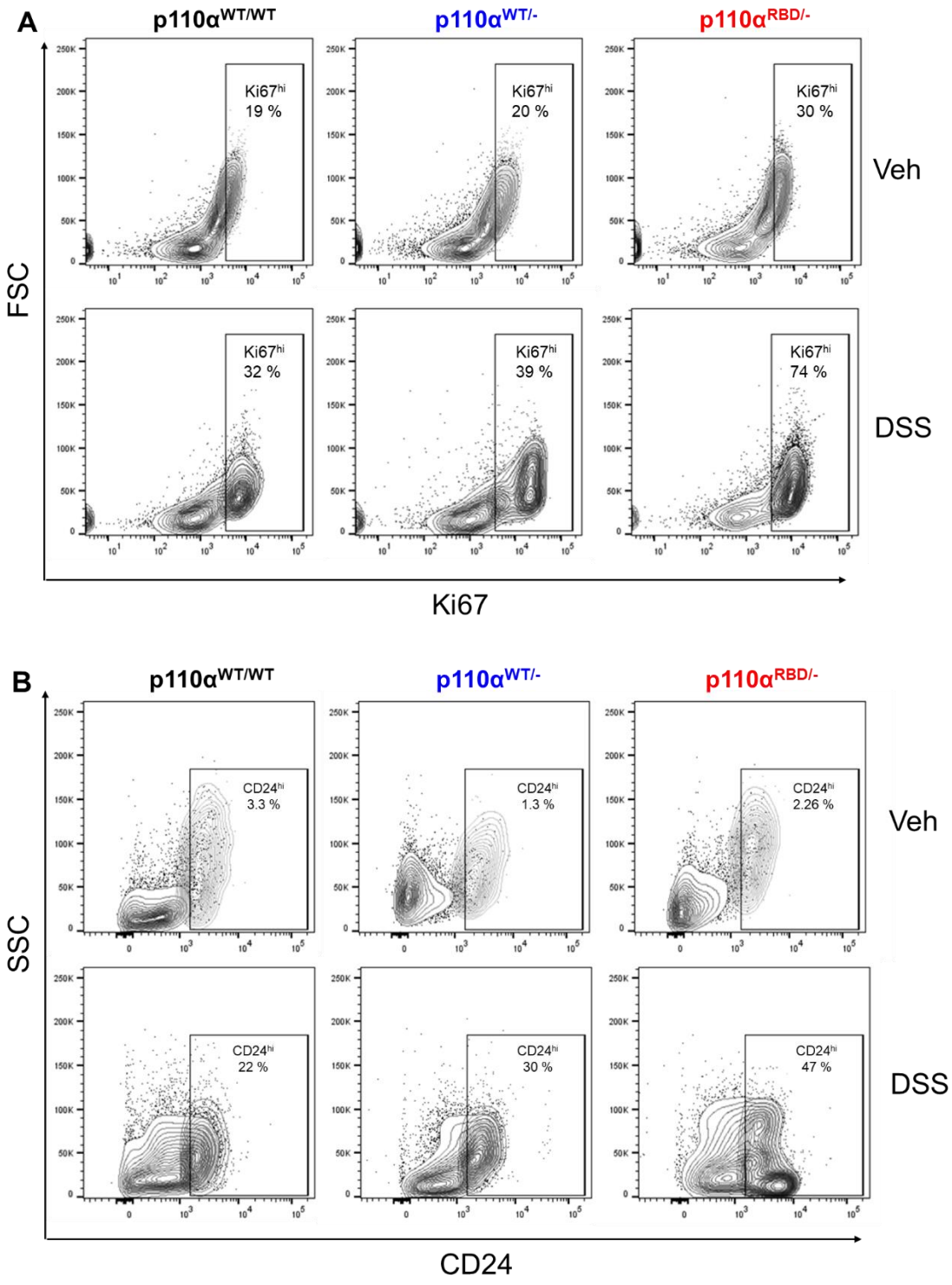
A
p110α^WT/WT
p110α^WT/-
p110α^RBD/-
Ki67^hi 19 %
Ki67^hi 20 %
Ki67^hi 30 %
Ki67^hi 32 %
Ki67^hi 39 %
Ki67^hi 74 %
Veh
DSS
FSC
Ki67
B
p110α^WT/WT
p110α^WT/-
p110α^RBD/-
CD24^hi 3.3 %
CD24^hi 1.3 %
CD24^hi 2.26 %
CD24^hi 22 %
CD24^hi 30 %
CD24^hi 47 %
Veh
DSS
SSC
CD24

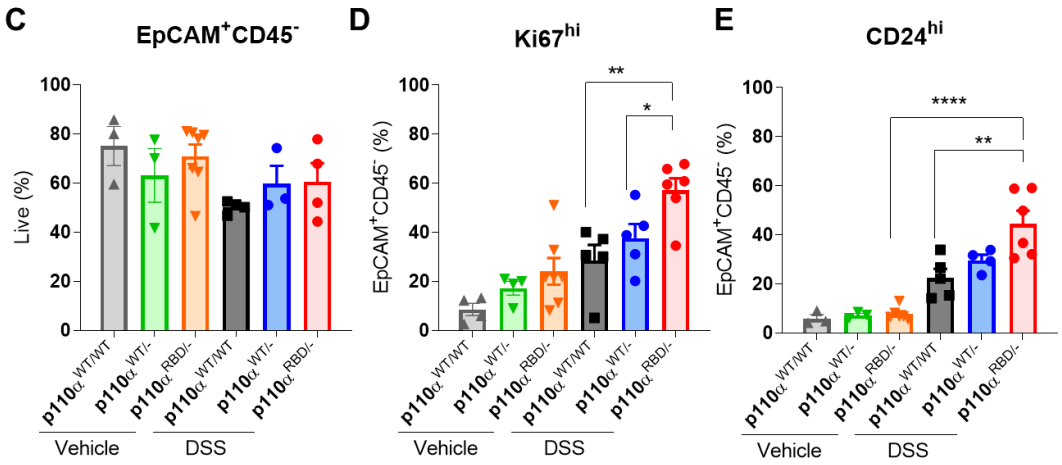

Figure 52: Acute DSS intestinal injury results in increased representation of Ki67^{hi} and CD24^{hi} IEC populations in p110α$^{RBD/-}$ mice. Gating examples show frequent of parent (EpCAM^{+}CD45^{-}) subpopulation of IECs isolated and stained from each mouse strain; p110α$^{WT/WT}$, p110α$^{WT/-}$, and p110α$^{RBD/-}$ after vehicle or DSS treatment. **(A)** Proliferative cells were selected from EpCAM^{+}CD45^{-} subpopulation (Ki67^{hi}). **(B)** Positive secretory/Paneth cells population (CD24^{hi}) were also selected from the EpCAM^{+}CD45^{-} subpopulation. One out of 4 from each mouse strain and condition is shown. **(C-E)** The graphs represent percentage of parent from **(C)** EpCAM^{+}CD45^{-}, **(D)** Ki67^{hi}, and **(E)** CD24^{hi} subpopulation from each mouse strain after vehicle or DSS treatment. Statistical analysis shows mean ± SEM (n=3–6) mice per group **(C)** ****p<0.0001 after vehicle treatment, **(D)** *p<0.05, and **(E)** **p<0.01 after DSS treatment by One-way ANOVA.

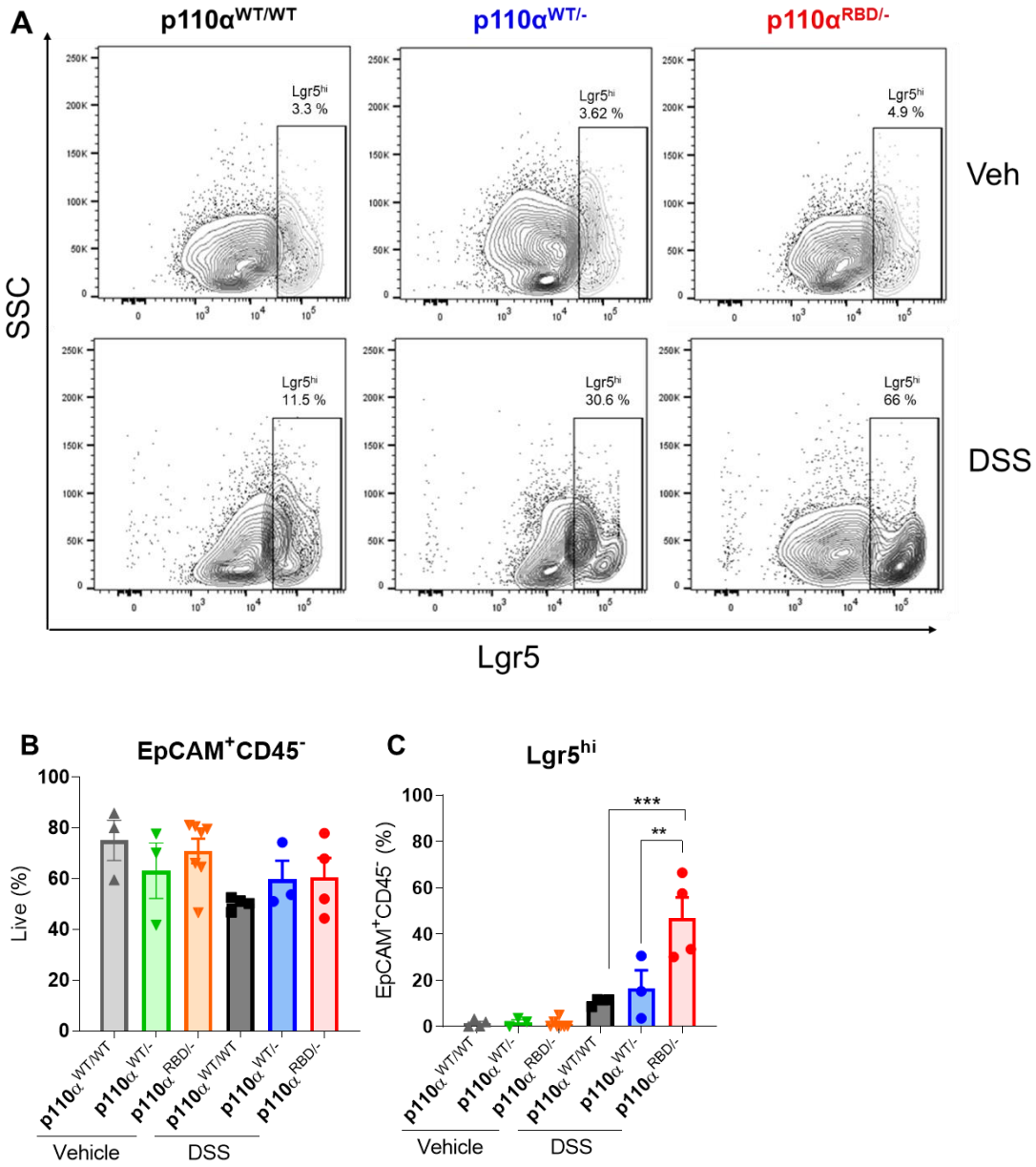

Figure 53: The p110α-RBD mice exhibit contracted Lgr5^{hi} IEC population under basal levels which is increased after DSS-mediated intestinal injury. Gating examples show frequent of parent (EpCAM^{+}CD45^{-}) subpopulation of small intestinal cells isolated and stained from each group; p110α$^{WT/WT}$, p110α$^{WT/-}$, and p110α$^{RBD/-}$ after vehicle or DSS treatment. **(A)** Lgr5^{hi} cells were selected from EpCAM^{+}CD45^{-} subpopulation. One out of 4 from each mouse strain and condition is shown. **(B-C)** The graphs represent percentage of parent from each mouse strain after vehicle or DSS treatment from **(B)** EpCAM^{+}CD45^{-}, and **(C)** Lgr5^{hi} subpopulations. **(B-C)** Statistical analysis show mean ± SEM (n=3–10) mice per group by One-way ANOVA are **(B)** ****p<0.0001 in p110α$^{WT/-}$ and p110α$^{RBD/-}$ after vehicle treatment compared to control counterparts, and **(C)** ****p<0.0001 in p110α$^{RBD/-}$ compared to control counterparts after DSS treatment.

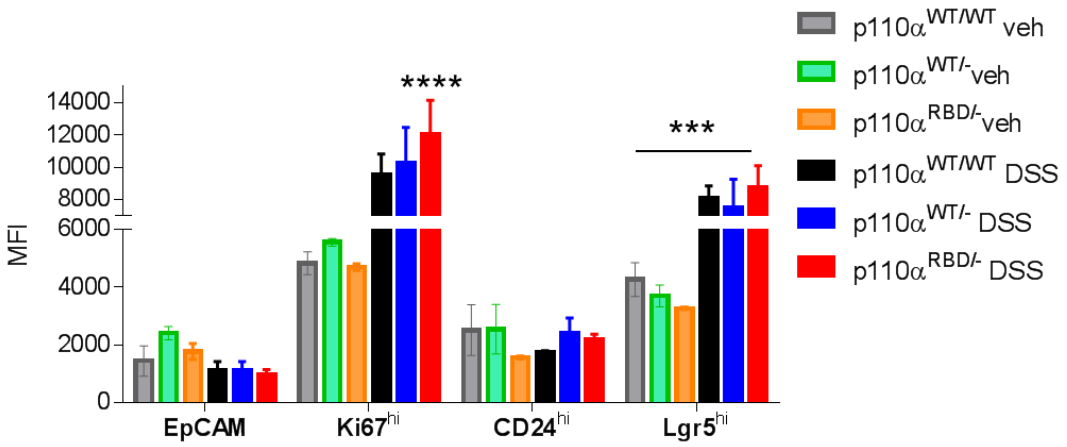

Figure 54: The p110α-RBD inactivation marginally alters the expression levels of Ki67^{hi} and Lgr5^{hi} subpopulations after acute DSS injury. The graph shows mean ±SEM of mean fluorescence intensity (MFI) levels of EpCAM^{+}CD45^{-}, Ki67^{hi}, CD24^{hi}, and Lgr5^{hi} subpopulations of p110α$^{WT/WT}$, p110α$^{WT/-}$, and p110α$^{RBD/-}$ adult mice after vehicle (veh) treatment or DSS-mediated intestinal injury (n=3-8). Statistical analysis shows mean ± SEM (n=3–10) mice per group by One-way ANOVA are ****p<0.0001 for Ki67^{hi} in p110α$^{RBD/-}$ compared to control counterparts after DSS treatment; and ***p<0.001 for Lgr5^{hi} in all mouse strains after DSS treatment compared to vehicle treatment.

Overall, these results showed that gene dosage-dependent loss of p110α expression together with disrupted p110α-RBD inactivity collectively increased CD24^{+} and Lgr5+ cell proliferation resulting in hyperplasia in the small intestine after DSS injury. In this scenario, injury-induced hyperplasia favoured Lgr5+ cell lineage as well as an increase in the secretory/Paneth cells, which could be due to injury induce dedifferentiation from differentiated IECs after injury as several studies had shown[127,213].

4.2.7. The p110α-RBD inactivation results in increased Bmi1 expression in IECs after acute DSS injury

Small intestine, colon, liver and spleen from each mouse euthanized were kept with RNAlater at -80ºC for further RNA isolation. Since we observed mainly differences in the small intestine between groups, we investigated the genetic expression in the small intestine for several transcription factors such as; EpCAM (lineage marker), Ascl2 (Wnt signalling), Notch signalling, Olfm4 (Lgr5+ stem cells), Bmi1 (+4 stem cells), Mmp7 (Paneth cells), Muc2 (goblet cells), Wdr43 (TA cells). RNA from >60 mg of small intestine from each mouse strain, was isolated and processed for reverse transcription assay in order to obtain cDNA for further RT-PCR assay as previously described (**Section 3.5**). These results showed significantly increased levels of Bmi1 in $p110\alpha^{RBD/-}$ mouse and $p110\alpha^{WT/-}$ compared to $p110\alpha^{WT/WT}$ after DSS treatment. Interestingly, levels of Bmi1 were already increased in the $p110\alpha^{RBD/-}$ mouse stain after vehicle treatment compared to $p110\alpha^{WT/-}$ and $p110\alpha^{WT/WT}$ mouse strains. Relative gene expression of Mmp7 was significantly increased in both mutant mouse strains ($p110\alpha^{WT/-}$ and $p110\alpha^{RBD/-}$) after vehicle or DSS treatment compared to compared to the control $p110\alpha^{WT/WT}$ mouse strain, which levels of Mmp7 increased after DSS treatment (**Figure 55**). Our results showed no significant (ns) differences between each mouse strain in other lineage markers such as Ascl2, Olfm4 and Wdr43. However, some limitations have to be considered on RT-PCR assays due to relative gene expression does not mean protein expression and therefore other assays should be carried such as immunohistochemistry at the tissue samples already embedded. Furthermore, other genes should be considered for future assays such as Atoh1 and Hes1 in order to look at IECs from absorptive lineage as they might be relevant for this study[133,214].

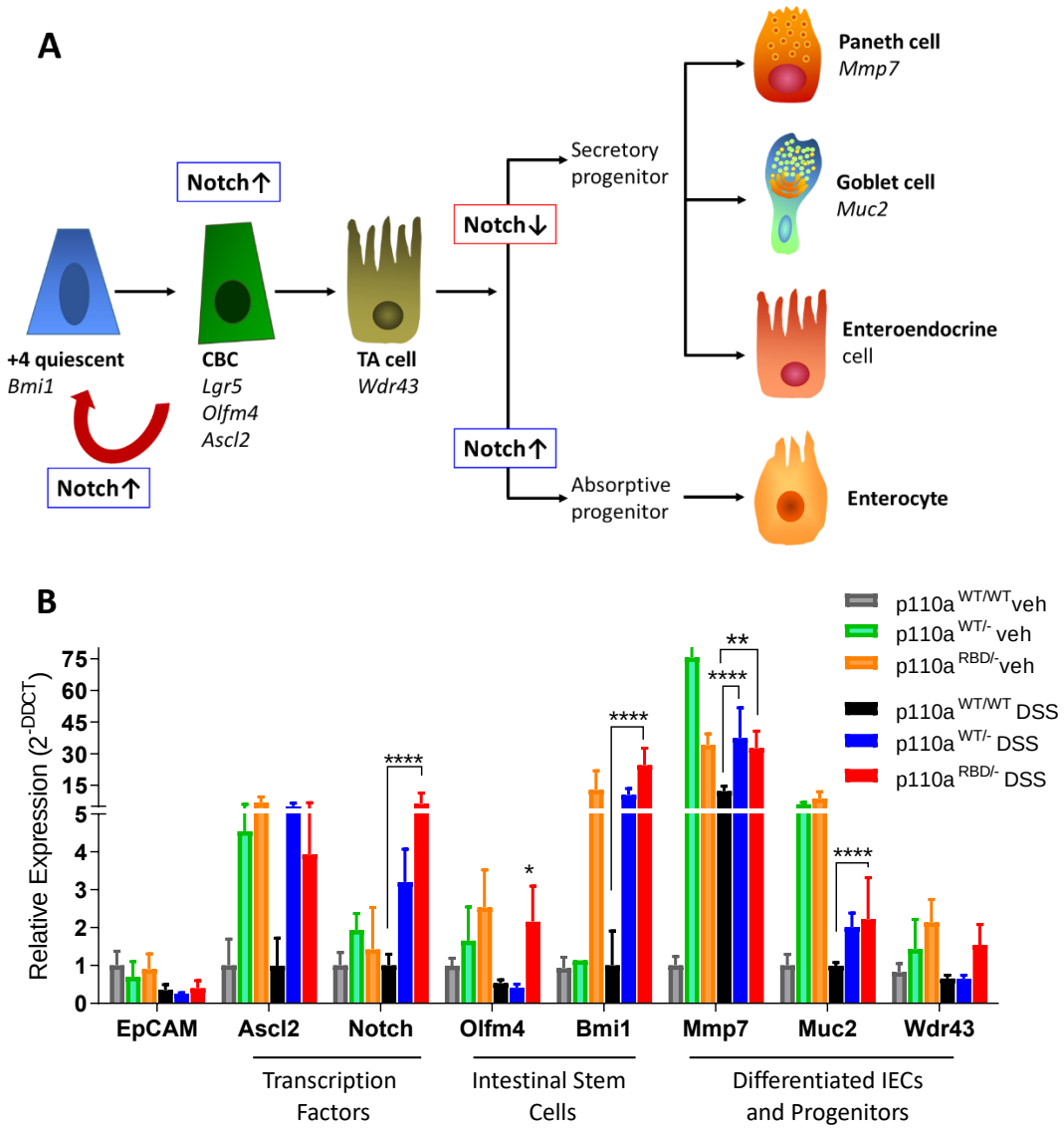

Figure 55: The p110α-RBD mutant mice exhibit increased Bmi1 gene expression along with high Notch and secretory lineage markers after acute DSS injury. (A) Schematic representation of murine ISCs differentiation. Illustration from (Laura Medrano-González). **(B)** The RNA was isolated from small intestines collected from p110α$^{WT/WT}$, p110α$^{WT/-}$, and p110α$^{RBD/-}$ adult mice after vehicle or DSS treatment. Samples were processed for further RT-PCR assay. The graph shows detection of the following transcription factors expressed in relative gene expression ($2^{-\Delta\Delta CT}$); EpCAM (lineage marker), Ascl2 (Wnt signalling), Notch signalling, Olfm4 (Lgr5+ stem cells), Bmi1 (+4 stem cells), Mmp7 (Paneth cells), Muc2 (goblet cells), Wdr43 (TA cells). GAPDH was used as reference gene and $2^{-\Delta\Delta CT}$ from each condition was normalised to p110α$^{WT/WT}$ mouse with vehicle (veh) treatment. Statistical analysis shows mean ± SEM by One way ANOVA (n=4-8): ****p<0.0001 of Notch, Bmi1, and Muc2 gene expression in p110α$^{WT/-}$ and p110α$^{RBD/-}$ compared to control counterparts after DSS treatment; ****p<0.0001 Mmp7 levels in

p110α$^{WT/-}$; and **p<0.01 p110α$^{RBD/-}$ compared to control counterparts after vehicle or DSS treatment.

4.2.1. Disruption of p110α-RBD *in vivo* is protective later in lifespan to DSS-mediated intestinal injury

As previously shown, p110α inactivation in young mice results into insulin resistance and glucose intolerance. However, recent studies showed that long-term p110α inactivation protects from fat accumulation in old mice[215]. This is an example of side-effect of kinase inactivation that leads to organismal adaptation with beneficial effects on metabolism in long-term. Following these studies, we sought to study the effects of p110α-RBD mutation in old mice after DSS treatment. Therefore, we used middle-aged mice (over 27 weeks, representing middle-late adulthood) and investigated the impact of p110α-RBD mutation in DSS-mediated injury *in vivo*. Our results showed that, compared to the p110α$^{WT/-}$ and p110α$^{RBD/-}$ mice, the control p110α$^{WT/WT}$ mouse strain weight loss under DSS was faster (**Figure 56A**). Surprisingly and in contrast to the young adult p110α$^{RBD/-}$ mice, the older p110α$^{RBD/-}$ mice exhibited significantly faster weight recovery time following DSS intestinal injury compared to p110α$^{WT/-}$ and p110α$^{WT/WT}$ mouse strains, with no sign of colitis severity and partial lethality, which was observed in younger p110α$^{RBD/-}$ counterparts. The p110α$^{RBD/-}$ percentage weight loss was significantly lower than p110α$^{WT/WT}$ controls, while p110α$^{WT/-}$ mice showed slightly delayed but not significantly altered recovery from DSS. However, we observed that p110α$^{RBD/-}$ mice, similar to their younger counterparts, still showed a significantly reduced colon length after DSS treatment (**Figure 56B**). Overall these results demonstrated that p110α-RBD loss of interaction differentially affects

intestinal injury responses *in vivo* and is partially protective in recovery from intestinal injury later in lifespan.

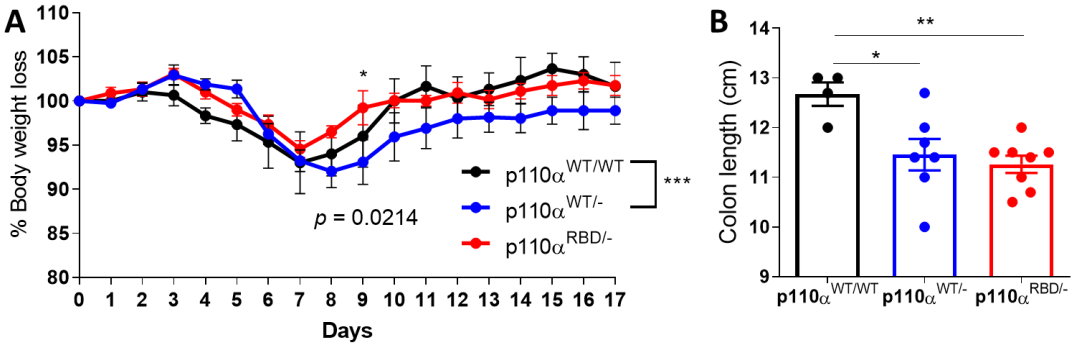

Figure 56: Inactivation of p110α-RBD interactions in aged mice accelerates recovery from weight loss after acute DSS injury. Healthy age and sex-matched p110α$^{WT/WT}$, p110α$^{WT/flox}$ and p110α$^{RBD/flox}$ strains received tamoxifen 2 weeks prior to 2.5% vehicle or DSS treatment for 5 consecutive days and surviving mice were euthanised at day 17. **(A)** The bar graph shows mean ± SEM percent weight loss after DSS treatment (n=9-11 mice per group). **(B)** The graph shows colon length after DSS treatment of p110α$^{WT/WT}$, p110α$^{WT/-}$ and p110α$^{RBD/-}$ adult mice, (n=4–8 mice per group). **(A-B)** Statistical analysis show mean ± SEM **(A)** ***p<0.001 by Two-way ANOVA, and **(B)** *p<0.05/**p<0.01 by One-way ANOVA.

4.3. The mechanism of p110α-RBD and nutrient sensing mTOR pathway

4.3.1. The p110α-RBD is minimally involved in RTK and NOD1/2 dependent mTORC1 activation, while restricts p38 MAPK activity under AA replete conditions *in vitro*

To investigate the role and mechanism of action of p110α-RBD interaction in NOD signalling, mouse embryonic fibroblasts (MEFs) immortalised cell lines from WT and p110α$^{RBD/RBD}$ mutant (αRBD) mice utilised. MEFs were reported to express NOD1 [216] and therefore are a good *in vitro* model to investigate NOD signalling. In the first set of experiments, MEFs were stimulated with EGF (EGFR ligand), or iE-DAP (NOD1 ligand) under AA-replete conditions and the kinetic activation of PI3K-AKT and mTORC1 targets were analysed by western blotting assays. In these experiments, phosphorylation levels of AKT Ser473 in WT and αRBD MEFs were found to be comparable with minimal under basal and EGF-activated conditions (**Figure 57A**). In a similar setting, iE-DAP ligand stimulation resulted in a low but detectable increase in the levels of AKT Ser473 phosphorylation, which was marginally, but noticeably enhanced in mutant αRBD MEFs (**Figure 57B**). In the same settings, phosphorylation of p70 S6K (Thr389) and its downstream target S6 Ribosomal (Ser253/236), correlating with the activation of the mTORC1 pathway, were variably decreased in mutant αRBD MEFs after EGF or iE-DAP stimulation compared to WT counterparts. An increase in the phosphorylation level of p38 MAPK was also detected in the mutant αRBD MEFs after EGF or iE-DAP stimulation compared to WT MEFs, indicating stress-associated signalling pathway is hyper-activated under conditions when p110α-

RBD interaction is inactivated (**Figure 57**). These results suggested that p110α-RBD interaction is minimally involved in the activation of mTORC1 pathway by EGF or NOD1 ligands, in presence of extracellular AA and was minimally involved in mTORC1 activity. Contrary to the observations reported, αRBD interaction was not involved in the activation of GFR- or NOD1-mediated AKT signalling module under these conditions.

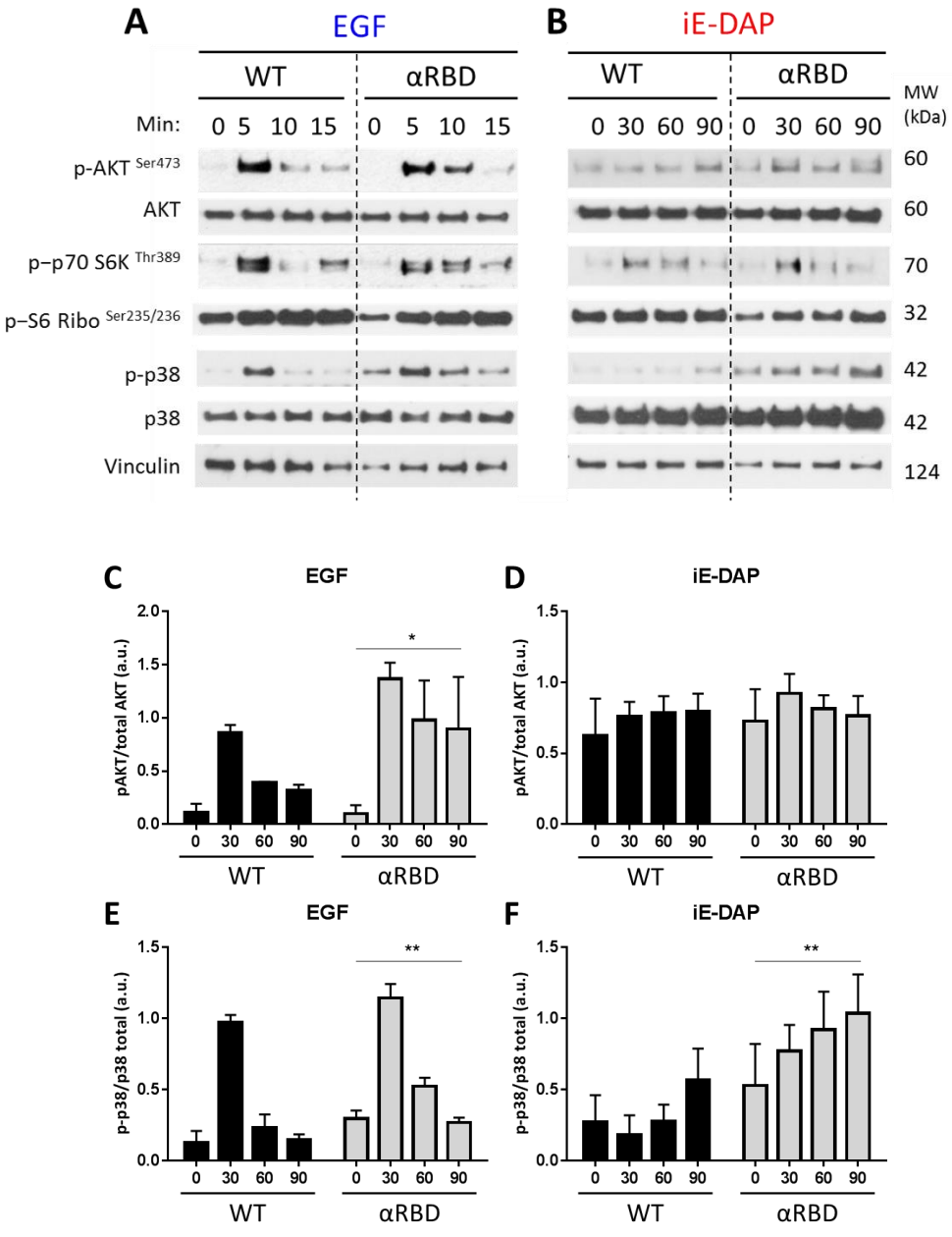

Figure 57: The p110α-BD interaction regulates mTORC1 and p38 MAPK through NOD1 stimulation in MEFs. Immortalised MEFs from WT and αRBD mutant mice were cultured in normal conditions and replaced with 5% FBS in DMEM 4 h prior to stimulations with **(A)** EGF (20 ng/mL), **(B)** iE-DAP (30 μg/mL), at indicated time intervals. Immunoblots were probed using; p-AKT^{Ser473}, AKT, p-p70 S6K^{Thr389}, p-S6 ribosomal$^{Ser235/236}$, p-p38$^{Thr180/182}$, p38, and Vinculin. Total AKT, p38, and vinculin were used as loading control. One representative out of three independently performed experiments is shown. **(C-F)** The graphs represent western blot quantification of **(C, D)** p-AKT^{Ser473}, and **(E, F)** p-p38$^{Thr180/182}$ levels after EGF or iE-DAP simulations from WT MEFs compared to mutant αRBD MEFs. **(C-F)** Statistical analysis show mean ± SEM **(C)** $^{*}p<0.05$, **(E)** $^{**}p<0.01$, and **(F)** $^{**}p<0.01$ by Two-way ANOVA.

4.3.2. The p110α-RBD supports AA sensing mTORC1 pathway by extracellular eukaryotic AAs and bacterial dipeptides under AA-depleted conditions *in vitro*

To further investigate the cellular and molecular mechanisms of p110α-RBD action on activation of mTORC1 pathway by bacterial peptides, we sought to investigate cellular events that have been ascribed to control extracellular AA dependent mTORC1 activation. The mTORC1 is stimulated in response to acute GFs or serum stimulation in presence of extracellular AAs[217]. However, internalization of AAs is required to activate mTORC1 in the lysosomes, which is predominantly initiated by the macropinocytosis process[218,219]. To investigate whether a similar type of cellular activity is required for bacterial dipeptide-mediated mTORC1 signalling, enabled by αRBD interaction, we sought to investigate whether extracellular bacteria-derived dipeptides, specifically iE-DAP can induce mTORC1 activity in a similar manner comparable to extracellular eukaryotic AAs and/or bulk proteins. Therefore, immortalised WT and mutant αRBD MEFs were starved from AAs (-AA) and then were incubated with the essential AA, L-Leucine (a well-described activator of mTORC1 pathway) and iE-

DAP. Acute stimulation of MEFs with L-Leucine resulted in a robust phosphorylation p70 S6K (Thr389), S6 Ribosomal (Ser253/236) and 4EBP1 (Thr37/46) in WT MEFs, which was completely abolished in mutant αRBD MEFs (**Figure 58A**). L-Leucine induced 4EBP1 (Thr37/46) was strongly inhibited in αRBD mutant counterparts. Interestingly in a similar setting, iE-DAP stimulation of WT MEFs also induced phosphorylation of p70 S6K (Thr389), S6 Ribosomal (Ser253/236) and 4EBP1 (Thr37/46), albeit weaker in comparison to L-Leucine, which was likewise abolished in mutant αRBD MEFs (**Figure 58B**). Surprisingly, an enhanced level of AKT Ser473 phosphorylation was detected in the mutant αRBD MEFs following iE-DAP stimulation in comparison to the levels in WT cells, possibly due to inhibited mTORC1 activity that provides retro-feedback control and inhibits AKT activity. Overall, these data demonstrated that p110α-RBD activates mTORC1 pathway mediated by eukaryotic AAs and bacterial dipeptides. Furthermore, our data suggested that the p110α-RBD mediated pathway restricts AKT pathway, a known downstream target of PI3Ks potentially by mTORC1-dependent negative regulatory loop.

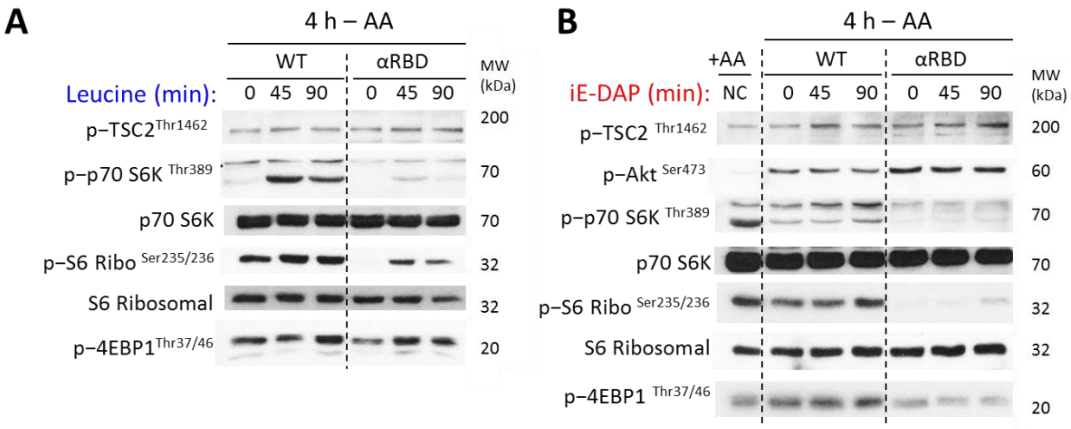

Figure 58: p110α-RBD regulates AA sensing mTORC1 pathway through eukaryotic and bacterial dipeptides. The effects of p110α-RBD mediated mTORC1 on AA starvation media (-AA) were analysed by immuno blotting assays using immortalised MEFs from WT and αRBD mutant mice. MEFs were plated in DMEM normal conditions (+AA) or in EBSS -

AA with 5% FBS dialyzed. MEFs with -AA conditions were stimulated with **(A)** L-Leucine (1 mM) or **(B)** iE-DAP or (30 μg/mL) at indicated time intervals. Immunoblots were probed using; p-TSC2^{Thr1462}, p-AKT^{Ser473}, p-p70 S6K^{Thr389}, p70 S6 Kinase, p-S6 Ribosomal$^{Ser253/256}$, S6 Ribosomal, and p-4EBP1^{Thr70}. Total p70 S6 Kinase and S6 Ribosomal protein were used as loading control. One representative out of three independently performed experiments is shown.

Having established that p110α-RBD supports mTORC1 activation by eukaryotic AAs, and in a similar manner by bacterial dipeptides, we next addressed the cellular mechanisms involved in the activation of mTORC1 under both conditions. It was previously reported that mTORC1 activation by AAs utilises macropinocytic pathway [219], bringing in a bulk amount of AAs into the lysosomes, where mTORC1 can be activated through Rheb GTPase activation at the lysosomal membrane. To test whether such mechanisms were involved in MEFs through utilisation of p110α-RBD, we used MEFs from WT and αRBD counterparts under AA-replete conditions, which were initially treated with bafilomycin A1 (a vacuolar (V)-ATPase inhibitor that blocks lysosomal fusion of vesicles) or a well-established macropinocytosis inhibitor EIPA (Na^+/H^+ exchanger inhibitor) and then acutely treated cells with the bacterial dipeptide, iE-DAP (NOD1 ligand). Remarkably in WT MEFs, bafilomycin A1 or EIPA pre-treatment resulted in the complete inhibition of the bacterial dipeptide, iE-DAP mediated p70 S6K and ribosomal S6 phosphorylation, (well-established targets of mTORC1 pathway) to the levels observed in iE-DAP-treated αRBD MEFs with or without drug treatment (**Figure 59A & B**). In a similar manner, control eukaryotic L-Leucine mediated activation of p70 S6K and ribosomal S6 phosphorylation in WT MEFs were similarly abolished in WT MEFs, to the levels observed in αRBD MEFs with or without bafilomycin A1 treatment (**Figure 60**). Our results established that p110α-RBD interaction is required for activation of eukaryotic AA and prokaryotic dipeptide sensing mTORC1 signalling *in vitro*.

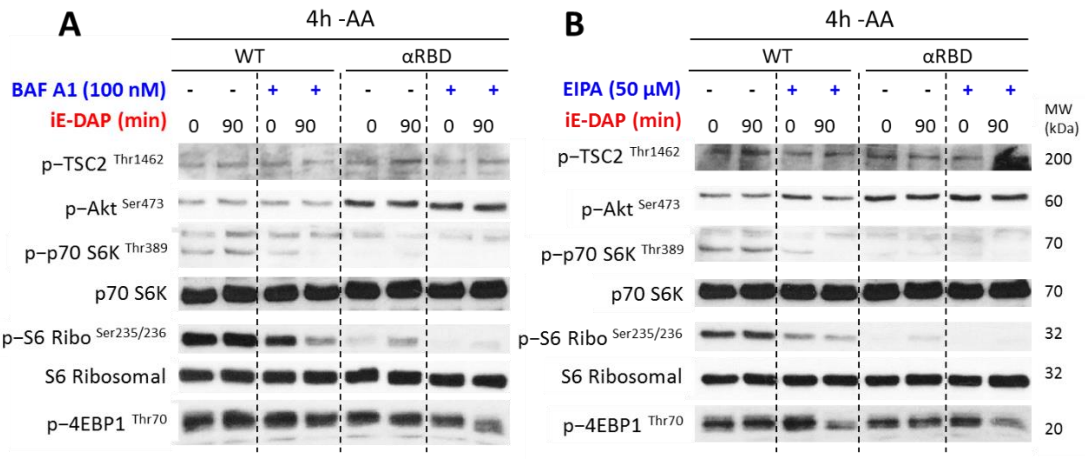

Figure 59: p110α-RBD mediated macropinocytosis regulates AA sensing mTORC1 pathway through bacterial dipeptides. Immortalised MEFs from WT and αRBD mutant mice were plated overnight and starved for 4 h in AA starvation medium with 5% FBS dialyzed in EBSS (-AA) prior to treatment. Inhibitors were added prior stimulation; **(A)** Bafilomycin A1 (BAF A1) (100 nM) for 20 min, or **(B)** EIPA (50 μM) for 45 min. **(A-B)** MEFs were stimulated with iE-DAP (30 μg/mL) at indicated time intervals. Immunoblots were probed using; p-TSC2^{Thr1462}, p-AKT^{Ser473}, p-p70 S6K^{Thr389}, p70 S6 Kinase, p-S6 Ribosomal$^{Ser253/256}$, S6 Ribosomal, and p-4EBP1^{Thr70}. Total p70S6 Kinase and S6 Ribosomal protein were used as loading control. One representative out of three independently performed experiments is shown.

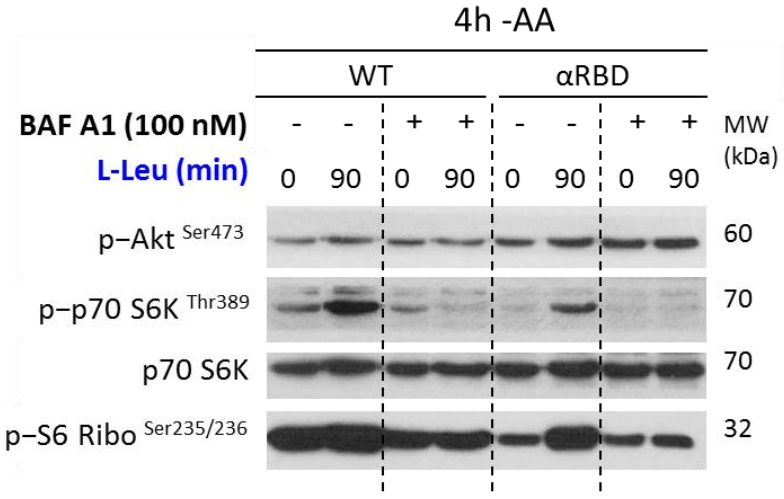

Figure 60: p110α-RBD mediated macropinocytosis regulates AA sensing mTORC1 pathway through L-Leucine. Immortalised MEFs from WT and αRBD mutant mice were plated overnight and starved for 4 h in AA starvation medium with 5% FBS dialyzed in EBSS (-

AA) prior to treatment. Bafilomycin A1 (BAF A1) was added prior stimulation (100 nM) for 20 min. MEFs were stimulated with L-Leucine (1 mM) at indicated time intervals. Immunoblots were probed using; p-AKT^{Ser473}, AKT, p-p70 S6K^{Thr389}, p70 S6 Kinase, and p-S6 Ribosomal$^{Ser253/256}$. Total p70 S6 Kinase was used as loading control. One representative out of two independently performed experiments is shown.

4.4. NOD1 & NOD2 induce intestinal protection

GWAS studies have identified several susceptibility genes which are related to inflammatory bowel diseases such as Cohn's diseases[177,199]. One of which is NOD2, a PRR involved in the immune system, NOD2 is expressed in haematopoietic cells, such as B and T lymphocytes, as well as non-haematopoietic cells such as Paneth cells and goblet cells in the intestine and are proposed to provide antimicrobial/viral defence. Previous studies have established that NOD1 and NOD2 are vital for intestinal epithelial protection and regeneration[168,182,220,221]. It has also been shown that NOD2 deficiency causes delayed wound healing, and that NOD2 stimulation provides protection to the stem cells as well as allow survival of intestinal crypts[183,222]. Since we previously showed the important role of class I PI3Ks signalling with NODs ligands in gut immunity and inflammation; we also investigated in this study in mice expressing a knocked out (KO) version of the gene encoding NOD1 or NOD2 ($NOD1^{KO}$ and $NOD2^{KO}$, respectively).

4.4.1. NOD1 and NOD2 deficiency results in increased susceptibility to DSS injury, indicating a protective role for bacterial dipeptide sensing during intestinal damage

$NOD1^{KO}$ and $NOD2^{KO}$ mice were administered 2.5% DSS in water for five 5 days in order to see effects and recovery of $NOD1^{KO}$ and $NOD2^{KO}$ mice after chemically induced acute inflammation. All mice were checked daily and weights were recorded in order to see effects and weight recovery of each group mice after acute inflammation. As expected, and previously published, $NOD1^{KO}$ and $NOD2^{KO}$ mice showed a significant susceptibility compared to control counterparts (WT)

after acute chemically DSS-induced colitis. Moreover, $NOD1^{KO}$ and $NOD2^{KO}$ mice showed significantly colon length decreased compared to WT mice at day 7 upon after DSS treatment (**Figure 61** & **Figure 62**). In these results, we observed that NOD1 and NOD2 cytosolic receptors regulate protection or wound healing via regeneration of their tissue after DSS intestinal injury comparable to p110α-Ras interaction inactive in mouse strains. However, the role and mechanism of p110α-Ras mediating NOD1 and NOD2 protection or tissue regeneration is still not clear.

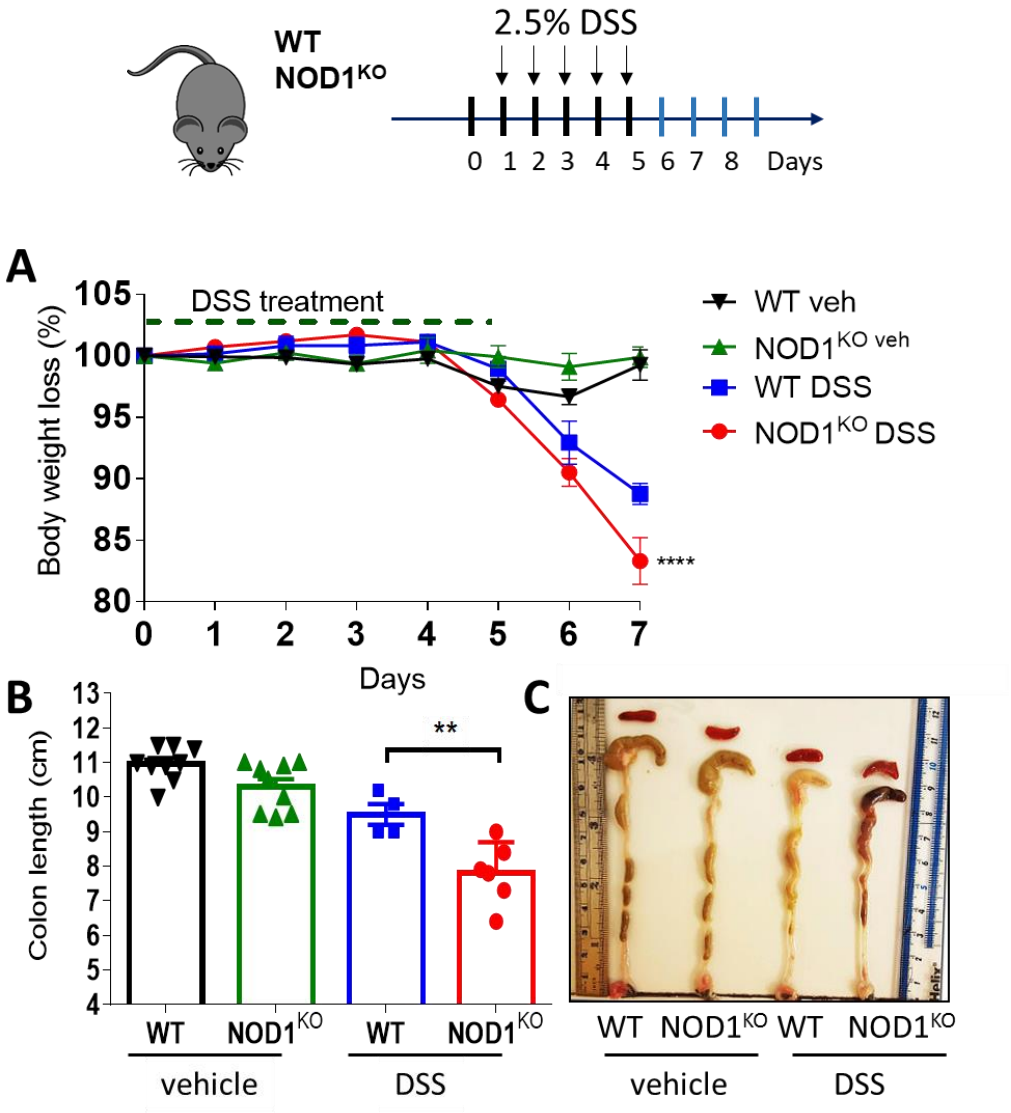

Figure 61: NOD1 deficiency in mice results in significant susceptibility after acute chemically increased DSS-induced injury. Healthy age and sex-matched WT and NOD1^{KO} mice, reared in conventional housing facility were orally treated with 2.5% DSS in drinking water for 5 days or vehicle (veh) to induce acute chemically-induced colitis. The mice engaged for acute analysis were euthanised at day 7. **(A)** The graph represents the percentage weight loss for 7 days ensuring DSS injury or vehicle treatment (n=6-13 mice per mouse strain). **(B)** The bar chart shows mean ± SEM colon length (n=4-9 mice per mouse strain). **(C)** The image shows colon length (cm) from WT and NOD1^{KO} mice after DSS treatment compared to vehicle. **(A-B)** Statistical analysis of data expressed as mean ± SEM was **(A)** ****p<0.0001 by Two-way ANOVA, and **(B)** **p<0.01 by Student t-test.

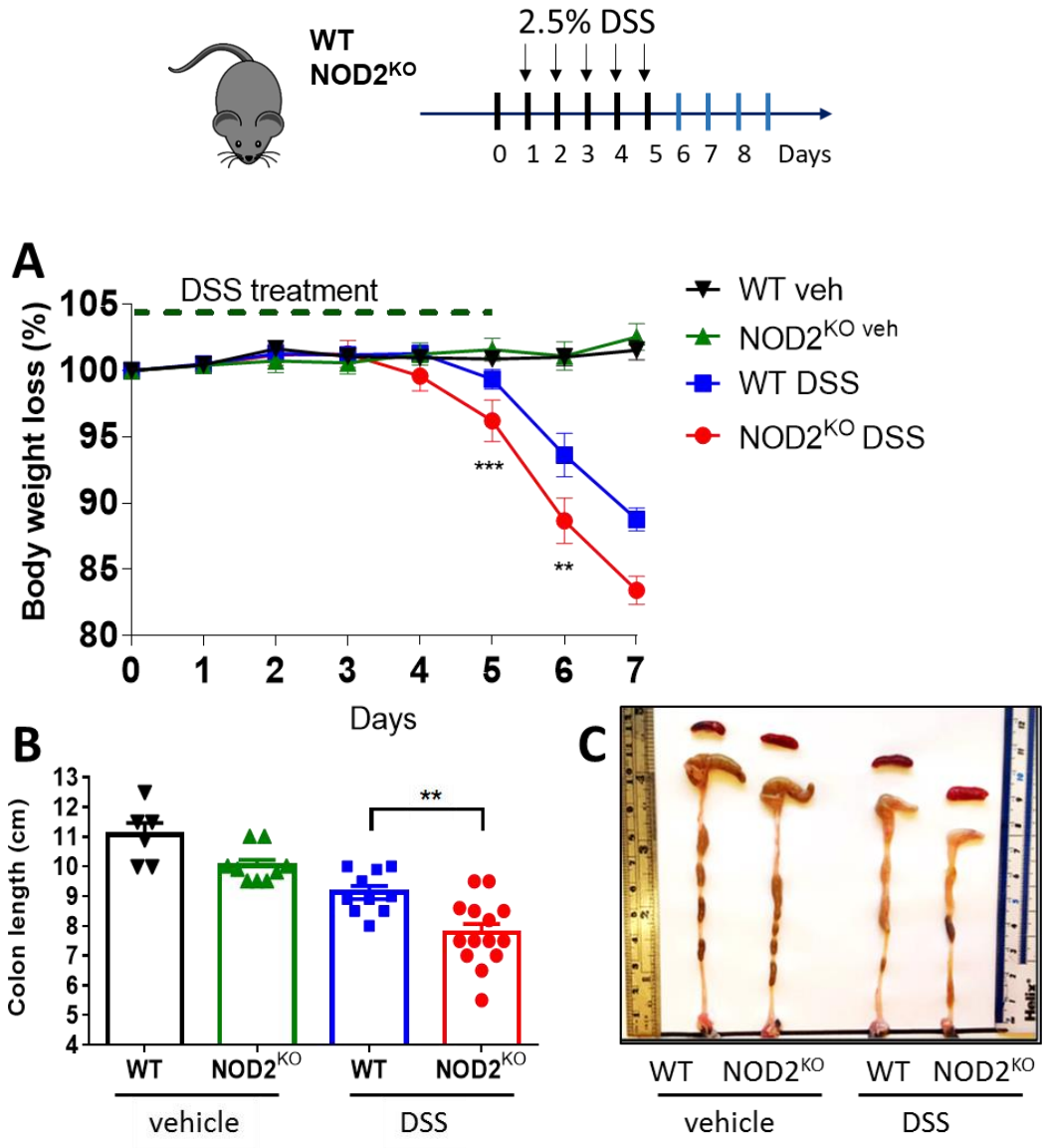

Figure 62: NOD2 deficiency in mice results in significant susceptibility after acute chemically DSS-induced injury. Healthy age and sex-matched WT and NOD2^{KO} mice, reared in conventional housing facility were orally treated with2.5% DSS in drinking water for 5 days or vehicle (veh) to induce acute chemically-induced colitis. The mice engaged for acute analysis were euthanised at day 7. **(A)** The graph represents the percentage weight loss for 7 days ensuring DSS injury or vehicle-treatment (n=11-15 mice per mouse strain). **(B)** The bar chart shows mean ± SEM colon length (n=10-14 mice per mouse strain). **(C)** The image shows colon length (cm) from WT and NOD2^{KO} mice after DSS-injury compared to vehicle. **(A-B)** Statistical analysis of data expressed as mean ± SEM was **(A)** ***p<0.001 by Two-way ANOVA, and **(B)** **p<0.01 by Student t-test.

4.4.2. NOD1 and NOD2 deficiency results in IECs dysregulation following DSS intestinal injury *in vivo*

IECs from NOD1^{KO} and NOD2^{KO} mice after vehicle or DSS treatment, were isolated and stained as previously described (**Section 3.7 & 3.8**) in order to quantify through FACS proliferative levels, using Ki67 antibody, and secretory/Paneth cells using CD24 antibody[212]. Cell sorting from IECs after vehicle or acute chemically DSS-mediated injury in the intestine from each mouse strain were analysed following gating strategy previously described in (**Figure 50** & **Figure 51**). NOD1^{KO} and NOD2^{KO} mice were observed to express comparable levels of EpCAM^{+}CD45^{-} population, but also significantly increased Ki67^{hi} subpopulation compared to WT mice. However, our results showed CD24^{hi} subpopulation to be significantly decreased after DSS treatment in both mutant mouse strains compared to WT control (**Figure 63**). Our results showed increased levels of mean fluorescence intensity (MFI) of EpCAM^{+}CD45^{-} subpopulation in all groups as well as Ki67^{hi} in the intestine (**Figure 64**). IECs from NOD2^{KO} mice and control counterparts were also stained for Lgr5+ after vehicle or DSS treatment. We observed a significantly increased expression of Lgr5^{hi} levels form EpCAM^{+}CD45^{-} subpopulation in the NOD2^{KO} mice after DSS treatment (**Figure 65**). These results showed NOD1 or NOD2 deficiency upregulate proliferation in the intestinal epithelium after acute DSS-mediated intestinal injury. NOD1 and NOD2-deficiency were observed to favour cycling IECs after DSS treatment, but not CD24^{hi} subpopulation. Furthermore, NOD2-deficiency favoured Lgr5+ cell lineage after DSS treatment in a similar manner as p110$\alpha^{RBD/-}$ mouse strain.

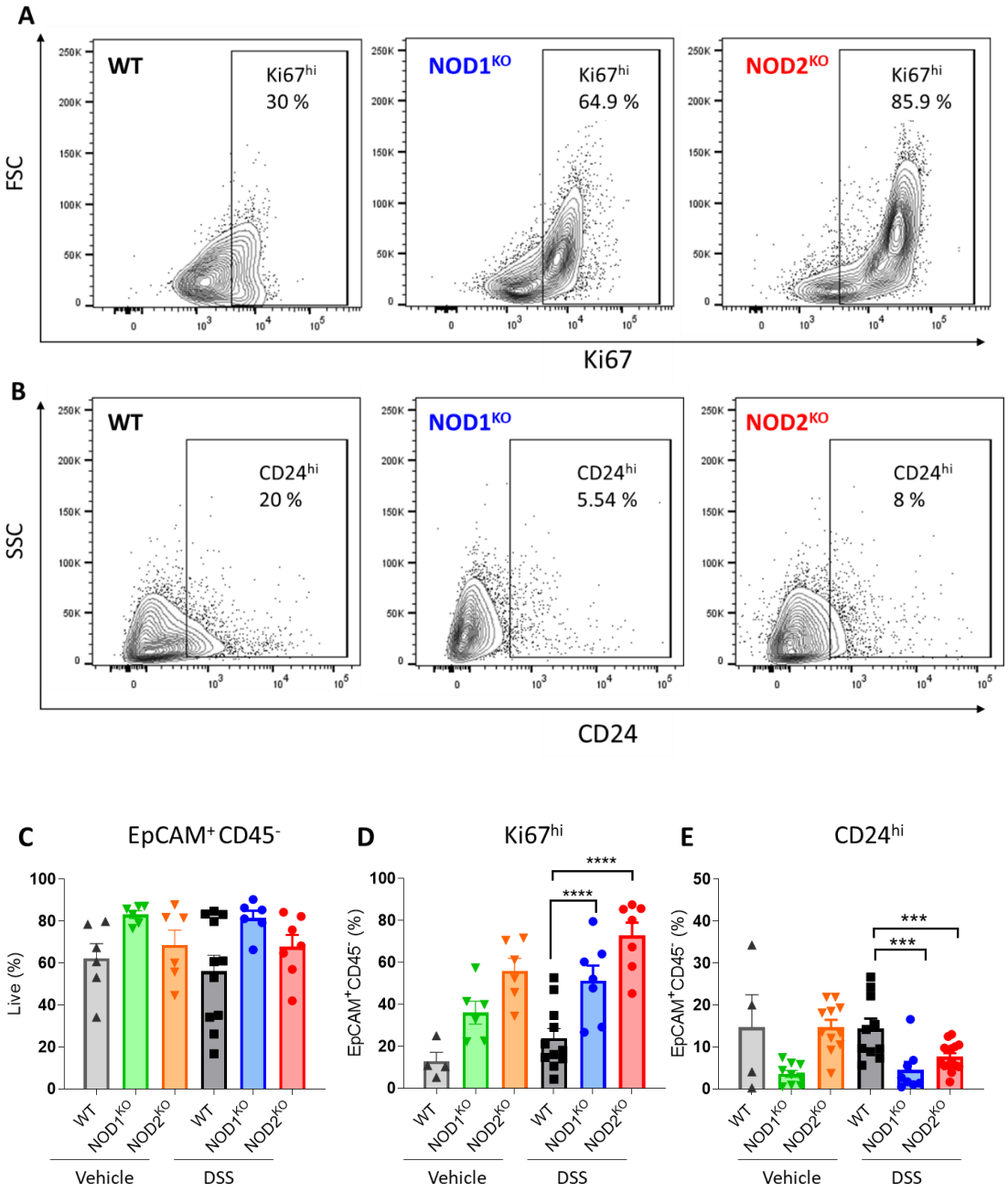

Figure 63: IECs isolation from NOD1^{KO} and NOD2^{KO} mouse strains showed increased Ki67^{hi} and decreased CD24^{hi} population after acute DSS treatment compared to WT mouse. (A-E) Healthy age and sex-matched WT, NOD1^{KO}, and NOD2^{KO} mice, were given vehicle or DSS treatment for 5 days. Mouse were euthanised and organs collected at day 7. IECs were isolated form each mouse strain and stained for further flow cytometry analysis. **(A-B)** An example of FACS gating strategy showing percentage of **(A)** proliferative cells selected from EpCAM^{+}CD45^{-} subpopulation (Ki67^{hi}), and **(B)** positive secretory/Paneth cells population (CD24^{hi}) after DSS treatment. One out of 4 from each mouse strain and condition is shown. **(C-E)** The graphs represent percentage of parent from **(C)**

EpCAM^{+}CD45^{-}, **(D)** Ki67^{hi}, and **(E)** CD24^{hi} subpopulation from each mouse strain after vehicle or DSS treatment. Statistical analysis shows mean ± SEM (n=4–13) by One-way ANOVA at indicated mouse strains and treatment **(C)** ****p<0.0001, *p<0.05, **(D)** ****p<0.0001, **(E)** and ***p<0.001.

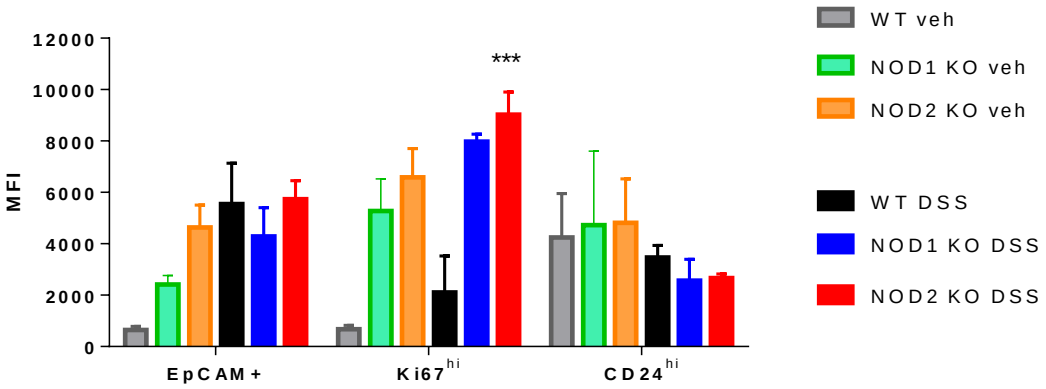

Figure 64: NOD1 and NOD2 deficiency in mice induces increased Ki67^{hi} subpopulation in the intestine after acute DSS injury. The graph shows mean ±SEM of mean fluorescence intensity (MFI) levels of EpCAM^{+}CD45^{-}, Ki67^{hi}, and CD24^{hi} subpopulations of WT, NOD1^{KO}, and NOD2^{KO} adult mice after vehicle (veh) or DSS treatment (n=3-8). Statistical analysis shows mean ± SEM (n=4–13) mice per group ***p<0.001 of Ki67^{hi} subpopulation in NOD2^{KO} mouse after DSS treatment compared to control counterparts by One-way ANOVA.

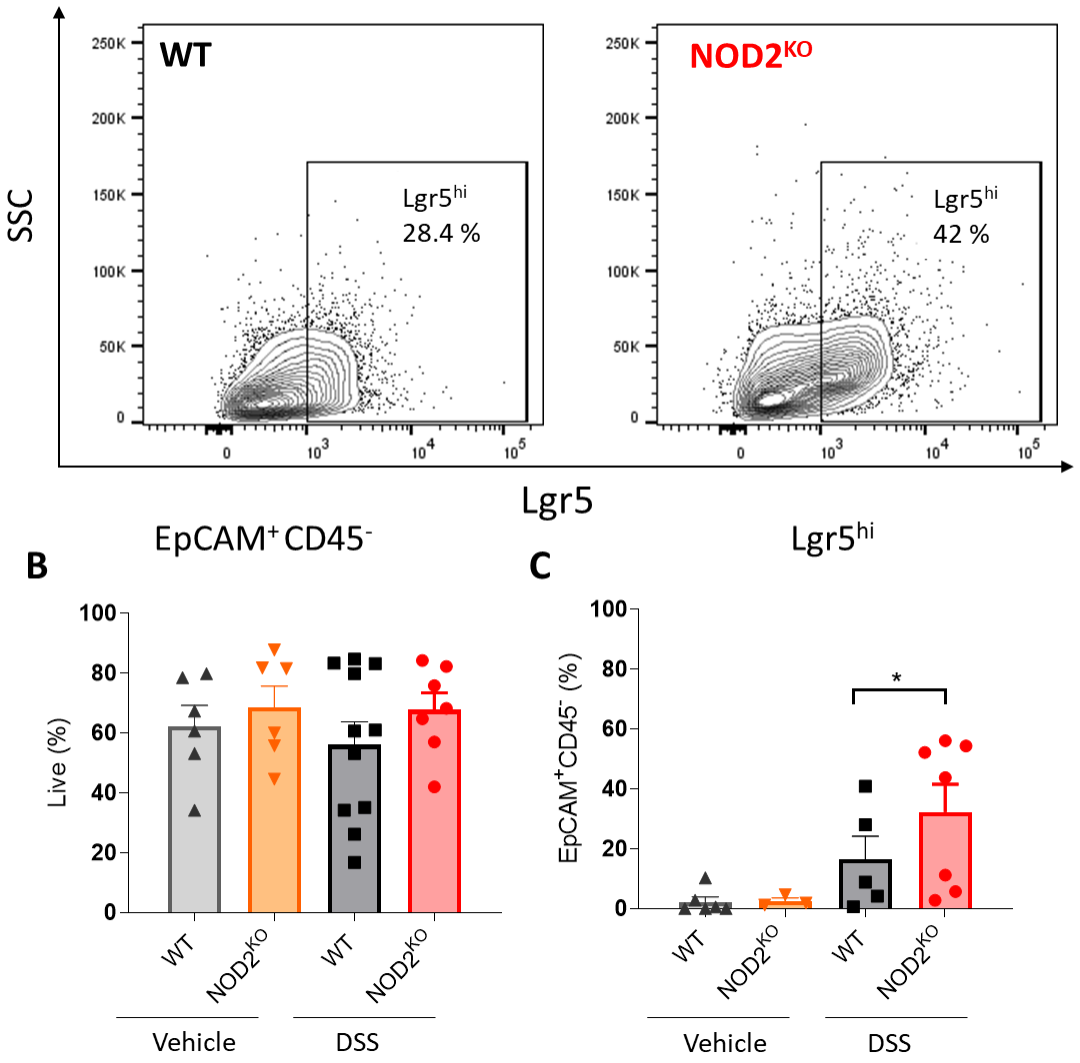

Figure 65: The NOD2^{KO} mice exhibit increased Lgr5+ cell lineage after DSS treatment. Gating examples show frequent of parent (EpCAM^{+}CD45^{-}) subpopulation of small intestinal cells isolated and stained from each group; p110α$^{WT/WT}$, p110α$^{WT/-}$, and p110α$^{RBD/-}$ after vehicle or DSS treatment. **(A)** Lgr5^{hi} cells were selected from EpCAM^{+}CD45^{-} subpopulation. One out of 8 from each mouse strain and condition is shown. **(B-C)** The graphs represent percentage of parent from **(B)** EpCAM^{+}CD45^{-}, and **(C)** Lgr5^{hi} from each mouse strain after vehicle or DSS treatment. **(B-C)** Statistical analysis show mean ± SEM (n=3–12) mice per group by One-way ANOVA **(B)** *p<0.05 after vehicle and DSS treatment, and **(C)** *p<0.05 after DSS treatment.

4.5. The role of Rheb in intestinal epithelial cells

In order to understand the precise role of mTORC1/Rheb in intestinal injury and inflammation, we therefore sought to investigate the role of Rheb GTPase in IEC populations *in vivo*. We have generated a conditional mouse model in order to delete Rheb specifically in IECs. Villin-Cre mice were crossed onto $Rheb^{flox/flox}$ transgenic mice ($Rheb^{\Delta IEC}$) to study the role of Rheb in the intestinal epithelium (*villin 1* promoter directing expression of Cre recombinase to villus and crypt epithelial cells of the small and large intestine). $Rheb^{\Delta IEC}$ mice were genotyped and followed up for two years in case they developed spontaneous colitis or other related phenotypes. Interestingly, there was no significant difference between $Rheb^{\Delta IEC}$ compared to Cre-negative strain ($Rheb^{flox/flox}$) in terms of macroscopic intestinal pathology and colon length, since the loss of Rheb in the villus did not cause any spontaneous abnormalities. All mouse models and groups used in this study are detailed in **Section 3.3.**

4.5.1. IEC-intrinsic Rheb-mTORC1 pathway is necessary for survival of mice upon DSS injury

In order to find out the specific role of mTORC1/Rheb in intestinal injury, acute DSS-induced intestinal injury model was carried using the conditional mouse model $Rheb^{\Delta IEC}$ and the $Rheb^{flox/flox}$ mouse strain as a control (**Figure 66**). The mice were checked daily and weights were recorded in order to observe any pathological effects and weight changes of each mouse strain. Strikingly, $Rheb^{\Delta IEC}$ mice showed approximately over 81% lethality, and statistically significant susceptibility to DSS-mediated acute intestinal injury in comparison to $Rheb^{flox/flox}$.

The Rheb$^{\Delta IEC}$ mice lost rapidly and significantly over 20% of body weight in comparison to Rheb$^{flox/flox}$, which required euthanasia in most cases of death. Colon lengths for each group were measured and shown that deletion of Rheb in the intestinal epithelium resulted in the significant shortening of the colon following DSS in comparison to the control counterparts (and most mouse mice tested within this study) with no changes under basal conditions.

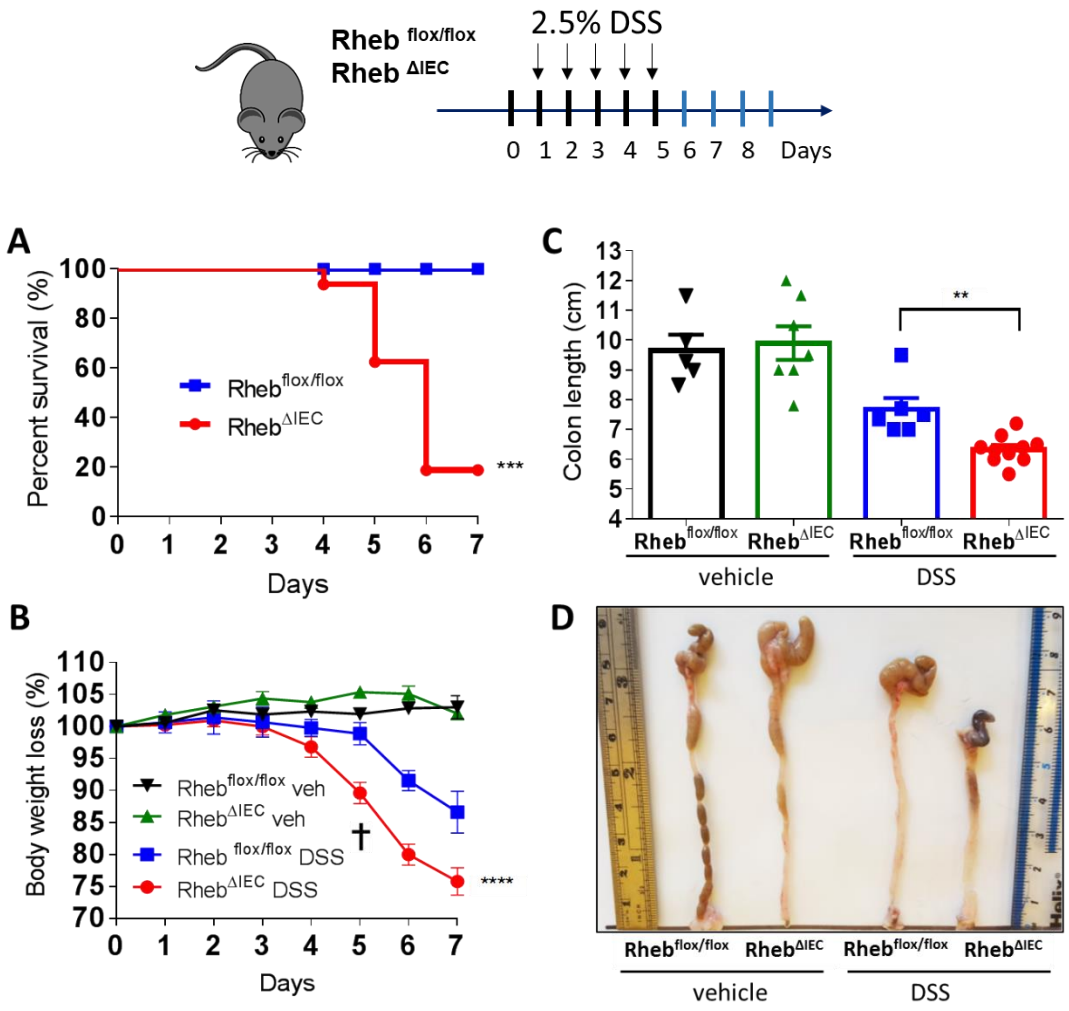

Figure 66: Specific Rheb inactivation in IECs (Rheb$^{\Delta IEC}$) in mice results in severe lethality following acute chemically induced DSS injury akin to p110α$^{RBD/-}$ mice. Healthy age and sex-matched Rheb$^{flox/flox}$ and Rheb$^{\Delta IEC}$ mice, reared in conventional housing facility were orally treated with 2.5% DSS in drinking water for 5 days or vehicle (veh) to induce acute chemically-induced colitis. The mice engaged for acute analysis were euthanised at day 7.

(A) The graph represents the percent survival after DSS injury (n=16 mice per mouse strain). **(B)** The graph represents the percentage of weight loss for 7 days ensuing DSS injury or vehicle treatment (n=11-15 mice per mouse strain). **(C)** The bar chart shows mean ± SEM colon length (n=9–11 mice per mouse strain). **(D)** The image shows colon lengths at day 7 after DSS injury in $Rheb^{\Delta IEC}$ mice compared to Cre-negative $Rheb^{flox/flox}$ mice at day 7 after DSS or vehicle treatment. **(A-C)** Statistical analysis show mean ± SEM **(A)** ***p<0.001 by by Log-rank (survival curve) test, **(B)** ****p<0.0001 by Two-way ANOVA, and **(C)** **p<0.01 unpaired Student t-test.

4.5.2. Rheb deficiency specifically in IECs results in severe intestinal damage due to perturbation in IEC populations following DSS injury

In order to study the strong phenotype observed in $Rheb^{\Delta IEC}$ mice after acute DSS injury, the small intestine and colons were collected, fixed and embedded for further histopathology examinations. Small intestines and colons fixed were scanned using NanoZoomer S210 digital microscope and pictures were analysed with NDP.view2 software. The initial H&E analyses showed a strong disruption in the small intestine and colon architectures in $Rheb^{\Delta IEC}$ mice after DSS injury compared to $Rheb^{flox/flox}$ control mice, reminiscent of intestinal enteritis. Under basal conditions, the H&E staining for $Rheb^{\Delta IEC}$ showed enteropathy, marked by disturbed differentiation of cells in the small intestine and colon, with signs of decreased villus height in the small intestines (**Figure 67**). Furthermore, small intestines from $Rheb^{\Delta IEC}$ mice showed decreased crypt size and numbers compared to the control $Rheb^{flox/flox}$ mice after DSS injury. There was also increased infiltration of granulocytes and polymorphonuclear cells in the colons of $Rheb^{\Delta IEC}$, showing DSS-induced intestinal damage increased inflammatory responses and flux of immune cells. These data indicated that IEC-intrinsic loss of Rheb might impact overall immune responses in an IEC-extrinsic manner, potentially due to

mucosal damage and increased bacterial translocation, recruiting immune cells to the injury site. Overall, our data demonstrated Rheb-deficiency in IECs (Villin-Cre mice) is critical for mouse survival and intestinal protection following DSS-mediated intestinal damage.

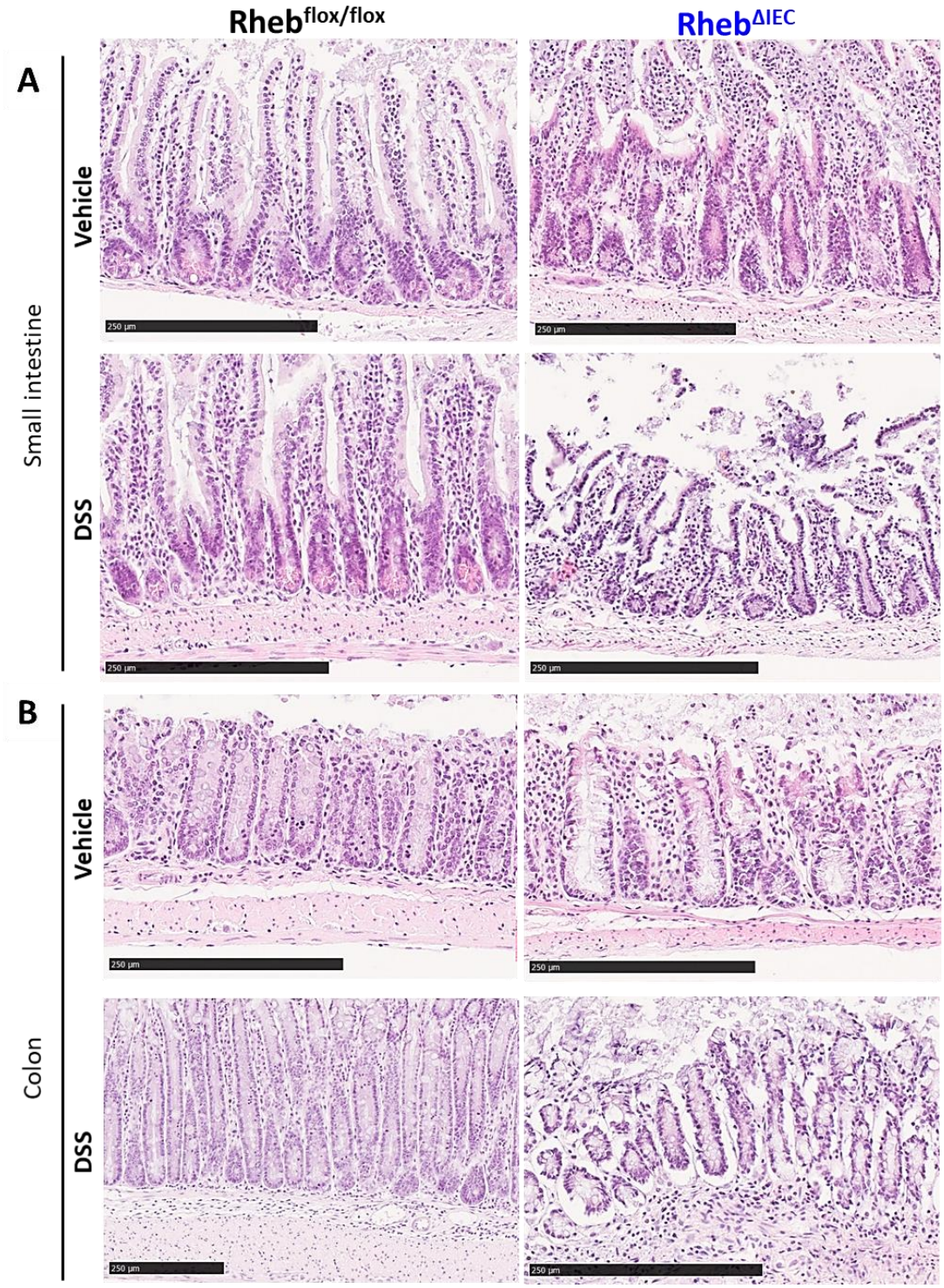

Figure 67: Conditional inactivation of Rheb in IECs result in disrupted crypt formation in the small intestine and in the colon after acute DSS-induced intestinal injury. The micrographs represent H&E staining of zinc fixative fixed and paraffin-embedded from **(A)** small intestine, and colon **(B)** from $Rheb^{\Delta IEC}$ and $Rheb^{flox/flox}$ adult mice (n=3-5) after vehicle or DSS treatment. H&E staining tissues were scanned using NanoZoomer S210 digital microscope and pictures were analysed with NDP.view2 software. The photos

micrographs one out of n=3-4 independent mouse from each strain and treatment tissue fixed and stained. Scale bars indicate **(A)** 250 μm and **(B)** 100 μm.

4.5.3. Rheb inactivation in IECs results in increased proliferation and decreased secretory lineage markers after acute DSS treatment

IECs from $Rheb^{flox/flox}$, and $Rheb^{\Delta IEC}$ mouse after vehicle or DSS treatment, were isolated and stained as previously described (**Section 3.7 & 3.8**) in order to quantify through FACS proliferative levels, using Ki67 antibody, and secretory/Paneth cells using CD24 antibody[212]. From whole sample of IECs isolated and stained (FSC-A, SSC-A), dead cells (Aqua, SSC-A) and doublets were excluded. IECs were positively selected with EpCAM-CD36 antibody and leukocytes discriminated with CD45 antibody ($EpCAM^{+}CD45^{-}$). Proliferative cells were selected from $EpCAM^{+}CD45^{-}$ subpopulation ($Ki67^{hi}$) as well as low proliferative cells ($Ki67^{hi}$). Positive secretory/Paneth cells population ($CD24^{hi}$) were also selected from the $EpCAM^{+}CD45^{-}$ subpopulation. Gating strategy used is described in (**Figure 50** & **Figure 51**). After DSS treatment, expression of $EpCAM^{+}CD45^{-}$ subpopulation of cells was significantly increased in $Rheb^{\Delta IEC}$ mouse compared to $Rheb^{flox/flox}$ as well the percentage of $Ki67^{hi}$ ($Ki67^{hi}$ FSC). The $Rheb^{\Delta IEC}$ mouse also tended to show increased percentage of $CD24^{hi}$ subpopulation ($CD24^{hi}$ SSC), although this was not significant (**Figure 68**). Overall, these data indicated that Rheb deficiency in the intestinal epithelium regulates cell proliferation but does not alter IEC numbers nor Paneth cells.

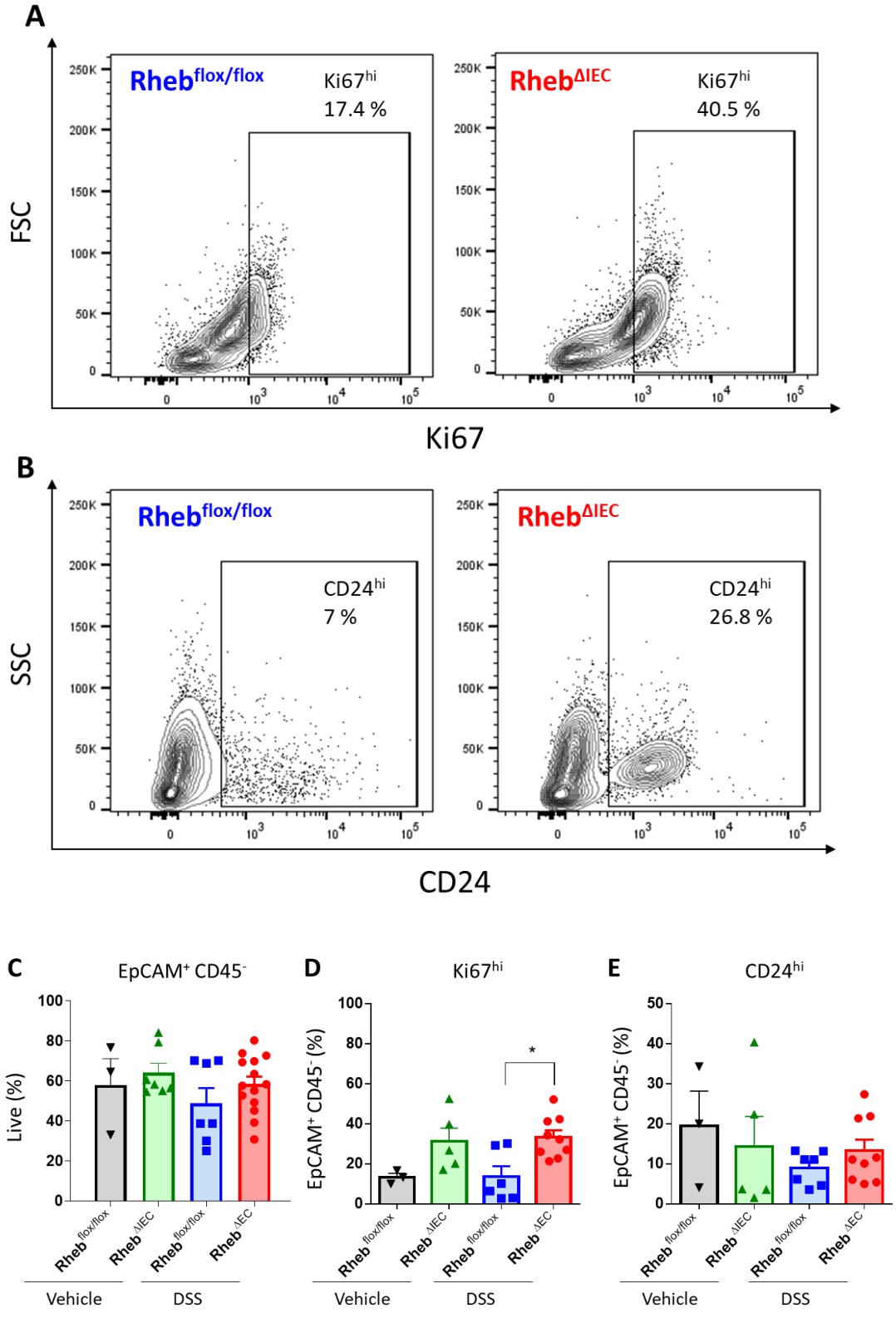

Figure 68: Rheb$^{\Delta IEC}$ mice showed increased Ki67^{hi} population after acute DSS injury. Gating examples show frequent of parent (EpCAM^{+}CD45^{-}) subpopulation of small intestinal cells isolated and stained from each group; Rheb$^{flox/flox}$, and Rheb$^{\Delta IEC}$ after vehicle or DSS

treatment. **(A)** Proliferative cells were selected from $EpCAM^{+}CD45^{-}$ subpopulation ($Ki67^{hi}$). **(B)** Positive secretory/Paneth cells population ($CD24^{hi}$) were also selected from the $EpCAM^{+}CD45^{-}$ subpopulation. One out of 4 from each mouse strain and condition is shown. **(C-E)** The graphs represent percentage of parent from **(C)** $EpCAM^{+}CD45^{-}$, **(D)** $Ki67^{hi}$, and **(E)** $CD24^{hi}$ subpopulation from each mouse strain after vehicle or DSS treatment. Statistical analysis shows mean ± SEM (n=3–9) mice per group by One-way ANOVA after DSS treatment were **(C)** ****$p<0.0001$, and **(D)** *$p<0.05$.

4.5.4. Rheb deficiency in IECs results in decreased Bmi1 expression in the intestine after acute DSS injury

Small intestine, colon, liver and spleen from each mouse euthanised were kept with RNAlater at -80ºC for further RNA isolation. Since we observed mainly differences in the small intestine between groups, we investigated the genetic expression in the small intestine for several transcription factors such as; EpCAM (lineage marker), c-Myc and Ki67 (proliferation), Notch (transcription factor (TF)), Olfm4 (Lgr5+ stem cells), Bmi1 (+4 stem cells), Mmp7 (Paneth cells), Muc2 (goblet cells), and Wdr43 (TA cells). RNA from >60 mg of small intestines from $Rheb^{flox/flox}$ and $Rheb^{\Delta IEC}$ mouse strains after vehicle treatment or DSS treatment, were isolated and processed for reverse transcription assay in order to obtain cDNA for further RT-PCR assay as previously described (**Section 3.5**). These results showed significantly increased levels of Bmi1 in $Rheb^{\Delta IEC}$ mouse strain after vehicle treatment compared to $Rheb^{flox/flox}$ control mouse strain. Surprisingly, after DSS injury our results showed significantly decreased levels of Bmi1 in $Rheb^{\Delta IEC}$ mouse strain after DSS injury compared to $Rheb^{flox/flox}$ control mouse strain (**Figure 69**). Our results showed no significant (ns) differences between each mouse strain in other genetic targets such as lineage markers (EpCAM), proliferation markers (c-Myc, Ki67), Notch, Olfm4, Mmp7, Muc2, and Wdr43.

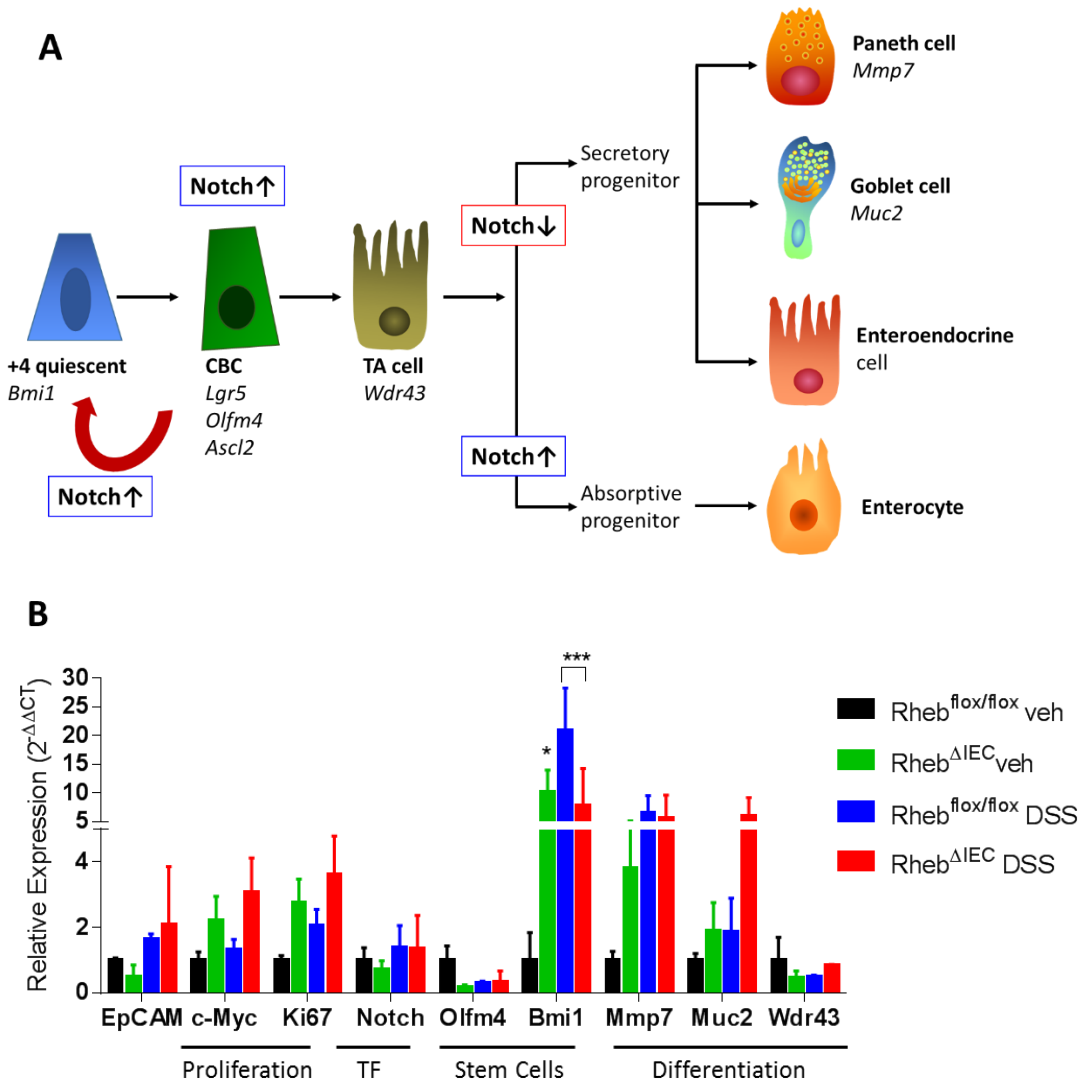

Figure 69: Conditional Rheb inactivity IECs-specific exhibited decreased Bmi1 genetic expression after acute DSS injury. RNA/cDNA was isolated from small intestines collected from $Rheb^{flox/flox}$ and $Rheb^{\Delta IEC}$ adult mice after DSS treatment or vehicle (veh). Samples were processed for further RT-PCR assay and detection of the following transcription factors was expressed in relative gene expression ($2^{-\Delta\Delta CT}$); EpCAM (lineage marker), c-Myc and Ki67 (proliferation), Notch (transcription factor (TF)), Olfm4 (Lgr5+ stem cells), Bmi1 (+4 stem cells), Mmp7 (Paneth cells), Muc2 (goblet cells), and Wdr43 (TA cells). GAPDH was used as reference gene and $2^{-\Delta\Delta CT}$ from each condition was normalised to $p110\alpha^{WT/WT}$ mouse with vehicle treatment. Statistical analysis shows mean ± SEM $^{*}p<0.05$ and $^{***}p<0.001$ by Two-way ANOVA (n=3-4).

5.CONCLUSIONS

"Go as far as you can see; when you get there, you will be able to see further"

5.1. The role of class I PI3K in intestinal immunity

In this thesis, p110δ KI mice responses were significantly more severe to acute chemically DSS induced intestinal injury compared to WT mice. Our results indicated that p110δ activity is required for dampening acute intestinal inflammation upon injury, and also showed that p110δ couples to NOD2 signalling in DCs to regulate inflammatory responses *in vitro* and *in vivo*. Moreover, when looking at specific innate cell subpopulations, deletion of p110δ in granulocytes ($p110\delta^{\Delta Lyz2}$) did not result in significant increased severity after DSS compared to control counterparts. However, deletion of p110δ in myeloid cells ($p110\delta^{\Delta CD11c}$) was observed to increase severity following DSS compared to control counterparts in a similar manner as the p110δ full KI mice. Therefore, we concluded that p110δ activity in DCs population plays a major role and regulates anti-inflammatory responses in mice form conventional facilities to intestinal injury, either mediated by microbial insult and/or the breach of the intestinal barrier by chemically-induced colitis. Data obtained in collaboration with Dr. María González Núñez, unpublished data for manuscript from our laboratory in preparation.

We concluded that cells of the immune compartment other than the intestinal phagocytes (DCs and macrophages, on their own), or loss of p110δ activity in both populations in a combinatorial manner, may be important in resistance to microbiota-mediated inflammation. Since intestinal barrier functions are initially mediated by IECs, we decided to focus on exploring the isoform-selective roles of class I PI3Ks in IECs, which may regulate their innate immune response to microbial components and impact inflammation, proliferation and survival in the gut. As expected, p110δ protein expression in human and mouse IECs is lower than the other class I PI3Ks isoforms, p110α and p110β being the

main isoforms *in vitro*. However, after stimulation with bacterial ligands and/or inflammatory stimuli, the expression of p110δ can be induced at a higher level in IECs. We have explored this link *in vivo* using a conditionally targeted mouse model, referred as $p110\delta^{\Delta IECs}$ to confirm the role of p110δ in IECs *in vivo*, in a DSS-injury model. Our results confirmed that conditional inactivation of p110δ in IECs does not alter susceptibility to DSS-mediated injury. To characterise which of the main class I PI3K isoform may couple and regulate innate NOD1/2 signalling pathway in the intestine, human and mouse IECs responses to NOD1/2 ligands were investigated *in vitro* in presence of isoform selective PI3K inhibitors. These results showed that p110α is the main class I PI3K isoform in IECs, regulating NOD1/2-mediated AKT/mTORC1 signalling. Therefore, we concluded that p110α regulates AKT-phosphorylation and mTORC1 downstream targets, p70-S6K, and S6 ribosomal protein in human and mouse IECs. In parallel, NOD1/2-induced p38 MAPK stress-associated MAPK pathway was under negative control by NOD1/2-activated p110α PI3Ks since p110α inhibition hyper-activated p38. In conclusion, PRR-mediated p110α PI3K activity supports the activation of its downstream targets AKT, p70-S6K, and S6 ribosomal protein in both human and mouse IECs.

In order to study the role of p110α *in vivo*, we used a conditional mouse model with disrupted p110α-RBD ($p110\alpha^{RBD/-}$) and one copy p110α deficient ($p110\alpha^{WT/-}$) mice. In comparison with the control counterpart, $p110\alpha^{RBD/-}$ and $p110\alpha^{WT/-}$ mice showed significantly increased severity of intestinal injury (but not inflammatory response of immune cells), partial lethality (55.56%), and abnormal intestinal architecture following DSS intestinal injury. In particular, it is important to highlight that the expression of a single copy of p110α-RBD demonstrated worst outcome in terms of DSS-induced lethality in comparison to the loss of single copy of the gene encoding p110α with respect to WT counterparts expressing two functional copies of p110α PI3K. These observations support the functional role of

p110α-RBD is distinct and additionally important for p110α mediated functions with respect to survival of the organism during intestinal injury. Furthermore, we observed that the heterozygous $p110\alpha^{RBD/flox}$ mice show increased severity to DSS intestinal injury in comparison to the control $p110\alpha^{WT/WT}$ mice without tamoxifen treatment, indicating the importance of the RBD-mediated intestinal repair during injury. Overall, these results indicated that both processes under control of the kinase activity and the RBD interaction of p110α are critical for survival of the organism following intestinal damage by promoting balanced repair/regenerative response of the intestinal tissue.

In order to understand the cause of this partial lethality in the $p110\alpha^{RBD/-}$ mouse after DSS treatment, the functional role of gene-dosage dependent loss of p110α and p110α-RBD interaction was studied in this project by scoring H&E staining from small intestine and colon tissues from each mouse strain after vehicle or DSS treatment. The semi-quantitative data showed a clear disrupted architecture of the small intestine and colon after DSS treatment in both mutant mouse strains in a dosage manner compared to our control. We also observed an increased hyperplasia in the small intestine of $p110\alpha^{RBD/-}$ mouse strain as well as increased goblet cells. Interestingly, no inflammation was observed following DSS intestinal injury in the $p110\alpha^{RBD/-}$ mouse strain H&E stained tissues. Small intestine and colon explants from each mouse strain were acutely stimulated with bacterial ligands for further quantification of inflammatory and anti-inflammatory cytokines by ELISA in order to verify our results. Our results showed that inflammatory and anti-inflammatory cytokine secretion in $p110\alpha^{RBD/-}$ mouse strain were comparable following LPS or MDP simulations to control counterparts with the exception of IL-33. Therefore, we sought to determine IECs specific subpopulation from each mouse strain via IECs isolation and staining for proliferative markers (Ki67), as well as CBCs/Paneth cells markers (CD24), and

Lgr5 for further flow cytometry analysis. We concluded that proliferation was higher in IECs from p110α$^{RBD/-}$ mouse strain compared to the control counterparts after DSS treatment. Although decreased under control conditions, we have observed increased percentages of CD24^{hi} levels in EpCAM^{+}CD45^{-} subpopulation, which may indicate an increase of Paneth cell lineage or cells undergoing proliferation. Finally, in order to identify a range of selective lineage markers, gene expression analysis was carried by real time RT-PCR using small intestinal RNAs. The RT-PCR results showed increased expression of Notch, Olfm4, and Bmi1 lineage marker as well as Mmpp7, and Muc2 differentiated markers in mutant mouse strain p110α$^{RBD/-}$compared to control counterparts. Therefore, we concluded that inactivation of the p110α catalytic isoform in a heterozygous manner impacts intestinal repair and regeneration of the intestinal tissue after acute chemically induced DSS injury. However, disruption of the p110α-RBD showed additional effects since the hyper-proliferative response was further increased skewing the IECs toward stem-like cells cycling. Next, we sought to decipher the mechanism by which NOD-mediated p110α kinase activity, particularly through p110α-RBD interaction controls tissue regeneration during intestinal injury. Therefore, the mechanism by which p110α-RBD regulates signalling processes associated with canonical PI3K/AKT and mTORC1 pathways mediated by NODs and AA uptake *in vitro* was investigated. These results demonstrated that p110α-RBD interaction is required for both eukaryotic AA and prokaryotic dipeptide mediated activation of mTORC1 pathway. In addition, p38 MAPK stress pathway was hyper-activated when p110α-RBD interaction was rendered inactive during NODs activation. These results demonstrated that p110α-RBD interaction through AA sensing mTORC1 and particularly through NODs pathway may enable host recovery from injury through IECs growth and repair by limiting proliferation and potentially initiating differentiation of cells, adding a further complexity to the existing symbiotic host-microbiome interactions even

under stressful conditions. Overall, p110α-RBD interaction couples to the canonical eukaryotic AA sensing mTORC1 signalling by eukaryotic essential AAs i.e. L-Leucine and furthermore by the bacterial dipeptides of prokaryotic origin downstream of NOD pathway.

Overall, the results shown in this study indicated that p110α and p110δ roles in intestinal health and immunity are dissimilar and are likely to act differentially in diverse cell populations. The p110α is the most prominent IEC-selective class I PI3K isoform under basal conditions, based on our *in vitro* analyses and appears to control IEC proliferative capacity *in vivo* after intestinal injury. While the p110δ PI3K (although being important in DC population) is inducible following PRR or inflammatory cytokine stimulations and may also be important in other aspects of gut repair and regeneration under inflammatory/infectious conditions. Yet, p110δ kinase deficient mice have thickened intestinal mucosa with hyperplasic glands and mixed inflammatory infiltration of the lamina propria[80] and a recent study has demonstrated that p110δ regulates apico-basal polarity axis and lumen formation in Madin–Darby canine kidney epithelial cells in 3D vitro studies[223]. Based on this project, we concluded that p110α PI3Ks restricts injury-mediated regenerative responses linked to IEC proliferation in the intestinal epithelium and its absence results in hyper-proliferation of IECs and skewing toward increased secretory cell lineage.

5.2. The PI3K-NOD-mTOR pathway in intestinal repair and regeneration

We aimed to replicate and further investigate NOD1 and NOD2 deficient mouse strains susceptibility after DSS intestinal injury, as previously described[158,181,221], and compare these deficient mouse models with the p110α-RBD mutant mouse strain. The results in $NOD1^{KO}$ and $NOD2^{KO}$ mouse strains acquired in this project showed significantly worsened colitis, marked by weight loss and reduced colon lengths analogous to the observations made in $p110\alpha^{RBD/-}$ mice. An important difference observed in $NOD1^{KO}$ and $NOD2^{KO}$ mice compared to p110α-RBD mutant mouse strains, was the survival in all $NOD1^{KO}$ and $NOD2^{KO}$ mice strains after DSS intestinal injury. However, macroscopic analyses from both $NOD1^{KO}$ and $NOD2^{KO}$ mice strains showed blood in stool after acute DSS-induced injury, indicating acute sever damage to the intestinal epithelium causing IEC death leading to haematocrit increase in the intestinal lumen. On the contrary, p110α-RBD mutant mouse strain showed absorbance defects with little or no stool and thinning of the intestine indicative of defects in nutrient absorption. These observations indicated a different type of damage in the intestine in NOD1 and NOD2 deficient mouse strains. Since NOD1 and NOD2 are also critical for the immune cells which regulate gut protection, the contrasting effect on intestinal damage may be caused by the cumulative loss of NOD proteins from both the IEC and immune cell populations, which requires addressing using conditionally targeted $NOD1^{KO}$ or $NOD2^{KO}$ models. Following flow cytometry analysis of IECs from $NOD1^{KO}$ and $NOD2^{KO}$ mouse strains, we concluded that the percentage of $Ki67^{hi}$ populations from IECs were significantly higher both under vehicle and DSS treatment conditions compared to the WT counterparts. After DSS treatment, the percentage of $Ki67^{hi}$ levels were significantly increased in both mutant strains compared to the controls analogous to the p110α-RBD mutant mouse strain.

However, $CD24^{hi}$ levels were significantly reduced in both $NOD1^{KO}$ and $NOD2^{KO}$ mouse strains after DSS. Overall, we concluded that the bacterial dipeptide sensing NOD pathways, which may couple and signal through p110α-RBD *in vivo*, are restricting proliferation capacity in a similar manner as p110α-RBD after DSS intestinal injury.

As previously described, temporal inactivation of p110α-RBD interaction in adult mice results in partial lethality (55.56%) following DSS intestinal injury. Since we previously showed that p110α-RBD interaction couples to AA sensing mTORC1 signalling, we sought to investigate the role of Rheb/mTORC1 activity in IEC-intrinsic Rheb deletion *in vivo*. Interestingly, $Rheb^{\Delta IEC}$ adult mice resulted in a severe lethality (81%) after DSS intestinal injury, as well as a significantly reduced colon length, analogous to $p110\alpha^{RBD/-}$ mouse strain. Therefore, Rheb/mTORC1 activity was observed to regulate a mechanism of protection and/or survival from intestinal injury after acute DSS intestinal injury. The histopathological examination of the small intestines and colons from $Rheb^{\Delta IEC}$ adult mice that have undergone DSS injury, showed increased tissue damage compared to $p110\alpha^{RBD/-}$ mouse strain with level of hyperplasia yet severe disruption of villus-crypt architecture. Furthermore, IECs were isolated from each $Rheb^{\Delta IEC}$ mouse strain and stained for proliferative markers (Ki67), as well as CBCs markers such as CD24. After DSS treatment, the percentage of $Ki67^{hi}$ levels were significantly higher in $Rheb^{\Delta IEC}$ mouse strain compared to the control analogous to the p110α-RBD, $NOD1^{KO}$, and $NOD2^{KO}$ mouse strains. However, our results showed no significant differences of the percentage of $CD24^{hi}$ in $Rheb^{\Delta IEC}$ mouse strain after DSS treatment although a tendency of an increased percentage of $CD24^{hi}$ levels was observed. We concluded that proliferation of IECs was higher in all mutant strains compared to the control counterparts after DSS treatment with the exception of $CD24^{hi}$ expressing IEC population, which was increased only in

p110α-RBD mutant mice after DSS treatment. Finally, in order to identify a range of selective lineage markers, a gene expression analysis by real time RT-PCR was carried using small intestinal RNAs. Our data obtained from real time RT-PCR showed increased expression of Bmi1 lineage marker as well as Mmp7 (Paneth cells), and Muc2 (goblet cells) in $Rheb^{\Delta IEC}$ mouse strain. Overall, our data indicated common pathways, regulated downstream of p110α-RBD-Rheb-mTORC1 pathways that may be important for the survival of mice under intestinal injury, herein mediated by DSS, overall resulting in the increased susceptibility and near complete lethality. Although our analysis showed differences in IEC subpopulations, since IEC intrinsic Rheb deletion *in vivo* resulted in an increased lethality after DSS intestinal injury, p110α-RBD interaction might be involved in intestinal protection in a different manner than Rheb/mTORC1.

6.DISCUSSION

"One never notices what has been done;

one can only see what remains to be done"

Marie Skłodowska Curie

6.1. Class I PI3K and gut immunology

PI3Ks control evolutionary complex pathways involving proliferation, growth, metabolic functions, and other essential cellular processes. For the past two decades, significant discoveries in PI3K molecular and functional biology, facilitated the development of class I PI3K specific-inhibitors used in clinical trials for important therapeutic approaches in cancer and inflammatory diseases. However, the specific role of class I PI3Ks in the gut remains not well-established and requires to be addressed. Recent studies, established that cytosolic receptors of bacterial peptidoglycans, known as NLRs, regulate many essential downstream pathways, being NOD1 and NOD2 the most studied and associated with intestinal epithelial tissue repair, restitution, and proliferation[5,172]. In this project, we investigated class I PI3K specific-isoforms crosstalk with NOD-signalling, regulating repair and protection at the intestinal epithelium by controlling the balance between proliferation and growth after injury. Moreover, we showed the mechanism of how p110α-RBD supports such process in the intestine *in vivo* and *in vitro*. We identified that the link between an evolutionarily conserved macropinocytosis process in IECs, which was previously attributed to cancer cells and phagocytes, is mediated via p110α-RBD interaction in MEFs. Furthermore, we discovered that bacterial dipeptides, enriched in the gut lumen utilise an analogous process to uptake AAs and bacterial dipeptides by macropinocytosis and induced mTORC1 signalling downstream of p110α. Finally, we showed that p110α is critically involved and supports uptake and signalling by eukaryotic AAs and prokaryotic dipeptides which overall regulate responses to intestinal injury and survival of the organism. How AA sensing pathway relays on p110α-RBD and the molecular interactions controlling this pathway remains to be established.

6.1.1. The role of p110δ vs. p110α PI3K in the gut

The first part of our data, reinforced by previous studies, showed that p110δ is the main isoform in DCs regulating intestinal protection[1,224,225]. Furthermore, we showed that p110δ is a key component of NOD2 signalling pathway and downregulates intestinal inflammation (upregulating AKT phosphorylation and downregulating p38-MAPK activation) in immune cells. However, inactivation of p110δ in specific innate immune cell populations was not sufficient to compromise mucosal immunity. Therefore, we concluded that cells of the immune compartment other than the intestinal phagocytes (DCs and macrophages, on their own), or loss of p110δ activity in both populations in a combinatorial manner maybe important in resistance to microbiota-mediated inflammation. Since p110δ can be expressed in other cell populations in an inducible manner, we hypothesised that other non-immune cells might play a role in intestinal repair and regeneration and so, a combined deficiency of p110δ in both innate and IECs might generate spontaneous colitis. However, we also studied the role of other class I PI3Ks in IECs and demonstrated that p110α is the main isoform regulating AKT activation as well as mTORC1, while p38-MAPK are downregulated, being p110β the second most expressed. We inhibited selective-isoforms of class I PI3Ks in human and mouse intestinal cell lines and showed that p110α activity was required for the activation of AKT but also mTORC1 mediated by bacterial dipeptide sensing NOD1/2 pathway *in vitro*. Our data showed IEC-intrinsic p110α activity link bacterial dipeptide sensing NOD1/2 pathways to AA sensing mTORC1 signalling *in vitro.*

The ubiquitously expressed p110α PI3K has been shown to be the main class I PI3K isoform regulating cellular proliferation[39,191,226], differentiation[113,227],

and development[206,228–232]. Mutations in p110α isoform are highly associated with cancer and overgrowth syndromes, and p110α inactivity in transgenic mouse models is lethal in early stages of embryogenesis. However, the role of p110α in the adult intestine has never been addressed. Therefore, in this project we compared an established model of p110δ kinase inactivated mice (p110δ KI), showing increased susceptibility and inflammatory responses after acute chemically induced DSS intestinal injury, to a conditional p110α-RBD transgenic mouse model, which did not correlate with the phenotype of p110δ KI. Whilst p110δ showed increased susceptibility and inflammatory responses (DSS-colitis response), p110α-RBD mice showed partial lethality and DSS-injury not related to colitis, showing no marked differences to the WT counterparts in the level of inflammation.

6.1.2. The p110α PI3K activity controls mTORC1 dependent AA sensing pathway *in vitro*

Since our data demonstrating that disruption of p110α-RBD interaction after intestinal acute injury in adult mice has functional consequences *in vivo*, we have investigated the mechanism of p110α-RBD interaction in the intestine. A possible future study from our findings could be to generate crypt cultures (also named organoids) from p110α-RBD mice intestines *ex vivo* and study these functions *ex vivo*. Linage tracing and histological characterisation such as immunohistochemistry (IHC) staining for specific IEC subpopulations could also be the following tools to address this project. We have made attempts, but unfortunately more exhaustive optimisation of the crypt culture methodologies and higher numbers of tissues processed for IHC staining was required to address this question. Therefore, we have investigated the selective role of p110α-RBD and

its mechanism of action *in vitro* in MEFs derived from homozygous ($p110\alpha^{RBD/RBD}$) mice and used $p110\alpha^{WT/WT}$ mice as controls. The AKT expression in mutant αRBD MEFs was comparable to WT MEFs after acute EGF stimulation, showing that p110α interactions with GTPases does not influence AKT activity mediated by RTKs. Therefore, we did not observe differences *in vitro* after GFs exposure mediated p110α-RBD interaction. However, our results showed mutations disrupting p110α-RBD interaction selectively downregulate mTORC1 activation mediated by AAs and bacterial ligands in a similar manner. Herein, we showed a new mechanism which p110α interaction with GTPases regulates mTORC1 independently of AKT activation, unlike previous studies indicating RTK mediated activation of PI3K/AKT pathway results in the activation of p70 S6K by phosphorylation-dependent inhibition of TSC2[233]. Our results confirmed that AKT should not be used as a unique readout for functional analyses of PI3K signalling pathway. Previous studies have shown that inhibition of mTORC1 through p110α-RBD affects growth and protein synthesis but not proliferation that is regulated through AKT signalling[215,231]. This could potentially be explained through p110α-RBD role downstream of Ras regulating macropinocytosis via Rac and overall resulting in the activation of mTORC1.

Furthermore, we observed that p110α-RBD interaction restricted NOD1 mediated p38 activity in MEFs, in a similar manner to the p110α inhibitor in IECs. Our results demonstrated that p38 MAPK signalling was increased in absence of p110α-RBD interaction that may indicate low AA availability inducing a cell protective stress response to activate autophagy via p38-autophagy-mTORC1 pathway, potentially to acquire AAs through cell catabolic processes. These data are in agreement with previous studies showing cell stress conditions such as oxidative stress or accumulation of protein aggregates in cells induces p38 MAPK, which is involved in the upregulation of autophagy related gene expression and/or

direct activation of the autophagy which later on can induce mTORC1 activation through protein catabolism in the lysosome system[234,235]. Since oncogenic Ras has been linked to increased macropinocytosis of extracellular proteins pathways[236], we therefore explored whether a similar pathway may be functional in healthy cells in the uptake mechanism of AAs. The p110α-RBD is established to interact with Ras isoforms and in this study, we have demonstrated that p110α-RBD in MEFs controls eukaryotic AA and prokaryotic dipeptide uptake, overall resulting in the activation of mTORC1 pathway. In addition, using established inhibitor of $Na^{+/}H^{+}$ exchanger (NHE) that arrests macropinocytosis (EIPA) and a v-ATPase inhibitor that blocks lysosomal fusion (bafilomycin A1), we have discovered that either inhibitor blocks AA and/or bacterial dipeptide uptake mediated activation of mTORC1 pathway. These data demonstrated that p110α-RBD interaction might be required for activation of both eukaryotic AA and prokaryotic dipeptide sensing mTORC1 signalling *in vitro.*

6.2. PI3K-NOD and mTOR axis in the gut

As previously described, all groups of transgenic mice analysed in this thesis were observed to share several commonalities. The p110α-RBD, Rheb$^{\Delta IEC}$, NOD1^{KO}, and NOD2^{KO} mouse models were all significantly susceptible after DSS mediated intestinal injury and the colon lengths were significantly decreased compared to control counterparts. Although, weight loss and colon length are not enough indicators of colitis pathology in mouse, in order to understand the functional role of p110α-RBD mouse strain, we compared histological samples from small intestines and colon tissues, as well as cell subpopulations lineage tracing between each mouse strain. However, several differences were observed between all mouse strains tested under vehicle treatment or DSS intestinal injury.

6.2.1. IECs proliferation is regulated by p110α-RBD dependent crosstalk to NOD1/2 and mTORC1

NOD1 and NOD2-deficiency have been previously shown to be associated with gut immunity and inflammation[180,181,237–239]. Our *in vitro* data showed that NOD1/2 coupling to p110α-RBD may restrict IEC nutrient sensing, growth, and cellular stress. GFR and mitogens that signal through p110α-p85 (independently of RBD interaction), can increase AKT signalling, through mTORC2, which we have shown is upregulated when mTORC1 pathway is abolished in the p110α-RBD MEFs. Therefore, GFRs may be sufficient to provide survival/proliferation signals to IECs under injury conditions and overcome the effects enforced by the loss of p110α-RBD mediated AA and dipeptide sensing mTORC1 activity. After

vehicle treatment, p110α-RBD, NOD1^{KO}, and NOD2^{KO} mouse strains showed increased proliferation levels (Ki67^{hi}) of IECs *in vivo.* Both p110α-RBD and NOD1/2^{KO} have reduced CD24^{hi} subpopulation under basal conditions even if proliferation is high in all strains, a possible explanation could be that p110α-RBD/NOD1 controls CBCs and/or Paneth cells survival and, as previously reported[212], can consequently indirectly impact CBC numbers in a non-CBC autonomous manner[212]. After DSS treatment, we observed significantly increased level of proliferation in IECs from p110α-RBD, NOD1^{KO}, and NOD2^{KO} mice strains. Interestingly, loss of p110α-RBD showed increased CD24^{+} cell population numbers under injury as well as Lgr5+ cell population.

Under injury conditions, the absence of both AA and bacterial dipeptide-mediated p110α-RBD signals (potentially activating mTORC1), appears to increase proliferation of IECs population. In our results, the percentage of CD24^{hi} subpopulation resulted to be reduced in the NOD1/2^{KO} mouse strains under DSS treatment, suggesting NOD2 being important for CBCs population, either providing protection signals within CBCs or via Paneth cells and supporting CBC self-renewal by bacterial dipeptides. NOD1-deficiet mice under injury, were observed to share overlapping functions as NOD2, which had been shown to be important for restricting IEC proliferation and acquisition of CD24 marker, representing the CBC population[182,240]. Overall, our data demonstrated that NOD1/2 mediated bacterial dipeptide sensing, potentially via p110α, restricts IEC hyperproliferative capacity, while supporting CBC lineage maintenance. The p110α-RBD interaction, likely in part through eukaryotic AA sensing mTORC1 pathway restricts proliferative capacity of IECs, potentially through ISCs lineage and restricts their conversion to CBC lineage. Therefore, lack of AA sensing together with loss of bacterial dipeptide signalling through NODs via p110α-RBD

cumulatively could possibly increase proliferation of cells either through reversion from differentiated cells to Lgr5+ ISCs or by directly acting on reserve stem cells.

6.2.2. IEC functions are controlled by Rheb GTPase downstream of mTORC1 pathway and is important for intestinal responses to injury

With regards to the conditional loss of Rheb in the intestinal epithelium, $Rheb^{\Delta IEC}$ mouse lethality was the highest (81%), followed by $p110\alpha^{RBD/-}$ (55.56%), and $p110\alpha^{WT/-}$ (30%) after DSS intestinal injury. On the contrary, all $NOD1^{KO}$ and $NOD2^{KO}$ mice survived DSS mediated intestinal injury. A possible explanation could be due to NOD1/2 not being required for IECs functions, particularly of absorption, and their loss of function do not result in lethality. Therefore, our data demonstrated that the conditional loss of Rheb in IECs under DSS injury was found detrimental to the survival of IECs and maintenance and lineage differentiation of the ISCs as previously shown in *Drosophila*[241]. However, important similarities were observed with p110α-RBD, $NOD1^{KO}$, and $NOD2^{KO}$ mouse models. Under basal conditions, Rheb appears to shut down eukaryotic AA signalling from p110α-RBD, dipeptide signalling from NODs, and GFR and other mitogen mediated mTORC1 signals converging on Rheb. Hence, it is a cumulative phenotype which is difficult to dissociate. In order to be able to comment on $Rheb^{\Delta IEC}$ effects, it would be useful to conditionally delete p110α in IECs or use p110α kinase dead transgenic mouse model (not yet available as full KI/KO p110α is lethal), to uncover how much of the RTK signals downstream of p110α-p85 and RBD interactions feeds into mTORC1 activity in comparison to RBD alone. Our analysis from the histopathological samples obtained from each mouse strain, indicated

differences to DSS treatment between p110α-RBD and Rheb$^{\Delta IEC}$ mouse strains, being the last model with the most lethal effects. The p110α$^{WT/-}$ and p110α$^{RBD/-}$ mouse strains showed a clear hyperplasia and damage, increased progressively from p110α$^{WT/-}$ to p110α$^{RBD/-}$ mouse strain after DSS treatment. One more highlight is that the p110α$^{RBD/-}$ mouse after vehicle treatment caused loss of crypts due to tamoxifen induced toxicity to CBCs, although we already observed this in the p110α$^{WT/WT}$ but in the mutant mouse the differences were more abrupt. Interestingly, after DSS treatment the p110α$^{RBD/-}$ mouse strain did not regenerate the intestinal epithelium as well as the control counterparts. On the other side, intestinal tissues from Rheb$^{\Delta IEC}$ mice were completely disrupted, and villus atrophy and crypt loss can be observed across small intestine and colon. The histological analyses of intestinal images from Rheb$^{\Delta IEC}$ mice under DSS treatment are somewhat reminiscent of anthropic enteropathy phenotypes observed under severe malnutrition or celiac disease[242]. Although more histological samples from Rheb$^{\Delta IEC}$ and Rheb$^{flox/flox}$ mice strains are required to be processed for future quantitative and semi-quantitative analysis (work in progress), our data suggested that mTORC1/Rheb plays an essential role in the balance between proliferation and differentiation of IECs upon injury[30,243].

Previous studies showed that neither irradiation-mediated loss of Lgr5+ ISCs, nor deletion of Lgr5+ cell populations by genetic targeting, affected regeneration and repair of tissue damage due to +4 quiescent ISCs (expressing Bmi1), being resistant to radiation and able to proliferate and replenish the tissue damage[244,245]. Therefore under basal conditions after tamoxifen treatment, +4 ISCs might be resistant to tamoxifen toxicity and are able to proliferate as WTs, but these ISCs may still require p110α-RBD to differentiate and repair the tissue damage, which in the absence of p110α-RBD interaction after tamoxifen treatment, may be compromised to differentiate normally in to distinct cell

lineages, resulting in colon shortening and delayed weight gain. Moreover, as shown in recent studies, under injury conditions Bmi1+ rapidly proliferating cells can be generated from differentiated IECs, most likely occurring by dedifferentiation from functional IECs into cycling Bmi1+ ISCs[246,247]. Under DSS injury, it is possible that the differentiated IECs such as enterocytes may revert to Bmi1+ cells, since we observed significant increase in their percentage and Bmi1+ gene expression. However, the p110α-RBD mutants, compared to WTs, under DSS injury showed upregulated proliferation and $CD24^{hi}$ cell percentage along with Bmi1 gene expression. These data indicate that inhibiting p110α-RBD may be able to restore $CD24^{+}$ cells and thus CBCs, and prematurely drive differentiation of the secretory lineages. Therefore, we suggest that interruption of p110α-RBD signals result in uncontrolled dedifferentiation of IECs into Bmi1+ or other adult progenitors, possibly at the expanse of differentiated absorptive enterocytes, since the levels of $CD24^{+}$ cells and other secretory lineage cell markers were comparable or markedly upregulated in p110α-RBD mice, which requires further investigation.

Furthermore, our results showed significant increase in the $Ki67^{hi}$ expression in IEC populations in p110α-RBD, $Rheb^{\Delta IEC}$, $NOD1^{KO}$, and $NOD2^{KO}$ mouse strains after DSS treatment. A possible explanation could be that +4 quiescent cells or any remaining ISCs population in the tissue, after injury may undertake proliferation but no differentiation into adult IECs, particularly of absorptive cells. However, we also quantified $CD24^{hi}$ (being used as a marker for CBC lineage and Paneth cells[138,212] in IECs isolation), and observed phenotypic differences between mouse strains. We observed significant increase in the levels of CD24 expression in IECs in $p110\alpha^{WT/-}$, $p110\alpha^{RBD/-}$ and $Rheb^{\Delta IEC}$ mouse strains which was decreased in $NOD1^{KO}/NOD2^{KO}$ mouse strains, indicating p110α and mTORC1 activation is important for intestinal survival and/or maintenance. The

divergent phenotype observed in p110α$^{WT/-}$, p110α$^{RBD/-}$ and Rheb$^{\Delta IEC}$ mouse strains can also result for compensatory RTK-PI3K-Akt signals upregulating proliferation at the expanse of differentiation. Finally, one more difference took our interest when comparing all mouse strains. Rheb$^{\Delta IEC}$ and NOD1/2^{KO} mice showed an increased severity of colitis and macroscopic observation of haematocrit in the stool compared to p110α-RBD mutant strain. We concluded that NOD deficient mouse models showed increased susceptibility and inflammatory responses (DSS-colitis response), analogous to p110δ KI mouse model; compared to p110α-RBD and Rheb$^{\Delta IEC}$ mice, which showed partial lethality and DSS-injury not related to colitis (having no inflammation). One possible explanation for these differences could be due to increased level of cell death in Rheb, which is dissimilar in p110α-RBD. It is possible that IECs in p110α$^{RBD/-}$ mouse strain might not be dying, but rather unable to differentiate towards absorptive cells therefore, the mice were not able to absorb nutrients and died by starvation after intestinal damage. This hypothesis can also be supported by the lack of weight gain following tamoxifen treatment in p110α$^{RBD/-}$ mouse strain. A possible solution to confirm this theory, could be the usage of specific markers from differentiated secretory and absorptive IECs such as Atoh1 and Hes1[133].

6.2.3. Future perspectives and work in line

Based on our *in vivo* data showing partial lethality due to p110α-RBD interaction, we foresee that future work is needed to address *in vitro* and *in vivo* mechanisms regarding cell proliferation and/or survival. Although p110α-RBD interaction has been previously shown to regulate proliferation of MEFs *in vitro*[25], we have not yet addressed whether the loss of p110α-RBD impacts eukaryotic AA- or bacterial dipeptide-mediated proliferative capacity and/or survival of

colonocytes and MEFs *in vitro*, which is to be addressed in the near future. Similar to mTOR$^{\Delta IEC}$ crypts, we observed that the loss of signalling through p110α-RBD, Rheb$^{\Delta IEC}$ and NODs do not impair adult crypt cell proliferation, which we have demonstrated by the observed increase in cell proliferation, suggesting that crypt cell proliferation may be restricted by NOD-p110α-RBD-mTORC1 axis. We have also observed in mutant αRBD MEFs that mTORC1-dependent signals repress PI3K-AKT activity, which was shown to be regulated through a negative feedback loop targeting IGFR by Grb10[248]. Both mTOR complexes are stimulated by mitogens and GFs, but only mTORC1 is under the control of nutrient and energy inputs, which may directly couple to Ras regulated macropinocytosis and uptake of nutrients, activating mTORC1 and providing a feedback inhibition of RTK-mediated PI3K-AKT pathway via Grp10 activation. Indeed, increased AKT phosphorylation was reported upon either mTORC1 or mTORC2 disruption in crypts, whereas elevated p-AKT^{Ser473}, an mTORC2 is associated with mTOR and Raptor disruption, regulating mTORC2 axis, signalling downstream of RTKs rather than Ras-PI3K axis[249]. Our *in vitro* data in MEFs is in line with these observations and confirms that RTK-PI3K-AKT pathway may be under control of p110α-RBD interaction with GTPases and may potentially contribute to mTORC1-inhibitor resistance observed in colon cancer types[250,251].

Rheb$^{\Delta IEC}$ mice represented the starkest severity from all strains regarding the decreased survival of mice being the most significantly affected. However, complete lack of absorptive functions cause death of mice in 24-48 h and in this case, we did not observe this. Hence, it is possible that perturbation in the differentiation capacity of cells, rather than a lack of differentiation, results in partial lethality. Rheb$^{\Delta IEC}$ mice start to die at day 4 and half of our mice were dead or had to be sacrificed by day 5, meaning earlier and hence the perturbed differentiation is clearly evident and alters survival of mice. We observed more +4

cells but no other IECs unlike in p110α-RBD mouse strain. In p110α-RBD mouse strain we observed increased Bmi1 gene expression and normal Lgr5+ population, hence these likely have come from Bmi1+ cells or Lgr5+ themselves. The loss of NODs alters and upregulate IEC numbers and proliferation as in p110α-RBD and Rheb$^{\Delta IEC}$. Therefore, NODs in IECs are likely to control cell differentiation through p110α-RBD and mTORC1 by restricting proliferation under basal and injury conditions, but differentiation might be still working for the absorptive lineage, while Paneth and goblet cells (secretory lineage) are increased in the p110α-RBD and Rheb$^{\Delta IEC}$. If Paneth cells are lower than Lgr5+ cells might be affected and lower, yet we observed more proliferating cells.

NODs are not only expressed by IECs. Under injury, NODs from immune cells may cumulatively result in cell death and increase of haematocrit. However, cell death does not necessarily lead to organismal death. This could mean an affect or impairment of repair hence also seen in NOD KOs, as the phenotype is not lethal. So, mTORC1 mediated nutrient sensing controls organismal survival during injury, through p110α-RBD-mediated activation of mTORC1. This could potentially be due to perturbed differentiation capacity, possibly toward absorptive lineage likely due to cell fate change toward secretory differentiation, but certainly not due to cell death. However, Rhebs do also couple to bacterial peptide sensing through NODs and NODs also control differentiation in IECs, hence the combined inhibition of both mTORC1 activation by eukaryotic and prokaryotic AAs cause bigger damage upon injury. It is important to delineate that our *in vitro* results do not capitulate exactly what happens *in vivo* in terms of isoform selective coupling to cell signalling and macropinocytosis. The p110α-RBD may not be the sole PI3K-RBD involved in AA sensing coupling to mTORC1 activation and other PI3Ks such as, p110β-RBD[252] may be important in macropinocytosis in IECs. Recent studies showed this *in vitro* in other epithelial cells as well as our own *in vitro* data in IECs

using TGX221. Therefore, in NOD KO system we observed a completely abolish a receptor activating a pathway, same for Rheb as it is the supreme controller of mTORC1 pathway but not p110α-RBD as PI3Ks can be compensated especially *in vivo* via other isoforms coupling to receptors such as GPCRs, here being p110β.

6.2.4. Therapeutic applications of PI3K/mTOR

The clinical effectiveness of PI3K inhibitors in the treatment of solid tumours remains imprecise and with certain limitations for human health. Targeting RBD of p110α has been suggested as a good target for therapy, particularly in lung cancers, since blocking RBD function appears to have limited toxicity in the adult mice, as also shown by our data, while being effective in tumour regression[226]. Based on our study, inhibiting p110α-RBD targets epithelial cell functions, which results in increased IEC proliferative capacity, potentially altering the balance between IEC proliferation and differentiation, possibly due to mTORC1-mediated growth signals, which may be equally important for cell differentiation and survival. This is in line with the studies indicating inhibition of mTORC1 pathway in adult mouse intestine increases stemness[3,253] and rapamycin treatment in adult mice increases stem cell regenerative capacity[254,255]. Therefore, targeting solely p110α-RBD may increase cell proliferative activity particularly in tumours with associated cancer stem cell types with highly undifferentiated cells, resembling cancer stem cells. Nevertheless, targeting p110α-RBD may be selectively beneficial for tumours with known RAS mutations that show cell survival advantage due to increased macropinocytosis and catabolism of extracellular proteins, likely occurring through lysosomal degradation of proteins, increasing mTORC1 pathway[236,256]. Therefore, we suggest that p110α or mTORC1 inhibitors may prove beneficial when used in combination of Ras-Raf inhibitors,

overall targeting proliferation of cells. Although, potential intestinal toxicity should be considered while using RAS inhibitors.

7.REFERENCES

"Science has only one commandment: contribution" **Bertolt Brecht**

"In the middle of difficulty lies opportunity" **Albert Einstein**

1. Steinbach, E. C. *et al.* Innate PI3K p110δ regulates Th1/Th17 development and microbiota-dependent colitis. *J. Immunol.* **192**, 3958–68 (2014).

2. Dbouk, H. A. *et al.* Characterization of a Tumor-Associated Activating Mutation of the p110β PI 3-Kinase. *PLoS One* **8**, e63833 (2013).

3. Sampson, L. L., Davis, A. K., Grogg, M. W. & Zheng, Y. mTOR disruption causes intestinal epithelial cell defects and intestinal atrophy postinjury in mice. *FASEB J.* **30**, 1263–75 (2016).

4. Barron, L. *et al.* Intestinal Epithelial-Specific mTORC1 Activation Enhances Intestinal Adaptation After Small Bowel Resection. *Cell. Mol. Gastroenterol. Hepatol.* **3**, 231–244 (2017).

5. Parlato, M. & Yeretssian, G. NOD-Like Receptors in Intestinal Homeostasis and Epithelial Tissue Repair. *Int. J. Mol. Sci.* **15**, 9594–9627 (2014).

6. Cruickshank, S.-M. *et al.* Evidence for the involvement of NOD2 in regulating colonic epithelial cell growth and survival. *World J. Gastroenterol.* **14**, 5834–41 (2008).

7. Couturier-maillard, A. *et al.* NOD2-mediated dysbiosis predisposes mice to transmissible colitis and colorectal cancer. doi:10.1172/JCI62236DS1

8. Hisamatsu, T. *et al.* CARD15/NOD2 functions as an antibacterial factor in human intestinal epithelial cells. *Gastroenterology* **124**, 993–1000 (2003).

9. Bozzaro, S. & Eichinger, L. The Professional Phagocyte Dictyostelium discoideum as a Model Host for Bacterial Pathogens. *Curr. Drug Targets* **12**, 942–954 (2011).

10. Vanhaesebroeck, B., Guillermet-Guibert, J., Graupera, M. & Bilanges, B. The emerging mechanisms of isoform-specific PI3K signalling. *Nat. Rev. Mol. Cell Biol.* **11**, 329–341 (2010).

11. Koyasu, S. The role of PI3K in immune cells. *Nat. Immunol.* **4**, 313–319 (2003).

12. Vanhaesebroeck, B., Leevers, S. J., Panayotou, G. & Waterfield, M. D. Phosphoinositide 3-kinases: A conserved family of signal transducers. *Trends Biochem. Sci.* **22**, 267–272 (1997).

13. Vanhaesebroeck, B., Stephens, L. & Hawkins, P. PI3K signalling: the path to discovery and understanding. *Nat. Rev. Mol. Cell Biol.* **13**, 195–203 (2012).

14. Clayton, E. *et al.* A crucial role for the p110delta subunit of phosphatidylinositol 3-kinase in B cell development and activation. *J. Exp. Med.* **196**, 753–63 (2002).

15. Thorpe, L. M., Yuzugullu, H. & Zhao, J. J. PI3K in cancer: divergent roles of isoforms, modes of activation and therapeutic targeting. *Nat. Rev. Cancer* **15**, 7–24 (2015).

16. Vanhaesebroeck, B., Ali, K., Bilancio, A., Geering, B. & Foukas, L. C. Signalling by PI3K isoforms: insights from gene-targeted mice. *Trends Biochem. Sci.* **30**, 194–204 (2005).

17. Carpenter, C. L. *et al.* Phosphoinositide 3-kinase is activated by phosphopeptides that bind to the SH2 domains of the 85-kDa subunit. *J. Biol. Chem.* **268**, 9478–83 (1993).

18. Samuels, Y. *et al.* High Frequency of Mutations of the PIK3CA Gene in Human Cancers. doi:10.1126/science.1096502

19. Cathomas, G. PIK3CA in colorectal cancer. (2014). doi:10.3389/fonc.2014.00035

20. Thorpe, L. M., Yuzugullu, H. & Zhao, J. J. PI3K in cancer: divergent roles of isoforms, modes of activation and therapeutic targeting. *Nat. Rev. Cancer* **15**, 7–24 (2015).

21. Sun, X. J. *et al.* Structure of the insulin receptor substrate IRS-1 defines a unique signal transduction protein. *Nature* **352**, 73–77 (1991).

22. Backer, J. M. *et al.* Phosphatidylinositol 3'-kinase is activated by association with IRS-1 during insulin stimulation. *EMBO J.* **11**, 3469–79 (1992).

23. Rodriguez-Viciana, P., Sabatier, C. & McCormick, F. Signaling Specificity by Ras Family GTPases Is Determined by the Full Spectrum of Effectors They Regulate. *Mol. Cell. Biol.* **24**, 4943 (2004).

24. Bos, J. Ras oncogenes in human cancer: a review. Available at: https://www.ncbi.nlm.nih.gov/pubmed/?term=2547513. (Accessed: 27th September 2019)

25. Gupta, S. *et al.* Binding of Ras to Phosphoinositide 3-Kinase p110α Is Required for Ras-Driven Tumorigenesis in Mice. *Cell* **129**, 957–968 (2007).

26. Orme, M. H., Alrubaie, S., Bradley, G. L., Walker, C. D. & Leevers, S. J. Input from Ras is required for maximal PI(3)K signalling in Drosophila. *Nat. Cell Biol.* **8**, 1298–1302 (2006).

27. Burke, J. E. & Williams, R. L. Synergy in activating class I PI3Ks. *Trends Biochem. Sci.* **40**, 88–100 (2015).

28. Vadas, O., Burke, J. E., Zhang, X., Berndt, A. & Williams, R. L. Structural basis for activation and inhibition of class I phosphoinositide 3-kinases. *Sci. Signal.* **4**, re2 (2011).

29. Yu, J. S. L. & Cui, W. Proliferation, survival and metabolism: the role of PI3K/AKT/mTOR signalling in pluripotency and cell fate determination. *Development* **143**, 3050–3060 (2016).

30. Wipperman, M. F., Montrose, D. C., Gotto, A. M. & Hajjar, D. P. Mammalian Target of Rapamycin. *Am. J. Pathol.* **189**, 492–501 (2019).

31. Schieke, S. M. *et al.* The Mammalian Target of Rapamycin (mTOR) Pathway Regulates Mitochondrial Oxygen Consumption and Oxidative Capacity. *J. Biol. Chem.* **281**, 27643–27652 (2006).

32. Xu, K., Liu, P. & Wei, W. mTOR signaling in tumorigenesis. *Biochim. Biophys. Acta* **1846**, 638–54 (2014).

33. Yoshida, S., Pacitto, R., Inoki, K. & Swanson, J. Macropinocytosis, mTORC1 and cellular growth control. *Cell. Mol. Life Sci.* **75**, 1227–1239 (2018).

34. Bloomfield, G. & Kay, R. R. Uses and abuses of macropinocytosis. (2016). doi:10.1242/jcs.176149

35. Recouvreux, M. V. & Commisso, C. Macropinocytosis: A Metabolic Adaptation to Nutrient Stress in Cancer. *Front. Endocrinol. (Lausanne).* **8**, 261 (2017).

36. Williams, T. D., Peak-Chew, S.-Y., Paschke, P. & Kay, R. R. Akt and SGK protein kinases are required for efficient feeding by macropinocytosis. *J. Cell Sci.* **132**, (2019).

37. Bloomfield, G. & Kay, R. R. Uses and abuses of macropinocytosis. (2016). doi:10.1242/jcs.176149

38. Palm, W. Metabolic functions of macropinocytosis. *Philos. Trans. R. Soc. Lond. B. Biol. Sci.* **374**, 20180285 (2019).

39. Murillo, M. M. *et al.* RAS interaction with PI3K p110α is required for tumor-induced angiogenesis. *J. Clin. Invest.* **124**, 3601–3611 (2014).

40. Yoshida, S., Pacitto, R., Yao, Y., Inoki, K. & Swanson, J. A. Growth factor signaling to mTORC1 by amino acid-laden macropinosomes. *J. Cell Biol.* **211**, 159–172 (2015).

41. Samuels, Y. *et al.* High Frequency of Mutations of the PIK3CA Gene in Human Cancers. *Science (80-.).* (2004).

42. Zhao, L. & Vogt, P. K. Helical domain and kinase domain mutations in p110 of phosphatidylinositol 3-kinase induce gain of function by different mechanisms. *Proc. Natl. Acad. Sci.* **105**, 2652–2657 (2008).

43. Wu, X. *et al.* Activation of diverse signalling pathways by oncogenic PIK3CA mutations. *Nat. Commun.* **5**, 4961 (2014).

44. Berenjeno, I. M. *et al.* Both p110 α and p110 β isoforms of PI3K can modulate the impact of loss-of-function of the PTEN tumour suppressor. **159**, 151–159 (2012).

45. Jia, S. *et al.* Essential roles of PI(3)K–p110β in cell growth, metabolism and tumorigenesis. *Nature* **454**, 776–779 (2008).

46. Sasaki, T. *et al.* Colorectal carcinomas in mice lacking the catalytic subunit of PI(3)Kγ. *Nature* **406**, 897–902 (2000).

47. Webb, L. M. C., Vigorito, E., Wymann, M. P., Hirsch, E. & Turner, M. Cutting edge: T cell development requires the combined activities of the p110gamma and p110delta catalytic isoforms of phosphatidylinositol 3-kinase. *J. Immunol.* **175**, 2783–7 (2005).

48. Falasca, M. & Maffucci, T. Targeting p110gamma in gastrointestinal cancers: attack on multiple fronts. *Front. Physiol.* **5**, 391 (2014).

49. Kurek, K. C. *et al.* Somatic Mosaic Activating Mutations in PIK3CA Cause CLOVES Syndrome. *Am. J. Hum. Genet.* **90**, 1108–1115 (2012).

50. Lindhurst, M. J. *et al.* Mosaic overgrowth with fibroadipose hyperplasia is caused by somatic activating mutations in PIK3CA. *Nat. Genet.* **44**, 928–933 (2012).

51. Castillo, S. D. *et al.* Somatic activating mutations in Pik3ca cause sporadic venous malformations in mice and humans. *Sci. Transl. Med.* **8**, 332ra43-332ra43 (2016).

52. Madsen, R. R., Vanhaesebroeck, B. & Semple, R. K. Cancer-Associated PIK3CA Mutations in Overgrowth Disorders. *Trends Mol. Med.* **24**, 856–870 (2018).

53. Worby, C. A. & Dixon, J. E. PTEN. *Annu. Rev. Biochem.* **83**, 641–669 (2014).

54. Wymann, M. P. & Marone, R. Phosphoinositide 3-kinase in disease: Timing, location, and scaffolding. *Curr. Opin. Cell Biol.* **17**, 141–149 (2005).

55. Angulo, I. *et al.* Phosphoinositide 3-kinase δ gene mutation predisposes to respiratory infection and airway damage. *Science* **342**, 866–71 (2013).

56. Ali, K. *et al.* Inactivation of PI(3)K p110δ breaks regulatory T-cell-mediated immune tolerance to cancer. *Nature* **510**, 407–11 (2014).

57. Dornan, G. L. *et al.* Conformational disruption of PI3Kδ regulation by immunodeficiency mutations in *PIK3CD* and *PIK3R1*. *Proc. Natl. Acad. Sci.* **114**, 1982–1987 (2017).

58. Sogkas, G. *et al.* Primary immunodeficiency disorder caused by phosphoinositide 3–kinase δ deficiency. *J. Allergy Clin. Immunol.* **142**, 1650-1653.e2 (2018).

59. Swan, D. J. *et al.* Immunodeficiency, autoimmune thrombocytopenia and enterocolitis caused by autosomal recessive deficiency of PIK3CD-encoded phosphoinositide 3-kinase δ. *Haematologica* haematol.2018.208397 (2019). doi:10.3324/haematol.2018.208397

60. Hudes, G. *et al.* Temsirolimus, Interferon Alfa, or Both for Advanced Renal-Cell Carcinoma. *N. Engl. J. Med.* **356**, 2271–2281 (2007).

61. Rodon, J., Dienstmann, R., Serra, V. & Tabernero, J. Development of PI3K inhibitors: lessons learned from early clinical trials. *Nat. Rev. Clin. Oncol.* **10**, 143–153 (2013).

62. Baselga, J. *et al.* Everolimus in Postmenopausal Hormone-Receptor–Positive Advanced Breast Cancer. *N. Engl. J. Med.* **366**, 520–529 (2012).

63. Chen, I.-C. *et al.* Phosphatidylinositol-3 Kinase Inhibitors, Buparlisib and Alpelisib, Sensitize Estrogen Receptor-positive Breast Cancer Cells to Tamoxifen. *Sci. Rep.* **7**, 9842 (2017).

64. Gopal, A. K. *et al.* PI3Kδ inhibition by idelalisib in patients with relapsed indolent lymphoma. *N. Engl. J. Med.* **370**, 1008–18 (2014).

65. LoRusso, P. M. Inhibition of the PI3K/AKT/mTOR pathway in solid tumors. *J. Clin. Oncol.* **34**, 3803–3815 (2016).

66. Brana, I. *et al.* A phase I dose-escalation study of the safety, pharmacokinetics (PK), and pharmacodynamics of XL765 (SAR245409), a PI3K/TORC1/TORC2 inhibitor administered orally to patients (pts) with advanced malignancies. *J. Clin. Oncol.* **28**, 3030–3030 (2010).

67. Jiménez, C. *et al.* Role of the Pi3k Regulatory Subunit in the Control of Actin Organization and Cell Migration. *J. Cell Biol.* **151**, 249–262 (2000).

68. Hill, K. M. *et al.* N-terminal domains of the class ia phosphoinositide 3-kinase regulatory subunit play a role in cytoskeletal but not mitogenic signaling. *J. Biol. Chem.* **276**, 16374–8 (2001).

69. Kang, H., Schneider, H. & Rudd, C. E. Phosphatidylinositol 3-kinase p85 adaptor function in T-cells. Co-stimulation and regulation of cytokine transcription independent of associated p110. *J. Biol. Chem.* **277**, 912–21 (2002).

70. Sapey, E. *et al.* Phosphoinositide 3-kinase inhibition restores neutrophil accuracy in the elderly: toward targeted treatments for immunosenescence. *Blood* **123**, 239–48 (2014).

71. Sasaki, T. *et al.* Function of PI3K in Thymocyte Development, T Cell Activation, and Neutrophil Migration. *Science (80-.).* **287**, 1040–1046 (2000).

72. Hirsch, E. *et al.* Central role for G protein-coupled phosphoinositide 3-kinase gamma in inflammation. *Science* **287**, 1049–53 (2000).

73. Patrucco, E. *et al.* PI3Kγ Modulates the Cardiac Response to Chronic Pressure Overload by Distinct Kinase-Dependent and -Independent Effects. *Cell* **118**, 375–387 (2004).

74. Chang, J. D. *et al.* Deletion of the phosphoinositide 3-kinase p110γ gene attenuates murine atherosclerosis. *Proc. Natl. Acad. Sci.* **104**, 8077–8082 (2007).

75. Vadas, O. *et al.* Molecular determinants of PI3Kγ-mediated activation downstream of G-

protein-coupled receptors (GPCRs). *Proc. Natl. Acad. Sci. U. S. A.* **110**, 18862–7 (2013).

76. Okkenhaug, K. *et al.* Impaired B and T Cell Antigen Receptor Signaling in p110δ PI 3-Kinase Mutant Mice. *Science (80-.).* **297**, 7–18 (2002).

77. Aksoy, E. *et al.* The p110δ isoform of the kinase PI(3)K controls the subcellular compartmentalization of TLR4 signaling and protects from endotoxic shock. *Nat. Immunol.* **13**, 1045–54 (2012).

78. Guillermet-Guibert, J. *et al.* Novel Role for p110? PI 3-Kinase in Male Fertility through Regulation of Androgen Receptor Activity in Sertoli Cells. *PLOS Genet.* **11**, e1005304 (2015).

79. Bi, L., Okabe, I., Bernard, D. J., Wynshaw-Boris, A. & Nussbaum, R. L. Proliferative defect and embryonic lethality in mice homozygous for a deletion in the p110alpha subunit of phosphoinositide 3-kinase. *J. Biol. Chem.* **274**, 10963–8 (1999).

80. Okkenhaug, K. *et al.* Impaired B and T Cell Antigen Receptor Signaling in p110delta PI 3-Kinase Mutant Mice. *Science (80-.).* **297**, 1031 (2002).

81. Okkenhaug, K., Bilancio, A., Meek, S. E., Salpekar, A. & Waterfield, M. D. Impaired B and T Cell Antigen Receptor Signaling in p110 ʕ PI 3-Kinase Mutant Mice. *Science (80-.).* **297**, 1031–1034 (2002).

82. Rolf, J. *et al.* Phosphoinositide 3-kinase activity in T cells regulates the magnitude of the germinal center reaction. *J. Immunol.* **185**, 4042–52 (2010).

83. Goorden, S. M. I. *et al.* Rheb is essential for murine development. *Mol. Cell. Biol.* **31**, 1672–8 (2011).

84. Zou, J. *et al.* Rheb1 Is Required for mTORC1 and Myelination in Postnatal Brain Development. *Dev. Cell* **20**, 97–108 (2011).

85. Tamai, T. *et al.* Rheb (Ras Homologue Enriched in Brain)-dependent Mammalian Target of Rapamycin Complex 1 (mTORC1) Activation Becomes Indispensable for Cardiac Hypertrophic Growth after Early Postnatal Period. *J. Biol. Chem.* **288**, 10176–10187 (2013).

86. Hallmann, D. *et al.* Altered signaling and cell cycle regulation in embryonal stem cells with a disruption of the gene for phosphoinositide 3-kinase regulatory subunit p85alpha. *J. Biol. Chem.* **278**, 5099–108 (2003).

87. Fruman, D. A. *et al.* Impaired B cell development and proliferation in absence of phosphoinositide 3-kinase p85alpha. *Science* **283**, 393–7 (1999).

88. Ueki, K. *et al.* Molecular balance between the regulatory and catalytic subunits of phosphoinositide 3-kinase regulates cell signaling and survival. *Mol. Cell. Biol.* **22**, 965–77 (2002).

89. Fruman, D. A. *et al.* Hypoglycaemia, liver necrosis and perinatal death in mice lacking all isoforms of phosphoinositide 3-kinase p85α. *Nat. Genet.* **26**, 379–382 (2000).

90. Mauvais-Jarvis, F. *et al.* Reduced expression of the murine p85alpha subunit of phosphoinositide 3-kinase improves insulin signaling and ameliorates diabetes. *J. Clin. Invest.* **109**, 141–9 (2002).

91. Terauchi, Y. *et al.* Increased insulin sensitivity and hypoglycaemia in mice lacking the p85α subunit of phosphoinositide 3–kinase. *Nat. Genet.* **21**, 230–235 (1999).

92. Suzuki, H. *et al.* Xid-like immunodeficiency in mice with disruption of the p85alpha subunit of phosphoinositide 3-kinase. *Science* **283**, 390–2 (1999).

93. Chen, D. *et al.* p50alpha/p55alpha phosphoinositide 3-kinase knockout mice exhibit enhanced insulin sensitivity. *Mol. Cell. Biol.* **24**, 320–9 (2004).

94. Ueki, K. *et al.* Increased insulin sensitivity in mice lacking p85 subunit of phosphoinositide 3-kinase. *Proc. Natl. Acad. Sci.* **99**, 419–424 (2002).

95. Bi, L., Okabe, I., Bernard, D. J., Wynshaw-Boris, A. & Nussbaum, R. L. Proliferative defect and embryonic lethality in mice homozygous for a deletion in the p110alpha subunit of phosphoinositide 3-kinase. *J. Biol. Chem.* **274**, 10963–8 (1999).

96. Jou, S.-T. *et al.* Essential, nonredundant role for the phosphoinositide 3-kinase p110delta in signaling by the B-cell receptor complex. *Mol. Cell. Biol.* **22**, 8580–91 (2002).

97. Ali, K. *et al.* Essential role for the p110δ phosphoinositide 3-kinase in the allergic response. *Nature* **431**, 1007–1011 (2004).

98. Laffargue, M. *et al.* Phosphoinositide 3-Kinase γ Is an Essential Amplifier of Mast Cell Function. *Immunity* **16**, 441–451 (2002).

99. Chagastelles, P. C. & Nardi, N. B. Biology of stem cells: an overview. *Kidney Int. Suppl.* **1**, 63–67 (2011).

100. Biehl, J. K. & Russell, B. Introduction to stem cell therapy. *J. Cardiovasc. Nurs.* **24**, 98–103; quiz 104–5 (2009).

101. Shahriyari, L. & Komarova, N. L. Symmetric vs. Asymmetric Stem Cell Divisions: An Adaptation against Cancer? *PLoS One* **8**, e76195 (2013).

102. Lopez-Garcia, C., Klein, A. M., Simons, B. D. & Winton, D. J. Intestinal stem cell replacement follows a pattern of neutral drift. *Science* **330**, 822–5 (2010).

103. Snippert, H. J. *et al.* Intestinal Crypt Homeostasis Results from Neutral Competition between Symmetrically Dividing Lgr5 Stem Cells. *Cell* **143**, 134–144 (2010).

104. de Sousa e Melo, F. & de Sauvage, F. J. Cellular Plasticity in Intestinal Homeostasis and Disease. *Cell Stem Cell* **24**, 54–64 (2019).

105. Paling, N. R. D., Wheadon, H., Bone, H. K. & Welham, M. J. Regulation of embryonic stem cell self-renewal by phosphoinositide 3-kinase-dependent signaling. *J. Biol. Chem.* **279**, 48063–48070 (2004).

106. Palomero, T. *et al.* Mutational loss of PTEN induces resistance to NOTCH1 inhibition in T-cell leukemia. *Nat. Med.* **13**, 1203–1210 (2007).

107. Li, T. *et al.* SMO Expression in Colorectal Cancer: Associations with Clinical, Pathological, and Molecular Features. *Ann. Surg. Oncol.* **21**, 4164–4173 (2014).

108. Tenbaum, S. P. *et al.* β-catenin confers resistance to PI3K and AKT inhibitors and subverts FOXO3a to promote metastasis in colon cancer. *Nat. Med.* **18**, 892–901 (2012).

109. Lindström, N. O., Carragher, N. O. & Hohenstein, P. The PI3K pathway balances self-renewal and differentiation of Nephron Progenitor Cells through β-catenin signaling. *Stem Cell Reports* **4**, 551–560 (2015).

110. Gregorieff, A. & Clevers, H. Wnt signaling in the intestinal epithelium : from endoderm to

cancer Wnt signaling in the intestinal epithelium : from endoderm to cancer. 877–890 (2005). doi:10.1101/gad.1295405

111. Lucas, C. L. *et al.* Dominant-activating germline mutations in the gene encoding the PI(3)K catalytic subunit p110δ result in T cell senescence and human immunodeficiency. *Nat. Immunol.* **15**, 88–97 (2014).

112. Chen, Y.-H. *et al.* Asymmetric PI3K Activity in Lymphocytes Organized by a PI3K-Mediated Polarity Pathway. *Cell Rep.* **22**, 860–868 (2018).

113. Lin, W. H. W. *et al.* Asymmetric PI3K Signaling Driving Developmental and Regenerative Cell Fate Bifurcation. *Cell Rep.* **13**, 2203–2218 (2015).

114. Rivas, S., Gómez-Oro, C., Antón, I. & Wandosell, F. Role of Akt Isoforms Controlling Cancer Stem Cell Survival, Phenotype and Self-Renewal. *Biomedicines* **6**, 29 (2018).

115. Scharl, M. & Rogler, G. Microbial sensing by the intestinal epithelium in the pathogenesis of inflammatory bowel disease. *Int. J. Inflam.* **2010**, 671258 (2010).

116. Gourbeyre, P. *et al.* Pattern recognition receptors in the gut: Analysis of their expression along the intestinal tract and the crypt/villus axis. *Physiol. Rep.* **3**, 1–15 (2015).

117. Greenwood-Van Meerveld, B., Johnson, A. C. & Grundy, D. Gastrointestinal physiology and function. *Handb. Exp. Pharmacol.* **239**, (2017).

118. Kamada, N., Seo, S.-U., Chen, G. Y. & Núñez, G. Role of the gut microbiota in immunity and inflammatory disease. *Nat. Rev. Immunol.* **13**, 321–335 (2013).

119. Peterson, L. W. & Artis, D. Intestinal epithelial cells: regulators of barrier function and immune homeostasis. *Nat. Rev. Immunol.* **14**, 141–153 (2014).

120. Lopez-Garcia, C., Klein, A. M., Simons, B. D. & Winton, D. J. Intestinal Stem Cell Replacement Follows a Pattern of Neutral Drift. *Science (80-.).* **330**, 822–825 (2010).

121. van der Flier, L. G. & Clevers, H. Stem Cells, Self-Renewal, and Differentiation in the Intestinal Epithelium. *Annu. Rev. Physiol.* **71**, 241–260 (2009).

122. Lei-Leston, A. C., Murphy, A. G. & Maloy, K. J. Epithelial Cell Inflammasomes in Intestinal Immunity and Inflammation. *Front. Immunol.* **8**, 1168 (2017).

123. Chu, H. *et al.* Gene-microbiota interactions contribute to the pathogenesis of inflammatory bowel disease. *Science (80-.).* **352**, 1116–1120 (2016).

124. Abreu, M. T. Toll-like receptor signalling in the intestinal epithelium: How bacterial recognition shapes intestinal function. *Nat. Rev. Immunol.* **10**, 131–143 (2010).

125. Peterson, L. W. & Artis, D. Specialized epithelial cells constitute barrier surfaces that separate mammalian hosts from the external environ. (2014). doi:10.1038/nri3608

126. Lanik, W., Mara, M., Mihi, B., Coyne, C. & Good, M. Stem Cell-Derived Models of Viral Infections in the Gastrointestinal Tract. *Viruses* **10**, 124 (2018).

127. Yu, S. *et al.* Paneth Cell Multipotency Induced by Notch Activation following Injury. *Cell Stem Cell* **23**, 46-59.e5 (2018).

128. Bjerknes, M. & Cheng, H. Clonal analysis of mouse intestinal epithelial progenitors. *Gastroenterology* **116**, 7–14 (1999).

129. Potten, C. S., Gandara, R., Mahida, Y. R., Loeffler, M. & Wright, N. A. The stem cells of small intestinal crypts: where are they? *Cell Prolif.* **42**, 731–50 (2009).

130. Cheng, H. Origin, differentiation and renewal of the four main epithelial cell types in the mouse small intestine IV. Paneth cells. *Am. J. Anat.* **141**, 521–535 (1974).

131. Blache, P. *et al.* SOX9 is an intestine crypt transcription factor, is regulated by the Wnt pathway, and represses the CDX2 and MUC2 genes. *J. Cell Biol.* **166**, 37–47 (2004).

132. Tan, C. W., Hirokawa, Y. & Burgess, A. W. Analysis of Wnt signalling dynamics during colon crypt development in 3D culture. *Sci. Rep.* **5**, 1–18 (2015).

133. Ishibashi, F. *et al.* Contribution of ATOH1+ Cells to the Homeostasis, Repair, and Tumorigenesis of the Colonic Epithelium. *Stem cell reports* **10**, 27–42 (2018).

134. Dominguez-Brauer, C. *et al.* Mule Regulates the Intestinal Stem Cell Niche via the Wnt Pathway and Targets EphB3 for Proteasomal and Lysosomal Degradation. *Cell Stem Cell* **19**, 205–216 (2016).

135. Park, I. *et al.* Bmi-1 is required for maintenance of adult self-renewing haematopoietic stem cells. *Nature* **423**, 302–305 (2003).

136. Yan, K. S. *et al.* The intestinal stem cell markers Bmi1 and Lgr5 identify two functionally distinct populations. *Proc. Natl. Acad. Sci. U. S. A.* **109**, 466–71 (2012).

137. Mustata, R. C. *et al.* Lgr4 is required for Paneth cell differentiation and maintenance of intestinal stem cells ex vivo. *EMBO Rep.* **12**, 558–564 (2011).

138. Sato, T. *et al.* Paneth cells constitute the niche for Lgr5 stem cells in intestinal crypts. *Nature* **469**, 415–418 (2011).

139. Barker, N. *et al.* Identification of stem cells in small intestine and colon by marker gene Lgr5. *Nature* **449**, 1003–1007 (2007).

140. Flier, L. G. van der & Clevers, H. Stem Cells, Self-Renewal, and Differentiation in the Intestinal Epithelium. *http://dx.doi.org/10.1146/annurev.physiol.010908.163145* (2009). doi:10.1146/ANNUREV.PHYSIOL.010908.163145

141. Sancho, R., Cremona, C. A. & Behrens, A. Stem cell and progenitor fate in the mammalian intestine: Notch and lateral inhibition in homeostasis and disease. *EMBO Rep.* **16**, 571–581 (2015).

142. Kaaij, L. T. *et al.* DNA methylation dynamics during intestinal stem cell differentiation reveals enhancers driving gene expression in the villus. *Genome Biol.* **14**, R50 (2013).

143. Ge, Y. *et al.* Stem Cell Lineage Infidelity Drives Wound Repair and Cancer. *Cell* **169**, 636-642.e14 (2017).

144. Ge, Y. & Fuchs, E. Stretching the limits: from homeostasis to stem cell plasticity in wound healing and cancer. *Nat. Rev. Genet.* (2018). doi:10.1038/nrg.2018.9

145. Ahmad, R., Sorrell, M. F., Batra, S. K., Dhawan, P. & Singh, A. B. Gut permeability and mucosal inflammation: bad, good or context dependent. *Mucosal Immunol.* **10**, 307–317 (2017).

146. Lazzeri, E., Peired, A., Ballerini, L. & Lasagni, L. Adult Stem Cells in Tissue Homeostasis and Disease. in *Current Frontiers and Perspectives in Cell Biology* (InTech, 2012).

doi:10.5772/33941

147. Krausova, M. & Korinek, V. Wnt signaling in adult intestinal stem cells and cancer. *Cell. Signal.* **26**, 570–579 (2014).

148. Gregorieff, A. & Clevers, H. Wnt signaling in the intestinal epithelium: From endoderm to cancer. *Genes and Development* **19**, 877–890 (2005).

149. Barker, N. Adult intestinal stem cells: critical drivers of epithelial homeostasis and regeneration. (2013). doi:10.1038/nrm3721

150. Janeway, C. A. & Medzhitov, R. I <scp>NNATE</scp> I <scp>MMUNE</scp> R <scp>ECOGNITION</scp>. *Annu. Rev. Immunol.* **20**, 197–216 (2002).

151. Medzhitov, R. Pattern recognition theory and the launch of modern innate immunity. *J. Immunol.* **191**, 4473–4 (2013).

152. Ahmad, R., Sorrell, M. F., Batra, S. K., Dhawan, P. & Singh, A. B. Gut permeability and mucosal inflammation: Bad, good or context dependent. *Mucosal Immunology* **10**, 307–317 (2017).

153. Xavier, R. J. & Podolsky, D. K. Unravelling the pathogenesis of inflammatory bowel disease. doi:10.1038/nature06005

154. Ramanan, D., Tang, M. S., Bowcutt, R., Loke, P. & Cadwell, K. Bacterial sensor Nod2 prevents inflammation of the small intestine by restricting the expansion of the commensal bacteroides vulgatus. *Immunity* **41**, 311–324 (2014).

155. Guo, L. *et al.* IL-1 family members and STAT activators induce cytokine production by Th2, Th17, and Th1 cells. *Proc. Natl. Acad. Sci. U. S. A.* **106**, 13463–8 (2009).

156. Triantafillidis, J. K., Merikas, E. & Georgopoulos, F. Current and emerging drugs for the treatment of inflammatory bowel disease. *Drug Design, Development and Therapy* **5**, 185–210 (2011).

157. Michail, S., Bultron, G. & Depaolo, R. W. Genetic variants associated with Crohn's disease. *Appl. Clin. Genet.* **6**, 25–32 (2013).

158. Zhan, Y., Seregin, S. S., Chen, J. & Chen, G. Y. Nod1 Limits Colitis-Associated Tumorigenesis by Regulating IFN-γ Production. *J. Immunol.* **196**, 5121–9 (2016).

159. Normand, S. *et al.* Nod-like receptor pyrin domain-containing protein 6 (NLRP6) controls epithelial self-renewal and colorectal carcinogenesis upon injury. doi:10.1073/pnas.1100981108

160. Zaki, M. H., Lamkanfi, M. & Kanneganti, T. D. The Nlrp3 inflammasome: Contributions to intestinal homeostasis. *Trends in Immunology* **32**, 171–179 (2011).

161. Thorley, A. J. *et al.* Innate immune responses to bacterial ligands in the peripheral human Lung - Role of alveolar epithelial TLR expression and signalling. *PLoS One* **6**, (2011).

162. Santaolalla, R. & Abreu, M. T. Innate immunity in the small intestine. doi:10.1097/MOG.0b013e3283506559

163. Kawai, T. & Akira, S. Toll-like Receptors and Their Crosstalk with Other Innate Receptors in Infection and Immunity. *Immunity* **34**, 637–650 (2011).

164. Brandl, K. *et al.* MyD88 signaling in nonhematopoietic cells protects mice against induced

colitis by regulating specific EGF receptor ligands. *Proc. Natl. Acad. Sci.* **107**, 19967–19972 (2010).

165. Jiminez, J. A., Uwiera, T. C., Inglis, G. D. & Uwiera, R. R. E. Animal models to study acute and chronic intestinal inflammation in mammals. *Gut Pathogens* **7**, (2015).

166. Dieleman, L. A. *et al.* Chronic experimental colitis induced by dextran sulphate sodium (DSS) is characterized by Th1 and Th2 cytokines. *Clin. Exp. Immunol.* **114**, 385–391 (1998).

167. Salim, T., Sershen, C. L. & May, E. E. Investigating the role of TNF-α and IFN-γ activation on the dynamics of iNOS gene expression in lps stimulated macrophages. *PLoS One* **11**, (2016).

168. Hiemstra, I. H., Bouma, G., Geerts, D., Kraal, G. & Haan, J. M. M. den. Nod2 improves barrier function of intestinal epithelial cells via enhancement of TLR responses. *Mol. Immunol.* **52**, 264–272 (2012).

169. Homer, C. R. *et al.* A dual role for receptor-interacting protein kinase 2 (RIP2) kinase activity in nucleotide-binding oligomerization domain 2 (NOD2)-dependent autophagy. *J. Biol. Chem.* **287**, 25565–25576 (2012).

170. Travassos, L. H. *et al.* Nod1 and Nod2 direct autophagy by recruiting ATG16L1 to the plasma membrane at the site of bacterial entry. *Nat. Immunol.* **11**, 55–62 (2010).

171. Manuscript, A. Crohn ' s disease : NOD2 , autophagy and ER stress converge. **60**, 1580–1588 (2014).

172. Philpott, D. J., Sorbara, M. T., Robertson, S. J., Croitoru, K. & Girardin, S. E. NOD proteins: regulators of inflammation in health and disease. *Nat. Rev. Immunol.* **14**, 9–23 (2014).

173. Corridoni, D., Chapman, T., Ambrose, T. & Simmons, A. Emerging Mechanisms of Innate Immunity and Their Translational Potential in Inflammatory Bowel Disease. *Front. Med.* **5**, 32 (2018).

174. Gutierrez, O. *et al.* Induction of Nod2 in Myelomonocytic and Intestinal Epithelial Cells via Nuclear Factor- B Activation *. **277**, 41701–41705 (2002).

175. Petnicki-Ocwieja, T. *et al.* Nod2 is required for the regulation of commensal microbiota in the intestine.

176. Couturier-Maillard, A. *et al.* NOD2-mediated dysbiosis predisposes mice to transmissible colitis and colorectal cancer. *J. Clin. Invest.* **123**, (2013).

177. Hugot, J.-P. *et al.* Association of NOD2 leucine-rich repeat variants with susceptibility to Crohn's disease. *Nature* **411**, 599–603 (2001).

178. Udden, S. M. N. *et al.* NOD2 Suppresses Colorectal Tumorigenesis via Downregulation of the TLR Pathways. *Cell Rep.* **19**, 2756–2770 (2017).

179. Ferrand, A. *et al.* NOD2 Expression in Intestinal Epithelial Cells Protects Toward the Development of Inflammation and Associated Carcinogenesis. *CMGH* **7**, 357–369 (2019).

180. Inohara, N., Chamaillard, M., McDonald, C. & Nuñez, G. NOD-LRR PROTEINS: Role in Host-Microbial Interactions and Inflammatory Disease. *Annu. Rev. Biochem.* **74**, 355–383 (2005).

181. Jing, X. *et al.* Peptidoglycan recognition protein 3 and Nod2 synergistically protect mice

from dextran sodium sulfate-induced colitis. *J. Immunol.* **193**, 3055–69 (2014).

182. Nigro, G., Rossi, R., Commere, P. H., Jay, P. & Sansonetti, P. J. The cytosolic bacterial peptidoglycan sensor Nod2 affords stem cell protection and links microbes to gut epithelial regeneration. *Cell Host Microbe* **15**, 792–798 (2014).

183. Nigro, G., Rossi, R., Commere, P. H., Jay, P. & Sansonetti, P. J. The cytosolic bacterial peptidoglycan sensor Nod2 affords stem cell protection and links microbes to gut epithelial regeneration. *Cell Host Microbe* **15**, 792–798 (2014).

184. Kawai, T. & Akira, S. The roles of TLRs, RLRs and NLRs in pathogen recognition. *Int. Immunol.* **21**, 317–337 (2009).

185. Takeuchi, O. & Akira, S. Pattern Recognition Receptors and Inflammation. *Cell* **140**, 805–820 (2010).

186. Fruman, D. A. *et al.* The PI3K Pathway in Human Disease. *Cell* **170**, 605–635 (2017).

187. Liu, P., Cheng, H., Roberts, T. M. & Zhao, J. J. Targeting the phosphoinositide 3-kinase (PI3K) pathway in cancer. *Nat. Rev. Drug. Discov.* **8**, 627–644 (2009).

188. Hawkins, P. T. & Stephens, L. R. PI3K signalling in inflammation. *Biochim. Biophys. Acta* **1851**, 882–97 (2015).

189. Robertson, S. J. *et al.* Nod1 and Nod2 signaling does not alter the composition of intestinal bacterial communities at homeostasis. *Gut Microbes* **4**, 222–231 (2013).

190. Caruso, R., Warner, N., Inohara, N. & Núñez, G. NOD1 and NOD2: Signaling, host defense, and inflammatory disease. *Immunity* **41**, 898–908 (2014).

191. Castellano, E. *et al.* RAS signalling through PI3-Kinase controls cell migration via modulation of Reelin expression. *Nat. Commun.* **7**, 11245 (2016).

192. Castellano, E., De Las Rivas, J., Guerrero, C. & Santos, E. Transcriptional networks of knockout cell lines identify functional specificities of H-Ras and N-Ras: significant involvement of N-Ras in biotic and defense responses. *Oncogene* **26**, 917–933 (2007).

193. Laemmli, U. K. Cleavage of structural proteins during the assembly of the head of bacteriophage T4. *Nature* **227**, 680–685 (1970).

194. Oh, S. Y., Cho, K. A., Kang, J. L., Kim, K. H. & Woo, S. Y. Comparison of experimental mouse models of inflammatory bowel disease. *Int. J. Mol. Med.* **33**, 333–340 (2014).

195. Barreau, F. *et al.* CARD15/NOD2 is required for Peyer's patches homeostasis in mice. *PLoS One* **2**, e523 (2007).

196. Bauer, C. *et al.* Colitis induced in mice with dextran sulfate sodium (DSS) is mediated by the NLRP3 inflammasome. *Gut* **59**, 1192–1199 (2010).

197. Umiker, B. *et al.* The NLRP3 inflammasome mediates DSS-induced intestinal inflammation in *Nod2* knockout mice. *Innate Immun.* **25**, 132–143 (2019).

198. Hugot, J. P. *et al.* Association of NOD2 leucine-rich repeat variants with susceptibility to Crohn's disease. *Nature* **411**, 599–603 (2001).

199. Ogura, Y. *et al.* A frameshift mutation in NOD2 associated with susceptibility to Crohn's disease. *Nature* **411**, 603–606 (2001).

200. Liu, J. Z. *et al.* Association analyses identify 38 susceptibility loci for inflammatory bowel disease and highlight shared genetic risk across populations. *Nat. Genet.* **47**, 979–986 (2015).

201. Cadwell, K. *et al.* A key role for autophagy and the autophagy gene Atg16l1 in mouse and human intestinal Paneth cells. *Nature* **456**, 259–263 (2008).

202. Aksoy, E. *et al.* The p110δ isoform of the kinase PI(3)K controls the subcellular compartmentalization of TLR4 signaling and protects from endotoxic shock. *Nat. Immunol.* **13**, 1045–54 (2012).

203. Inohara, N., Ogura, Y., Chen, F. F., Muto, A. & Nuñez, G. Human Nod1 confers responsiveness to bacterial lipopolysaccharides. *J. Biol. Chem.* **276**, 2551–4 (2001).

204. Kok, K., Geering, B. & Vanhaesebroeck, B. Regulation of phosphoinositide 3-kinase expression in health and disease. *Trends Biochem. Sci.* **34**, 115–127 (2009).

205. Marone, R., Cmiljanovic, V., Giese, B. & Wymann, M. P. Targeting phosphoinositide 3-kinase-Moving towards therapy. *Biochim. Biophys. Acta - Proteins Proteomics* **1784**, 159–185 (2008).

206. Graupera, M. *et al.* Angiogenesis selectively requires the p110α isoform of PI3K to control endothelial cell migration. *Nature* **453**, 662–666 (2008).

207. Wang, Q. *et al.* Tamoxifen enhances stemness and promotes metastasis of ERα36+ breast cancer by upregulating ALDH1A1 in cancer cells. *Cell Res.* **28**, 336–358 (2018).

208. Kobori, A. *et al.* Interleukin-33 expression is specifically enhanced in inflamed mucosa of ulcerative colitis. *J. Gastroenterol.* **45**, 999–1007 (2010).

209. Duan, L. *et al.* Interleukin-33 ameliorates experimental colitis through promoting Th2/Foxp3^{+} regulatory T-cell responses in mice. *Mol. Med.* **18**, 753–61 (2012).

210. Jiang, W. *et al.* Recognition of gut microbiota by NOD2 is essential for the homeostasis of intestinal intraepithelial lymphocytes. *J. Exp. Med.* **210**, (2013).

211. Jie Chen, Yan He, L. T. and L. D. Dual immune functions of IL-33 in inflammatory bowel diseaseistopathol, Vol 34, Chen et al. Available at: http://www.hh.um.es/Abstracts/Vol_/_/__18149.htm. (Accessed: 6th September 2019)

212. Yilmaz, Ö. H. *et al.* mTORC1 in the Paneth cell niche couples intestinal stem-cell function to calorie intake. *Nature* **486**, 490–5 (2012).

213. Schmitt, M. *et al.* Paneth Cells Respond to Inflammation and Contribute to Tissue Regeneration by Acquiring Stem-like Features through SCF/c-Kit Signaling. *Cell Rep.* **24**, 2312-2328.e7 (2018).

214. VanDussen, K. L. *et al.* Notch signaling modulates proliferation and differentiation of intestinal crypt base columnar stem cells. *Development* **139**, 488–497 (2011).

215. Foukas, L. C. *et al.* Long-term p110a PI3K inactivation exerts a beneficial effect on metabolism. doi:10.1002/emmm.201201953

216. Travassos, L. H. *et al.* Nod1 and Nod2 direct autophagy by recruiting ATG16L1 to the plasma membrane at the site of bacterial entry. *Nat. Immunol.* **11**, 55–62 (2010).

217. Manifava, M. *et al.* Dynamics of mTORC1 activation in response to amino acids. *Elife* **5**, (2016).

218. Nofal, M., Zhang, K., Han, S. & Rabinowitz, J. D. mTOR Inhibition Restores Amino Acid Balance in Cells Dependent on Catabolism of Extracellular Protein. *Mol. Cell* **67**, 936-946.e5 (2017).

219. Yoshida, S., Pacitto, R., Yao, Y., Inoki, K. & Swanson, J. A. Growth factor signaling to mTORC1 by amino acid-laden macropinosomes. *J. Cell Biol.* **211**, 159–72 (2015).

220. Zanello, G. *et al.* The Cytosolic Microbial Receptor Nod2 Regulates Small Intestinal Crypt Damage and Epithelial Regeneration following T Cell–Induced Enteropathy. *J. Immunol.* **197**, 345–355 (2016).

221. Chen, G. Y., Shaw, M. H., Redondo, G. & Nunez, G. The Innate Immune Receptor Nod1 Protects the Intestine from Inflammation-Induced Tumorigenesis. *Cancer Res.* **68**, 10060–10067 (2008).

222. Lee, C. *et al.* NOD2 Supports Crypt Survival and Epithelial Regeneration after Radiation-Induced Injury. *Int. J. Mol. Sci.* **20**, 4297 (2019).

223. Peng, J. *et al.* Phosphoinositide 3-kinase p110δ promotes lumen formation through the enhancement of apico-basal polarity and basal membrane organization. *Nat. Commun.* **6**, 5937 (2015).

224. Lo, Y., Sauve, J. P., Menzies, S. C., Steiner, T. S. & Sly, L. M. Phosphatidylinositol 3-kinase p110δ drives intestinal fibrosis in SHIP deficiency. *Mucosal Immunol.* **12**, 1187–1200 (2019).

225. Brown, J. B. & Barrett, T. A. p110δ mutant mice reveal central role for PI3K signaling in intestinal macrophages. *Gastroenterology* **139**, 1451–3 (2010).

226. Castellano, E. *et al.* Requirement for Interaction of PI3-Kinase p110α with RAS in Lung Tumor Maintenance. *Cancer Cell* **24**, 617–630 (2013).

227. Zhao, J. J. *et al.* The p110alpha isoform of PI3K is essential for proper growth factor signaling and oncogenic transformation. *Proc. Natl. Acad. Sci. U. S. A.* **103**, 16296–300 (2006).

228. Soler, A. *et al.* Therapeutic benefit of selective inhibition of p110a PI3-kinase in pancreatic neuroendocrine tumors. *Clin. Cancer Res.* (2016). doi:10.1158/1078-0432.CCR-15-3051

229. Lindhurst, M. J. *et al.* Mosaic overgrowth with fibroadipose hyperplasia is caused by somatic activating mutations in PIK3CA. *Nat. Genet.* **44**, 928–933 (2012).

230. Soler, A. *et al.* Inhibition of the p110α isoform of PI 3-kinase stimulates nonfunctional tumor angiogenesis. *J. Exp. Med.* **210**, 1937–45 (2013).

231. Foukas, L. C. *et al.* Critical role for the p110α phosphoinositide-3-OH kinase in growth and metabolic regulation. *Nature* **441**, 366–370 (2006).

232. Berenjeno, I. M. *et al.* Both p110α and p110β isoforms of PI3K can modulate the impact of loss-of-function of the PTEN tumour suppressor. *Biochem. J.* **442**, 151 (2012).

233. Murillo, M. M. *et al.* Disruption of the Interaction of RAS with PI 3-Kinase Induces Regression of EGFR-Mutant-Driven Lung Cancer. *Cell Rep.* **25**, 3545-3553.e2 (2018).

234. McClung, J. M., Judge, A. R., Powers, S. K. & Yan, Z. p38 MAPK links oxidative stress to autophagy-related gene expression in cachectic muscle wasting. *Am. J. Physiol. - Cell Physiol.* **298**, (2010).

235. Tang, G. *et al.* Autophagy induced by Alexander disease-mutant GFAP accumulation is regulated by p38/MAPK and mTOR signaling pathways. *Hum. Mol. Genet.* **17**, 1540–1555 (2008).

236. Commisso, C. *et al.* Macropinocytosis of protein is an amino acid supply route in Ras-transformed cells. *Nature* **497**, 633–637 (2013).

237. Zhou, Y.-J., Zhou, H., Li, Y. & Song, Y.-L. NOD1 activation induces innate immune responses and insulin resistance in human adipocytes. *Diabetes Metab.* **38**, 538–543 (2012).

238. Michail, S., Bultron, G. & Depaolo, R. W. Genetic variants associated with Crohn's disease. *Appl. Clin. Genet.* **6**, 25–32 (2013).

239. Ogura, Y. *et al.* A frameshift mutation in NOD2 associated with susceptibility to Crohn's disease. *Nature* **411**, 603–606 (2001).

240. Fritz, J. H. Nod-like receptors have a grip on stem cells. *Cell Host Microbe* **15**, 659–661 (2014).

241. Patel, P. H. *et al.* Drosophila Rheb GTPase is required for cell cycle progression and cell growth. *J. Cell Sci.* **116**, 3601–3610 (2003).

242. Singhi, A. D. *et al.* Pediatric autoimmune enteropathy: An entity frequently associated with immunodeficiency disorders. *Mod. Pathol.* **27**, 543–553 (2014).

243. Groenewoud, M. J. *et al.* Mammalian Target of Rapamycin Complex I (mTORC1) Activity in Ras Homologue Enriched in Brain (Rheb)-Deficient Mouse Embryonic Fibroblasts. *PLoS One* **8**, e81649 (2013).

244. Yan, K. S. *et al.* Intestinal Enteroendocrine Lineage Cells Possess Homeostatic and Injury-Inducible Stem Cell Activity. *Cell Stem Cell* **21**, 78-90.e6 (2017).

245. Kim, C. K., Yang, V. W. & Bialkowska, A. B. The Role of Intestinal Stem Cells in Epithelial Regeneration Following Radiation-Induced Gut Injury. *Current Stem Cell Reports* **3**, 320–332 (2017).

246. Suh, H. N. *et al.* Quiescence Exit of Tert+ Stem Cells by Wnt/β-Catenin Is Indispensable for Intestinal Regeneration. *Cell Rep.* **21**, 2571–2584 (2017).

247. Tian, H. *et al.* A reserve stem cell population in small intestine renders Lgr5-positive cells dispensable. *Nature* **478**, 255–259 (2011).

248. Yu, Y. *et al.* Phosphoproteomic analysis identifies Grb10 as an mTORC1 substrate that negatively regulates insulin signaling. *Science* **332**, 1322–6 (2011).

249. You, J.-S. *et al.* The role of raptor in the mechanical load-induced regulation of mTOR signaling, protein synthesis, and skeletal muscle hypertrophy. *FASEB J.* **33**, 4021–4034 (2019).

250. Francipane, M. G. & Lagasse, E. mTOR pathway in colorectal cancer: an update. *Oncotarget* **5**, 49–66 (2014).

251. Dann, S. G., Selvaraj, A. & Thomas, G. mTOR Complex1-S6K1 signaling: at the crossroads of obesity, diabetes and cancer. *Trends Mol. Med.* **13**, 252–9 (2007).

252. Fritsch, R. *et al.* RAS and RHO families of GTPases directly regulate distinct phosphoinositide 3-kinase isoforms. *Cell* **153**, 1050–63 (2013).

253. Meng, D., Frank, A. R. & Jewell, J. L. mTOR signaling in stem and progenitor cells. *Development (Cambridge)* **145**, (2018).

254. Haller, S. *et al.* mTORC1 Activation during Repeated Regeneration Impairs Somatic Stem Cell Maintenance. *Stem Cell* **21**, 806-818.e5 (2017).

255. Chen, C., Liu, Y., Liu, Y. & Zheng, P. mTOR Regulation and Therapeutic Rejuvenation of Aging Hematopoietic Stem Cells. *Sci. Signal.* **2**, ra75–ra75 (2009).

256. Palm, W., Araki, J., King, B., Dematteo, R. G. & Thompson, C. B. Critical role for PI3-kinase in regulating the use of proteins as an amino acid source. doi:10.1073/pnas.1712726114